Exogenous Ligand Assisted Rare-earth Complexes: Catalyst Design, Applications in Ring-Opening Polymerization and Reaction Kinetics

Xiang Dong

A DISSERTATION

in

Chemistry

Presented to the Faculties of Brown University

in

Partial Fulfillment of the Requirement of

Degree of Doctor of Philosophy

2022

Supervisor of Dissertation:

Dr. Jerome R. Robinson, Assistant Professor of Chemistry

Graduate Group Chairperson:

Dr. Lai-Sheng Wang, Jesse H. and Louisa D. Sharpe Metcalf Professor of Chemistry

Dissertation Committee:

Dr. Ou Chen, Associate Professor of Chemistry

Dr. Jerome R. Robinson, Assistant Professor of Chemistry

Dr. Matthew B. Zimmt, Professor of Chemistry

This dissertation by Xiang Dong is accepted in its present form by the Department of Chemistry as satisfying the dissertation requirement for the degree of Doctor of Philosophy.

Date _____   _____

Jerome R. Robinson, Ph.D.

Advisor

Recommended to the Graduate Council

Date _____   _____

Ou Chen, Ph.D.

Reader

Date _____   _____

Matthew B. Zimmt, Ph.D.

Reader

Approved by the Graduate Council

Date _____   _____

Andrew G. Campbell, Ph.D.

Dean of the Graduate School

Curriculum Vitae

Xiang Dong

EDUCATION

08/2016-05/2022	Ph.D., Chemistry	**Brown University**
	Advisor: Prof. Jerome R. Robinson	Providence, RI, USA

08/2007-06/2011	B.S. Chemical Physics	**University of Science and Technology of China**
		Hefei, Anhui, China

RESEARCH EXPERIENCE

01/2017–05/2022 **Brown University** — Graduate Research Assistant
- Department of Chemistry — Providence, RI, USA
Advisor: Prof. Jerome R. Robinson
- Synthesis, characterization, and reactivity of novel rare-earth catalysts
- Stereospecific ring-opening (co)polymerization of oxygenated monomers

07/2011–07/2013 **Shanghai Institute of Organic Chemistry,** — Research Assistant
Chinese Academy of Sciences — Shanghai, China
Supervisor: Prof. Min Shi
- Trifluoromethylation induced intramolecular cascade reactions
- Transition metal catalyzed reactions of highly strained molecules

10/2010–06/2011 **University of Science and Technology of China** — Undergraduate Research Assistant
- Department of Chemical Physics — Hefei, Anhui, China
Advisor: Prof. Xiao-Guo Zhou
- Photofragment-ion imaging and dynamics of photodissociation

06/2009–09/2009 **Dalian Institute of Chemical Physics,** — Undergraduate Research Assistant
Chinese Academy of Sciences — Dalian, Liaoning, China
Advisor: Prof. Yong-Gui Zhou
- Asymmetric hydrogenation of heteroaromatic compounds
- Synthesis of novel chiral ligands

PUBLICATIONS

Brown University

10. **Dong, X.**; Brown, A. M.; Woodside, A. J.; Robinson, J. R.* "N-Oxides Amplify Catalyst Reactivity and Isoselectivity in the Ring-Opening Polymerization of rac-β-Butyrolactone" *Chem. Comm.* **2022,** *58,* 2854-2857. (Part of the themed collection: 2021 Emerging Investigators)

9. **Dong, X.**; Robinson, J. R.* "The Versatile Roles of Neutral Donor Ligands in Tuning Catalyst Performance for the Ring-Opening Polymerization of Cyclic Esters" *New J. Chem.*, **2022**, *46*, 444-453. (Part of the themed collection: NJC Emerging Investigators)

8. Shen, M.; Yu, C.; Guan, H.; **Dong, X.**; Harris, C.; Xiao, Z.; Yin, Z., Muzzio, M.; Lin, H.; Robinson, J. R.; Colvin, V. L. Sun, H.* "Nanoparticle-Catalyzed Green Chemistry Synthesis of Polybenzoxazole" *J. Am. Chem. Soc.* **2021**, *143*, 2115–2122.

7. **Dong, X.**; Robinson, J. R.* "The Role of Neutral Donor Ligands in the Isoselective Ring-Opening Polymerization of rac-β-Butyrolactone" *Chem. Sci.* **2020**, *11*, 8184-8195.

Prior to Brown:

6. Zhang, X. N.; **Dong, X.**; Wei, Y.*; Shi, M.* "Access to 2',3'-dihydro-1'H-spiro[indoline-3,4'-pyridin]-2-ones via amino acid derived phosphine-catalyzed asymmetric [4+2] annulation with easily available oxindole-derived α,β-unsaturated imines" *Tetrahedron* **2014**, *70*, 2838-2846.

5. **Dong, X.**; Sang, R.; Wang, Q.; Tang, X. Y.*; Shi, M.* "Copper-Catalyzed Trifluoromethylation and Cyclization of Aromatic-Sulfonyl-Group-Tethered Alkenes for the Construction of 1,2-Benzothiazinane Dioxide Type Compounds" *Chem. Eur. J.* **2013**, *19*, 16910–16915.

4. Zhang, X. N.; Chen, G. Q.; **Dong, X.**; Wei, Y.*; Shi, M.* "Phosphine-Catalyzed Asymmetric [4+2] Annulation of Vinyl Ketones with Oxindole-Derived α,β-Unsaturated Imines: Enantioselective Syntheses of 2',3'-Dihydro-1'H-spiro[indoline-3,4'-pyridin]-2-ones" *Adv. Synth. Catal.* **2013**, *355*, 3351-3357.

3. Yuan, W.; **Dong, X.**; Shi, M.*; McDowell P.; Li, G.* "Rh(I)-catalyzed Pauson-Khand-type Cycloaddition Reaction of Ene-vinylidenecyclopropanes with Carbon Monoxide (CO)" *Org. Lett.* **2012**, *14*, 5582-5585.

2. Yuan, W.; **Dong, X.**; Wei, Y.*; Shi, M.* "An Efficient Method for the Synthesis of Alkylidenecyclobutanones by Gold-Catalyzed Oxidative Ring Enlargement of Vinylidenecyclopropanes" *Chem. Eur. J.* **2012**, *18*, 10501-10505.

1. Chen, Q. A.; **Dong, X.**; Chen, M. W.; Wang, D. S; Zhou, Y. G.*; Li, Y. X. "Highly Effective and Diastereoselective Synthesis of Axially Chiral Bis-sulfoxide Ligands via Oxidative Aryl Coupling" *Org. Lett.* **2010**, *12*, 1928-1931.

PATENTS

1. Robinson, J. R.; **Dong, X.** (2021). "Catalyst and process for ring opening polymerization" *U.S. Patent Application No. 2021/0188878 A1*. Washington, DC: U.S. Patent and Trademark Office.

Acknowledgment

This dissertation could not have been possible without the support, inspiration, and expertise of Prof. Jerome R. Robinson, my advisor, who contributed immensely to my scientific development over the last six years. I had the great fortune to meet Prof. Robinson in the Department of Chemistry at Brown University when I started my graduate study in Fall 2016 and join his group in the following semester. It was an experience that changed my life. I have never had an experience that I was not impressed by his vast knowledge and profound thought after any discussion with him. Besides his guidance, I greatly appreciate the freedom and opportunities he granted to me to investigate problems that I found interesting and to learn the knowledge that I felt constructive to my scientific development.

I gratefully thank the other members of my committee, Prof. Ou Chen and Prof. Matthew B. Zimmt, for their helpful comments, suggestions, and career advice. To Prof. Ou Chen, I would like to especially thank the generous emotional support he offered me after he considerately noticed I was in a somewhat unhealthy and depressing state. To Prof. Matthew B. Zimmt, I would like to acknowledge his influence seen throughout my studies, especially by .helping me rigorously approaching research by asking and answering thought-provoking questions in multiple ways in each of my committee meeting.

I owe immense thanks to many other faculty members in and out of the Department of Chemistry. I would like to thank Prof. Eunsuk Kim for hosting weekly literature meeting that including both her and our group. It is a great chance for me to broaden my scientific view and she has been teaching me (and probably all students joining the meetings) a lot and brought insightful thoughts. I would also express my gigantic gratitude and esteem to Prof. Richard M. Stratt for the course Statistical Mechanics he presented and Prof. Robert A. Pelcovits, in the Department of Physics, for his Quantum Mechanics II and Solid State Physics. I could not be more fortunate to have attended their classes, which were (and certainly will be) of tremendously extraordinary quality. In their class, they elucidate profound and magnificent scientific principals in concise and comprehensive language and laid a great part of solid cornerstones of my scientific development. I would also like to thank Prof. Mary (Rebecca)

Table of Contents

List of Tables

Chapter 4:
Quantitative Study of Kinetic of Polymerization of *rac-β*-BBL
Accompanied by Time-dependent Concentration of Catalyst

List of Figures

Chapter 1:
Introduction to Rare-earth Catalyzed Polymerization of *β*-Butyrolactone

Chapter 2:
OPPh3 Assisted Rare-earth Catalyst of Iso-selective
Ring-Opening Polymerization of *rac-β*-BBL

Chapter 3:
***N*-Oxides Amplify Catalyst Reactivity and Iso-selectivity in**
the Ring-Opening Polymerization of *rac-β*-BBL

Chapter 4:
Quantitative Study of Kinetic of Polymerization of *rac-β*-BBL
Accompanied by Time-dependent Concentration of Catalyst

List of Schemes

Exogenous Ligand Assisted Rare-earth Complexes: Catalyst Design, Applications in Ring-Opening Polymerization and Reaction Kinetics

Xiang Dong

Jerome R. Robinson

Abstract

Complexes of rare-earth elements (REs, Sc, Y, La-Lu) are among the most successful catalysts for ring-opening polymerization (ROP) of lactones. However, there are gaps in synthesizing the polymers with both high efficiency and good steric selectivity. Our studies provided a novel way of constructing RE catalyst and tuning its catalytic performance by introducing exogenous ligands [phosphine oxides or lutidine-oxides (LO)]. We applied this catalytic system on the ROP of *rac-β*-butyrolactone (*rac*-BBL), which usually displays relatively low reactivity among lactone monomers and challenges in polymerization with high iso-tacticity ($P_m \geqslant 0.80$) and got unprecedent success in both high reactivity (TOF up to 1,900 /h) and good iso-selectivity (P_m up to 0.82). Furthermore, the critical side reaction were systematically examined that significantly affected distribution of molecular weights of macromolecular product and reaction rate. In the study of raction kinetics, a method of track evolution of active catalytic species was developed and applied to quantatively determine kinetic parameters of the primary propagation and the coupling side reaction. These results may direct further developments of this exogenous ligand assisted RE catalytic system.

Chapter 1: Introduction to Rare-earth Catalyzed Polymerization of β-Butyrolactone

Plastics derived from polyolefins enable many applications and provide incredible benefits to society; however, there is growing environmental concern for the immense amount of polymer waste entering landfills and waterways and its unfavorable environmental persistence.[1-4]. Poly-3-hydroxybutyrate (P3HB), the most common poly(hydroxyalkanoate) (PHA), is a biodegradable aliphatic polyester which can have properties similar to isotactic polypropylene and applications ranging from packaging to bio-medical applications.[5-13] The polymer's relative stereochemistry (tacticity) plays a critical role in the observed properties (thermal, mechanical, degradation).[5, 10, 12, 14-17] Several microorganisms can produce perfectly isotactic P3HB through fermentation; however, production costs remain high, the highly crystalline material is brittle, and the material's decomposition temperature is close to its melting temperature.[5, 18-21]
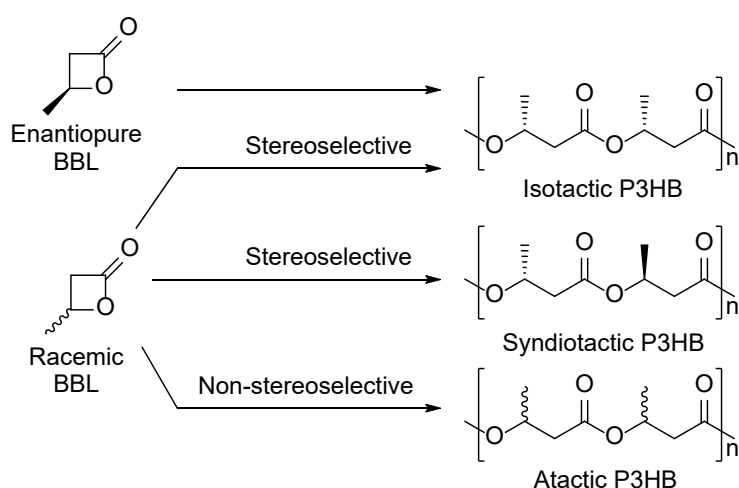
Scheme 1.1. Access to P3HBs with different microstructures from BBL

2

Alternatively, a variety of synthetic catalysts can produce P3HB with various microstructures through stereoselective ring-opening polymerization (ROP) of β-butyrolactone (BBL) (Scheme 1.1),[22-42]. The ratio between *racemic* and *meso* diads manipulates physical, chemical and biological properties of the material, and thus tuning this ratio makes P3HB and ideal candidate that fulfills a wide range of applications. However, stereocontrol has been challenging.[35, 43-46] Intensive labors in catalyst design[16, 26, 31-32, 36, 47-58] have led to highly syndiotactic P3HB ($P_r \geq 0.9$; P_r: percent *racemic* diads),[16, 35-36, 50-51] yet despite numerous efforts,[38-39, 45-47, 59-66] a single system[39]. has managed to produce isotactic P3HB with $P_m \geq$ 0.80 (P_m: percent *meso* diads). Chen and coworkers developed an elegant alternative to access perfectly isotactic P3HB from a designer 8-membered cyclic diolide. Although this avoids selectivity challenges associated with *rac*-BBL, it requires multi-step monomer synthesis (14–60% yield).[12, 66-67]

R^1	CMe$_2$*t*-Bu	*t*-Bu	CMe$_2$Ph	CPh$_3$
P_r	0.70	0.81	0.91	0.95
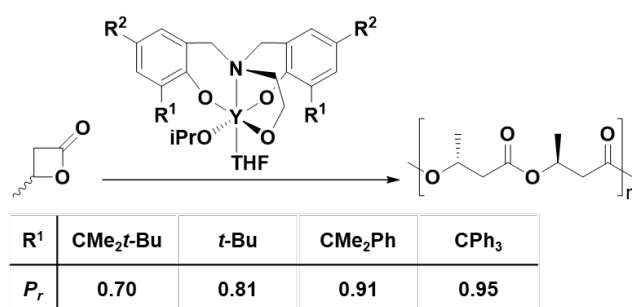
Scheme 1.2. Syndioselective ROP of *rac*-BBL promoted by amido and alkyl Y(ONXOR^1,R^2) complexes (R^2 = tBu or CMe$_2$Ph)

Of all the catalyst platforms, rare-earth (RE) complexes supported by tetradentate tripodal amino-bisphenolate ligands developed by Carpentier and coworkers (Scheme 1.2) stand out as "privileged" structures due to their exceptional activity and syndioselectivity.[16, 35-36]

Numerous modifications have been explored (e.g. aryloxide substitution, donor identity, tether/linker, initiator, and RE[III]); however, none have led to isotactic P3HB.[68-70]

Conventional catalyst design and reaction optimization have focused on systematic covalent modifications of ancillary ligand frameworks; however, labile, exogenous neutral donor ligands have emerged as an important class of additives that can rapidly modify catalyst properties to access new, mechanistically distinct pathways in an inexpensive and operationally simple manner. These neutral donors can dynamically tune the stereoelectronics of catalyst active-sites and attenuate reactivity and selectivity by modulating position(s) of critical catalyst equilibria. Improved mechanistic-level understanding of these additives has enabled exciting advances in the fields of homogeneous[71-72] and heterogeneous[73] catalysis, including an increasing number in polymerization methodologies.[74-81] Unfortunately, with the exception of ligands which promote Lewis-pair polymerization (LPP)[82-83] and introduction of neutral *N*-donor ligands to catalysts for the ROP of lactide[84] the effects of added neutral donors in the ROP of cyclic esters are scattered throughout the literature.
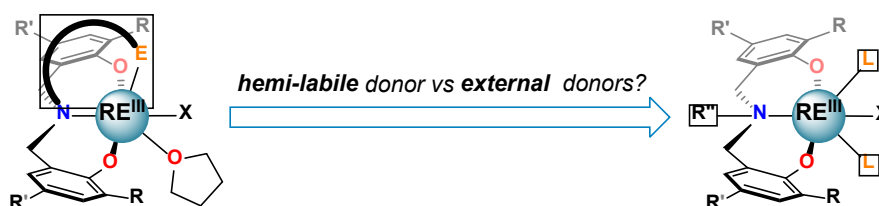
Scheme 1.3. Motivation of the design of neutral donor supported rare-earth catalyst

Instead of extensive covalent modification of catalyst frameworks, which can be costly and time-intensive, it would be highly desirable to access new selectivity preferences through

choice of simple external neutral donor ligand(s). We envisioned replacing the tethered donor in Carpentier's catalysts with a non-coordinating substituent to generate more accessible catalyst active sites that could be further shaped by neutral donor ligands. (Scheme 1.3)

References:

1.   Geyer, R.; Jambeck, J. R.; Law, K. L., Production, use, and fate of all plastics ever made. *Science Advances* **2017,** *3* (7), e1700782.

2.   Worm, B.; Lotze, H. K.; Jubinville, I.; Wilcox, C.; Jambeck, J., Plastic as a Persistent Marine Pollutant. *Annual Review of Environment and Resources* **2017,** *42* (1), 1-26.

3.   de Souza Machado, A. A.; Kloas, W.; Zarfl, C.; Hempel, S.; Rillig, M. C., Microplastics as an emerging threat to terrestrial ecosystems. *Global Change Biology* **2018,** *24* (4), 1405-1416.

4.   Chiba, S.; Saito, H.; Fletcher, R.; Yogi, T.; Kayo, M.; Miyagi, S.; Ogido, M.; Fujikura, K., Human footprint in the abyss: 30 year records of deep-sea plastic debris. *Marine Policy* **2018,** *96*, 204-212.

5.   Rieger, B.; Künkel, A.; Coates, G. W.; Reichardt, R.; Dinjus, E.; Zevaco, T. A., Synthetic Biodegradable Polymers. Springer Berlin: Berlin, 2014; pp 49-90.

6.   Gross, R. A.; Kalra, B., Biodegradable Polymers for the Environment. *Science* **2002,** *297* (5582), 803-807.

7.   Bugnicourt, E.; Cinelli, P.; Lazzeri, A.; Alvarez, V., Polyhydroxyalkanoate (PHA): Review of synthesis, characteristics, processing and potential applications in packaging. *Express Polymer Letters* **2014,** *8* (11), 791-808.

8. Zhu, Y.; Romain, C.; Williams, C. K., Sustainable polymers from renewable resources. *Nature* **2016,** *540*, 354.

9. Raza, Z. A.; Abid, S.; Banat, I. M., Polyhydroxyalkanoates: Characteristics, production, recent developments and applications. *International Biodeterioration & Biodegradation* **2018,** *126*, 45-56.

10. Tang, X.; Chen, E. Y. X., Chemical synthesis of perfectly isotactic and high melting bacterial poly(3-hydroxybutyrate) from bio-sourced racemic cyclic diolide. *Nat. Commun.* **2018,** *9* (1), 1-11.

11. Sangroniz, A.; Zhu, J.-B.; Tang, X.; Etxeberria, A.; Chen, E. Y. X.; Sardon, H., Packaging materials with desired mechanical and barrier properties and full chemical recyclability. *Nature Communications* **2019,** *10* (1), 3559.

12. Tang, X.; Westlie, A. H.; Watson, E. M.; Chen, E. Y.-X., Stereosequenced crystalline polyhydroxyalkanoates from diastereomeric monomer mixtures. *Science* **2019,** *366* (6466), 754-758.

13. Tang, X.; Westlie, A.; Caporaso, L.; Cavallo, L.; Falivene, L.; Chen, E. Y.-X., Biodegradable Polyhydroxyalkanoates by Stereoselective Copolymerization of Racemic Diolides: Stereocontrol Mechanism and Polyolefin-Like Properties. *Angewandte Chemie* **2020,** *132* (20), 7955-7964.

14. Jedliński, Z.; Kowalczuk, M.; Kurcok, P.; Brzoskowska, L.; Franek, J., Anionic block polymerization of β-lactones initiated by potassium solutions, 1. Synthesis of poly(4-methyl-2-oxetanone-block-2-oxetanone). *Die Makromolekulare Chemie* **1987,** *188* (7), 1575-1582.

15. He, Y.; Shuai, X.; Kasuya, K.-i.; Doi, Y.; Inoue, Y., Enzymatic Degradation of Atactic

Poly(R,S-3-hydroxybutyrate) Induced by Amorphous Polymers and the Enzymatic Degradation Temperature Window of an Amorphous Polymer System. *Biomacromolecules* **2001,** *2* (3), 1045-1051.

16. Ajellal, N.; Bouyahyi, M.; Amgoune, A.; Thomas, C. M.; Bondon, A.; Pillin, I.; Grohens, Y.; Carpentier, J.-F., Syndiotactic-Enriched Poly(3-hydroxybutyrate)s via Stereoselective Ring-Opening Polymerization of Racemic β-Butyrolactone with Discrete Yttrium Catalysts. *Macromolecules (Washington, DC, U. S.)* **2009,** *42* (4), 987-993.

17. Haslböck, M.; Klotz, M.; Sperl, J.; Sieber, V.; Zollfrank, C.; Van Opdenbosch, D., Mechanical and Thermal Properties of Mixed-Tacticity Polyhydroxybutyrates and Their Association with Iso- and Atactic Chain Segment Length Distributions. *Macromolecules* **2019,** *52* (14), 5407-5418.

18. Chen, G. Q., A microbial polyhydroxyalkanoates (PHA) based bio- and materials industry. *Chemical Society Reviews* **2009,** *38* (8), 2434-2446.

19. Anjum, A.; Zuber, M.; Zia, K. M.; Noreen, A.; Anjum, M. N.; Tabasum, S., Microbial production of polyhydroxyalkanoates (PHAs) and its copolymers: A review of recent advancements. *International Journal of Biological Macromolecules* **2016,** *89*, 161-174.

20. Rehm, B. H. A., Bacterial polymers: biosynthesis, modifications and applications. *Nature Reviews Microbiology* **2010,** *8* (8), 578-592.

21. Noda, I.; Green, P. R.; Satkowski, M. M.; Schechtman, L. A., Preparation and Properties of a Novel Class of Polyhydroxyalkanoate Copolymers. *Biomacromolecules* **2005,** *6* (2), 580-586.

22. Hall, H. K.; Schneider, A. K., Polymerization of Cyclic Esters, Urethans, Ureas and

Imides. *Journal of the American Chemical Society* **1958,** *80* (23), 6409-6412.

23. Inoue, S.; Tomoi, Y.; Tsuruta, T.; Furukawa, J., Organometallic-catalyzed polymerization of propiolactone. *Die Makromolekulare Chemie* **1961,** *48* (1), 229-233.

24. Agostini, D. E.; Lando, J. B.; Shelton, J. R., Synthesis and characterization of poly-β-hydroxybutyrate. I. Synthesis of crystalline DL-poly-β-hydroxybutyrate from DL-β-butyrolactone. *Journal of Polymer Science Part A-1: Polymer Chemistry* **1971,** *9* (10), 2775-2787.

25. Yasuda, T.; Aida, T.; Inoue, S., Living polymerization of β-butyrolactone catalysed by tetraphenylporphinatoaluminum chloride. *Die Makromolekulare Chemie, Rapid Communications* **1982,** *3* (9), 585-588.

26. Kemnitzer, J. E.; McCarthy, S. P.; Gross, R. A., Syndiospecific ring-opening polymerization of .beta.-butyrolactone to form predominantly syndiotactic poly(.beta.-hydroxybutyrate) using tin(IV) catalysts. *Macromolecules* **1993,** *26* (23), 6143-6150.

27. Rieth, L. R.; Moore, D. R.; Lobkovsky, E. B.; Coates, G. W., Single-Site β-Diiminate Zinc Catalysts for the Ring-Opening Polymerization of β-Butyrolactone and β-Valerolactone to Poly(3-hydroxyalkanoates). *Journal of the American Chemical Society* **2002,** *124* (51), 15239-15248.

28. Shaik, M.; Peterson, J.; Du, G., Cyclic and Linear Polyhydroxylbutyrates from Ring-Opening Polymerization of β-Butyrolactone with Amido-Oxazolinate Zinc Catalysts. *Macromolecules* **2019,** *52* (1), 157-166.

29. Gao, J.; Zhu, D.; Zhang, W.; Solan, G. A.; Ma, Y.; Sun, W.-H., Recent progress in the application of group 1, 2 & 13 metal complexes as catalysts for the ring opening

polymerization of cyclic esters. *Inorganic Chemistry Frontiers* **2019,** *6* (10), 2619-2652.

30. Quan, S. M.; Diaconescu, P. L., High activity of an indium alkoxide complex toward ring opening polymerization of cyclic esters. *Chemical Communications* **2015,** *51* (47), 9643-9646.

31. Ebrahimi, T.; Hatzikiriakos, S. G.; Mehrkhodavandi, P., Synthesis and Rheological Characterization of Star-Shaped and Linear Poly(hydroxybutyrate). *Macromolecules* **2015,** *48* (18), 6672-6681.

32. Jeffery, B. J.; Whitelaw, E. L.; Garcia-Vivo, D.; Stewart, J. A.; Mahon, M. F.; Davidson, M. G.; Jones, M. D., Group 4 initiators for the stereoselective ROP of rac-β-butyrolactone and its copolymerization with rac-lactide. *Chemical Communications* **2011,** *47* (45), 12328-12330.

33. Brulé, E.; Gaillard, S.; Rager, M.-N.; Roisnel, T.; Guérineau, V.; Nolan, S. P.; Thomas, C. M., Polymerization of Racemic β-Butyrolactone Using Gold Catalysts: A Simple Access to Biodegradable Polymers. *Organometallics* **2011,** *30* (10), 2650-2653.

34. Lyubov, D. M.; Tolpygin, A. O.; Trifonov, A. A., Rare-earth metal complexes as catalysts for ring-opening polymerization of cyclic esters. *Coordination Chemistry Reviews* **2019,** *392*, 83-145.

35. Carpentier, J.-F., Rare-Earth Complexes Supported by Tripodal Tetradentate Bis(phenolate) Ligands: A Privileged Class of Catalysts for Ring-Opening Polymerization of Cyclic Esters. *Organometallics* **2015,** *34* (17), 4175-4189.

36. Amgoune, A.; Thomas, C. M.; Ilinca, S.; Roisnel, T.; Carpentier, J.-F., Highly active, productive, and syndiospecific yttrium initiators for the polymerization of racemic β-

butyrolactone. *Angew. Chem., Int. Ed.* **2006,** *45* (17), 2782-2784.

37. Alaaeddine, A.; Amgoune, A.; Thomas, C. M.; Dagorne, S.; Bellemin-Laponnaz, S.; Carpentier, J.-F., Bis[bis(oxazolinato)] Complexes of Yttrium and Lanthanum: Molecular Structure and Use in Polymerization of dl-Lactide and dl-β-Butyrolactone. *European Journal of Inorganic Chemistry* **2006,** *2006* (18), 3652-3658.

38. Reichardt, R.; Vagin, S.; Reithmeier, R.; Ott, A. K.; Rieger, B., Factors Influencing the Ring-Opening Polymerization of Racemic β-Butyrolactone Using CrIII(salphen). *Macromolecules (Washington, DC, U. S.)* **2010,** *43* (22), 9311-9317.

39. Ajellal, N.; Durieux, G.; Delevoye, L.; Tricot, G.; Dujardin, C.; Thomas, C. M.; Gauvin, R. M., Polymerization of racemic β-butyrolactone using supported catalysts: a simple access to isotactic polymers. *Chem. Commun. (Cambridge, U. K.)* **2010,** *46* (7), 1032-1034.

40. Kiesewetter, M. K.; Shin, E. J.; Hedrick, J. L.; Waymouth, R. M., Organocatalysis: Opportunities and Challenges for Polymer Synthesis. *Macromolecules* **2010,** *43* (5), 2093-2107.

41. Jeong, W.; Hedrick, J. L.; Waymouth, R. M., Organic Spirocyclic Initiators for the Ring-Expansion Polymerization of β-Lactones. *Journal of the American Chemical Society* **2007,** *129* (27), 8414-8415.

42. Jaffredo, C. G.; Carpentier, J. F.; Guillaume, S. M., Controlled ROP of β-Butyrolactone Simply Mediated by Amidine, Guanidine, and Phosphazene Organocatalysts. *Macromolecular Rapid Communications* **2012,** *33* (22), 1938-1944.

43. Li, H.; Shakaroun, R. M.; Guillaume, S. M.; Carpentier, J.-F., Recent Advances in Metal-Mediated Stereoselective Ring-Opening Polymerization of Functional Cyclic Esters towards

Well-Defined Poly(hydroxy acid)s: From Stereoselectivity to Sequence-Control. *Chemistry – A European Journal* **2020,** *26* (1), 128-138.

44. Guillaume, S. M.; Kirillov, E.; Sarazin, Y.; Carpentier, J.-F., Beyond Stereoselectivity, Switchable Catalysis: Some of the Last Frontier Challenges in Ring-Opening Polymerization of Cyclic Esters. *Chemistry – A European Journal* **2015,** *21* (22), 7988-8003.

45. Thomas, C. M., Stereocontrolled ring-opening polymerization of cyclic esters: synthesis of new polyester microstructures. *Chemical Society Reviews* **2010,** *39* (1), 165-173.

46. Carpentier, J.-F., Discrete Metal Catalysts for Stereoselective Ring-Opening Polymerization of Chiral Racemic β-Lactones. *Macromolecular Rapid Communications* **2010,** *31* (19), 1696-1705.

47. Altenbuchner, P. T.; Kronast, A.; Kissling, S.; Vagin, S. I.; Herdtweck, E.; Pöthig, A.; Deglmann, P.; Loos, R.; Rieger, B., Mechanistic Investigations of the Stereoselective Rare Earth Metal-Mediated Ring-Opening Polymerization of β-Butyrolactone. *Chemistry – A European Journal* **2015,** *21* (39), 13609-13617.

48. Ajellal, N.; Lyubov, D. M.; Sinenkov, M. A.; Fukin, G. K.; Cherkasov, A. V.; Thomas, C. M.; Carpentier, J.-F.; Trifonov, A. A., Bis(guanidinate) Alkoxide Complexes of Lanthanides: Synthesis, Structures and Use in Immortal and Stereoselective Ring-Opening Polymerization of Cyclic Esters. *Chemistry – A European Journal* **2008,** *14* (18), 5440-5448.

49. Grunova, E.; Kirillov, E.; Roisnel, T.; Carpentier, J.-F., Group 3 metal complexes supported by tridentate pyridine- and thiophene-linked bis(naphtholate) ligands: synthesis, structure, and use in stereoselective ring-opening polymerization of racemic lactide and β-butyrolactone. *Dalton Transactions* **2010,** *39* (29), 6739-6752.

50. Klitzke, J. S.; Roisnel, T.; Kirillov, E.; Casagrande, O. d. L.; Carpentier, J.-F., Yttrium– and Aluminum–Bis(phenolate)pyridine Complexes: Catalysts and Model Compounds of the Intermediates for the Stereoselective Ring-Opening Polymerization of Racemic Lactide and β-Butyrolactone. *Organometallics* **2014,** *33* (1), 309-321.

51. Fang, J.; Tschan, M. J. L.; Roisnel, T.; Trivelli, X.; Gauvin, R. M.; Thomas, C. M.; Maron, L., Yttrium catalysts for syndioselective β-butyrolactone polymerization: on the origin of ligand-induced stereoselectivity. *Polymer Chemistry* **2013,** *4* (2), 360-367.

52. Pappalardo, D.; Bruno, M.; Lamberti, M.; Pellecchia, C., Ring-Opening Polymerization of Racemic β-Butyrolactone Promoted by Salan- and Salen-Type Yttrium Amido Complexes. *Macromolecular Chemistry and Physics* **2013,** *214* (17), 1965-1972.

53. Kemnitzer, J. E.; McCarthy, S. P.; Gross, R. A., Preparation of predominantly syndiotactic poly(.beta.-hydroxybutyrate) by the tributyltin methoxide catalyzed ring-opening polymerization of racemic .beta.-butyrolactone. *Macromolecules* **1993,** *26* (6), 1221-1229.

54. Arcana, M.; Giani-Beaune, O.; Schué, F.; Amass, W.; Amass, A., Structure and morphology of poly(β-hydroxybutyrate) synthesized by ring-opening polymerization of racemic (R,S)-β-butyrolactone with distannoxane derivatives. *Polymer International* **2000,** *49* (11), 1348-1355.

55. Liu, Y. C.; Lin, C. H.; Ko, B. T.; Ho, R. M., Ring-opening polymerization of β-butyrolactone catalyzed by efficient magnesium and zinc complexes derived from tridentate anilido-aldimine ligand. *Journal of Polymer Science Part A: Polymer Chemistry* **2010,** *48* (23), 5339-5347.

56. Bouyahyi, M.; Ajellal, N.; Kirillov, E.; Thomas, C. M.; Carpentier, J.-F., Exploring

Electronic versus Steric Effects in Stereoselective Ring-Opening Polymerization of Lactide and β-Butyrolactone with Amino-alkoxy-bis(phenolate)-Yttrium Complexes. *Chem. - Eur. J.* **2011,** *17* (6), 1872-1883, S1872/1-S1872/82.

57. Ebrahimi, T.; Aluthge, D. C.; Hatzikiriakos, S. G.; Mehrkhodavandi, P., Highly Active Chiral Zinc Catalysts for Immortal Polymerization of β-Butyrolactone Form Melt Processable Syndio-Rich Poly(hydroxybutyrate). *Macromolecules* **2016,** *49* (23), 8812-8824.

58. Nie, K.; Fang, L.; Yao, Y.; Zhang, Y.; Shen, Q.; Wang, Y., Synthesis and Characterization of Amine-Bridged Bis(phenolate)lanthanide Alkoxides and Their Application in the Controlled Polymerization of rac-Lactide and rac-β-Butyrolactone. *Inorganic Chemistry* **2012,** *51* (20), 11133-11143.

59. Le Borgne, A.; Spassky, N., Stereoelective polymerization of β-butyrolactone. *Polymer* **1989,** *30* (12), 2312-2319.

60. Spassky, N.; Pluta, C.; Simic, V.; Thiam, M.; Wisniewski, M., Stereochemical aspects of the controlled ring-opening polymerization of chiral cyclic esters. *Macromolecular Symposia* **1998,** *128* (1), 39-51.

61. Wu, B.; Lenz, R. W., Stereoregular Polymerization of [R,S]-3-Butyrolactone Catalyzed by Alumoxane−Monomer Adducts. *Macromolecules* **1998,** *31* (11), 3473-3477.

62. Terrier, M.; Brule, E.; Vitorino, M. J.; Ajellal, N.; Robert, C.; Gauvin, R. M.; Thomas, C. M., Supported Neodymium Catalysts for Isoprene and rac-β-Butyrolactone Polymerization: Modulation of Reactivity by Controlled Grafting. *Macromol. Rapid Commun.* **2011,** *32* (2), 215-219.

63. Vagin, S.; Winnacker, M.; Kronast, A.; Altenbuchner, P. T.; Deglmann, P.; Sinkel, C.;

Loos, R.; Rieger, B., New Insights into the Ring-Opening Polymerization of β-Butyrolactone Catalyzed by Chromium(III) Salphen Complexes. *ChemCatChem* **2015,** *7* (23), 3963-3971.

64. Zhuo, Z.; Zhang, C.; Luo, Y.; Wang, Y.; Yao, Y.; Yuan, D.; Cui, D., Stereo-selectivity switchable ROP of rac-β-butyrolactone initiated by salan-ligated rare-earth metal amide complexes: the key role of the substituents on ligand frameworks. *Chemical Communications* **2018,** *54* (85), 11998-12001.

65. Tani, H.; Yamashita, S.; Teranishi, K., Stereospecific Polymerization of β-Methyl-β-propiolactone1. *Polymer Journal* **1972,** *3* (3), 417-418.

66. donTang, X.; Chen, E. Y. X., Chemical synthesis of perfectly isotactic and high melting bacterial poly(3-hydroxybutyrate) from bio-sourced racemic cyclic diolide. *Nat. Commun.* **2018,** *9* (1), 1-11.

67. Tang, X.; Westlie, A.; Caporaso, L.; Cavallo, L.; Falivene, L.; Chen, E. Y.-X., Biodegradable Polyhydroxyalkanoates by Stereoselective Copolymerization of Racemic Diolides: Stereocontrol Mechanism and Polyolefin-Like Properties. *Angewandte Chemie n/a* (n/a).

68. Dyer, H. E.; Huijser, S.; Susperregui, N.; Bonnet, F.; Schwarz, A. D.; Duchateau, R.; Maron, L.; Mountford, P., Ring-Opening Polymerization of rac-Lactide by Bis(phenolate)amine-Supported Samarium Borohydride Complexes: An Experimental and DFT Study. *Organometallics* **2010,** *29* (16), 3602-3621.

69. Deng, L.-Q.; Zhou, Y.-X.; Tao, X.; Wang, Y.-L.; Hu, Q.-S.; Jin, P.; Shen, Y.-Z., Synthesis and structure of amine-bridged bis(phenolate) lanthanide complexes and their application in the polymerization of ε-caprolactone. *Journal of Organometallic Chemistry* **2014,** *749*, 356-

363.

70. Zhu, J.-B.; Chen, E. Y.-X., Catalyst-Sidearm-Induced Stereoselectivity Switching in Polymerization of a Racemic Lactone for Stereocomplexed Crystalline Polymer with a Circular Life Cycle. *Angewandte Chemie International Edition* **2019,** *58* (4), 1178-1182.

71. Walsh, P. J.; Lurain, A. E.; Balsells, J., Use of Achiral and Meso Ligands To Convey Asymmetry in Enantioselective Catalysis. *Chemical Reviews* **2003,** *103* (8), 3297-3344.

72. Hong, L.; Sun, W.; Yang, D.; Li, G.; Wang, R., Additive Effects on Asymmetric Catalysis. *Chemical Reviews* **2016,** *116* (6), 4006-4123.

73. Lu, L.; Zou, S.; Fang, B., The Critical Impacts of Ligands on Heterogeneous Nanocatalysis: A Review. *ACS Catalysis* **2021**, 6020-6058.

74. Aoshima, S.; Higashimura, T., Living cationic polymerization of vinyl monomers by organoaluminum halides. 3. Living polymerization of isobutyl vinyl ether by ethyldichloroaluminum in the presence of ester additives. *Macromolecules* **1989,** *22* (3), 1009-1013.

75. Slugovc, C.; Demel, S.; Stelzer, F., Ring opening metathesis polymerisation in donor solvents. *Chemical Communications* **2002,** (21), 2572-2573.

76. Baskaran, D., Strategic developments in living anionic polymerization of alkyl (meth)acrylates. *Progress in Polymer Science* **2003,** *28* (4), 521-581.

77. Pintauer, T.; Matyjaszewski, K., Structural aspects of copper catalyzed atom transfer radical polymerization. *Coordination Chemistry Reviews* **2005,** *249* (11), 1155-1184.

78. Tang, W.; Kwak, Y.; Braunecker, W.; Tsarevsky, N. V.; Coote, M. L.; Matyjaszewski, K., Understanding Atom Transfer Radical Polymerization: Effect of Ligand and Initiator

Structures on the Equilibrium Constants. *Journal of the American Chemical Society* **2008,** *130* (32), 10702-10713.

79. Karasawa, Y.; Kimura, M.; Kanazawa, A.; Kanaoka, S.; Aoshima, S., New initiating systems for cationic polymerization of plant-derived monomers: GaCl3/alkylbenzene-induced controlled cationic polymerization of β-pinene. *Polymer Journal* **2015,** *47* (2), 152-157.

80. Dau, H.; Keyes, A.; Basbug Alhan, H. E.; Ordonez, E.; Tsogtgerel, E.; Gies, A. P.; Auyeung, E.; Zhou, Z.; Maity, A.; Das, A.; Powers, D. C.; Beezer, D. B.; Harth, E., Dual Polymerization Pathway for Polyolefin-Polar Block Copolymer Synthesis via MILRad: Mechanism and Scope. *Journal of the American Chemical Society* **2020,** *142* (51), 21469-21483.

81. Jones, G. R.; Basbug Alhan, H. E.; Karas, L. J.; Wu, J. I.; Harth, E., Switching the Reactivity of Palladium Diimines with "Ancillary" Ligand to Select between Olefin Polymerization, Branching Regulation, or Olefin Isomerization. *Angewandte Chemie International Edition* **2021,** *60* (3), 1635-1640.

82. Hong, M.; Chen, J.; Chen, E. Y. X., Polymerization of Polar Monomers Mediated by Main-Group Lewis Acid–Base Pairs. *Chemical Reviews* **2018,** *118* (20), 10551-10616.

83. McGraw, M. L.; Chen, E. Y. X., Lewis Pair Polymerization: Perspective on a Ten-Year Journey. *Macromolecules* **2020,** *53* (15), 6102-6122.

84. dos Santos Vieira, I.; Herres-Pawlis, S., Lactide Polymerisation with Complexes of Neutral N-Donors – New Strategies for Robust Catalysts. *European Journal of Inorganic Chemistry* **2012,** *2012* (5), 765-774.

Chapter 2: OPPh₃ Assisted Rare-earth Catalyst of Iso-selective Ring-Opening Polymerization of *rac-β*-BBL

Abstract

Isoenriched poly-3-hydroxybutyrate (P3HB) is a biodegradable material with properties similar to isotactic polypropylene, yet efficient routes to this material are lacking after 50+ years of extensive efforts in catalyst design. In this contribution, a novel lanthanum aminobisphenolate catalyst (**1-La**) can access isoenriched P3HB through the stereospecific ring-opening polymerization (ROP) of *rac*-β-butyrolactone (*rac*-BBL). Replacing the tethered donor group of a privileged supporting ligand with a non-coordinating benzyl substituent generates a catalyst whose reactivity and selectivity can be tuned with inexpensive achiral neutral donor ligands (e.g. phosphine oxides, OPR₃). The **1-La**/OPR₃ (R = *n*-octyl, Ph) systems display high activity and are the most isoselective homogeneous catalysts for the ROP of *rac*-BBL to date (0 °C: P_m = 0.80, TOF ~190 h⁻¹). Combine d reactivity and spectroscopic studies provide insight into the active catalyst structure and ROP mechanism. Both **1-La(TPPO)₂** and a structurally related catalyst with a tethered donor group (**2-Y**) operate under chain-end stereocontrol; however, **2-RE** favors formation of P3HB with opposite tacticity (syndioenriched) and its ROP activity and selectivity are totally unaffected by added neutral donor ligands. Our studies uncover new roles for neutral donor ligands in stereospecific ROP, including supression of chain-scission events, and point to new opportunities for catalyst design.

2.1. Introduction

Since Carpentier's tetradentate tripodal amino-bisphenolate rare-earth catalyst is so effective and isoselective in ROP of BBL,[1-3] We were curious about the role and effect of the tethered donors in those catalysts and, consequently, how the reactivity would change if the tethered donor was removed from structure. However, the later question had not been well answered yet in previous works, except some comparison done by Mountford and coworkers in 2010. They compared Sm^{III} borohydrides supported by amino-bisphenolate with different tethered donors and non-coordinating propyl in ROPs of ε-caprolactone and lactide, which are more prone to polymerize, and found the one with propyl was less active than those with tethered donors (Scheme 2.1.)[4].
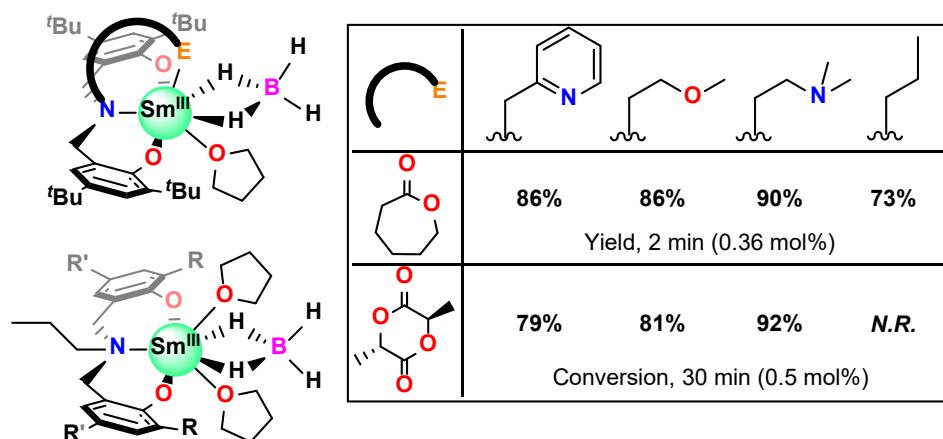
Scheme 2.1. ROP reactivities of Sm^{III} amino-bisphenolates with coordinating and non-coordinating arms.

According to Mountford's results, when the tethered donor is replaced by a less coordinating solvent molecule (tetrahydrofuran, THF), the activity drops. It can be accounted to that the lack of the chelate feature reduce the affinity of the dative group, which seems crucial to the reactivity. We then asked if it was a stronger monodentate ligand that filled the space left by the absence of the tethered donor rather than a THF, would the reactivity be affected.

Driven by this question, we report the synthesis, characterization, and catalytic activity of RE^{III} benzyl-substituted amino-bisphenolate complexes for the isoselective ROP of *rac*-BBL. Replacing the tethered donor fragment of a tetradentate aminobisphenolate ligand with a non-coordinating benzyl substituent leads to a La catalyst whose reactivity and selectivity are amplified by the addition of inexpensive neutral achiral donor ligands (e.g. phosphine oxides, OPR$_3$). The La^{III}/OPR$_3$/^{i}PrOH (R: Ph, *n*-octyl) species display high activity and are the most isoselective homogeneous catalysts for the ROP of *rac*-BBL to date (P_m = 0.8 at 0 °C, TOF = ~190 h^{-1}). Despite the prevalence of such ligands in the coordination chemistry of RE's[5] and other metal-ions,[6] this is the first report of added phosphine oxides enhancing catalyst reactivity or selectivity in ROP. Evidence that strong neutral donors can suppress unwanted side-reactions such as chain-scission through base-promoted elimination are also presented for the first time. Statistical analysis of P3HB microstructure confirms that **1-La(TPPO)$_2$** is the first catalyst to access isoenriched P3HB through chain-end stereocontrol. While a structurally related catalyst with a tethered donor (**2-Y**) also operates under chain-end stereocontrol, **2-RE** favor the *opposite* polymer tacticity (syndioenriched P3HB) and their performance in ROP are unaffected by added neutral donor ligands. Our studies uncover the effects of neutral donors on catalyst structure and function, and provide new opportunities for the design of catalysts for stereospecific ROP.

2.2. Results and Discussion

2.2.1. Synthesis and Structures of Catalysts

The white crystalline benzyl-amino-bisphenol ligand was synthesized in one step by a Mannich condensation of benzyl amine, 2,4-ditertbutylphenol and paraformaldehyde in 47% yield (Scheme 2.2.). $H_2{}^1L$ was then treated with one equivalent of RE^{III} amide (RE^{III}: La, Y), $RE^{III}[N(SiHMe_2)_2]_3(THF)_2$, to afford the corresponding RE^{III} complexes, $La^{III}({}^1L)[N(SiHMe_2)_2](THF)_2$ (**1-La**) and $\{Y^{III}({}^1L)[N(SiHMe_2)_2]\}_2$ (**1-Y₂**), in nearly quantitative yields (Scheme 2.2.).
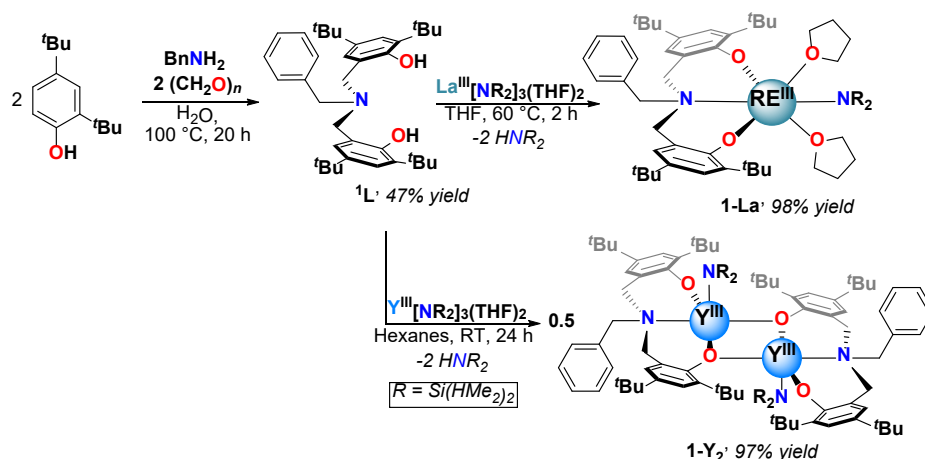
Scheme 2.2. Synthesis of ${}^1L$ and RE^{III} complexes (**1-La** and **1-Y₂**).

1-La is a monomer in both the solid- and solution-state as determined by single-crystal X-ray diffraction (Figure 2.1.) and Diffusion Ordered NMR Spectroscopy (DOSY, Table 2.1.). While X-ray quality crystals could not be grown of the THF adduct, slow evaporation of Et_2O solutions enabled the structural determination of the mixed THF/Et_2O adduct (Figure 2.1.). The geometry of the six-coordinate La^{III} center in the solid-state is best described as a distorted trigonal prism comprised of tridentate ${}^1L$, $-N(SiHMe_2)_2$, and two coordinated solvent molecules (THF and Et_2O). ${}^1L$ adopts a propeller-like conformation at nitrogen and enforces

fac-coordination. Agostic β-H–Si interactions (La⤙H–Si) were observed in the solid-state as supported by the smaller angle ∠La(1)–N(2)–Si(1) compared to ∠La(1)–N(2)–Si(2) (~15°), close La(1)–Si(1)–H contact (3.3497(13) Å), and lower energy Si-H stretch in the IR spectrum (non-agostic: 2075 cm^{-1}, agostic: 2011 cm^{-1}).[7-11] Unlike **1-La**, the yttrium derivative (**1-Y$_2$**) exists as a dimer in solution as determined by ^{1}H-DOSY NMR (Table 2.1.).
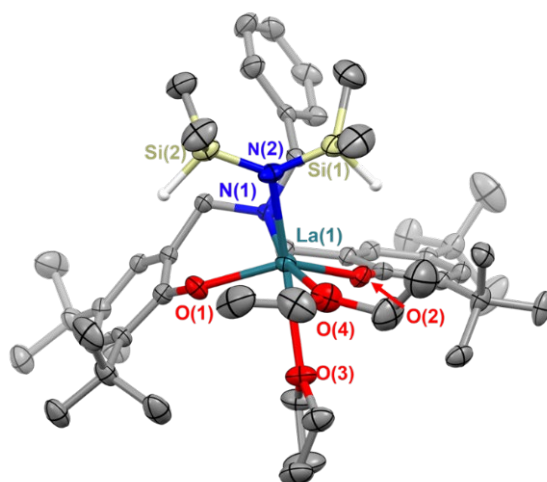
Figure 2.1. Thermal ellipsoid plot of **1-La** (THF, Et$_2$O adduct) displayed at 50% probability. Crystallographic data are available on Cambridge Crystallographic Data Centre. CCDC ID: LUSFUD.

Table 2.1. Diffusion coefficients, *D*, and estimated hydrodynamic radii, r$_H$, measured by ^{1}H DOSY NMR of **1-La** and **1-Y$_2$**

Species	D_{Fc} (10^{-10} m^2/s)^a	D (10^{-10} m^2/s)	D_{Fc}/D	r$_H$(DOSY)^b (Å)	r$_H$(theo.)^c (Å)
Fc^d	-	-	-	-	2.166
1-La	13.2	5.10	2.59	5.61	6.011
1-Y$_2$	11.8	3.56	3.31	7.18	7.361^e

a – DOSY measured diffusion coefficient of ferrocene (Fc) in the experiment of the corresponding complex. DOSY measured diffusion coefficient of the sample *b* – r$_H$ = D_{Fc}/D_{sample}·r$_H$(Fc, theo.). *c* – r$_H$(theo.) is the average of half lengths of the principal axes of the homogeneous ellipsoid with the same densities and principal moments of inertia of the molecule, which are determined from the crystal structure. *d* – Fc was added to each sample as an internal standard to cancel the fluctuation of temperature and viscosity, of which the diffusion coefficient varies. *e* – Estimated according to structure of **3-Y$_2$**,[12] due to the lack of X-ray structure of **1-Y$_2$**.
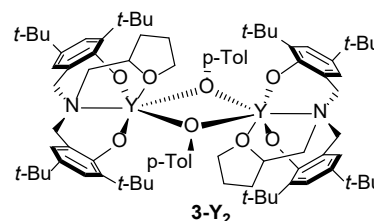
2.2.2. Reaction Optimization and Neutral Donor Ligand Effects.

1-La and **1-Y₂** were evaluated as catalysts for the ROP of *rac*-BBL (Table 2.2). Amide initiators

displayed low efficiency for the ROP of *rac*-BBL, where **1-Y₂** was completely inactive and **1-**

La formed 35% P3HB in 48 h at RT (Table 2.2, entries 1 and 3). While **1-La** was sluggish

compared to Carpentier's **2-Y**,[3, 13] formation of P3HB was encouraging as the related Sm[III]

borohydride complex supported by the propyl-amino-bisphenolate ligand reported by

Mountford and coworkers was inactive for ROP of an arguably easier substrate, *rac*-lactide.[4]

Table 2.2. ROP of *rac*-BBL catalyzed by **1-La** and **1-Y₂**.
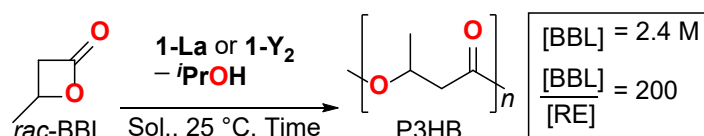
Entry	Cat.	[BBL]/[RE]//[^{i}PrOH]	Solvent	Time (h)^a	Conv. (%)^b	$M_{n, calc}{}^c$ (kg/mol)	$M_{n, exp}{}^d$ (kg/mol)	$Đ^{d,e}$	$P_m{}^f$
1	**1-Y₂**	200/1/0	Tol	1	0	--	n.d.	n.d.	n.d.
2	**1-Y₂**	200/1/1	Tol	1	5	0.9	n.d.	n.d.	n.d.
3	**1-La**	200/1/0	Tol	48	35	5.9	2.1	1.46	0.54
4	**1-La**	200/1/1	Tol	1	21	3.6	2.9	1.04	0.57

a – Reaction times not optimized. *b* – Determined by ^{1}H-NMR integration of BBL and PHB methine resonances in the crude reaction mixture. *c* – [BBL]/[RE]/[^{i}PrOH] × Conv. × 0.08609 kg•mol^{-1}. When [^{i}PrOH] = 0, [BBL]/[La] × Conv. × 0.08609 kg•mol^{-1}. *d* – Determined by gel permeation chromatography (GPC) at 30 °C in THF using polystyrene standards and corrected by Mark-Houwink factor of 0.54.[18] *e* – M_w/M_n. *f* – Probability of *meso*-linkages between repeat units. Determined by integration of P3HB <u>C</u>=O resonances using inverse gated (IG) ^{13}C-NMR.

Similar to other RE[III] catalysts,[3, 13-14] in situ generation of alkoxide initiators by adding one

equiv ^{i}PrOH with respect to RE[III] (Table 2.2, entries 1 and 3 *vs* entries 2 and 4) increased

reactivity and furnished polymers with narrow M_w/M_n (*Đ*). Microstructural analysis of P3HB

determined by integration of polymer C=O resonances by inverse-gated ^{13}C-NMR revealed a

slight isotactic preference (P_m = 0.57) using **1-La**. While modest, the polymer tacticity was

opposite that generated by **2-Y** and other amino-bisphenolate catalysts with tethered donors.[1, 3, 15] Given the increased degree of coordinative unsaturation of **1-RE** compared to **2-RE** and the attributed importance of steric congestion to selectivity for other stereospecific ROP,[13, 16-17] we posited that added neutral donor ligands could improve catalyst reactivity and selectivity through enhanced steric pressure.

Table 2.3. Influence of neutral donor ligand in the ROP of (*rac*)-BBL catalyzed by **1-RE**
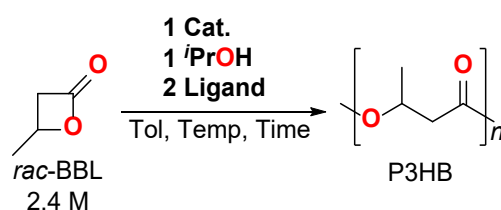
Entry	Cat.	[BBL]/[RE]	Ligand	Temp (°C)	Time (h)[a]	Conv. (%)[b]	$M_{n, calc}$[c] (kg/mol)	$M_{n, exp}$[d] (kg/mol)	$Đ$[d, e]	P_m[f]
1	**1-Y₂**	200	-	25	1	5	0.9	n.d.	n.d.	n.d.
2	**1-La**	200	-	25	1	21	3.6	2.9	1.04	0.57
3	**1-La**	200	DMAP	25	1	22	3.8	3.6	1.07	0.59
4	**1-La**	200	DABCO	25	1	7	1.2	n.d.	n.d.	n.d.
5	**1-La**	200	PPh₃	25	1	25	4.3	1.7	1.38	n.d.[g]
6	**1-La**	200	TPPO	25	1	97	16.7	9.6	1.18	0.71
7	**1-La**	200	HMPA	25	1	99	17.0	9.4	1.29	0.73
8	**1-La**	200	TOPO	25	1	99	17.0	9.5	1.23	0.75
9	**1-La**	200	OP(OPh)₃	25	1	25	4.3	1.6	1.35	0.63

a – Reaction times not optimized. *b* – Determined by ^{1}H-NMR integration of BBL and PHB methine resonances in the crude reaction mixture. *c* – [BBL]/[RE]/[^{i}PrOH] × Conv. × 0.08609 + 0.0601 kg·mol^{-1}. *d* – Determined by gel permeation chromatography (GPC) at 30 °C in THF using polystyrene standards and corrected by Mark-Houwink factor of 0.54.[18] *e* – M_w/M_n. *f* – Probability of *meso*-linkages between repeat units. Determined by integration of P3HB $\underline{C}$=O resonances using inverse gated (IG) ^{13}C-NMR. *g* – 0.52 at 6 h (36% conversion).

We initially tested this hypothesis by screening **1-La** with two equiv of neutral monodentate ligands. Representative classes included ethers (THF), tertiary amines (1,4-diazabicyclo-[2.2.2]octane, DABCO), pyridines (4-dimethylaminopyridine, DMAP), phosphines, (PPh₃), and phosphine oxides (OPPh₃, TPPO). Unlike some literature reports for group 13, 14, and RE^{III}-based systems,[19-28] weaker neutral ligands had a minor impact on ROP reactivity and

stereoselectivity (Table 2.3, entries 2–5). In contrast, the harder phosphine oxide ligand, TPPO (entry 6), led to nearly quantitative conversion in 1 h (97%) and improved isoselectivity (P_m = 0.71). Notably, [**1-La**]:[TPPO] ratios of at least 1:2 were needed to achieve maximum reactivity and selectivity, where a 1:1 ratio only led to 71% conversion and a P_m of 0.67 after 6 h (Table 2.4). While simple monodentate phosphine oxides have been reported as additives in asymmetric catalysis with hard metal-ions,[29-33] this is the first time they have been used to enhance reactivity and/or selectivity in ROP.

Given the unprecedented and dramatic enhancement in catalyst performance, we evaluated representative classes of phosphine oxides (aromatic, aliphatic, phosphoramide, and phosphate; Table 2.3, entries 6–9). Electron-rich donors, such as hexamethylphosphoramide (HMPA, entry 7) and trioctylphosphine oxide (TOPO, entry 8) increased reactivity and isoselectivity (P_m = 0.73 and 0.75 respectively). In contrast, triphenylphosphate ($OP(OPh)_3$, entry 9), a weaker donor, didn't increase reactivity and showed small improvements in selectivity (P_m = 0.63). Our results suggest both electronic and steric contributions to catalyst reactivity and selectivity, and a more comprehensive evaluation is warranted in future studies. This is affirmed by reports of stereospecific ROP of (*rac*)-Lactide by RE^{III} and group 13 complexes supported by chelating alkoxides,[34-36] amides,[37-38] and pyrazolyl scorpionates[39-40] with *tethered* phosphine-oxides, which display varied catalyst response depending on ligand substituents. Given the diverse array of phosphine oxides that can be derived from commercially available phosphines, this represents an exciting untapped opportunity to optimize catalyst performance in stereoselective ROP.

Table 2.4. Impact of TPPO equivalents on the ROP of *rac*-BBL catalyzed by **1-La**.
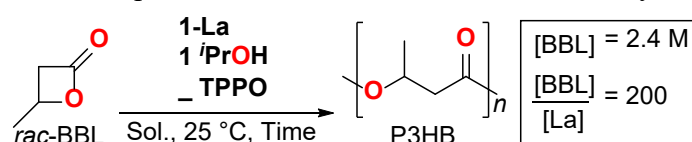
Entry	[TPPO]/[RE]	Time (h)[a]	Conv. (%)[b]	$M_{n, calc}$[c] (kg/mol)	$M_{n, exp}$[d] (kg/mol)	$Đ$[d,e]	P_m[f]
1	0	1	21	3.6	2.9	1.04	0.57
2	1	6	71	12.2	4.7	1.04	0.67
3	2	1	97	16.7	9.6	1.18	0.71
4	3	1	97	16.7	9.1	1.27	0.71

a – Reaction times not optimized. *b* – Determined by ^{1}H-NMR integration of BBL and PHB methine resonances in the crude reaction mixture. *c* – [BBL]/[RE]/[^{i}PrOH] × Conv. × 0.08609 kg•mol^{-1}. When [^{i}PrOH] = 0, [BBL]/[La] × Conv. × 0.08609 kg•mol^{-1}. *d* – Determined by gel permeation chromatography (GPC) at 30 °C in THF using polystyrene standards and corrected by Mark-Houwink factor of 0.54.[18] *e* – M_w/M_n. *f* – Probability of *meso*-linkages between repeat units. Determined by integration of P3HB $\underline{C}$=O resonances using inverse gated (IG) ^{13}C-NMR.

Table 2.5. Further optimization of the ROP of (*rac*)-BBL catalyzed by **1-RE** in the presence of TPPO or TOPO
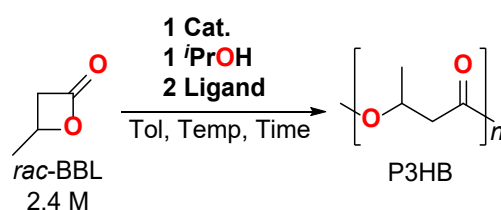
Entry	[BBL]/[RE]	Ligand	Temp (°C)	Time (h)[a]	Conv. (%)[b]	$M_{n, calc}$[c] (kg/mol)	$M_{n, exp}$[d] (kg/mol)	$Đ$[d,e]	P_m[f]
1	200	TPPO	25	1	97	16.7	9.6	1.18	0.71
2	200	TPPO	0	1	96	16.5	11.2	1.15	0.76
3	400	TPPO	0	4	77	26.5	15.3	1.20	0.75
4	200	TPPO	–30	24	99	17.0	11.5	1.12	0.80
5	200	TOPO	25	1	99	17.0	9.5	1.23	0.75
6	200	TOPO	0	1	99	17.0	12.9	1.20	0.80
7	400	TOPO	0	4	96	33.1	19.2	1.09	0.80
8	200	TOPO	–30	6	99	17.0	13.0	1.09	0.80

a – Reaction times not optimized. *b* – Determined by ^{1}H-NMR integration of BBL and PHB methine resonances in the crude reaction mixture. *c* – [BBL]/[RE]/[^{i}PrOH] × Conv. × 0.08609 + 0.0601 kg•mol^{-1}. *d* – Determined by gel permeation chromatography (GPC) at 30 °C in THF using polystyrene standards and corrected by Mark-Houwink factor of 0.54.[18] *e* – M_w/M_n. *f* – Probability of *meso*-linkages between repeat units. Determined by integration of P3HB $\underline{C}$=O resonances using inverse gated (IG) ^{13}C-NMR.

Key polymer attributes could be tuned by adjusting reaction temperature, catalyst loading, and chain-transfer agent. Lowering the reaction temperature from RT to 0 and –30 °C with TPPO and TOPO (Table 2.5) increased catalyst isoselectivity to a maximum (P_m = 0.80). This represents the highest values achieved for the ROP of *rac*-BBL by a homogeneous catalyst to date.[17] Furthermore, increased [*rac*-BBL]/[RE] ratios (400) lead to higher molecular weight P3HB with reasonable rates, identical selectivities, and narrow Đ (entries 3 and 7). Overall, **1-La**/OPR$_3$/^{i}PrOH systems display excellent reactivity (TOF up to 200 h^{-1}) and selectivity (P_m up to 0.80) with respect to the state-of-the-art for isoselective ROP of *rac*-BBL (P_m up to 0.77[17] and 0.85,[41] TOF ~5-6 h^{-1}).

Table 2.6. Impact of alcohol equivalents on the ROP of *rac*-BBL catalyzed by **1-La(TPPO)₂**.
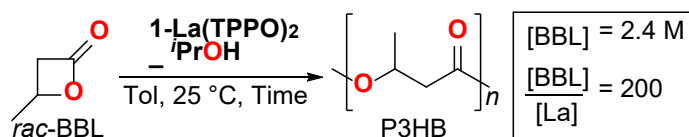
Entry	[^{i}PrOH]/[RE]	Time (h)^a	Conv. (%)^b	$M_{n, calc}{}^c$(kg/mol)	$M_{n, exp}{}^d$(kg/mol)	Đ^{d,e}	$P_m{}^f$
1	0	5	87	15.0	13.5	1.45	0.71
2	1	1	93	16.0	9.4	1.16	0.71
3	2	1	95	8.2	6.6	1.14	n.d.
4	4	1	93	4.0	3.3	1.07	0.70

a – Reaction times not optimized. *b* – Determined by ^{1}H-NMR integration of BBL and PHB methine resonances in the crude reaction mixture. *c* – [BBL]/[La]/[^{i}PrOH] × Conv. × 0.08609 kg•mol^{-1}. When [^{i}PrOH] = 0, [BBL]/[La] × Conv. × 0.08609 kg•mol^{-1}. *d* – Determined by gel permeation chromatography (GPC) at 30 °C in THF using polystyrene standards and corrected by Mark-Houwink factor of 0.54.[18] *e* – M_w/M_n. *f* – Probability of *meso*-linkages between repeat units. Determined by integration of P3HB C=O resonances using inverse gated (IG) ^{13}C-NMR.

Alcohols can serve as chain-transfer agents in living polymerizations to access "immortal" polymerization conditions,[42] offering further opportunities to control polymer molecular weight.[14, 43-44] A La catalyst was isolated from a toluene solution of **1-La** and TPPO in a 1:2 molar ratio (vide infra), which displays similar reactivity in the ROP of *rac*-BBL as the in situ

generated catalyst from adding 2 equivalents of TPPO to **1-La** (Table 2.6, entry 2 and Table 2.3, entry 6). Adding ^{i}PrOH (0–4 equiv) to **1-La(TPPO)$_2$** maintained high catalyst activity and P_m, while producing P3HB with the expected changes in molecular weight (Table 2.6).
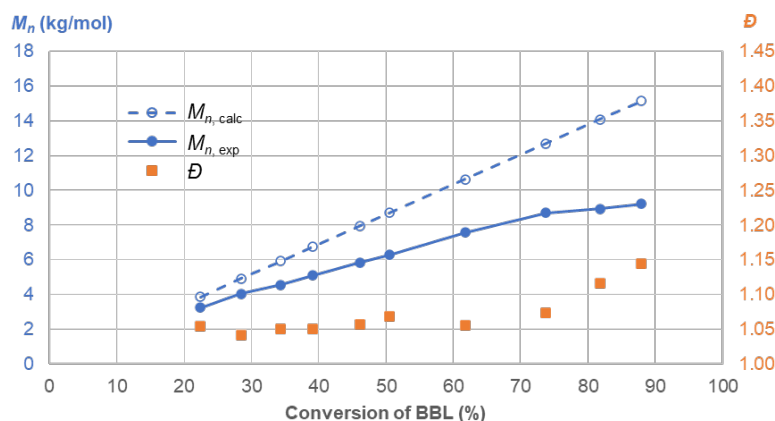
Figure 2.2. Calculated M_n (blue circle), Experimental M_n (blue dot) and Đ (orange squares) as functions of conversion of BBL. Reaction was performed in toluene at ambient temperature with [BBL]/[**1-La(TPPO)$_2$**]/[^{i}PrOH] = 200/1/1 and [BBL] = 2.4 M.

Table 2.7. ROP of *rac*-BBL with **1-La(TPPO)$_2$** + ^{i}PrOH quenched at different time points.
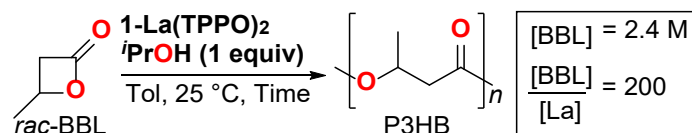
Entry	Time (min)	Conv. (%)[a]	$M_{n, calc}$[c](kg/mol)	$M_{n, exp}$[c](kg/mol)	Đ[c,d]
1	0.25	22	3.9	3.2	1.054
2	0.50	28	4.9	4.0	1.042
3	0.75	34	5.9	4.6	1.050
4	1.0	39	6.7	5.1	1.050
5	1.5	46	7.9	5.8	1.056
6	2.0	50	8.7	6.3	1.069
7	5.0	62	10.6	7.6	1.056
8	15	74	12.7	8.7	1.074
9	30	82	14.1	8.9	1.116
10	60	88	15.1	9.2	1.145

a – Determined by ^{1}H-NMR integration of BBL and PHB methine resonances in the crude reaction mixture. *b* – [BBL]/[La]/[^{i}PrOH] × Conv. × 0.08609 kg•mol^{-1}. *c* – Determined by gel permeation chromatography (GPC) at 30 °C in THF using polystyrene standards and corrected by Mark-Houwink factor of 0.54.[18] d – M_w/M_n.

The ROP of *rac*-BBL (200 equiv) catalyzed by **1-La(TPPO)$_2$** (1 equiv) with ^{i}PrOH (1 equiv)

displayed characteristics of a living polymerization, such as narrow Đ throughout the reaction

and reasonable agreement between experimental and calculated M_n (Table 2.7 and Figure 2.2a).

2.2.3. Binding and Characterization of RE-TPPO Species
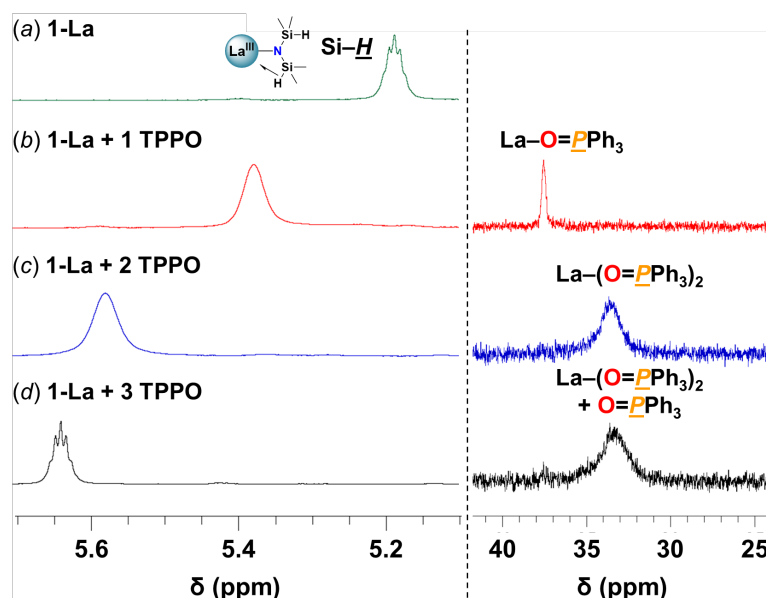
Figure 2.3. Selected spectral regions of (*Left*) ^{1}H- and (*Right*) ^{31}P{^{1}H}-NMR studies in C$_6$D$_6$ at RT of: (*a*) **1-La(TPPO)$_2$** (27 mM) (*b*) + 1 TPPO (*c*) + 2 TPPO (*d*) + 3 TPPO.

We set out to isolate discrete RE^{III}–TPPO species to better understand the isoselectivity for **1-La**/OPR$_3$. Adding one and two equiv. of TPPO to **1-La** led to distinct mono- and bis-TPPO

adducts (Figure 2.3; ^{31}P-NMR: mono: 37.5 ppm, bis: 33.3 ppm). Addition of TPPO also

resulted in a downfield shift of the Si–*H* resonances, consistent with weakening and

displacement of the β-H–Si interactions (La⁀H–Si) and TPPO coordination (Figure 2.3, *left*).[10]

The bis-TPPO adduct displays a single significantly broadened ^{31}P signal, indicative of

exchange on the NMR timescale. Isolation of crystalline bis-TPPO adducts,

RE^{III}(^{1}L)(N(SiHMe$_2$)$_2$)(TPPO)$_2$ (**1-RE(TPPO)$_2$**; RE^{III}: Y, La), was accomplished in high yields

by adding two equiv. TPPO per RE^{III} (**1-La** or **1-Y$_2$**) in toluene followed by layering with

hexanes (Scheme 2.3). Although under active investigation, attempts to crystallize the mono-TPPO adduct, **1-La(TPPO)**, have only led to isolation of crystalline **1-La(TPPO)$_2$**.
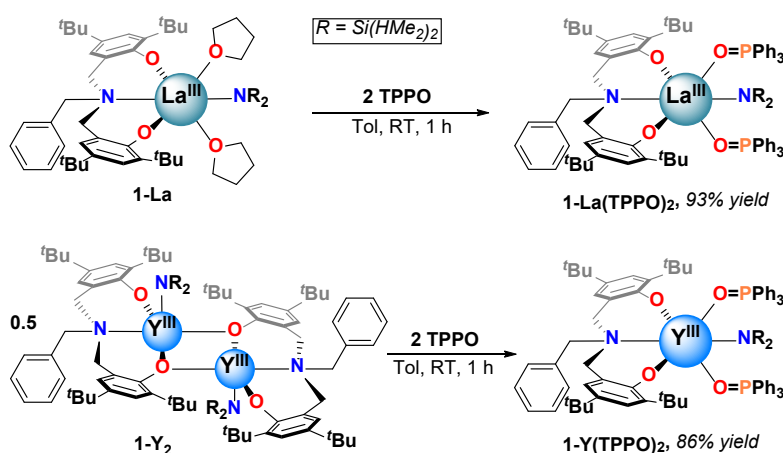
Scheme 2.3. Synthesis of **1-RE(TPPO)$_2$**

The solid-state structures of **1-RE(TPPO)$_2$** were determined unambiguously by single crystal X-ray diffraction experiments (Figures 2.4). In the solid-state, **^{1}L** coordinates in a *mer*-arrangement for **1-RE(TPPO)$_2$** rather than the *fac*-arrangement for **1-La**. The isostructural compounds contain six-coordinate RE^{III} centers in a distorted octahedron with equatorial sites occupied by **^{1}L** and -N(SiHMe$_2$)$_2$ and axial sites occupied by TPPO. Comparison of **1-RE(TPPO)$_2$** and tethered donor system, **2-Y**,[45] revealed largely conserved equatorial sites and significantly perturbed axial sites (Figure 2.4). In **2-Y**, the geometrically constrained tethered donor leads to a small N^2_L–Y–O$_{Me}$ angle (68°) and a large O$_{OMe}$–Y–O$_{THF}$ angle (203°) compared to **1-La(TPPO)$_2$** (Figure 2.4, ∠N^1_L–La–O$_{TPPO}$: 86°, ∠O$_{TPPO}$–La–O$_{TPPO}$: 169°). The differences in bond angles reflect increasing steric pressure from the axial donors, and suggest a plausible structural origin for the selectivity in **1-La**/OPR$_3$.
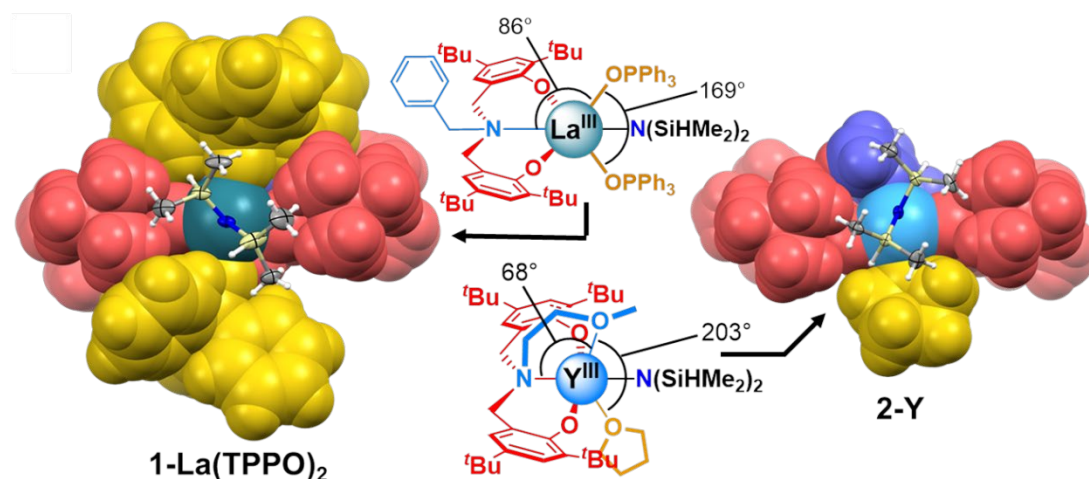
Figure 2.4. Partial space-filling diagrams comparing **1-La(TPPO)₂** and **2-Y**. Fragment color coding: phenolate (red), amine (blue), labile neutral donors (gold). N(SiHMe₂)₂ shown as ellipsoids (50% probability).

2.2.4. Insight into the Catalyst Resting State and Active Specie(s).

With **1-La(TPPO)₂** in hand, we pursued further spectroscopic studies to determine relevant catalyst speciation and resting states. Variable temperature NMR experiments performed in toluene-d_8 over the range of –30 to +30 °C allowed for an estimation of TPPO exchange at the two axial sites ($\Delta G^{\ddagger}$ ~58 kJ/mol; Figure 2.5),[46] which is consistent with other RE[III]–TPPO exchange processes reported in the literature.[47-48] At –30 °C, **1-La(TPPO)₂** displays two well-resolved ³¹P resonances indicating slow-exchange of the two-bound TPPO at this temperature (Figure 2.5). Adding one equiv ^{i}PrOH to **1-La(TPPO)₂** led to generation of HN(SiHMe₂)₂ and a La isopropoxide species as determined by ¹H-NMR (Figure 2.6). Bound TPPO exchanges much faster as evidenced by the nearly coalesced ³¹P resonances at –30 °C (Figure 2.7), while a small amount of free TPPO was generated alongside another minor species (tentatively assigned as a mono-phosphine oxide species, **1-La(TPPO)**).
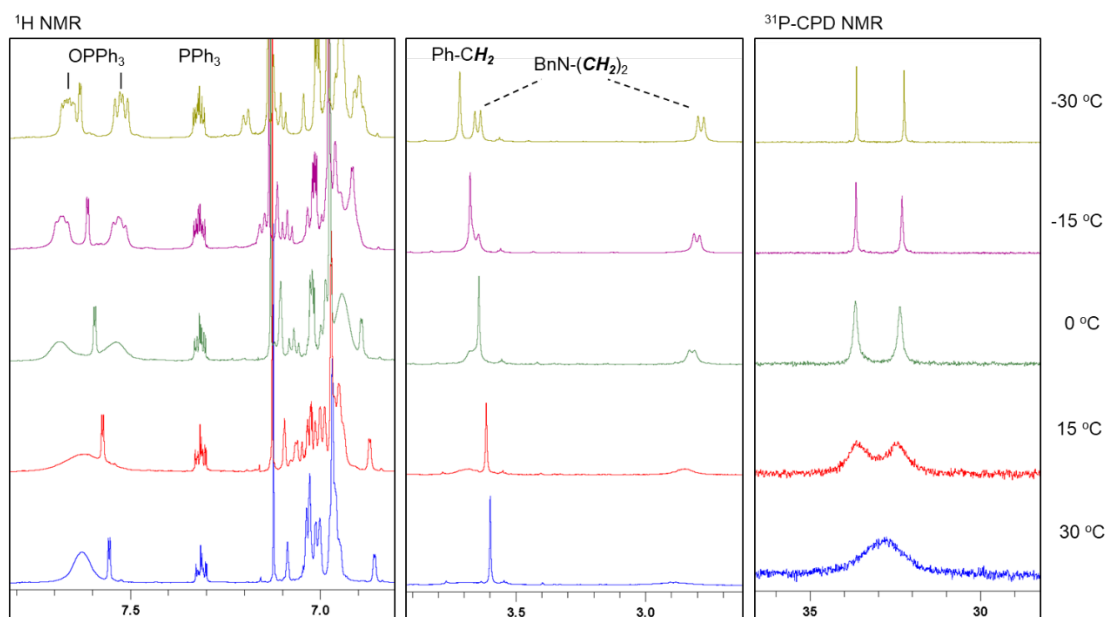
Figure 2.5. ^{1}H-NMR (600 MHz, toluene-d_8) and ^{31}P{^{1}H}-NMR (243 MHz, toluene-d_8) of **1-La(TPPO)$_2$** at –30, –15, 0, 15 and 30 °C.
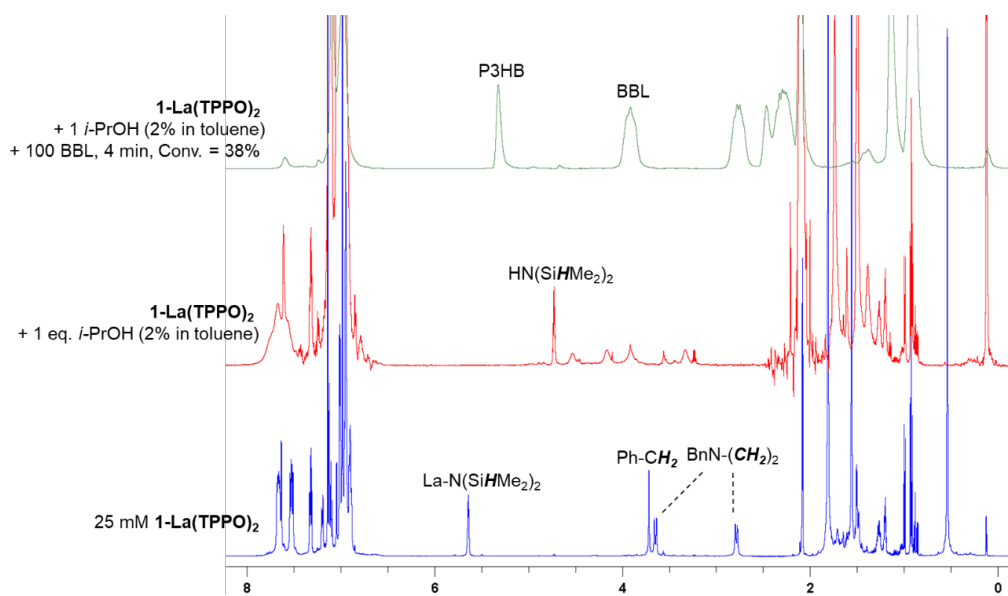
Figure 2.6. ^{1}H-NMR (600 MHz, toluene-d_8, –30 °C) of **1-La(TPPO)$_2$** (25 mM, blue, bottom), **1-La(TPPO)$_2$** + ^{i}PrOH (red, middle), and **1-La(TPPO)$_2$** + ^{i}PrOH + 100 BBL at 4 min (green, top).
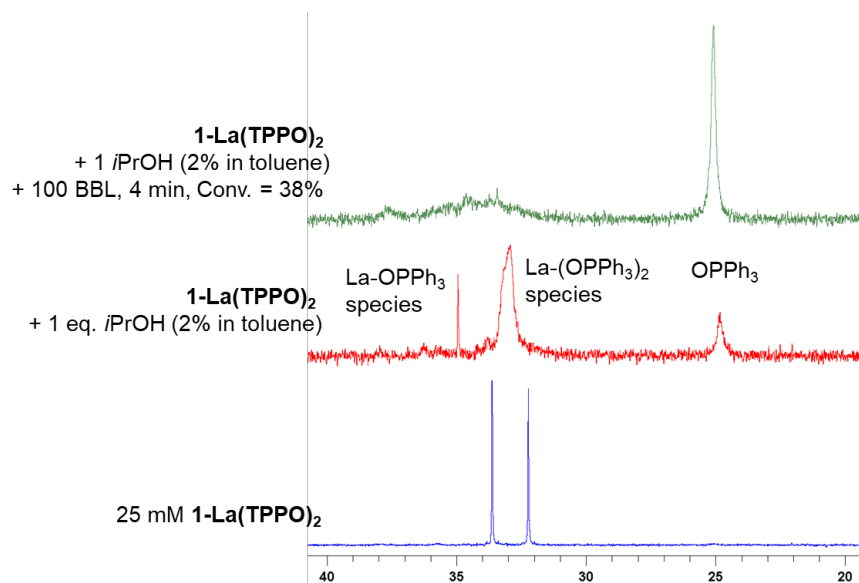
Figure 2.7. $^{31}P\{^1H\}$-NMR (600 MHz, toluene-d_8, –30 $^{\circ}$C) of **1-La(TPPO)₂** (25 mM, blue, bottom), **1-La(TPPO)₂** + ^{i}PrOH (red, middle), and **1-La(TPPO)₂** + ^{i}PrOH + 100 BBL at 4 min (green, top).
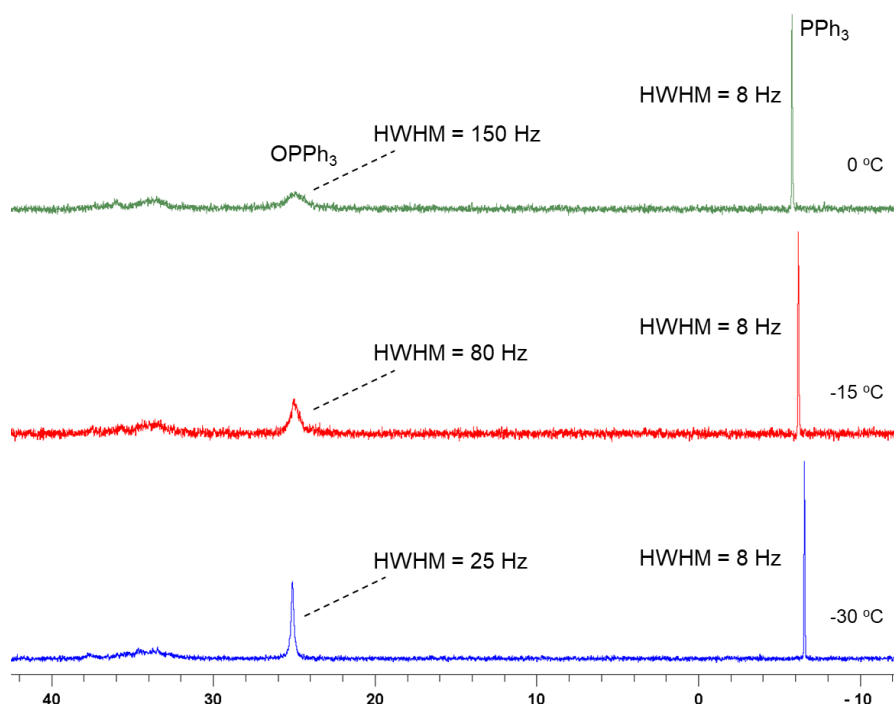
Figure 2.8. $^{31}P\{^1H\}$-NMR (600 MHz, toluene-d_8, –30 $^{\circ}$C – 0 $^{\circ}$C) of the ROP of BBL by **1-La(TPPO)₂** and ^{i}PrOH initially performed at –30 $^{\circ}$C (38% conversion), followed by warming to –15 $^{\circ}$C (55% conversion) and 0 $^{\circ}$C (67% conversion).

Addition of *rac*-BBL (100 equiv) increases the signal for free TPPO signficantly, while resonances associated with **La(TPPO)$_n$** (*n* = 1, 2) were dramatically broadened (Figure 2.7).

Warming the reaction mixture from –30 $^{\circ}$C to –15 $^{\circ}$C and 0 $^{\circ}$C (Figure 2.8) increased exchange

of free and bound TPPO as evidenced by the increasing line-width of free TPPO (half-width at half-maximum, HWHM; 25, 80, and 150 Hz respectively), and RT experiments produced similar species (Figure 2.9b). Reactions performed at RT with one equiv TPPO formed similar species without generation of free TPPO (Figure 2.9a); however, optimal catalyst reactivity and selectivity required at least two equiv of TPPO (Table 2.4). Taken together, our reaction optimization and in situ spectroscopic studies support dissociation of one equiv TPPO from the pre-catalyst, **1-La(TPPO)$_2$**, and dynamic phosphine oxide exchange during catalysis. While **La(TPPO)** was identified as a catalyst resting state, the observed TPPO-dependent reactivity and observed speciation implicates both **La(TPPO)$_n$** (n = 1, 2) as catalytically relevant species.
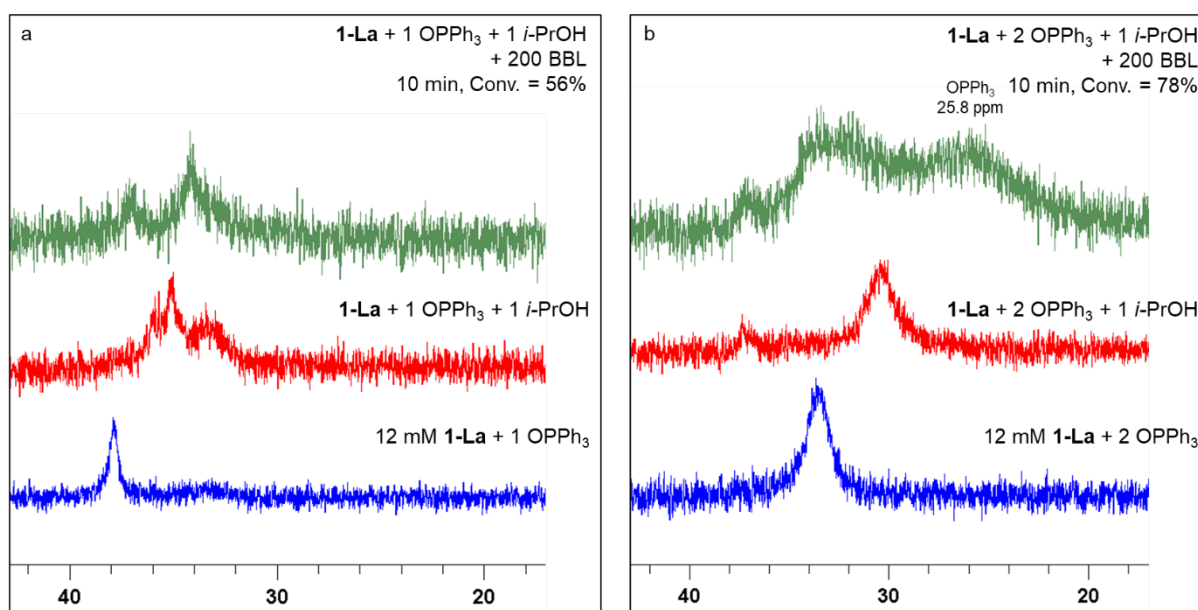
Figure 2.9. ^{31}P{^{1}H}-NMR (243 MHz, toluene, 298 K) of: **1-La** + n TPPO (bottom, blue), **1-La** + n TPPO + ^{i}PrOH (middle, red), and **1-La** + n TPPO + ^{i}PrOH + 200 BBL (top, green), where n = 1 (a), 2 (b).

2.2.5. Stereocontrol and Polymerization Mechanism.

Insights into the polymerization mechanism were made possible through evaluation of isolated P3HB samples (M_n, Đ, end-groups, statistical analysis of microstructure) and reactivity studies

aimed at establishing the viability of relevant side-reactions during the ROP of *rac*-BBL using the small molecule, (*R*)-3-acetoxybutyric acid methylester [**(*R*)-3-OAcB^Me**].

Stereocontrol: As described by Thomas and Carpentier,[3] diad and triad distribution can provide insight into the mechanism of stereocontrol for the ROP of *rac*-BBL. Two types of stereocontrol may contribute to the tacticity of BBL polymerization: (1) *enantiomorphic site control*, under which the selectivity of incoming monomer is determined by the asymmetric environment of catalyst, and (2) *chain-end control*, in which the asymmetric nature of the active end of growing polymer differentiates the two enantiomers of the monomer.

In the context that the isotactic diad (meso diad) is dominant, one can consider a mis-insertion (e.g. …RRRR$\underline{S}$, where $\underline{S}$ is the mis-insertion) is immediately corrected and followed by insertions that are favored. For site control, error correction leads to propagation with the favored enantiomer (e.g., …RRR$\underline{S}$RRR, where $\underline{S}$ is the mis-insertion). For chain-end control, it will continue to propagate the meso diad and propagate the enantiomer that was mis-inserted (e.g. …RRR$\underline{S}$SSS). Therefore, the resulting minor triads for site control are 1 *mr*, 1 *rr* and 1 *rm*, while the minor triads for chain-end control are 1 *mr* and 1 *rm*. Therefore, the two methods of stereocontrol can be differentiated by their triad distribution.

The triad distribution was obtained from the $\underline{C}$H2 signals of P3HB using IG-^{13}C-NMR. We fit the signals in the form of a Cauchy-Lorentz distribution. The result contains 4 components, each of which represents a triad ratio with its area (Figure 2.10). A representative example is

P3HB obtained from Table 2.3, entry 6 (**1-La** + 2 TPPO + 1 ^{i}PrOH; $P_m = 0.71$).

triad	δ_0, Chemical Shift/ppm	γ, Width/ppm	I_0, Intensity	rel. Area (%)
rm	40.864(1)	0.025(4)	0.59(6)	20.38
mm	40.809(1)	0.026(2)	1.38(6)	51.01
rr	40.727(2)	0.019(6)	0.32(7)	8.46
mr	40.662(1)	0.021(3)	0.68(7)	20.15
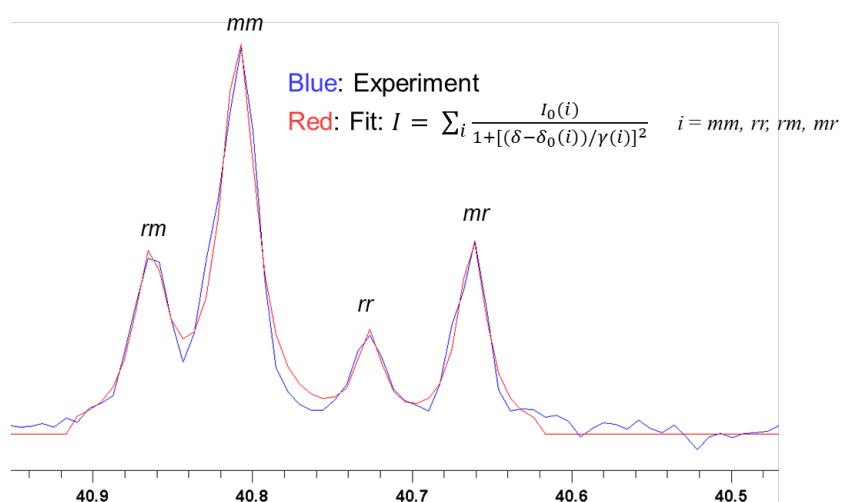
Figure 2.10. Experimental and fitted IG-^{13}C-NMR (152 MHz, CDCl$_3$) signal of P3HB (Table 2.3, entry 6; **1-La** + 2 TPPO + 1 ^{i}PrOH, $P_m = 0.71$)

For chain-end control, the triad distribution obeys a binominal distribution, i.e.: P (*mm*) = P_m^2, P(*rr*) = (1-P_m)^2, P (*mr*) = P (*rm*) = P_m(1-P_m). Applying the Bernoulli model triad test, B = 4P(*mm*)P(*rr*)/[P(*mr*)+P(*rm*)]^2, where B = 1 for a purely chain-end controlled process. For P3HB obtained from entry 6 in Table 2.3, B = (4*51.01*8.46)/(20.38+20.15)^2 = 1.05. This is close to the theoretical value and confirms chain-end control as the mechanism for stereocontrol. While chain-end stereocontrol is operative for several syndioselective catalysts,[13, 49-52] this is the first example with an isoselective catalyst. Other catalysts which produce isoenriched P3HB proceed through enantiomorphic site-control[53-55] or their mechanism of stereocontrol have not yet been determined.

End group analysis: Additional insights into the polymerization mechanism were facilitated by end-group analyses using ^{1}H-NMR and MALDI-TOF techniques. ROP of *rac*-BBL and other β-lactones catalyzed by neutral metal alkoxides commonly proceed through coordination-insertion or anionic pathways.[56] The coordination-insertion mechanism proceeds through acyl cleavage (ester and alcohol end-groups), while the anionic mechanism proceeds through alkyl cleavage (ether and carboxylate end-groups). The ^{i}Pr methine of 2-isopropoxyl butyrate, if any, should appear at ~3.6 ppm, analogous to that of 4-isopropoxypentan-2-one (3.60-3.66, m, CDCl$_3$)[57]. ^{1}H-NMR spectra of isolated P3HB samples revealed the presence of an isopropyl ester end-group (Figure 2.11 and 2.12), while signals for an isopropyl ether were notably absent. These observations are consistent with a coordination-insertion mechanism for ROP with inititation occurring from a metal-isopropoxide.

Following a coordination-insertion mechanism, the other end-group should be a terminal secondary alcohol, which would be obtained upon hydrolysis of the propagating metal-alkoxide. As expected, the secondary alcohol end-group (-CHOHCH$_3$) was observed in a ~1:1 molar ratio with respect to the ester end-group (COO^{i}Pr). However, additional C–H resonances which correspond to a crotyl end-group were observed by ^{1}H-NMR spectroscopy (crotyl:CHOHCH$_3$:COO^{i}Pr; ~1:1:1).
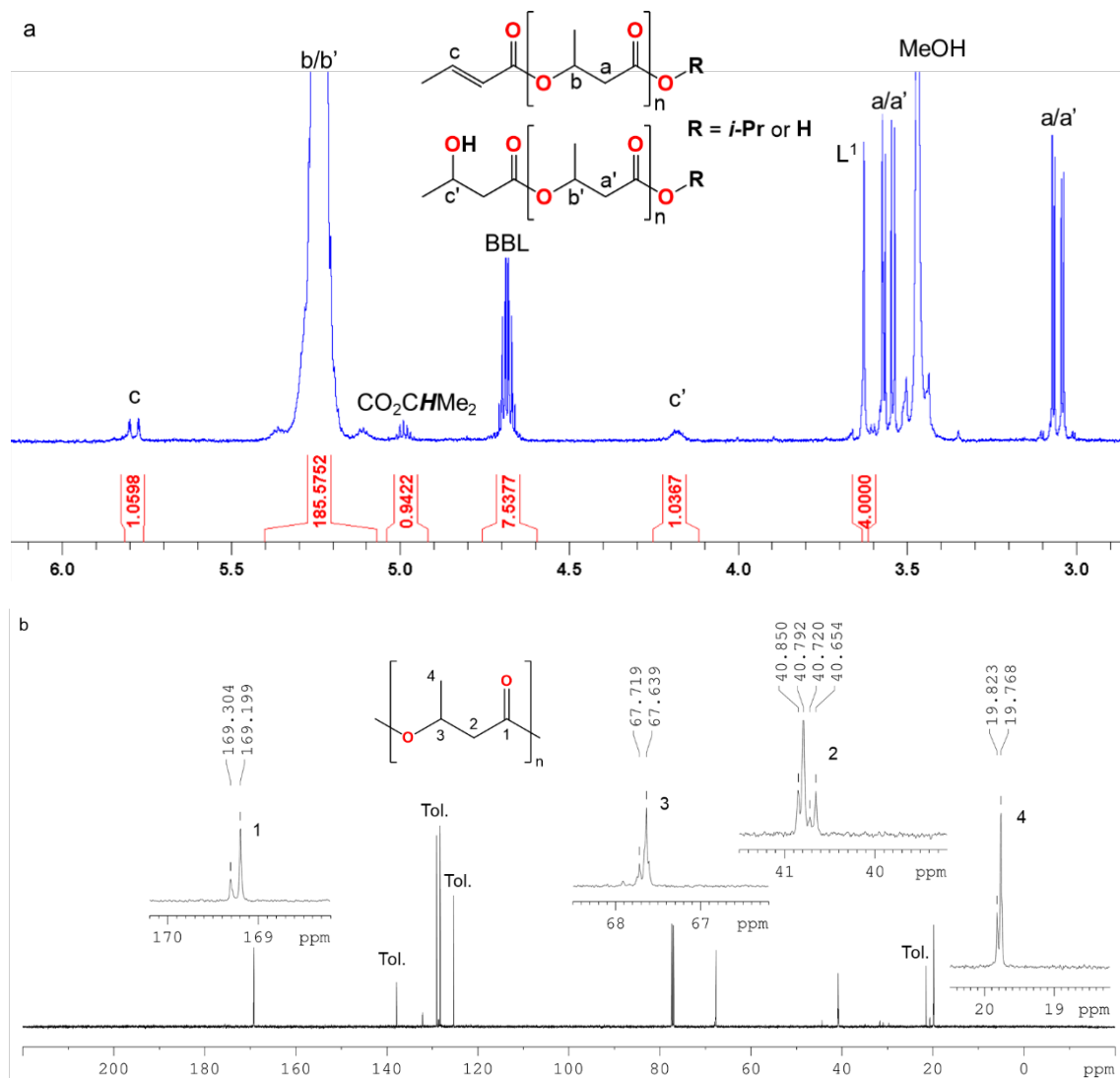
Figure 2.11. (*a*) ^{1}H-NMR (600 MHz, CDCl$_3$), (*b*) ^{13}C-NMR (152 MHz, CDCl$_3$) spectra of P3HB (Table 2.3, entry 6). Reaction was performed in toluene at ambient temperature with [BBL]/[**1-La**]/[TPPO]/[^{i}PrOH] = 200/1/2/1 and [BBL] = 2.4 M within 1 h. Conversion = 97%, M$_n$ = 9.6 kg/mol (corrected by Mark-Houwink factor of 0.54), Đ = 1.18.
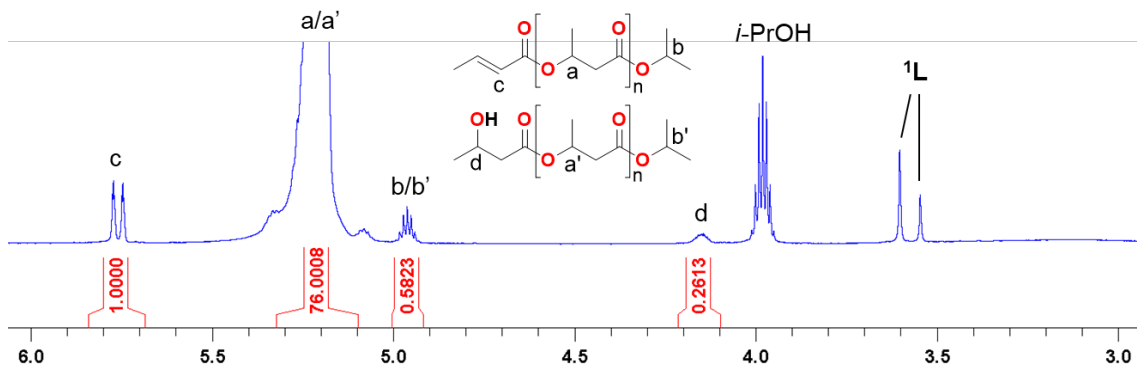
Figure 2.12. ^{1}H-NMR (400 MHz, CDCl$_3$) of the P3HB for MALDI analysis.

Further evidence of the crotyl end-group was established by MALDI-TOF measurements of P3HB obtained from ROP of 40 equiv *rac*-BBL using the **1-La(TPPO)$_2$** / iPrOH catalyst system. MALDI-TOF spectra corroborated ^{1}H-NMR end-group assignments, and clearly supported crotyl end-group formation during the reaction (Figure 2.12, 2.13).
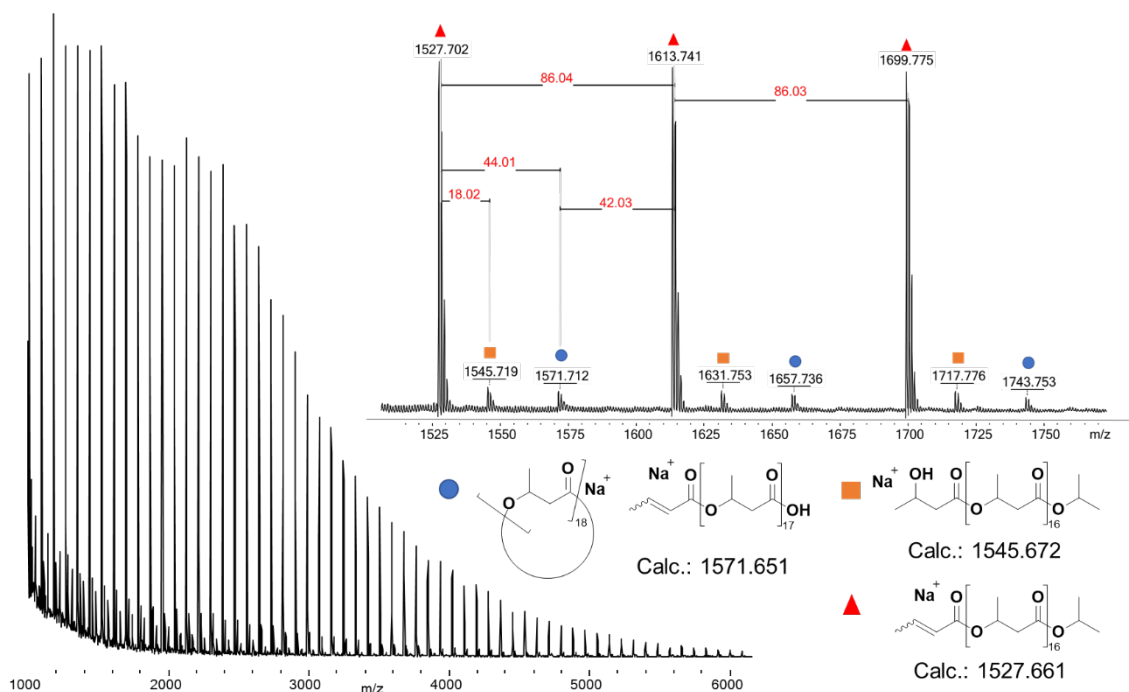
Figure 2.13. MALDI-TOF spectrum of P3HB, produced in toluene at ambient temperature with [BBL]/[**1-La**]/[TPPO]/[^{i}PrOH] = 40/1/2/1 and [BBL] = 2.4 M within 1 h. Conversion = 99%.   M$_n$ = 3.8 kg/mol (corrected by Mark-Houwink factor of 0.54), Đ = 1.30.

Elimination studies: Generation of crotyl end-groups after polymerization could proceed through several possible pathways : (*i*) elimination of water, hydroxide, or oxide from the alcohol end-group under acidic or basic conditions respectively,[44, 58-60] (*ii*) thermal scission,[61-64] or (*iii*) base-induced elimination of internal ester units,[65-67] (*iv*) terminal elimination from a metal alkoxide. While pathway (*i*) has been proposed to explain generation of crotyl end-groups after quenching polymerizations with weak acids,[44, 53] this stands in contrast to the stability of such 3-hydroxybutanoate monomer and oligomers under strong-acid conditions.[68] Furthermore,

elimination from a metal alkoxide during the reaction would convert the secondary alcohol end-group to an inactive crotyl end-group and broaden Đ. The relative amounts of crotyl, secondary alcohol, and isopropyl ester end groups observed (~1:1:1, vide supra) and narrow Đ are inconsistent with expectations for this pathway. Pathway (*ii*) can be excluded due to the reaction temperatures evaluated in our studies (ambient or below).

Side-reactions such as deprotonation, transesterification, and elimination were proposed in early reports for the ROP of *rac*-BBL; [59, 69-71] however, detailed examination of the elimination pathway (*iii*) under mild temperatures (< 100 °C) has been limited to the independent studies of Kricheldorf (K catalysts) and Coates (Zn beta-diketiminate catalysts).[65-66] Reactivity of internal P3HB linkages were established by the use of small molecule models, which enabled detailed identification of the resulting organic products. Despite the superior performance of many RE-based catalysts and the observation of crotyl formation in several reports,[15, 17, 53, 72-76] investigations into elimination pathways for RE-based catalysts are notably absent. Therefore, we examined the reactivity of **1-La** and **1-La(TPPO)₂** with a new small molecule model, (*R*)-3-acetoxybutyric acid methylester [(***R***)**-3-OAcB**$^{\textbf{Me}}$], to establish the viability of such side-reactions [e.g. pathway (*iii*)] during ROP.

Addition of one equiv iPrOH at RT to **1-La** and **1-La(TPPO)₂** cleanly generated the La isopropoxide species, **1'-La** and **1'-La(TPPO)₂**, and one equiv HN(SiHMe2)2 (▲). 15 equiv of (***R***)**-3-OAcB**$^{\textbf{Me}}$ was added, and reactivity was monitored by ^{1}H-NMR after 0.5 and 7 h (Figure 2.14 and 2.15). Our initial expectations were that (***R***)**-3-OAcB**$^{\textbf{Me}}$ would react with **1'-**

La and **1'-La(TPPO)₂** through base-promoted elimination to form crotonate (***trans*-Crot^Me**),

*i*PrOH, and a La acetate species.
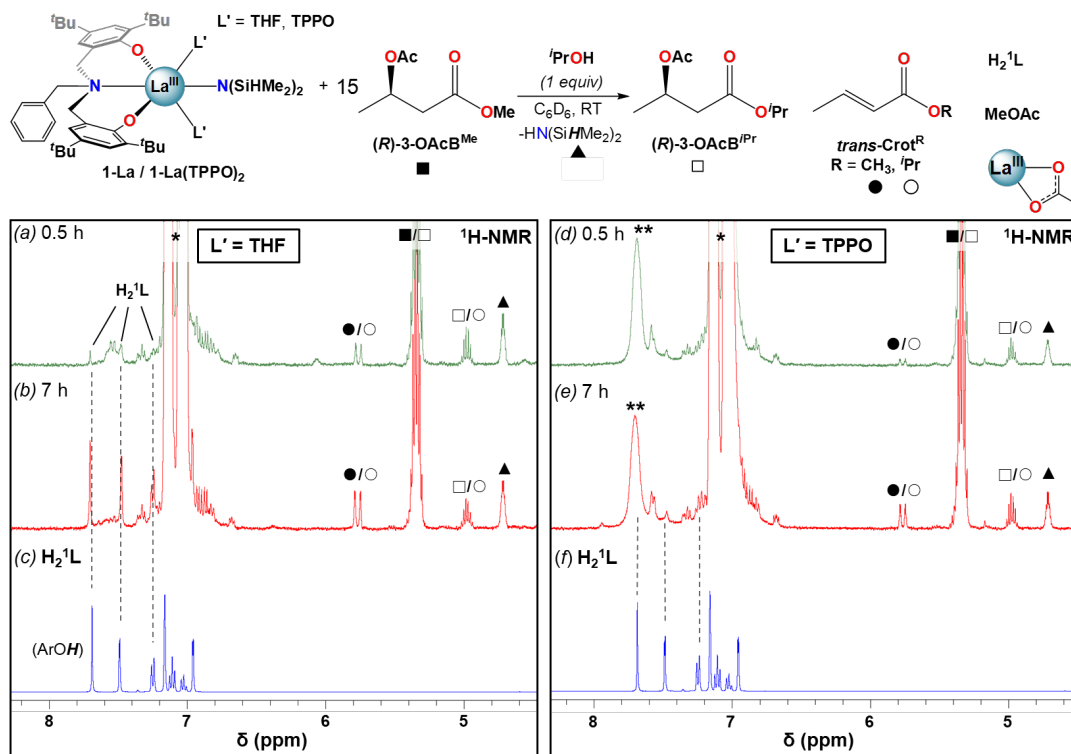
Figure 2.14. Reactivity studies of **1-La** and **1-La(TPPO)₂** in the presence of one equiv *i*PrOH and 15 equiv **(*R*)-3-OAcB^Me** followed by ¹H-NMR after 0.5 h (a, d), 7 h (b, e). Dashed lines provided to help track the formation of **H₂¹L** (c, f) during the reaction time course. * = Toluene (from *i*PrOH stock solution), ** = TPPO. Detailed assignments of full spectra provided as Figure 2.15.

1'-La readily produced crotonate (0.5 h: 0.6 equiv; 7 h: 1.2 equiv); however, free *i*PrOH was

not observed. Instead, the transesterification products, isopropyl butyrate/crotonate [**(*R*)-3-**

OAcB^*iPr*/*trans*-Crot^*iPr*] and methyl acetate (**MeOAc**)[77], were readily identified (Figure 2.15

for detailed assignments). Transesterification between the La isopropoxide and **(*R*)-3-OAcB^Me**

/***trans*-Crot^Me** would lead to a La methoxide and **(*R*)-3-OAcB^*iPr*/*trans*-Crot^*iPr***, while

transesterification between the La methoxide and the 3-acetoxy group of **(*R*)-3-OAcB^*iPr***

would generate **MeOAc** and a La 3-alkoxybutyrate species. The observed reactivity is

consistent with reports of neutral La alkoxides as extremely efficient transesterification catalysts under mild conditions.[78-80] In addition to the aforementioned products, quantifiable amounts of free ligand ($H_2{}^1L$; 0.5 h: 0.1 equiv, 7 h: 0.6 equiv) were also detected. The formation of crotonate and the direct (conjugate acids) or indirect (transesterification) products of base-promoted elimination provide clear evidence for pathway (*iii*) occuring readily at RT with **1'-La**.

In contrast to **1'-La**, **1'-La(TPPO)₂** generated less crotonate (0.5 h: 0.14 equiv, 7 h: 0.73 equiv) and only trace amounts of $H_2{}^1L$ after 7 h. These results highlight two additional and beneficial roles that strong neutral donor ligands (e.g. TPPO) can play in the ROP of *rac*-BBL. First, strong neutral donors can suppress elimination, as evidenced by the significantly decreased amount of crotonate formed with **1'-La(TPPO)₂** compared to **1'-La**. Supressing this side-reaction is critical, as the resulting La carboxylates would be inactive towards coordination-insertion ROP at RT (ie - dormant chains), while chain-scission would also broaden $Đ$ and lower M_n. Second, strong neutral donors can effectively supress the kinetic basicity of the supporting ligand, as evidenced by significant amounts of $H_2{}^1L$ generated with **1'-La**. While RE aryloxides have been leveraged as efficient multi-functional catalysts through cooperative Lewis-Acid/Lewis-base reactions (e.g. Michael, aldol, hydrophosphination),[81-83] RE aryloxides have been considered as innocent supporting ligands for the ROP of *rac*-BBL. Although rapid transesterification was observed for **1-La** and **1-La(TPPO)₂**, the low $Đ$ and high P_m support that this side-reaction is less significant under catalytic conditions. The pronounced tendency towards transesterification should correspond to the lower steric-bulk of the methyl ester found

in **(R)-3-OAcB^Me** compared to the more hindered ester linkages in P3HB.
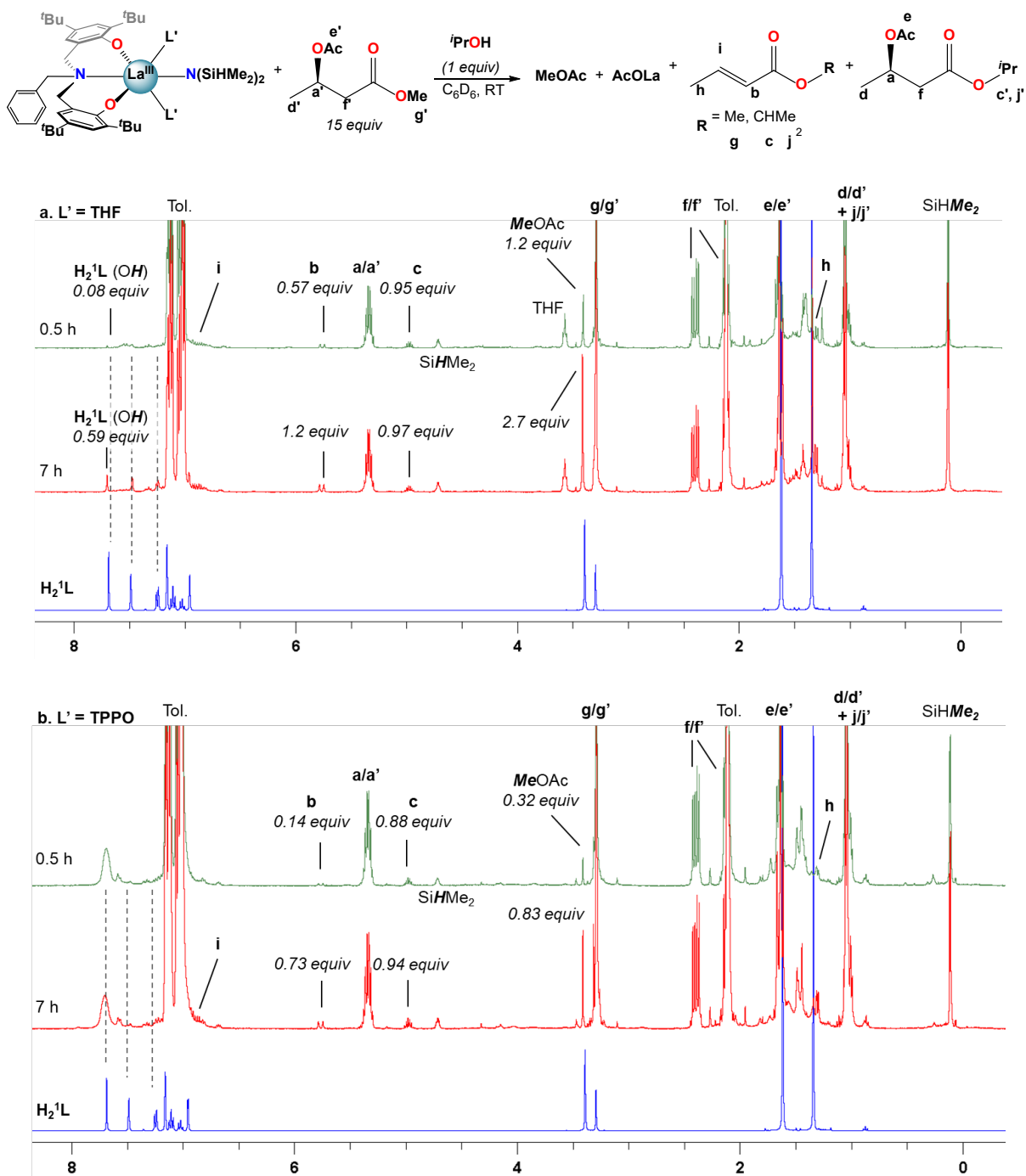
Figure 2.15. Reactivity studies of (a) **1-La** and (b) **1-La(TPPO)$_2$** in the presence of 1 equiv *i*PrOH and 15 equiv **(R)-3-OAcB^Me** in C$_6$D$_6$ followed by ^{1}H-NMR after 0.5 h, 7 h. (There are minor singlets, other than **(R)-3-OAcB^Me** and **(R)-3-OAcB^{iPr}**, from 1.6-1.7 ppm, representing La acetate species and other transesterification products, but cannot be unambiguously assigned)

The Effect of Neutral Donors on ROP Catalyzed by 1-RE and 2-RE: Given the observed benefits of adding strong neutral donor ligands to **1-RE** (vide supra), we set out to evaluate whether similar enhancements would occur in structurally related catalysts with a tethered donor group (**2-Y** and **2-La**). This was motivated by reports of solvent-dependent[3] and tethered-donor dependent[15, 84] ROP reactivity for **2-RE** and its derivatives.
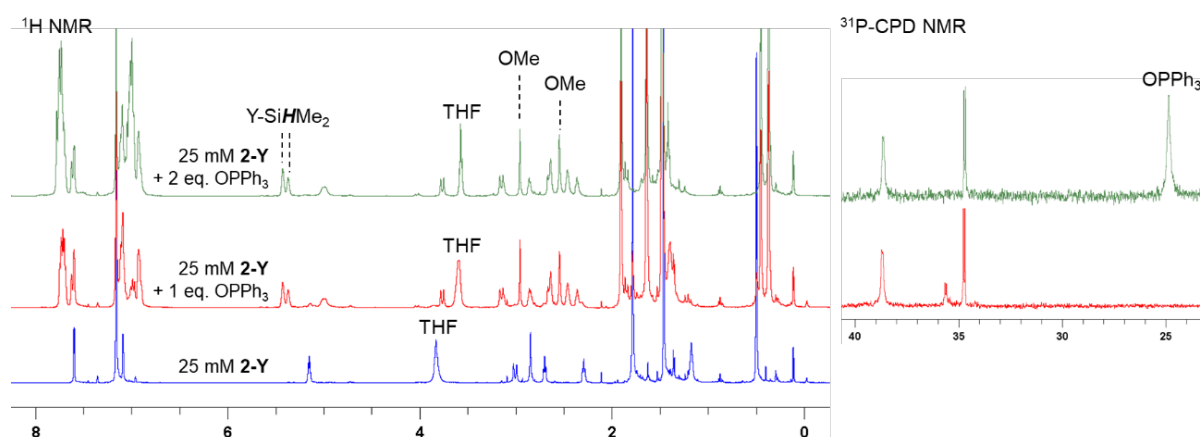
Figure 2.16. ^{1}H-NMR (400 MHz, C$_6$D$_6$, 298 K), ^{31}P{^{1}H}-NMR (162 MHz, C$_6$D$_6$, 298 K) of adding 0, 1 and 2 equiv. of OPPh$_3$ to **2-Y**.

^{1}H- and ^{31}P{^{1}H}-NMR studies indicate that TPPO readily binds to **2-RE** in solution (Figure 2.16); however, unlike **1-RE**, rates and selectivity for the ROP of *rac*-BBL were totally unaffected by added TPPO (Table 2.8, entries 3 – 5 and 8 – 10). While initially unanticipated, we suspect this is due to the much high concentrations of the weaker donor ligands (solvent) compared to our studies (two equiv).[3, 13] Under our experimental conditions, the tethered donor of **2-RE** dominates the observed reactivity and stereoselectivity, indicating that propagation from the corresponding TPPO adducts of **2-RE** is a higher energy pathway.

Table 2.8. Effects of TPPO on **1-RE** and **2-RE** ROP activity with *rac*-BBL
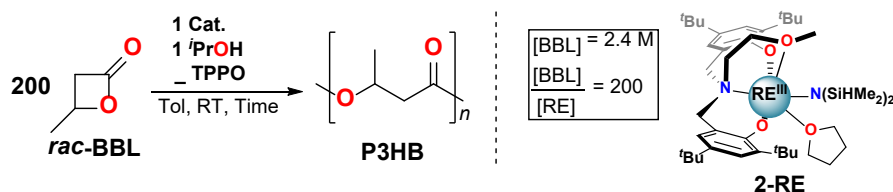
Entry	Cat.	[TPPO]/[RE]	Time (h)[a]	Conv. (%)[b]	$M_{n,\ exp}$[c] (kg/mol)	Đ[c,d]	P_m[e]
1	**1-La**	0	24	40	2.2	1.23	0.57
2	**1-La**	2	1	97	9.6	1.18	0.71
3	**2-La**	0	24	22	1.4	1.17	0.45
4	**2-La**	1	24	21	1.6	1.14	0.49
5	**2-La**	2	24	21	1.7	1.16	0.48
6	**1-Y₂**	0	24	33	5.9	1.15	0.55
7	**1-Y₂**	2	3	95	14.0	1.18	0.50
8	**2-Y**	0	1	91	14.2	1.16	0.22
9	**2-Y**	1	1	99	17.6	1.12	0.22
10	**2-Y**	2	1	99	15.9	1.14	0.22

a – Reaction times not optimized. *b* – Determined by ¹H-NMR integration of BBL and PHB methine resonances in the crude reaction mixture. *c* –Determined by gel permeation chromatography (GPC) at 30 °C in THF using polystyrene standards and corrected by Mark-Houwink factor of 0.54.[18] *d* – M_w/M_n. *e* – Probability of *meso*-linkages between repeat units. Determined by integration of P3HB *C*=O resonances using inverse gated (IG) ¹³C-NMR.

The presence or absence of a tethered donor also manifests opposite size-dependent reactivity and selectivity trends for **1-RE** and **2-RE**. Smaller ions are more reactive and selective for **2-RE**,[13, 16, 50] while larger ions are more reactive for **1-RE**/OPR₃. While both catalysts display chain-end stereocontrol and feature labile coordination sites *cis* to an initiator (two for **1-RE**, one for **2-RE**), amplified selectivity is only observed with the largest and most coordinatively unsaturated catalyst, **1-La**. Furthermore, the presence (**2-RE**) or absence (**1-RE**/OPR₃) of a tethered donor group favors opposite polymer tacticities (**2-RE**: syndio, **1-RE**: iso).

Proposed Mechanism: Given the results of our catalytic and mechanistic studies, we propose the following mechanism for the ROP of *rac*-BBL catalyzed by **1-La** & **1-La(TPPO)₂** (Figure 2.17; L' = THF or TPPO).
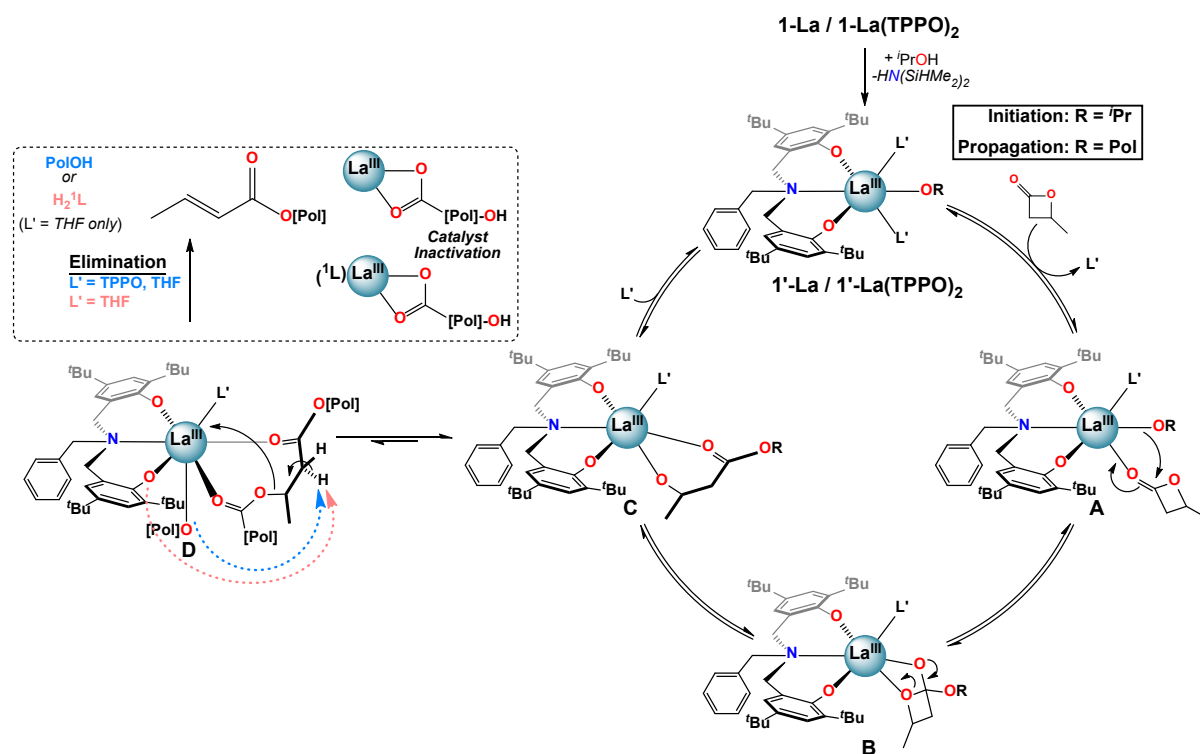
Figure 2.17. Proposed mechanism for the ROP of *rac*-BBL catalyzed by **1-La** or **1-La(TPPO)₂**.

Addition of *i*PrOH to **1-La** or **1-La(TPPO)₂** leads to a highly reactive initiator, **1′-La** or **1′-La(TPPO)₂**. Ligand exchange of L′ for *rac*-BBL generates **A**, which can then undergo insertion of the La alkoxide to generate **B**. Ring-opening would lead to **C**, which is involved in two competing ligand-exchange equilibria that gates productive (propagation) and unproductive (elimination) pathways. Upon binding of one equiv L' to **C**, the catalytic cycle is successfully completed with the regeneration of **1'-La**. Our low-temperature NMR studies of **1-La(TPPO)₂** support a mono-TPPO resting state during ROP, while our catalytic studies indicate that more than one equiv of TPPO is required to achieve maximum rate and selectivity enhancements (Table 2.4). While we have depicted **A**, **B**, and **C** as mono-L' adducts, we cannot exclude the

possibility that one or more of these intermediates may be bis-L' adducts.

Alternatively, at high reaction conversions or with weaker donor ligands, binding of ester linkages to **C** may become competitive with L' to form the key intermediate for base-promoted elimination, **D**. Chain cleavage through elimination would generate two polymer fragments that are inactive for further ROP at RT: (i) a terminated polymer with ester and crotyl end-groups, and (ii) a dormant polyester chain terminated by rare-earth carboxylate and secondary alcohol end-groups. With weak and sterically unencumbered donors (e.g. L' = THF), both the propagating alkoxide chain and ^{1}**L** could act as competent bases, while the kinetic basicity of ^{1}**L** is supressed with strong and bulky neutral donors (e.g. L' = TPPO). While intermediate **D** is depicted with coordination of a neighbouring polyester chain, we expect that both intra- and inter-molecular pathways are viable.

While the exact origin of the unique isoselectivity remains unresolved, we hypothesize that strong neutral donors such as TPPO lead to a sterically crowded axial environment in **1-La(TPPO)₂** compared to **1-La** and **2-RE** (Figure 2.17). Non-covalent C–H···π (arene) interactions between ligand and substrate have been proposed to explain the high syndioselectivity for the ROP of *rac*-BBL with a Yttrium catalyst supported by a cumyl-substituted tetradentate amino-bisphenolate ligand.[50] In contrast, we observed similar reactivity and selectivity with phosphine oxides containing aromatic (TPPO) or aliphatic (TOPO) substituents, which suggests other origins for the unique isoselective chain-end stereocontrol. Rieger and coworkers recently carried out an extensive computational study investigating the

ROP of *rac*-BBL catalyzed by **2-Y.**[16] The syndioselective pathway is favored kinetically and thermodynamically by the propagating P3HB chain adopting a κ^3 binding mode. The authors suggest that alternative P3HB binding modes (e.g. κ^1 or κ^2) may lead to iso-enriched P3HB. Such intermediates (Figure 2.17: **A** or **B**) could be favored by the stronger binding and enhanced steric bulk of phosphine oxides, opening up new pathways that are disfavored for **2-Y**.

Finally, our mechanistic studies uncover new roles for neutral donor ligands in ROP. Previous studies have provided evidence for decreased transesterification[19-20, 23, 85-86] and control of catalyst aggregation state[26, 85, 87-89] with added neutral donor ligands; however, their role in suppressing base-promoted elimination (i.e. crotyl end-group) was previously unknown. Our results suggest that neutral donor groups play a critical role in suppressing or shifting ligand-exchange equilibria for both productive and non-productive pathways in the ROP of *rac*-BBL, and addition of these simple ligands provide a facile and inexpensive way to further modulate catalyst performance.

2.3. Conclusions

In summary, we have synthesized, characterized, and evaluated the reactivity of novel benzyl-substituted amino-bisphenolate rare-earth complexes, **1-RE**, as catalysts for the isoselective ROP of *rac*-BBL. **1-RE** display ROP rates and selectivities that are tuned by the identity of exogenous neutral donor ligands (e.g. OPR$_3$). **1-La**/OPR$_3$/^{i}PrOH display excellent reactivity and selectivity ($P_m = 0.8$ at 0 °C, TOF = ~190 h^{-1}), and are the most isoselective homogeneous catalysts for ROP of *rac*-BBL (R: *n*-octyl, Ph). The use of simple monodentate OPR$_3$ to enhance catalyst performance in stereoselective ROP is unprecedented, and the relative ease and accessibility to a diverse array of phosphine oxides makes this an attractive and operationally simple strategy to further optimize catalyst performance.

Our preliminary mechanistic studies indicate that (*i*) **1-La(TPPO)$_2$** is a precatalyst for the isoselective ROP of *rac*-BBL, (*ii*) **La(TPPO)$_n$** ($n = 1,2$) are implicated as catalytically relevant species, (*iii*) isoselective ROP proceeds with chain-end stereocontrol through a coordination-insertion mechanism, and (*iv*) addition of neutral donor ligands can suppress elimination side-reactions. This is the first investigation into elimination pathways of RE-based catalysts in the ROP of *rac*-BBL, and **1-La(TPPO)$_2$** is the first catalyst to access isoenriched P3HB with chain-end stereocontrol. While structurally related catalysts with a tethered donor group (**2-RE**) also operate under chain-end stereocontrol, ROP activity and selectivity of **2-RE** (*i*) are unaffected by added neutral donor ligands and (*ii*) display opposite stereoselectivity (syndioselective) compared to **1-La**/OPR$_3$. Our study uncovers new roles for neutral donor ligands in stereospecific ROP, and begins to connect their effect on catalyst structure and function.

Removing the tethered donor fragment and increasing axial steric bulk with strong neutral donor ligands favors isoenriched P3HB. Similar donor-related enhancements may require catalysts with enhanced metal accessibility (i.e. several labile coordination sites), and highlight new opportunities in catalyst design and optimization.

2.4. Experimental Section

2.4.1. General Methods.

Instruments and measurements: Unless specified, all reactions were performed under inert conditions (N_2) using standard Schlenk techniques or in a MBraun drybox equipped with a standard catalyst purifier and solvent trap. Glassware was oven-dried for at least 2 h at 150 °C prior to use. Celite and 3 Å molecular sieves were heated under reduced pressure at 300 °C for at least 24 h and then cooled under vacuum prior to use. The following spectrometers were used for NMR characterization: Bruker Avance III HD Ascend (^{1}H: 600 MHz, ^{13}C: 152 MHz, ^{31}P: 243 MHz) and a Bruker DRX (^{1}H: 400 MHz, ^{13}C: 101 MHz, ^{31}P: 162 MHz). ^{1}H- and ^{13}C-NMR shifts are referenced relative to the solvent signal ($CDCl_3$: ^{1}H: 7.26 ppm, ^{13}C: 77.16 ppm; C_6D_6: ^{1}H: 7.16 ppm, ^{13}C: 128.06 ppm), while ^{31}P-NMR shifts are referenced relative to external solution standards (H_3PO_4, 0 ppm). Both instruments were equipped with Z-gradient BBFO probes. Probe temperatures were calibrated using ethylene glycol and methanol as previously described.[90] Polymer tacticity (P_m, percentage of *meso* diads) was measured using a ^{13}C inverse-gated pulse sequence, followed by integration of the $\underline{C}$=O resonances (Figure 2.30). The mechanism for stereocontrol was determined by statistical analysis of stereochemical triads in P3HB (*rr*, *mm*, and *rm*/*mr*; integration of $\underline{C}H_2$ resonances from ^{13}C-NMR using an inverse-gated pulse sequence) as described by Thomas and Carpentier.[3]

Gel permeation chromatography (GPC) measurements were performed using an Agilent 1260 equipped with two Poroshell 120 EC-C18 columns heated at 35 °C (4.6 x 100 mm, 2.7 μm) and a UV-vis diode-array detector and refractive detector. The eluent was inhibitor-free THF,

and the system was calibrated with standard polystyrene standards ranging from 580 to 1,500,000 Da. Reported molecular weights are those obtained from GPC corrected by a Mark-Houwink factor of 0.54.[18] Unless stated otherwise, all GPC samples were of the quenched crude reaction mixtures (not precipitated or purified polymers). P3HB samples (10 mg/mL in THF) using a DCTB/NaTFA matrix (v/v, 10:1) were analysed using MALDI TOF MS under positive-ion reflectron mode on a Bruker Ultraflex III ToF/ToF mass spectrometer at the University of Akron. IR spectra were recorded on Jasco 4100 FTIR spectrometers using Nujol mulls sandwiched between KBr plates. Elemental analyses were performed by Robertson Microlit Laboratories (Ledgewood, NJ) and Midwest Microlab, LLC (Indianapolis, IN) for bench-stable (**^{1}L**) and air-sensitive compounds (**1-RE** and **1-RE(TPPO)$_2$**) respectively. Samples were shipped in a sealed 2 mL vial that was placed in a 20 mL scintillation vial and sealed, which were then placed in a vacuum-sealed plastic bag.

Materials: Tetrahydrofuran, diethyl ether, toluene, hexanes, and pentane were purchased from Fisher Scientific. Solvents were sparged for 20 min with dry Ar and dried using a commercial two-column solvent purification system (LC Technologies). Solvents were further dried by storing them over 3 Å molecular sieves for at least 48 h prior to use. Ultrapure, deionized water (18.2 MΩ) was obtained from a Millipore Direct-Q 3 UV Water Purification System. Deuterated solvents were purchased from Cambridge Isotope Laboratories, Inc. C_6D_6 was degassed with 3 freeze-pump-thaw cycles and stored over 3 Å molecular sieves for at least 48 h prior to use. Qualitative assessment of moisture-content in these solvents was performed by adding 1 drop of a concentrated solution of a sodium benzophenone radical anion (purple) to

10 mL of solvent where maintenance of a dark blue color for at least 5 minutes was sufficient for use.

2,6-ditertbutyl phenol (Oakwood Chemical; 99% purity), para-formaldehyde (Alfa Aesar; 97% purity), benzylamine (TCI; 99% purity), 2-methoxyethylamine (Sigma-Aldrich; 99% purity), triphenylphosphine oxide (Acros; 99% purity), trioctylphosphine oxide (Sigma-Aldrich; 99% purity), hexamethylphosphoramide (TCI; 98% purity), triphenylphosphate (Sigma-Aldrich; 99% purity), triphenyl phosphine (Sigma-Aldrich; 99% purity), 4-dimethylaminopyridine (Chem-Impex; 99% purity), 1,4-diazabicyclo[2.2.2]octane (Sigma-Aldrich; 99% purity), potassium hexamethyldisilazide (Sigma-Aldrich; 95% purity), 1,1,3,3-tetramethyldisilazane (TCI, 97% purity), $RECl_3$ (Strem; RE = La, Y; 99.9% purity), (R)-methyl 3-hydroxybutanoate (Oakwood; 99% purity), acetyl chloride (Acros; 99% purity) 2-propanol (Alfa-Aesar, anhydrous, 99.5% purity) and pyridine (Sigma-Aldrich; 99% purity) were purchased and used as received. Racemic butyrolactone (Sigma-Aldrich; 98% purity) was freshly distilled from CaH_2 under nitrogen and degassed by freeze-pump-thaw cycles prior to use. $RE[N(SiMe_3)_2]_3$ (RE = La and Y),[91] $RE[N(SiHMe_2)_2]_3(THF)_2$ (RE = La and Y),[92] 6,6'-(((2-methoxyethyl)azanediyl)bis-(methylene))bis(2,4-di-tert-butylphenol) (^2L),[93] $RE(^2L)THF$ (RE = La[93] and Y[94]) were prepared according to reported procedures.

X-ray Crystallography: Samples were collected in Paraton™ oil on a petri dish in a glovebox and then quickly evaluated and mounted with the assistance of an optical microcope. X-ray reflection intensity data were collected on a Bruker D8 Quest with a Photon 100 CMOS

detector employing graphite-monochromated Mo-Kα radiation (λ = 0.71073 Å) at a temperature of 173(1) K. Rotation frames were integrated using SAINT,[95] producing a listing of unaveraged F^2 and $\sigma(F^2)$ values which were then passed to the SHELXT[96] program package for further processing and structure solution. The intensity data were corrected for Lorentz and polarization effects and for absorption using SADABS.[97] The structures were solved by direct methods (SHELXT).[96] Refinement was by full-matrix least squares based on F^2 using SHELXL.[96] All reflections were used during refinements. Non-hydrogen atoms were refined anisotropically and hydrogen atoms were refined using a riding model. Two tert-butyl groups and one of the Si(HMe2) groups were found to be disordered over two positions in [La(^{1}L)(N(SiHMe2)2)(TPPO)2] (**1-La(TPPO)₂**). Two tert-butyl groups were found to be disordered over two positions in [Y(^{1}L)(N(SiHMe2)2)(TPPO)2] (**1-Y(TPPO)₂**). Disorders were refined with the help of similarity restraints using standard/default values on 1,2 and 1,3 distances (SADI) and rigid bond restraints (RIGU) of the disordered groups.[98-99] For the structures [La(^{1}L)(N(SiHMe2)2)(TPPO)2] (**1-La(TPPO)₂**) and [Y(^{1}L)(N(SiHMe2)2)(TPPO)2] (**1-Y(TPPO)₂**) there were areas of disordered solvent (toluene, 2 molecules in the asymmetric unit) for which reliable disorder models could not be devised; the X-ray data were corrected for the presence of disordered solvent using SQUEEZE.[100] Crystallographic parameters are summarized in Table 2.10, and thermal ellipsoid plots (50 % probability) are shown in Figures 2.31-2.33.

2.4.2. Synthetic Details and Characterization.
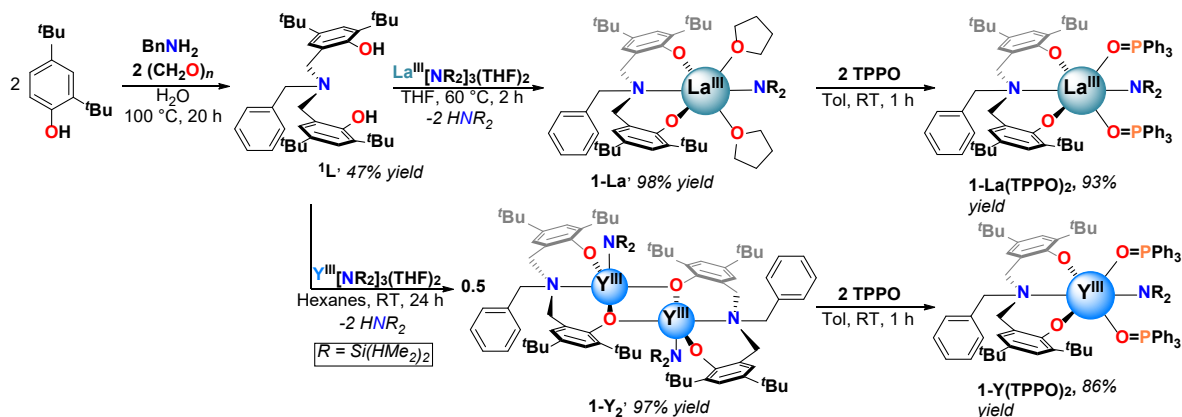
Scheme 2.4. Synthesis of benzyl-amino bisphenol and corresponding rare-earth complexes

6,6'-((benzylazanediyl)bis(methylene))bis(2,4-di-tert-butylphenol), (^{1}L)
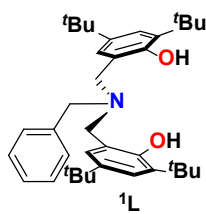
A 250 mL round-bottomed flask was charged with benzyl amine (3.27 g, 30.5 mmol, 1.0 equiv.; MW: 107.16 g•mol^{-1}), DI water (50 mL), a Teflon-coated stir bar, and paraformaldehyde (1.83 g; 30.5 mmol; 2.0 equiv.; MW: 30.03 g•mol^{-1}) paraformaldehyde, resulting in a colorless solution. To the stirring mixture, 2,6-ditertbutyl phenol (12.59 g, 30.5 mmol, 2.0 equiv.; MW: 206.33 g•mol^{-1}) was added and floated on the top of the solution. The reaction was heated in an oil bath at 110 °C for 20 h. The mixture became a yellow emulsion during heating. After cooling to RT, a solid was formed out of the cooled liquid. The aqueous layer was decanted. The residual solid was dissolved in EtOH (20 mL) at 60 °C and then cooled to RT, affording a colorless crystalline solid after standing overnight. The solid was isolated by vacuum filtration over a course porosity fritted filter, washed with EtOH (2 × 10 mL), and dried under reduced pressure to furnish compound ^{1}L as a white solid. Yield: 7.8 g (14.3 mmol, 47% yield; MW:

543.84 g•mol^{-1}).

^{1}H-NMR (400 MHz, CDCl$_3$, 298 K): δ = 1.28 (s, 18H; 2-^{t}Bu), 1.42 (s, 18H; 4-^{t}Bu), 3.60 (s, 2H; NC*H*$_2$Bn), 3.66 (s, 4H; NC*H*$_2$ArOH), 6.94 (d, *J* = 2.4 Hz, 2H; 5-H$_{Ar}$), 7.22 (d, *J* = 2.4 Hz, 2H; 3-H$_{Ar}$), 7.30-7.42 ppm (m, 7H; Bn, OH);

^{13}C{^{1}H}-NMR (101 MHz, CDCl$_3$, 298 K): δ = 29.8 (C*Me*$_3$), 31.8 (C*Me*$_3$), 34.3 (*C*Me$_3$), 35.0 (*C*Me$_3$), 57.0 (N*C*H$_2$ArOH), 58.6 (N*C*H$_2$Bn), 121.5, 123.7, 125.3, 128.0, 129.1, 129.7, 136.1, 137.6, 141.6, 152.3 ppm (*C*$_{Ar}$–OH);

^{1}H-NMR (400 MHz, C$_6$D$_6$, 298 K): δ = 1.34 (s, 18H; 2-^{t}Bu), 1.62 (s, 18H; 4-^{t}Bu), 3.29 (s, 2H; NC*H*$_2$Bn), 3.39 (s, 4H; NC*H*$_2$ArOH), 6.96 (d, *J* = 2.4 Hz, 2H; 5-H$_{Ar}$), 7.02 (t, *J* = 7.2 Hz, 1H; *p*-H$_{Bn}$), 7.11 (t, *J* = 7.2 Hz, 2H; *m*-H$_{Bn}$), 7.26 (d, *J* = 7.2 Hz, 2H; *o*-H$_{Bn}$), 7.49 (d, *J* = 2.4 Hz, 2H; 3-H$_{Ar}$), 7.69 ppm (m, 2H; OH);

Elemental Analysis calcd. (%) for C$_{37}$H$_{53}$NO$_2$: C 81.72, H 9.82, N 2.58; found: C 81.94, H 9.78, N 2.56.

La(^{1}L)[N(SiHMe$_2$)$_2$](THF)$_2$ (1-La)
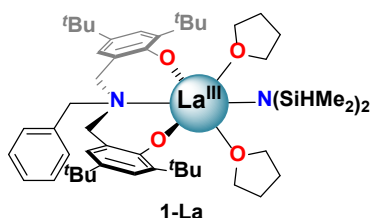
A 20 mL scintillation vial was charged with ^{1}L (335 mg, 0.62 mmol, 1.0 equiv.; MW: 543.84 g•mol^{-1}), a Teflon-coated stir-bar, and THF (2 mL). To the stirring, clear, and colorless solution, La[N(SiHMe$_2$)$_2$]$_3$(THF)$_2$ (419 mg, 0.62 mmol, 1.0 equiv.; MW: 680.12 g•mol^{-1}) was added.

The solution was heated at 60 °C for 2 h. All volatiles were removed under reduced pressure, affording **1-La** as a white solid. Yield: 580 mg (0.61 mmol, 98% yield; MW: 957.27 g•mol^{-1}).

^{1}H-NMR (600 MHz, C$_6$D$_6$, 298 K): δ = 0.42 (d, ^{3}J = 3.0 Hz, 12H; SiH*Me$_2$*), 1.23 (s, 8H; 3,4-H$_{THF}$), 1.46 (s, 18H; 2-^{t}Bu), 1.74 (s, 18H; 4-^{t}Bu), 3.45 (d, ^{2}J = 12.8 Hz, 2H; NC*H$_2$*ArO), 3.65 (s, 8H; 2,5-H$_{THF}$), 3.79 (s, 2H; NC*H$_2$*Bn), 4.00 (d, ^{2}J = 12.8 Hz, 2H; NC*H$_2$*ArO), 5.21 (quint, ^{3}J = 3.0 Hz, $^{1}J_{Si(29)-H}$ = 167 Hz, 2H; Si-H), 7.04 (t, J = 7.2 Hz, 1H; p-H$_{Bn}$), 7.15 (t, J = 7.2 Hz, 2H; m-H$_{Bn}$), 7.19 (d, J = 7.2 Hz, 2H; o-H$_{Bn}$), 7.20 (d, J = 2.4 Hz, 2H; 5-H$_{ArO}$), 7.62 ppm (d, J = 2.4 Hz, 2H; 3-H$_{ArO}$);

^{13}C{^{1}H}-NMR (152 MHz, C$_6$D$_6$, 298 K): δ = 4.0 (SiH*Me$_2$*), 25.3 (β-C$_{THF}$), 30.5 (C*Me$_3$*), 32.3 (C*Me$_3$*), 34.3 (*C*Me$_3$), 35.6 (*C*Me$_3$), 52.0 (N*C*H$_2$Bn), 61.6 (N*C*H$_2$ArO), 69.7 (α-C$_{THF}$), 124.0, 125.0, 127.8, 128.3, 128.7, 131.6, 135.7, 135.9, 136.9, 162.6 ppm (*C*$_{Ar}$–O);

IR (Nujol): 2075 [m, ν(SiH)], 2011 [w, ν(La←*H–Si*)], 1774 (w), 1602 (w), 1414 (m), 1305 (s), 1279 (s), 1241 (s), 1232 (s), 1201 (m), 1165 (m), 1133 (m), 1051 (m), 1030 (m), 962 (m), 899 (s), 883 (s), 835 (s), 802 (m), 787 (m), 762 (m), 700 (m), 644 (w), 629 (m), 598 (m), 528 (m), 489 (w), 444 (m) cm^{-1};

Elemental Analysis calcd. (%) for C$_{49}$H$_{81}$LaN$_2$O$_4$Si$_2$: C 61.75, H 8.30, N 2.92; found: C 61.48, H 8.53, N 2.93.

{Y(^{1}L)[N(SiHMe$_2$)$_2$]}$_2$ (1-Y$_2$)
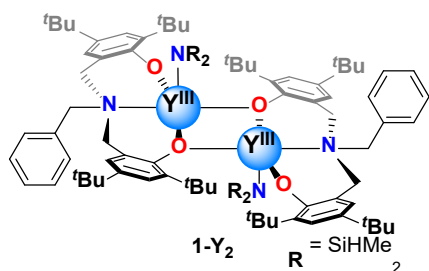
A 20 mL scintillation vial was charged with ^{1}**L** (253 mg, 0.47 mmol, 1.0 equiv.; MW: 543.84 g•mol^{-1}), a Teflon-coated stir-bar, and hexanes (2 mL). To the stirring, clear, and colorless solution, Y[N(SiHMe$_2$)$_2$]$_3$(THF)$_2$ (294 mg, 0.47 mmol, 1.0 equiv.; MW: 630.12 g•mol^{-1}) was added. The solution was stirred at ambient temperature for 24 h. All volatiles were removed under reduced pressure, affording **1-Y$_2$** as a white solid. Yield: 345 mg (0.23 mmol, 97% yield; MW: 1526.12 g•mol^{-1}).

^{1}H-NMR (600 MHz, C$_6$D$_6$, 298 K): δ = -0.09 (d, ^3J = 2.9 Hz, 12H; SiH_Me$_2$_), 0.18 (d, ^3J = 2.9 Hz, 12H; SiH_Me$_2$_), 1.23 (s, 18H; 2-^{t}Bu), 1.32 (s, 18H; 4-^{t}Bu) , 1.37 (s, 18H; 4-^{t}Bu) , 1.62 (s, 18H; 2-^{t}Bu), 3.79 (d, ^2J = 13.2 Hz, 2H; NC_H$_2$_ArO), 3.93 (d, ^2J = 14.4 Hz, 2H; NC_H$_2$_ArO), 4.40 (d, ^2J = 14.4 Hz, 2H; NC_H$_2$_Bn), 4.55 (d, ^2J = 14.4 Hz, 2H; NC_H$_2$_Bn), 4.73 (d, ^2J = 13.2 Hz, 2H; NC_H$_2$_ArO), 4.94 (d, ^2J = 14.4 Hz, 2H; NC_H$_2$_ArO), 5.00-5.03 (m, 4H; Si-H), 7.06 (d, J = 2.4 Hz, 2H; 5-H$_{ArO}$), 7.17 (t, J = 7.2 Hz, 2H; p-H$_{Bn}$), 7.22 (d, J = 2.4 Hz, 2H; 5-H$_{ArO}$), 7.27 (t, J = 7.2 Hz, 4H; m-H$_{Bn}$), 7.38 (d, J = 2.4 Hz, 4H; 3-H$_{ArO}$), 7.47 (d, J = 2.4 Hz, 4H; 3-H$_{ArO}$), 7.60 ppm (d, J = 7.2 Hz, 4H; o-H$_{Bn}$);

^{13}C{^{1}H}-NMR (152 MHz, C$_6$D$_6$, 298 K): δ = 2.6 (SiH_Me$_2$_), 3.1 (SiH_Me$_2$_), 29.6 (C_Me$_3$_), 31.6 (C_Me$_3$_), 32.0 (C_Me$_3$_), 34.22 (_C_Me$_3$), 34.26 (_C_Me$_3$), 34.33 (_C_Me$_3$), 35.1 (_C_Me$_3$), 36.7 (_C_Me$_3$), 52.1 (NC_H$_2$_Bn), 59.3 (NC_H$_2$_ArO), 62.1 (NC_H$_2$_ArO), 123.3, 123.8, 125.5, 126.7, 128.29,

128.31, 128.34, 129.4, 132.8, 133.4, 136.4, 137.7, 137.9, 142.6, 155.0 ($\underline{C}_{Ar}$–O), 161.1 ppm (d, J_{Y-C} = 3.3 Hz, $\underline{C}_{Ar}$–O);

IR (Nujol): 2096 [m, ν(SiH)], 2054 [w, ν(SiH)], 1936 [br, m, ν(Y←$\underline{H-Si}$)], 1605 (w), 1415 (m), 1307 (m), 1279 (m), 1248 (m), 1246 (m), 1225 (m), 1201 (m), 1165 (m), 1128 (m), 1086 (w), 1012 (s), 964 (m), 901 (s), 877 (s), 834 (s), 802 (m), 768 (m), 746 (m), 704 (m), 648 (w), 631 (m), 613 (m), 534 (m), 521 (w), 501 (w), 455 (m) cm^{-1};

Elemental Analysis calcd. (%) for $C_{82}H_{130}N_4O_4Si_4Y_2$: C 64.76, H 8.63, N 3.63; found: C 64.54, H 8.59, N 3.67.

The assignment of the ^{1}H- and ^{13}C{^{1}H}-NMR spectrum for **1-Y$_2$** was made by heteronuclear multiple bond correlation (HMBC) spectroscopy. Assignment for the bridging versus terminal phenolate in the ^{13}C-NMR was made based on comparison of the mononuclear **1-La**. The bridging phenolate $\underline{C}_{Ar}$–O is significantly shifted up-field (155.0 ppm) in comparison to the corresponding terminal $\underline{C}_{Ar}$–O (**1-Y$_2$**: 161.1 ppm; **1-La**: 162.6 ppm). The HMBC experiment was done at 600 MHz, with filtered ^1J coupling constant (cnst2) = 145 Hz, long rang ^nJ coupling constant (cnst13) = 10 Hz.

La(^{1}L)[N(SiHMe$_2$)$_2$](TPPO)$_2$ (1-La(TPPO)$_2$)

1-La(TPPO)$_2$
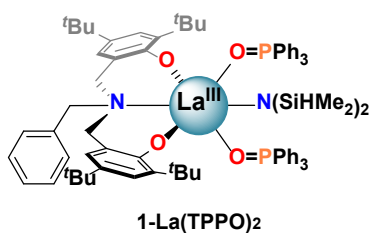
A 20 mL scintillation vial was charged with **1-La** (173 mg, 0.18 mmol, 1.0 equiv.; MW: 957.27

g•mol^{-1}), TPPO (101 mg, 0.36 mmol, 2.0 equiv.; MW: 278.29 g•mol^{-1}) and toluene (0.5 mL). After all solids were dissolved, hexane (3 mL) was layered on top of the toluene solution. After the two layers mixed (~ 1 h), the vial was cooled in the glovebox freezer at –35 °C for 3 h, affording a white crystalline solid. The mother liquor was decanted and volatiles were removed under reduced pressure, affording **1-La(TPPO)$_2$** as a white solid. Yield: 230 mg (0.17 mmol, 93% yield; MW: 1369.64 g•mol^{-1}). X-ray quality crystals were grown by layering hexane (2 mL) on top of a solution of **1-La(TPPO)$_2$** (200 mg / 0.5 mL toluene) and allowing the solution to stand and mix undisturbed at RT.

^{1}H-NMR (600 MHz, C$_6$D$_6$, 298 K): δ = 0.50 (d, J_3 = 3.0 Hz, 12H; SiH*Me$_2$*), 1.51 (s, 18H; 2-^{t}Bu), 1.81 (s, 18H; 4-^{t}Bu), 2.95 (br, 2H; NC*H$_2$*ArO), 3.74 (s, 2H; NC*H$_2$*Bn), 3.78 (br, 2H; NC*H$_2$*ArO), 5.63 (quint, ^3J = 3.0 Hz, $^1J_{Si(29)\text{-}H}$ = 174 Hz, 2H; Si-H), 6.94 (d, J = 2.4 Hz, 2H; 5-H$_{ArO}$), 6.96-7.04 (m, 19H; p-H$_{Bn}$, m,p-H$_{TPPO}$), 7.12 (t, J = 7.5 Hz, 2H; m-H$_{Bn}$), 7.19 (d, J = 7.5 Hz, 2H; o-H$_{Bn}$), 7.63 (d, J = 2.4 Hz, 2H; 3-H$_{ArO}$), 7.65 ppm (br, 12H; o-H$_{TPPO}$);

^{13}C{^{1}H}-NMR (152 MHz, C$_6$D$_6$, 298 K): δ = 5.0 (SiH*Me$_2$*), 31.0 (C*Me$_3$*), 32.5 (C*Me$_3$*), 34.3 (*C*Me$_3$), 36.0 (*C*Me$_3$), 51.2 (N*C*H$_2$Bn), 61.0 (N*C*H$_2$ArO), 123.1, 125.5, 127.0, 127.3, 128.3, 128.5, 128.9 (d, $J_{P(31)\text{-}C(13)}$ = 12.5 Hz; m-C$_{TPPO}$), 130.3 (d, $J_{P(31)\text{-}C(13)}$ = 107 Hz; C–P), 132.5 (p-C$_{TPPO}$), 133.0 (d, $J_{P(31)\text{-}C(13)}$ = 10.5 Hz; o-C$_{TPPO}$), 134.2, 135.5, 135.8, 164.3 ppm (C$_{Ar}$–O);

^{31}P{^{1}H}-NMR (243 MHz, C$_6$D$_6$, 298 K): δ = 33.3 (br) ppm;

IR (Nujol): 2048 [m, ν(Si-H)], 1959 (w), 1593(w), 1414 (m), 1331 (m), 1298 (m), 1259 (w), 1236 (m), 1200 (w), 1155 [s, ν(P=O)], 1120 (m), 1089(m), 1074 (w), 1043 (m), 1024 (m), 999 (w), 937 (m), 883 (m), 741 (m), 694 (m), 673 (w), 648 (w), 625 (w), 606 (w), 542 [s, ν(P-C)],

461 (w), 440 (w), 426 (w) cm^{-1};

Elemental Analysis calcd. (%) for C$_{77}$H$_{95}$LaN$_2$O$_4$P$_2$Si$_2$: C 66.98, H 6.77, N 1.86; found: C 67.52, H 6.99, N 2.05.

Y(^{1}L)[N(SiHMe$_2$)$_2$](TPPO)$_2$ (1-Y(TPPO)$_2$)

1-Y(TPPO)$_2$
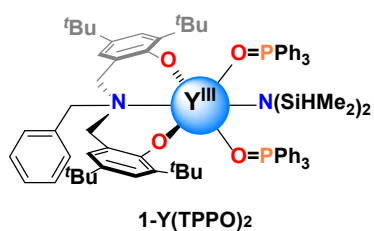
A 20 mL scintillation vial was charged with **1-Y$_2$** (129 mg, 0.085 mmol, 1.0 equiv.; MW: 1526.12 g•mol^{-1}), TPPO (94 mg, 0.34 mmol, 4.0 equiv.; MW: 278.29 g•mol^{-1}) and toluene (0.5 mL). After all solids were dissolved, hexane (3 mL) was layered on top of the toluene solution. After the two layers mixed (~ 1 h), the vial was cooled in the glovebox freezer at –35 °C for 3 h, affording a white crystalline solid. The mother liquor was decanted, and volatiles were removed under reduced pressure, affording **1-Y(TPPO)$_2$** as a white solid. Yield: 192 mg (0.15 mmol, 86% yield; MW: 1319.64 g•mol^{-1}). X-ray quality crystals were grown by layering hexanes (1 mL) on top of a solution of **1-Y(TPPO)$_2$** (100 mg / 0.2 mL toluene) and allowing the solution to stand and mix undisturbed at RT.

Note: The solution behaviour of **1-Y(TPPO)$_2$** and **1-Y** + 2 TPPO is complex and concentration-dependent. Crystallized **1-Y(TPPO)$_2$** has limited solubility in C$_6$D$_6$, and some TPPO dissociation was observed by ^{1}H- and ^{31}P-NMR. The major species observed at low concentration ([Y] = 25 mM) correspond to monomeric and dimeric Y-TPPO adducts (1:2).

Concentrated ([Y] = 75 mM) C_6D_6 solutions of **1-Y(TPPO)$_2$** were made by adding 4 equiv. TPPO to C_6D_6 solution of **1-Y$_2$**, in which **1-Y(TPPO)$_2$**, **[1-Y(TPPO)$_2$]$_2$** and **1-Y(TPPO)** was observed. The speciation is readily seen from DOSY NMR spectra (Figures 2.27 and 2.28).

^{1}H-NMR (400 MHz, C_6D_6, 298 K, 25 mM): δ = 0.10 (d, ^3J = 2.9 Hz, 12H; SiH*Me$_2$* of **[1-Y(TPPO)$_2$]$_2$**), 1.37-1.85 (m; ^{t}Bu), 2.72 (d, J = 13.7 Hz, 2H; NC*H$_2$*ArO of **1-Y(TPPO)**), 2.95 (br), 3.22 (d, J = 13.7 Hz, 2H; NC*H$_2$*ArO of **1-Y(TPPO)**), 3.50 (s, 2H; NC*H$_2$*Bn of **1-Y(TPPO)**), 3.66 (br; **1-Y(TPPO)$_2$**), 3.76 (d, J = 15.3 Hz, 1H; NC*H$_2$*ArO), 3.78 (d, J = 13.7 Hz, 1H; NC*H$_2$*ArO), 4.04 (br; **1-Y(TPPO)$_2$**), 4.64 (d, J = 14.1 Hz, 1H; NC*H$_2$*Bn), 4.70 (br; **1-Y(TPPO)$_2$**), 4.77 (d, J = 14.1 Hz, 1H; NC*H$_2$*Bn), 4.99 (quint, ^3J = 3.0 Hz, 2H; Si-H), 5.16 (d, J = 15.3 Hz, 1H; NC*H$_2$*ArO), 5.17 (d, J = 13.7 Hz, 1H; NC*H$_2$*ArO), 5.49 (br; Si-H of **1-Y(TPPO)$_2$**), 6.62-6.68 (m), 7.01-7.16 (m), 7.29-7.36 (m), 7.44-7.82 (m),;

^{31}P{^{1}H}-NMR (162 MHz, C_6D_6, 298 K, 15 mM): δ = 25.2 (br, free TPPO), 25.2 (br, **1-Y(TPPO)$_2$**), 34.6 (d, $J_{Y-P(31)}$ = 12.6 Hz; **1-Y(TPPO)**), 38.4 (d, $J_{Y-P(31)}$ = 11.1 Hz; **[1-Y(TPPO)$_2$]$_2$**), 39.1 (d, $J_{Y-P(31)}$ = 10.9 Hz; **1-Y(TPPO)**) ppm;

IR (Nujol): 2081 [m, ν(SiH)], 2015 (w), 1959 (w), 1591(w), 1416 (m), 1331 (m), 1300 (m), 1259 (m), 1240 (m), 1201 (w), 1153 [s, ν(P=O)], 1120 (m), 1090 (m), 1018 (m), 997 (m), 933 (m), 897 (m), 885 (m), 835 (m), 802 (w), 789 (w), 744 (m), 694 (m), 671 (w), 646 (w), 629 (w), 540 [s, ν(P-C)], 464 (m), 447 (m) cm^{-1};

Elemental Analysis calcd. (%) for $C_{77}H_{95}YN_2O_4P_2Si_2$: C 69.75, H 7.59, N 1.65; found: C 70.08, H 7.26, N 2.12.

^{1}H-NMR (600 MHz, C_6D_6, 298 K, 75 mM, prepared *in-situ*): δ = 0.09 (d, ^3J = 3.0 Hz, 12H;

SiH*Me₂*), 1.45 (s, 9H; *^t*Bu), 1.49 (s, 9H; *^t*Bu), 1.58 (s, 9H; *^t*Bu), 1.69 (s, 9H; *^t*Bu), 3.76 (d, J = 15.3 Hz, 1H; N$\underline{CH_2}$ArO), 3.78 (d, J = 13.7 Hz, 1H; N$\underline{CH_2}$ArO), 4.64 (d, J = 14.1 Hz, 1H; N$\underline{CH_2}$Bn), 4.77 (d, J = 14.1 Hz, 1H; N$\underline{CH_2}$Bn), 4.99 (quint, ^3J = 3.0 Hz, 2H; Si-H), 5.16 (d, J = 15.3 Hz, 1H; N$\underline{CH_2}$ArO), 5.17 (d, J = 13.7 Hz, 1H; N$\underline{CH_2}$ArO), 6.86 (t, J = 6.0 Hz, 6H; p-H$_{TPPO}$), 6.99-7.09 (m, 12H), 7.13 (t, J = 7.5 Hz, 1H; p-H$_{Bn}$), 7.17-7.22 (m, 10H), 7.33 (t, J = 7.5 Hz, 2H; m-H$_{Bn}$), 7.46 (d, J = 2.4 Hz, 1H; 3-H$_{ArO}$), 7.50 (d, J = 2.4 Hz, 1H; 3-H$_{ArO}$), 7.73 (br, 4H), 7.79 ppm (d, J = 7.5 Hz, 2H; o-H$_{Bn}$);

^{13}C{^{1}H}-NMR (152 MHz, C$_6$D$_6$, 298 K, 75 mM, prepared *in-situ*): δ = 3.7 (SiH*Me₂*), 30.6 (C*Me₃*), 30.8 (C*Me₃*), 32.6 (C*Me₃*), 32.7 (C*Me₃*), 34.2 (*C*Me₃), 34.3 (*C*Me₃), 35.6 (*C*Me₃), 35.7 (*C*Me₃), 50.6 (N*C*H₂Bn), 61.67 (N*C*H₂ArO), 61.7 (N*C*H₂ArO), 122.8, 122.9, 123.4, 124.3, 127.2, 127.3, 127.4, 127.6, 128.3 (p-C$_{TPPO}$), 128.9 (d, $J_{P(31)-C(13)}$ = 115 Hz; P-C), 129.1 (d, $J_{P(31)-C(13)}$ = 12.6 Hz; m-C$_{TPPO}$), 132.9 (d, $J_{P(31)-C(13)}$ = 10.9 Hz; o-C$_{TPPO}$), 133.1, 133.4, 133.8, 135.7, 136.0, 136.4, 164.3 (O-C),164.6 ppm (O-C);

^{31}P{^{1}H}-NMR (243 MHz, C$_6$D$_6$, 298 K, 75 mM, prepared *in-situ*): δ = 25.0 (br, free TPPO), 34.6 (d, $J_{Y-P(31)}$ = 10.4 Hz; **1-Y(TPPO)**), 38.3 (d, $J_{Y-P(31)}$ = 12.8 Hz; **[1-Y(TPPO)₂]₂**), 38.9 (d, $J_{Y-P(31)}$ = 10.3 Hz; **1-Y(TPPO)**) ppm;

(*R*)-3-acetoxybutyric acid methylester [(*R*)-3-OAcB^{Me}]
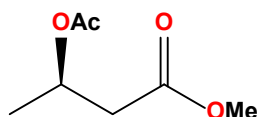
In a 50 mL flask, acetyl chloride (2.40 g, 30.6 mmol, 1.2 equiv.; MW = 78.50) was added to a solution of (*R*)-Methyl 3-hydroxybutanoate (3.01 g, 25.5 mmol, 1.0 equiv.) and pyridine (3.02

g, 38.2 mmol, 1.5 equiv.) in 15 mL CH_2Cl_2. The reaction was stirred at ambient temperature for 6 h. Saturated NH_4Cl solution (15 mL) was added to the reaction, followed by deionized water (15 mL) to dissolve all solids. The organic phase was isolated and washed with saturated NH_4Cl solution (3 x 10 mL). The combined organic layer was evaporated under reduced pressure and redissolved with Et_2O (20 mL). The mixture was dried with Na_2SO_4, filtrated through activated carbon and Celite®, and dried under reduced pressure to yield **(R)-3-OAcB**^{Me} as a colorless oil. Yield: 3.25 g (20.3 mmol, 80% yield; MW: 160.17 g•mol^{-1}). The ^{1}H-NMR spectrum is in agreement with the previous report.[101]

^{1}H-NMR (400 MHz, CDCl$_3$, 298 K): δ = 1.29 (d, J = 6.3 Hz, 3H; CH_Me_), 2.02 (s, 3H; CO_Me_), 2.50 (dd, J = 15.6, 5.8 Hz, 1H; COC_H2_), 2.64 (dd, J = 15.6, 7.4 Hz, 1H; COC_H2_), 3.68 (s, 3H; O_Me_), 5.26 ppm (hex, J = 6.2 Hz, 1H; C_H_);

^{1}H-NMR (400 MHz, C$_6$D$_6$, 298 K): δ = 1.05 (d, J = 6.3 Hz, 3H; CH_Me_), 1.64 (s, 3H; CO_Me_), 2.14 (dd, J = 15.6, 5.6 Hz, 1H; COC_H2_), 2.40 (dd, J = 15.6, 7.4 Hz, 1H; COC_H2_), 3.30 (s, 3H; O_Me_), 5.33 ppm (hex, J = 6.2 Hz, 1H; C_H_).

2.4.3. Experimental Procedures

Typical polymerization procedures

Reactions at ambient temperature:

In a glovebox, a 2 mL scintillation vial was charged with Rare-earth catalyst [e.g. **1-La(TPPO)₂** (5.7 mg, 0.0060 mmol, 1.0 equiv.; MW: 957.27 g•mol^{-1})], neutral ligand [if needed, e.g. TPPO (3.4 mg, 0.012 mmol, 2.0 equiv.; MW: 278.29 g•mol^{-1})] and toluene (0.382 mL). A toluene solution of ^{i}PrOH (2% m/m, 0.021 mL, ρ = 0.867 g/mL; 0.36 mg, 0.0060 mmol, 1.0 equiv.; MW: 60.10 g•mol^{-1}) was then added to the clear colorless solution. After approximately one minute, *rac*-BBL (103 mg, 1.20 mmol, 200 equiv.; MW: 86.09 g•mol^{-1}) was added to the catalyst solution. After 1 h, the reaction was quenched by a methanol solution of AcOH (10% v/v, ca. 0.1 mL), and volatiles were removed under reduced pressure.

Analysis of reaction progress prior to quenching:

An aliquot of the reaction is removed and dissolved in CDCl₃ for NMR analysis without additional quenching. The CDCl₃ solution is evaporated in vacuo for GPC analysis.

Reactions at 0 and –30 °C:

In a glovebox, a J-Young NMR tube was charged with **1-La(TPPO)₂** (8.2 mg, 0.0060 mmol, 1.0 equiv.; MW: 1369.64 g•mol^{-1}) and toluene (0.382 mL). A toluene solution of ^{i}PrOH (2% m/m, 0.021 mL, ρ = 0.867 g/mL; 0.36 mg, 0.0060 mmol, 1.0 equiv.; MW: 60.10 g•mol^{-1}) was then added to the clear colorless solution. After approximately one minute, the solution was then chilled to –30 °C in the glovebox freezer and pre-chilled (–30 °C) *rac*-BBL (103 mg, 1.20 mmol, 200 equiv.; MW: 86.09 g•mol^{-1}) was added to the catalyst solution. The tube was then

immediately removed from the glovebox and reacted in a 0 °C or –30 °C bath. After 1 h, the reaction was quenched by a methanol solution of AcOH (10% v/v, ca. 0.1 mL), and all volatiles were removed under reduced pressure.

NMR studies of relevant catalyst species in the ROP of *rac*-BBL

*Room Temperature (**1–La** + 1 ^{i}PrOH + 1 or 2 equiv. TPPO)*

A screw-capped NMR tube was charged with **1-La** (5.7 mg, 0.0060 mmol, 1.0 equiv.; MW: 957.27 g•mol^{-1}), TPPO (1.7 mg, 0.0060 mmol, 1.0 equiv.; 3.4 mg, 0.012 mmol, 2.0 equiv.; MW: 278.29 g•mol^{-1}), toluene (0.382 mL), and C$_6$D$_6$ (0.025 mL). The sample was removed from the glovebox and NMR spectra were taken. A toluene solution of ^{i}PrOH (2% m/m, 0.021 mL, ρ = 0.867 g/mL; 0.36 mg, 0.0060 mmol, 1.0 equiv.; MW: 60.10 g•mol^{-1}) was added inside the glovebox, and NMR spectra were recorded. *rac*-BBL (103 mg, 1.20 mmol, 200 equiv.; MW: 86.09 g•mol^{-1}) was then added to catalyst solution and NMR spectra were recorded at varying time points. Reaction conversion was determined by ^{1}H-NMR taken immediately before and after the ^{31}P{^{1}H}-NMR spectra were taken.

*–30 °C (**1-La(TPPO)$_2$** + 1 ^{i}PrOH)*

A J-Young NMR tube was charged with **1-La(TPPO)$_2$** (12.0 mg, 0.0088 mmol, 1.0 equiv.; MW: 1369.64 g•mol^{-1}) and toluene-d_8 (0.350 mL). PPh$_3$ (1.0 mg, 0.0040 mmol, 0.45 equiv.; MW: 262.29 g•mol^{-1}) was also added to calibrate line width in the ^{31}P-NMR spectra. The sample was removed from the glovebox, cooled to –30 °C in the NMR spectrometer, and spectra were taken. The sample was then brought inside of the glovebox, and a toluene solution of ^{i}PrOH (2% m/m, 0.031 mL, ρ = 0.867 g/mL; 0.53 mg, 0.0088 mmol, 1.0 equiv; MW: 60.10

g•mol^{-1}) was added to the tube. The sample was cooled to –30 °C in the NMR spectrometer, and spectra were recorded. The sample was then brought inside of the glovebox and chilled in the glovebox freezer to –30 °C. *rac*-BBL (75 mg, 0.88 mmol, 100 equiv.; MW: 86.09 g•mol^{-1}) was chilled at –30 °C, and then added to the NMR tube. The tube was immediately removed from the glovebox and chilled to –78 °C (^{i}PrOH-dry ice bath) for the brief period of time needed to transport the sample to the spectrometer. The sample was then loaded to the pre-cooled spectrometer (–30 °C) and spectra were taken immediately.

After 25 min, the spectrometer was warmed to –15 °C and 0 °C and spectra were recorded after 5 min of thermal equilibration. The total warming process was 30 min, and corresponded to an increase in reaction conversion from 48 to 67% during this time.

Sample for end-group analysis (MALDI-TOF and NMR)

In a glovebox, a 2 mL scintillation vial was charged with **1-La** (37 mg, 0.031 mmol, 1.0 equiv.; MW: 1369.64 g•mol^{-1}) and toluene (0.310 mL). A toluene solution of ^{i}PrOH (2% m/m, 0.109 mL, ρ = 0.867 g/mL; 1.86 mg, 0.031 mmol, 1.0 equiv.; MW: 60.10 g•mol^{-1}) was then added to the clear colorless solution. After approximately one minute, *rac*-BBL (108 mg, 1.25 mmol, 40 equiv.; MW: 86.09 g•mol^{-1}) was added to the catalyst solution. After 1 h, the reaction reached full conversion, was quenched by a drop of acetic acid, and all volatiles were removed under reduced pressure. ^{i}PrOH (1 mL) was added to the residual material precipitating the polymer and the liquid was decanted. The polymer was washed with ^{i}PrOH (1 mL) and dried under reduced pressure. This material was used for NMR, GPC and MALDI analysis.

Measurement of M$_n$ and Đ as a function of conversion

In a glovebox, a 20 mL scintillation vial was charged with **1-La(TPPO)₂** (16.4 mg, 0.012 mmol, 1.0 equiv.; MW: 1369.64 g•mol⁻¹), a Teflon-coated stirbar and toluene (0.763 mL). A toluene solution of ^{i}PrOH (2.0% m/m, 0.042 mL, ρ = 0.867 g/mL; 0.72 mg, 0.012 mmol, 1.0 equiv.; MW: 60.10 g•mol⁻¹) was added to the clear colorless solution. After approximately one minute, *rac*-BBL (207 mg, 2.40 mmol, 200 equiv.; MW: 86.09 g•mol⁻¹) was added to the stirring catalyst solution. After various time, 0.050 mL reaction solution was added to 0.050 mL 5%(m/m) benzoic acid solution in toluene to quench. The quenched mixture was dissolved in 0.5 mL CDCl₃ for NMR analysis. The NMR sample was evaporated under reduced pressure and dissolved in 1 mL THF for GPC analysis.

Reactivity studies of 1-La and 1-La(TPPO)₂ in the presence of 1 equiv ^{i}PrOH and 15 equiv. (*R*)-3-acetoxybutyric acid methylester [(*R*)-3-OAcB^Me]

A screw-capped NMR tube was charged with **1-La** (6.9 mg, 0.0072 mmol, 1.0 equiv.; MW: 957.27 g•mol⁻¹) or **1-La(TPPO)₂** (9.9 mg, 0.0072 mmol, 1.0 equiv.; MW: 1369.64 g•mol⁻¹) and C₆D₆ (0.558 mL). A toluene solution of ^{i}PrOH (2% m/m, 0.025 mL, ρ = 0.867 g/mL; 0.43 mg, 0.0072 mmol, 1.0 equiv.; MW: 60.10 g•mol⁻¹) and **(*R*)-3-OAcB^Me** (17.3 mg, 0.105 mmol, 15 equiv.; MW: 160.17 g•mol⁻¹) were added. NMR spectra were taken at 0.5 h and 7 h.

2.4.4. Supporting Data and Spectra
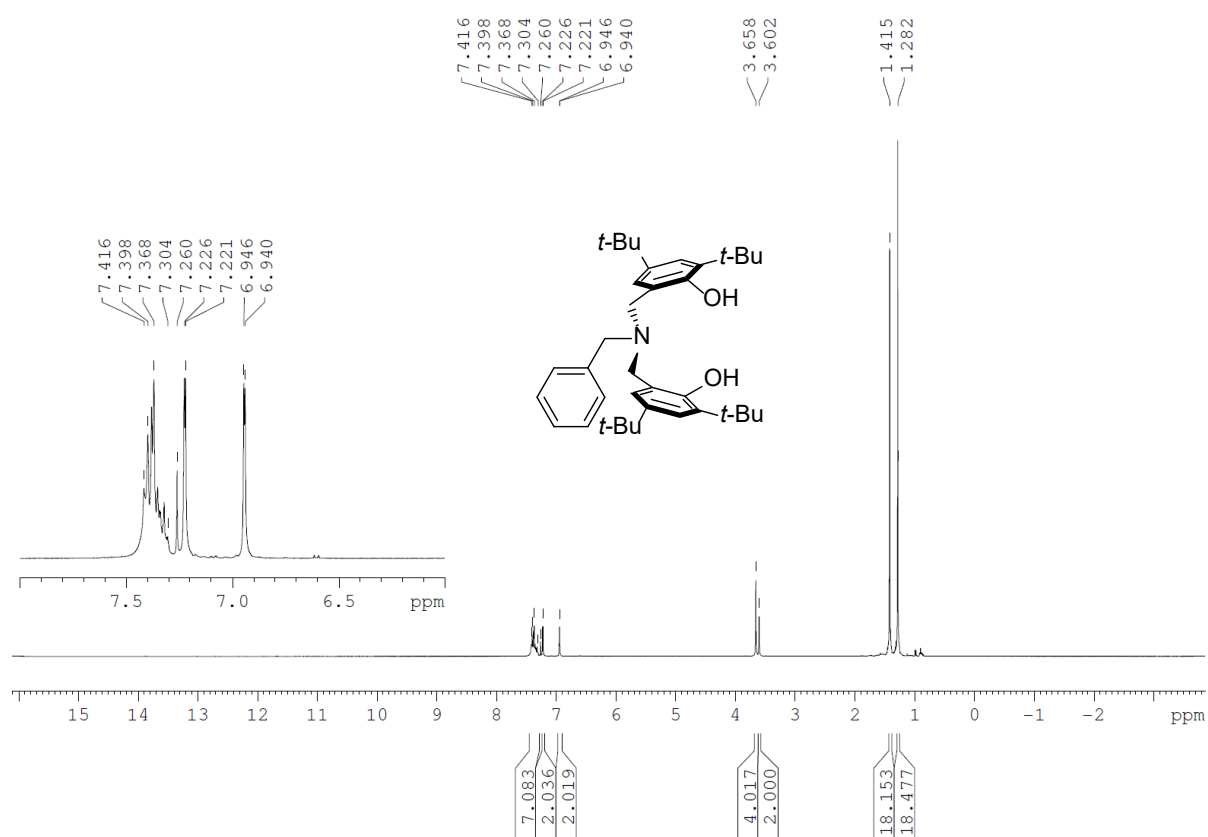
Figure 2.18a. ^{1}H-NMR (CDCl$_3$, 400 MHz) spectra of **H$_2$^{1}L**.
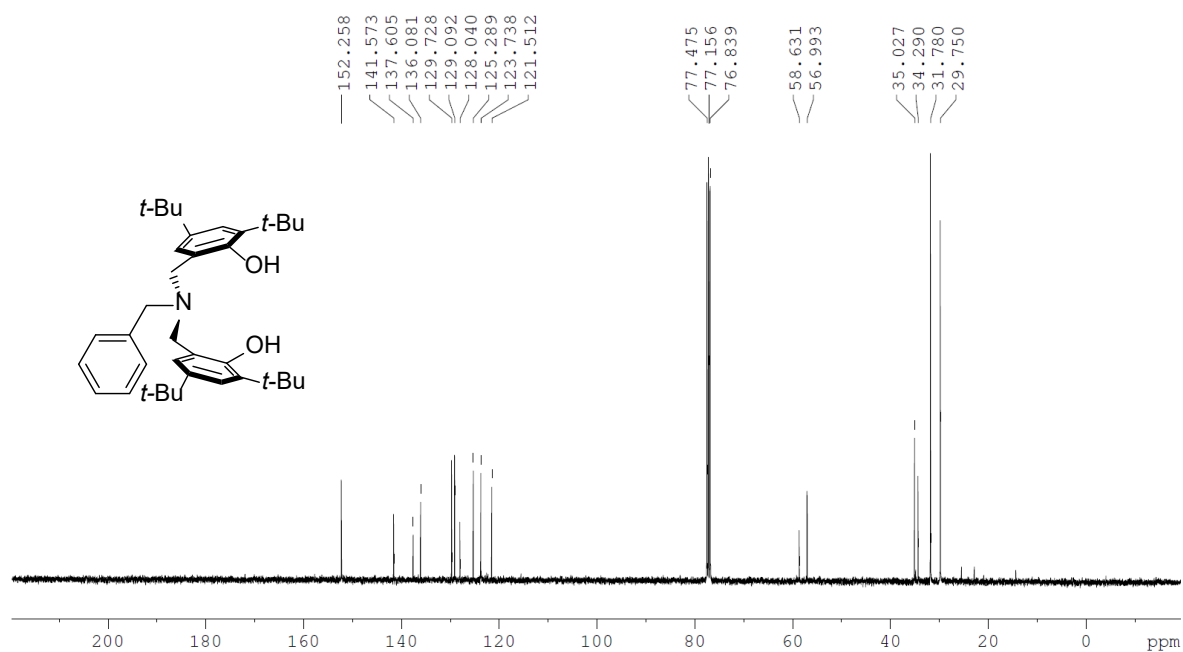
Figure 2.18b. ^{13}C-NMR (CDCl$_3$, 101 MHz) spectra of **H$_2$^{1}L**.
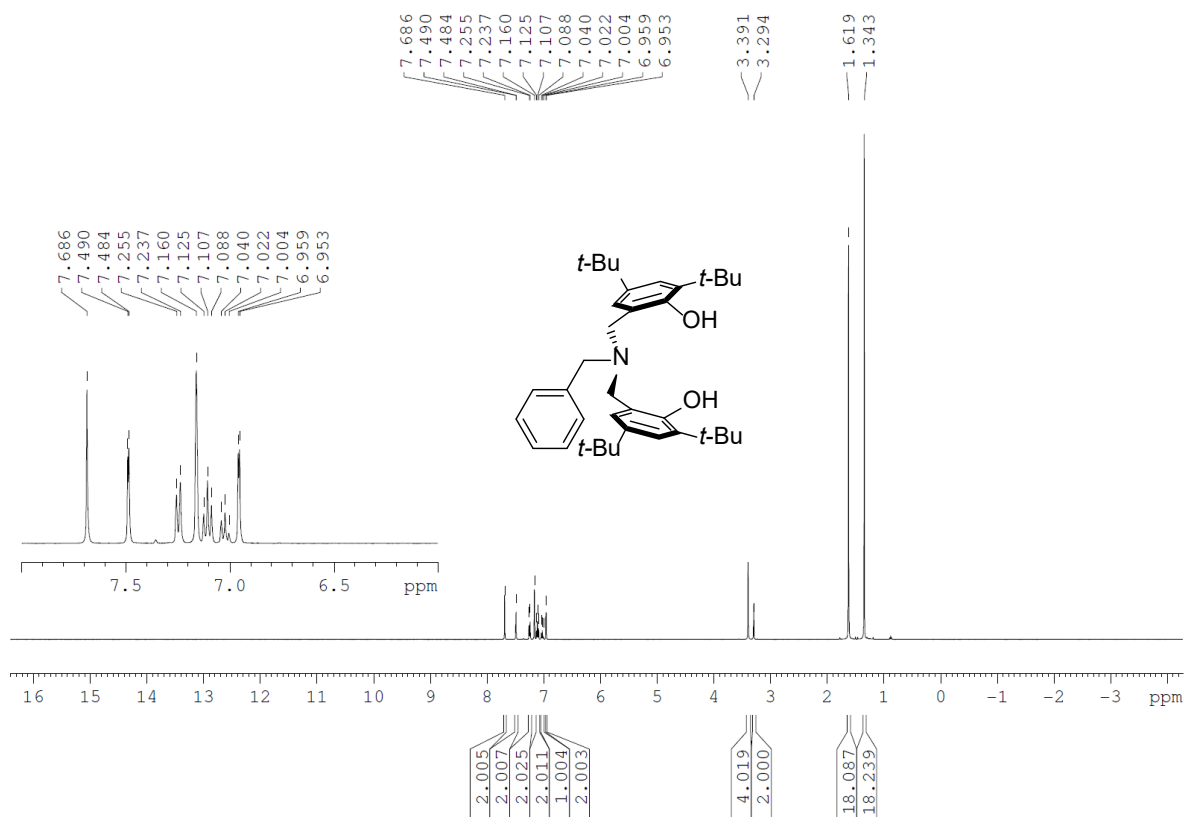
Figure 2.18c. ^{1}H-NMR (C$_6$D$_6$, 400 MHz) spectra of **H$_2$^{1}L**.
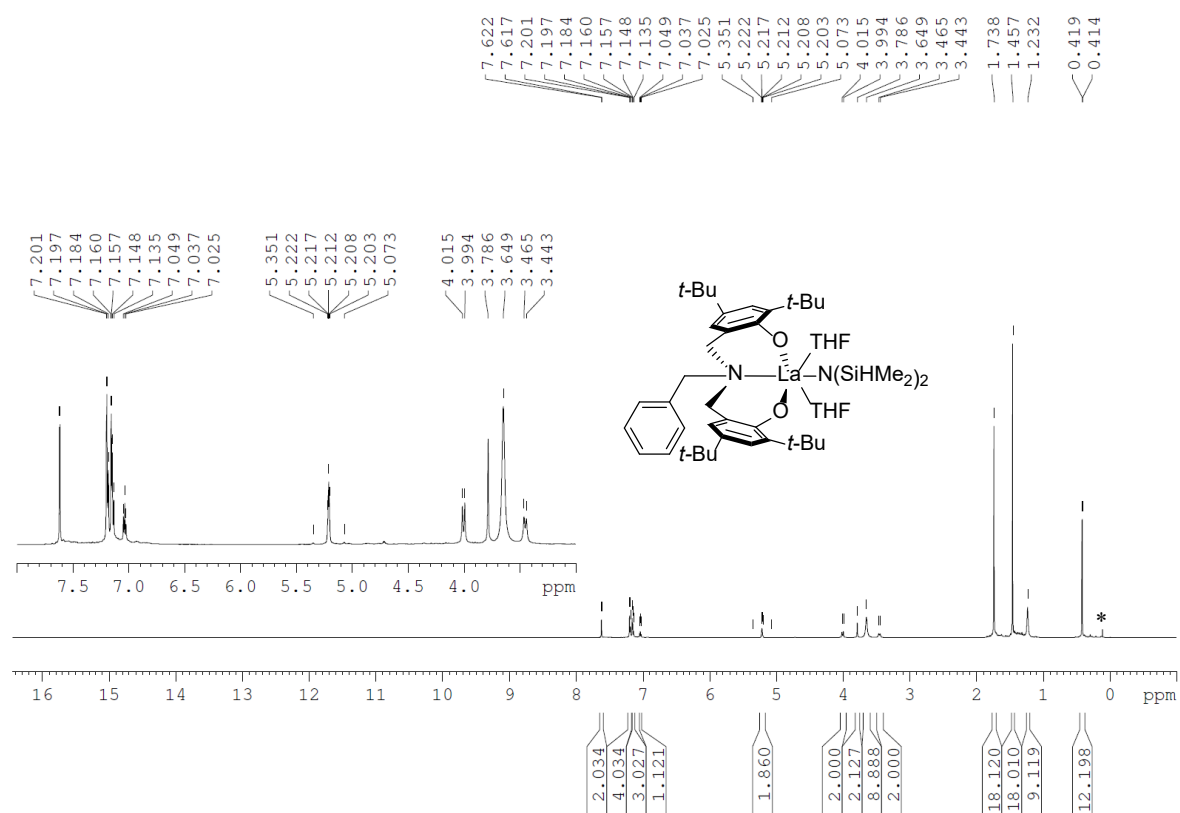
Figure 2.19a. ^{1}H-NMR (C$_6$D$_6$, 600 MHz) spectra of **1-La**.
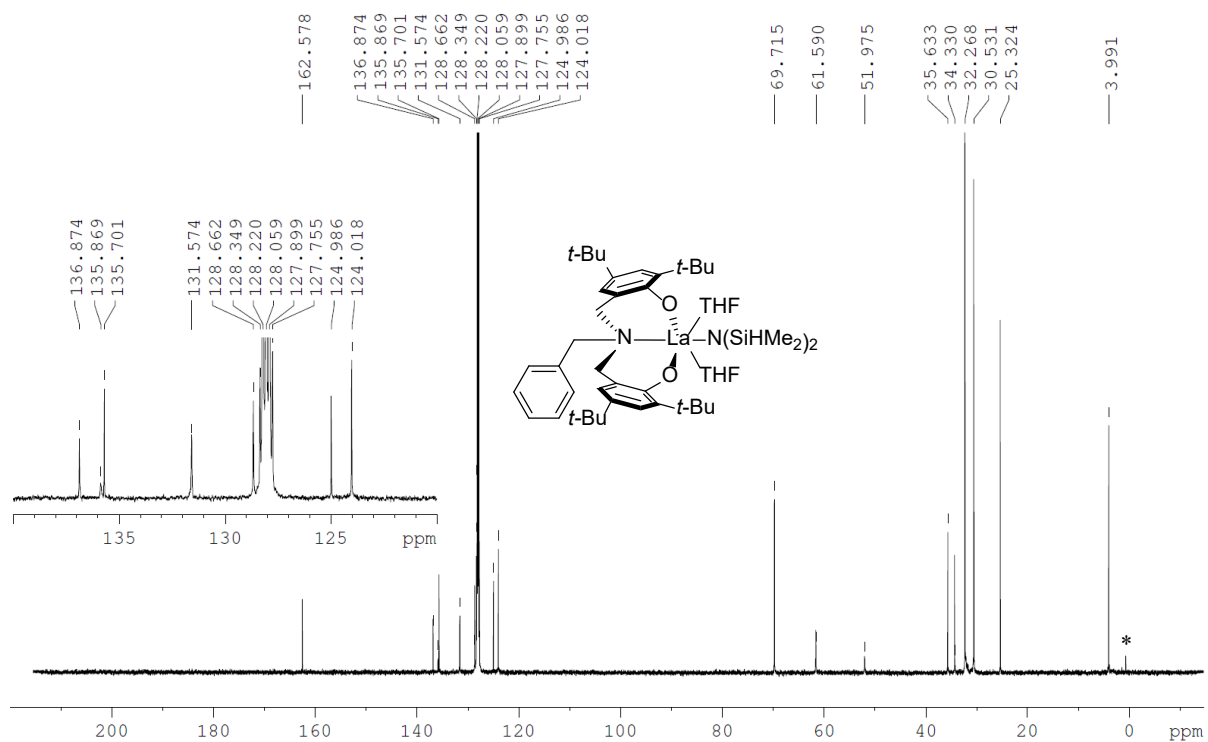
Figure 2.19b. ^{13}C-NMR (C$_6$D$_6$, 152 MHz) spectra of **1-La**.
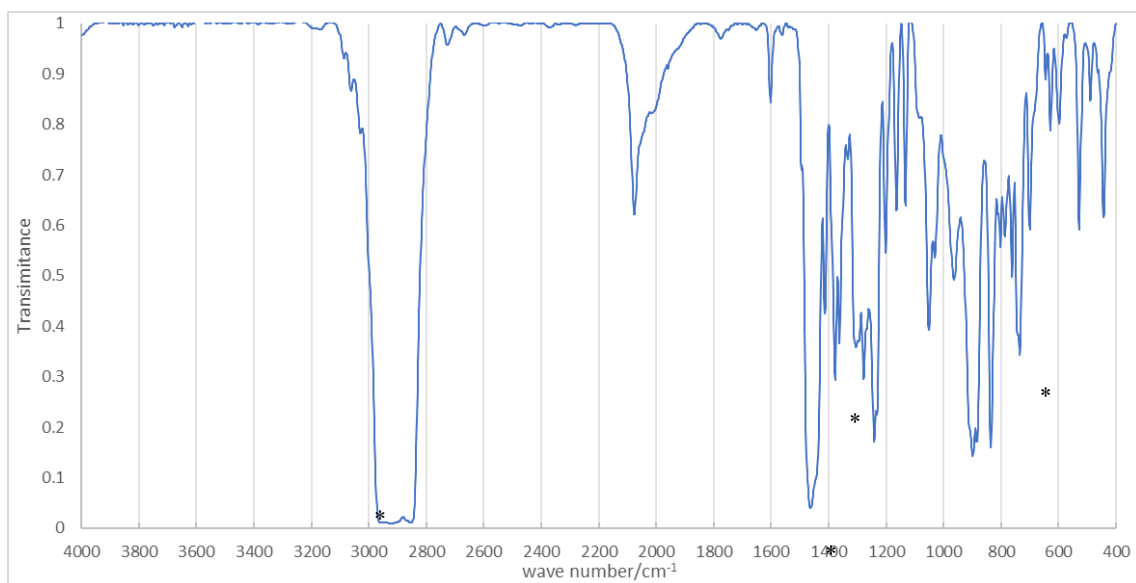
Figure 2.19c. IR (Nujol) spectra of **1-La**. (*: Nujol).
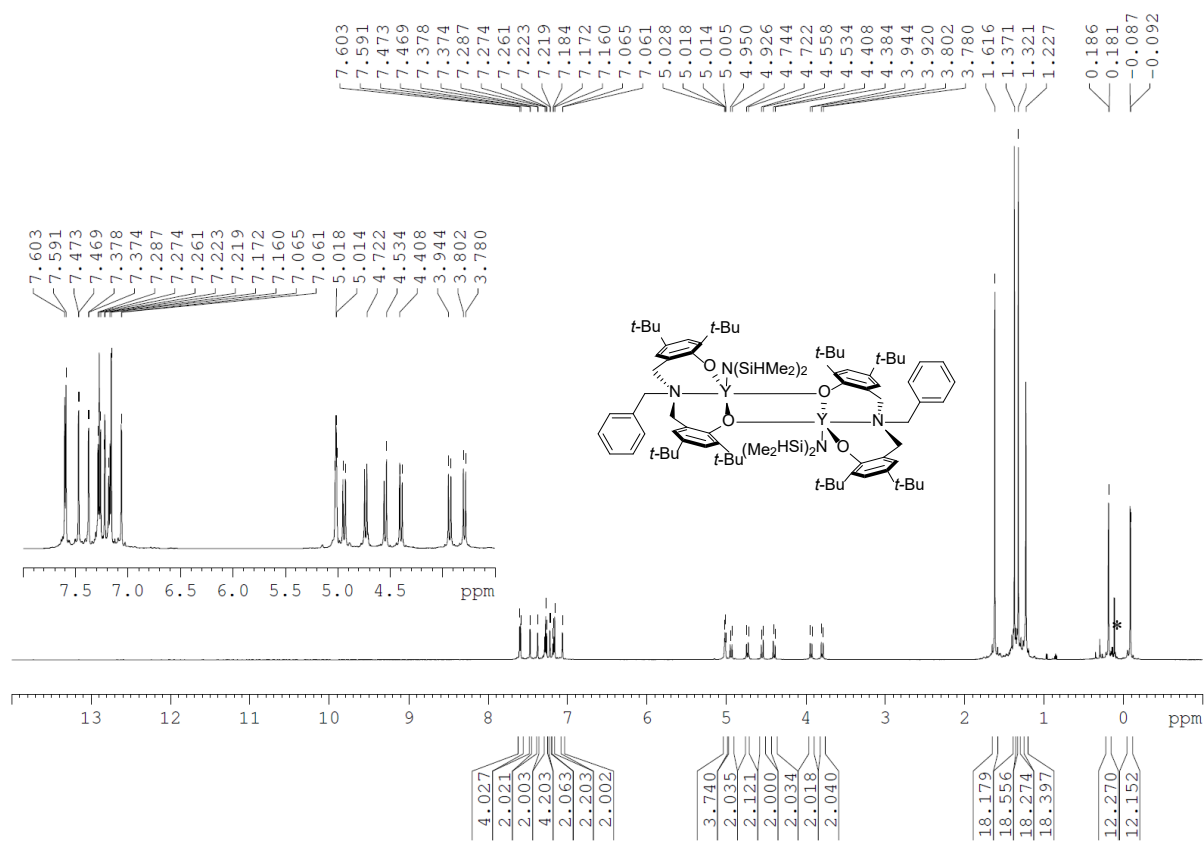
Figure 2.20a. ^{1}H-NMR (C$_6$D$_6$, 600 MHz) spectra of **1-Y$_2$**. (*: HN(SiHMe$_2$)$_2$).
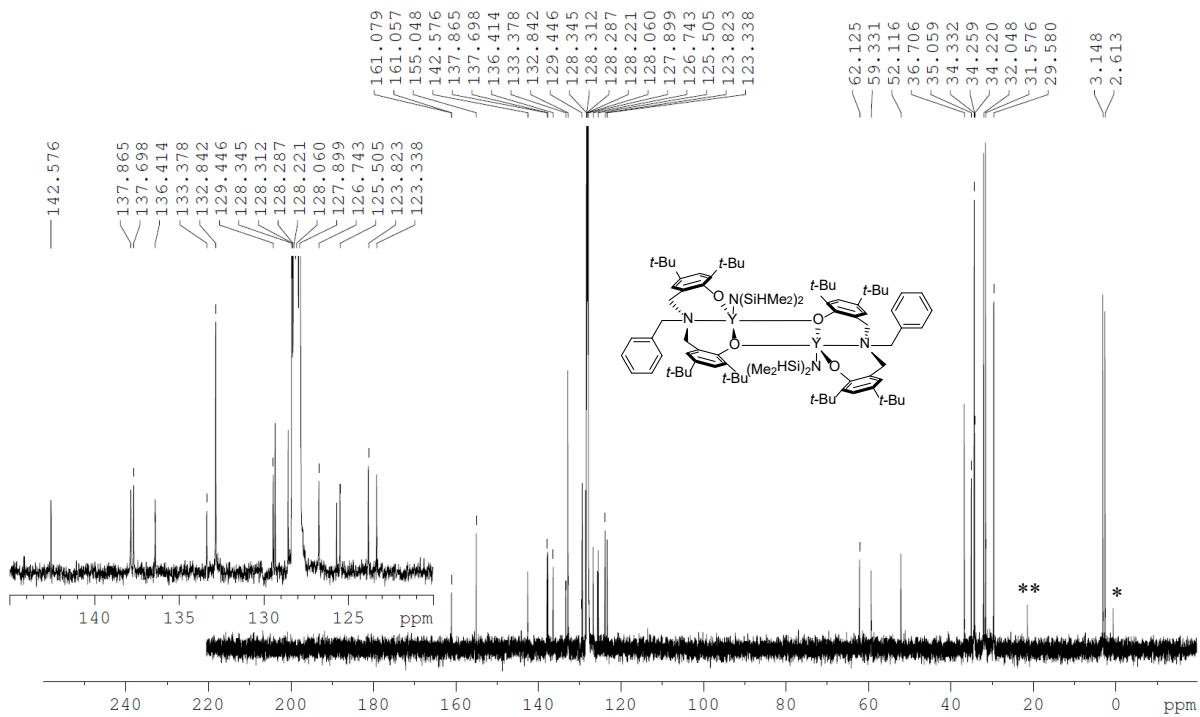
Figure 2.20b. ^{13}C-NMR (C$_6$D$_6$, 152 MHz) spectra of **1-Y$_2$**. (*: HN(SiHMe$_2$)$_2$, **: toluene).
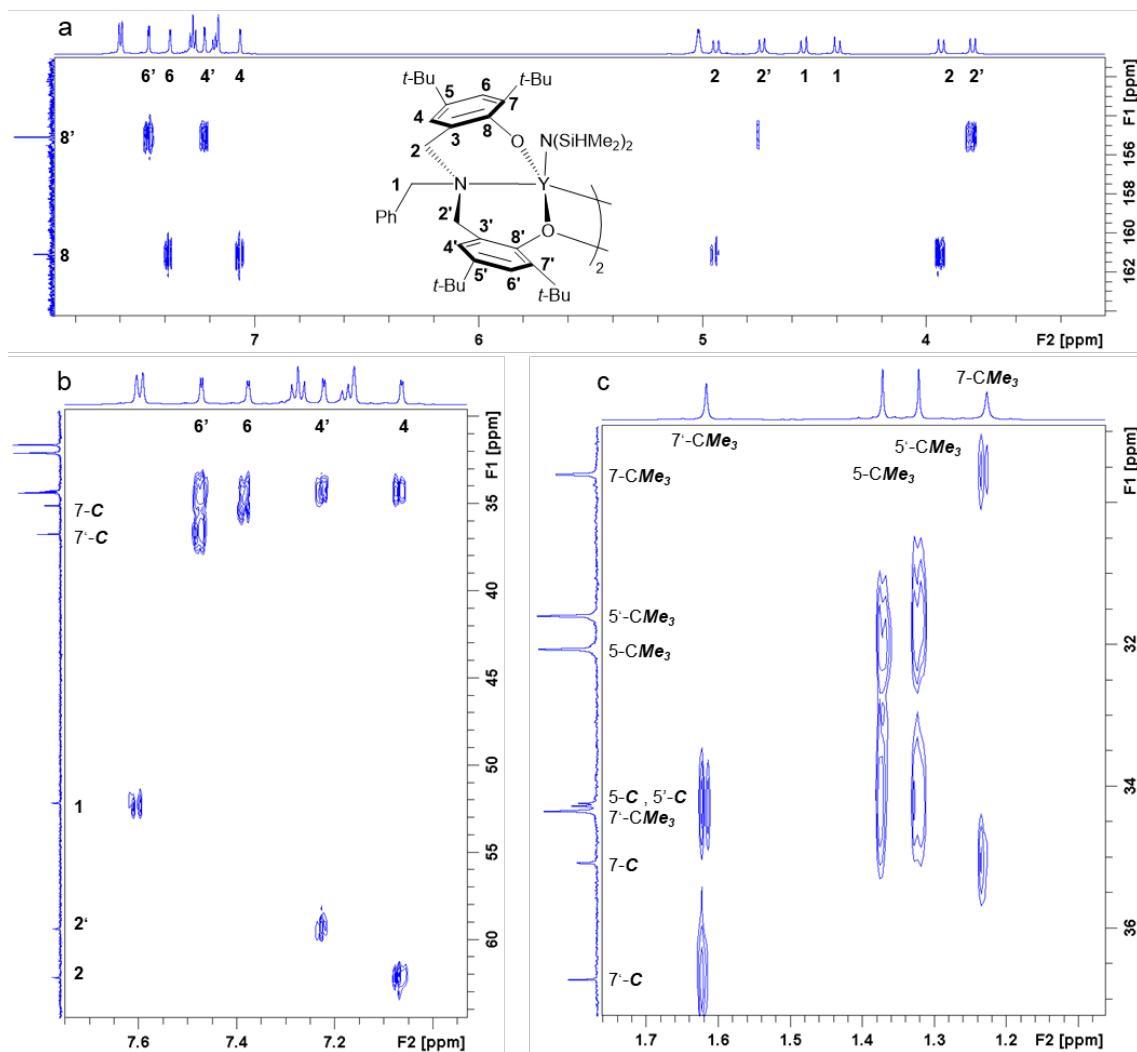
Figure 2.20c. Selected regions of ^{1}H-^{13}C HMBC (600 MHz for ^{1}H in C_6D_6) of **1-Y$_2$**
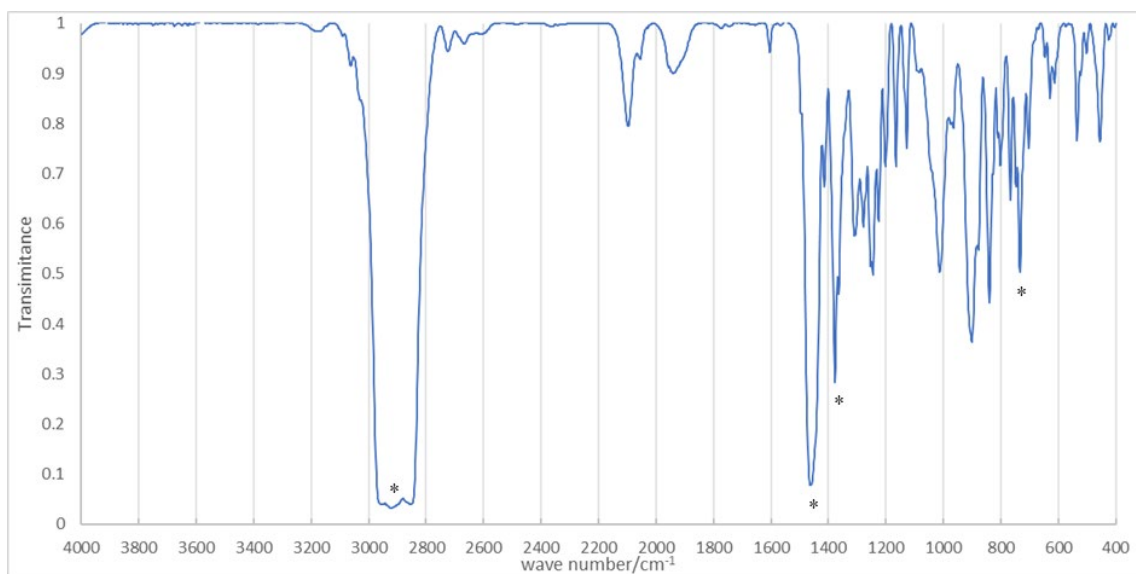
Figure 2.20d. IR (Nujol) spectra of **1-Y$_2$**. (*: Nujol).
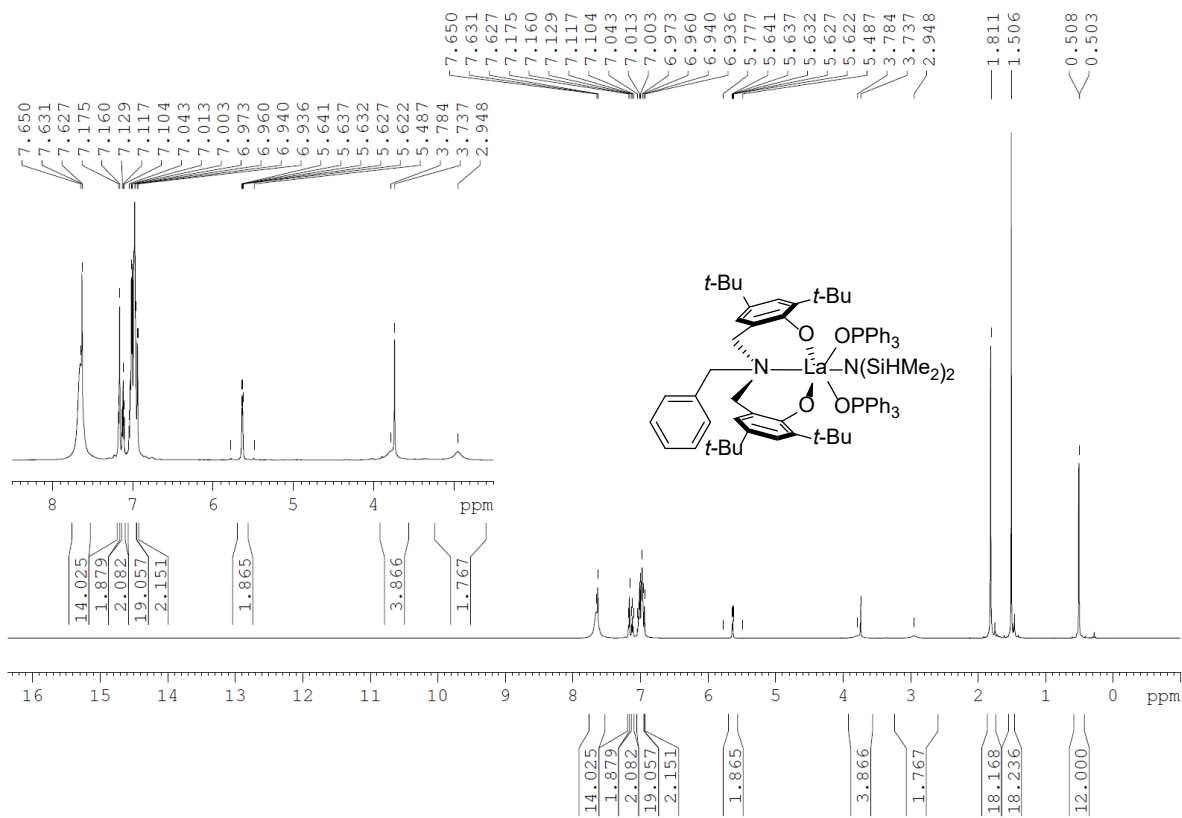
Figure 2.21a. ^{1}H-NMR (C$_6$D$_6$, 600 MHz) spectra of **1-La(TPPO)$_2$**.
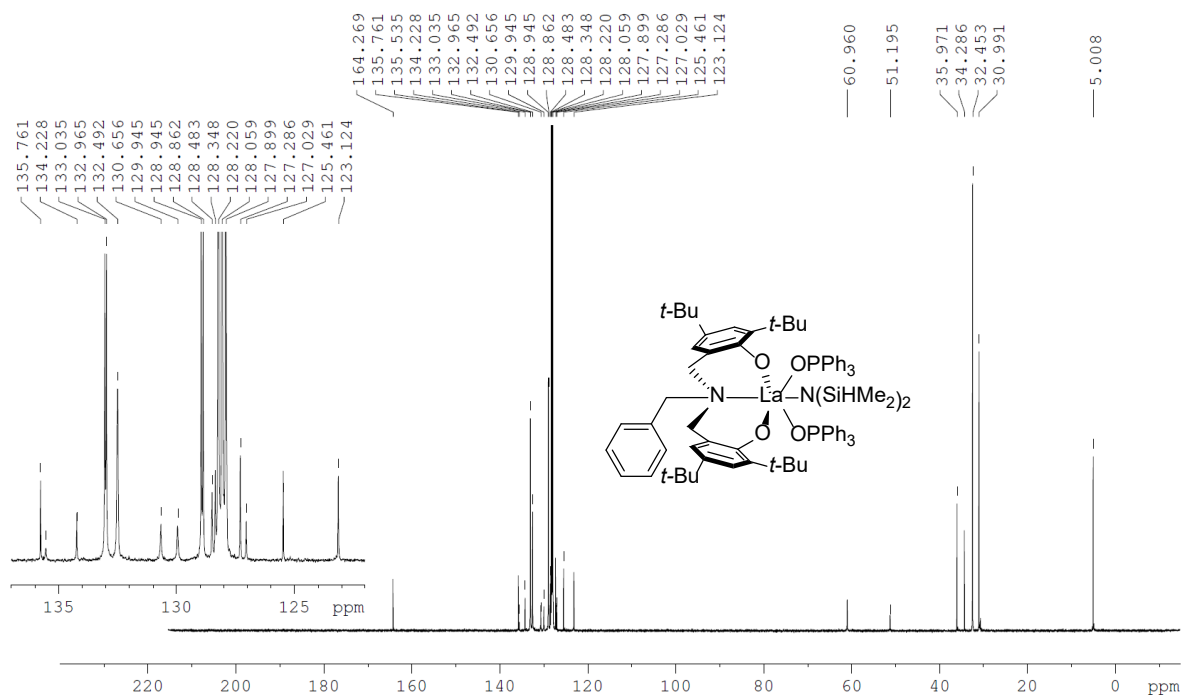
Figure 2.21b. ^{13}C-NMR (C$_6$D$_6$, 152 MHz) spectra of **1-La(TPPO)$_2$.**
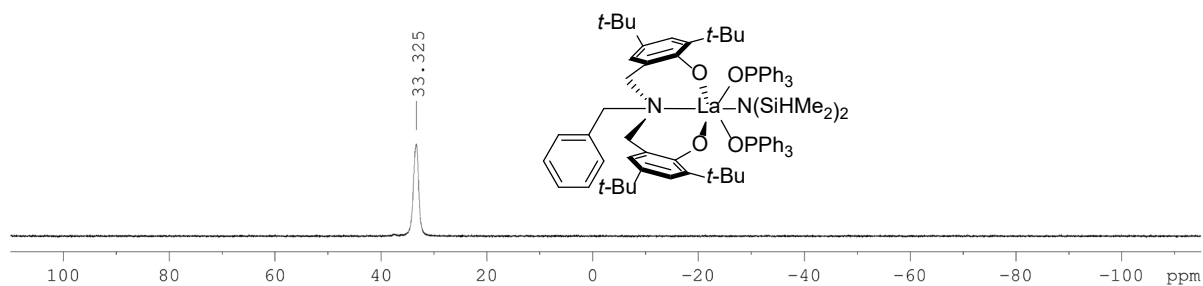
Figure 2.21c. $^{31}P\{^1H\}$-NMR (C$_6$D$_6$, 243 MHz) spectra of **1-La(TPPO)$_2$.**
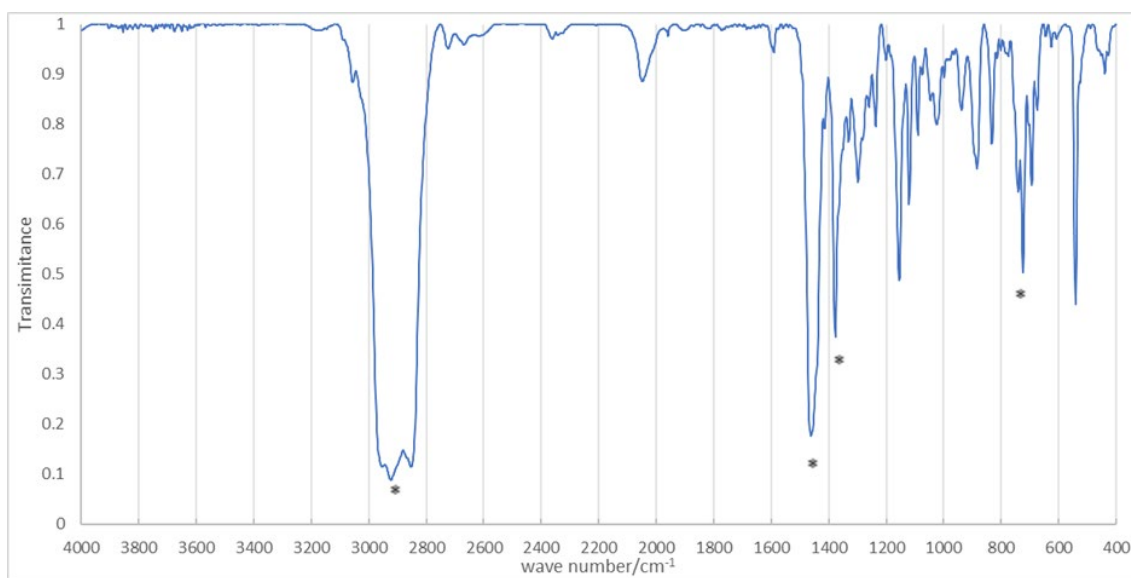
Figure 2.21d. IR (Nujol) spectra of **1-La(TPPO)$_2$**. (*: Nujol).
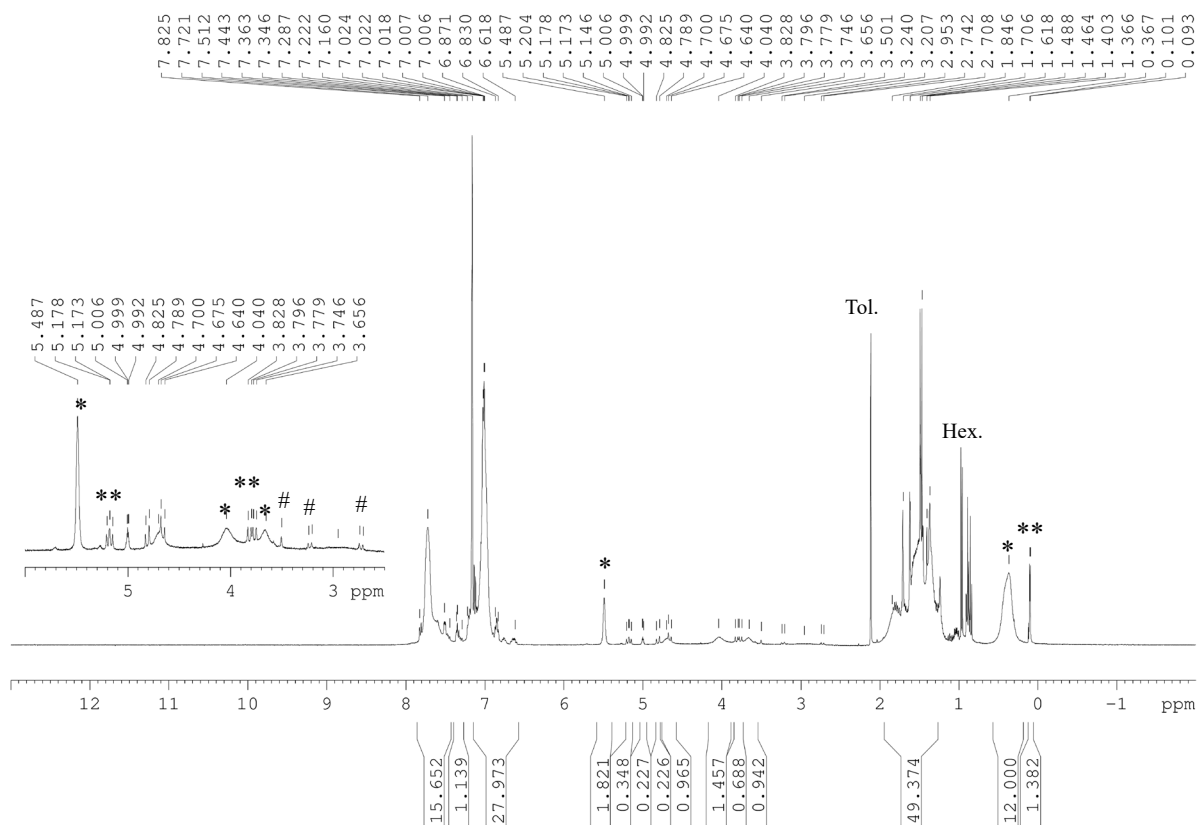
Figure 2.22a. ^{1}H-NMR (C$_{6}$D$_{6}$, 400 MHz, 25 mM) spectra of crystallized **1-Y(TPPO)$_{2}$**. (*: **1-Y(TPPO)$_{2}$**; **: **[1-Y(TPPO)$_{2}$]$_{2}$**; #: **1-Y(TPPO)**).
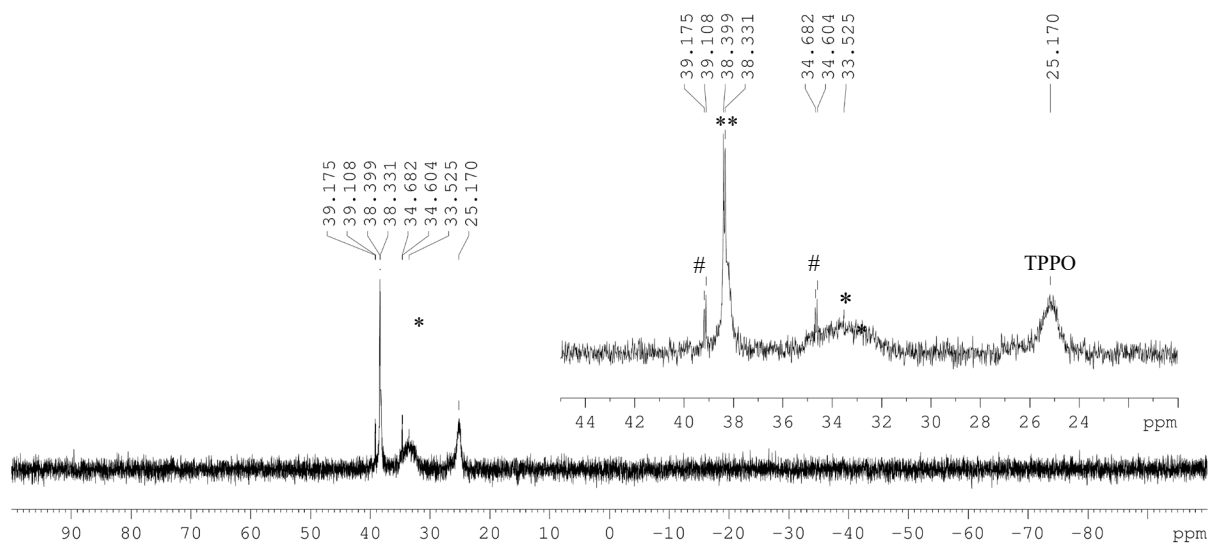
Figure 2.22b. ^{31}P{^{1}H}-NMR (C$_{6}$D$_{6}$, 162 MHz, 25 mM) spectra of crystallized **1-Y(TPPO)$_{2}$**. (*: **1-Y(TPPO)$_{2}$**; **: **[1-Y(TPPO)$_{2}$]$_{2}$**; #: **1-Y(TPPO)**).
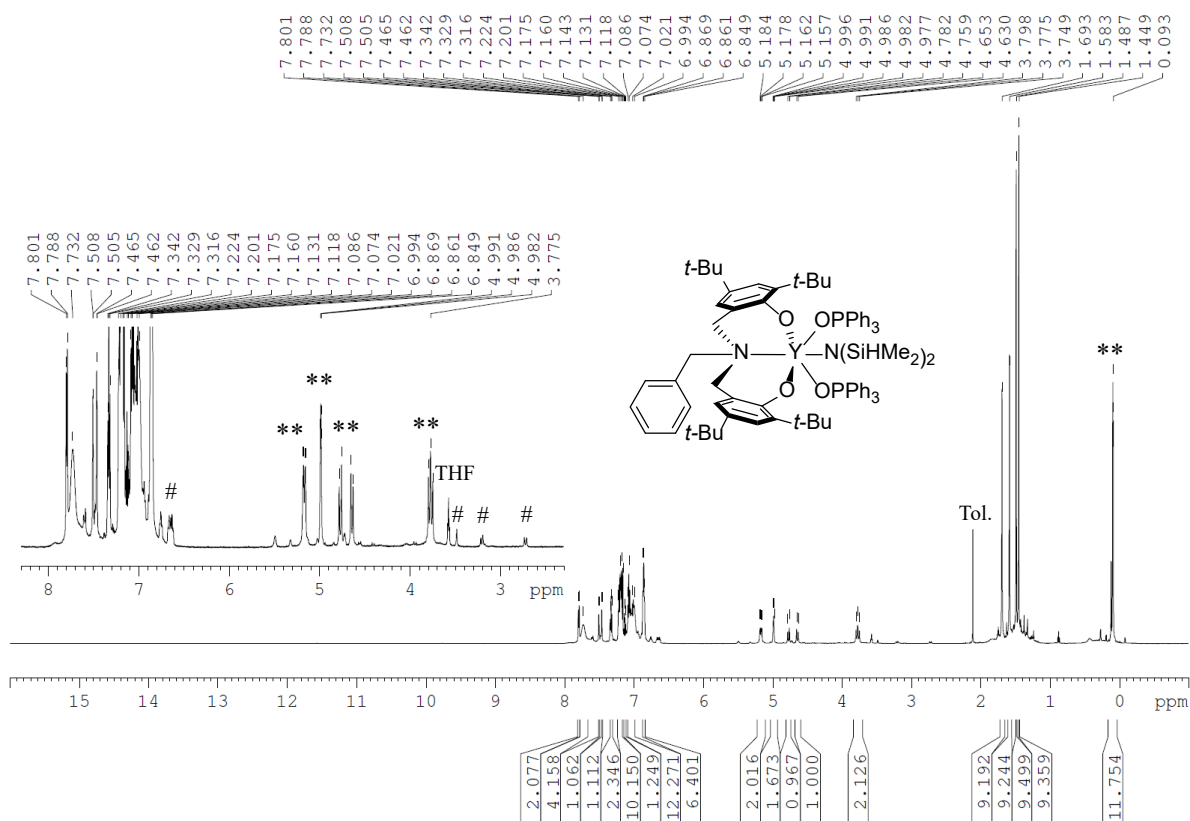
Figure 2.22c. ^{1}H-NMR (C$_6$D$_6$, 600 MHz, 75 mM) spectra of *in-situ* prepared **1-Y(TPPO)$_2$**. (**: [1-Y(TPPO)$_2$]$_2$; #: 1-Y(TPPO)**).
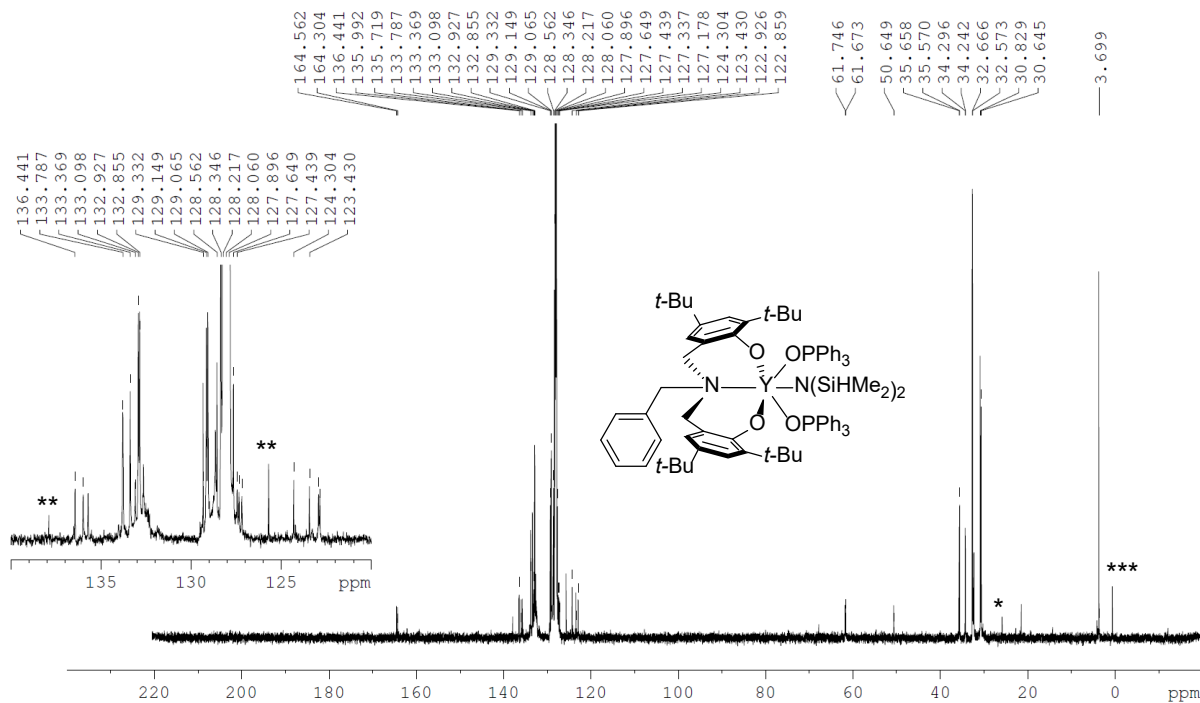
Figure 2.22d. ^{13}C-NMR (C$_6$D$_6$, 152 MHz, 75 mM) spectra of *in-situ* prepared **1-Y(TPPO)$_2$.** (*: THF; **: toluene; ***: HN(SiHMe$_2$)$_2$).
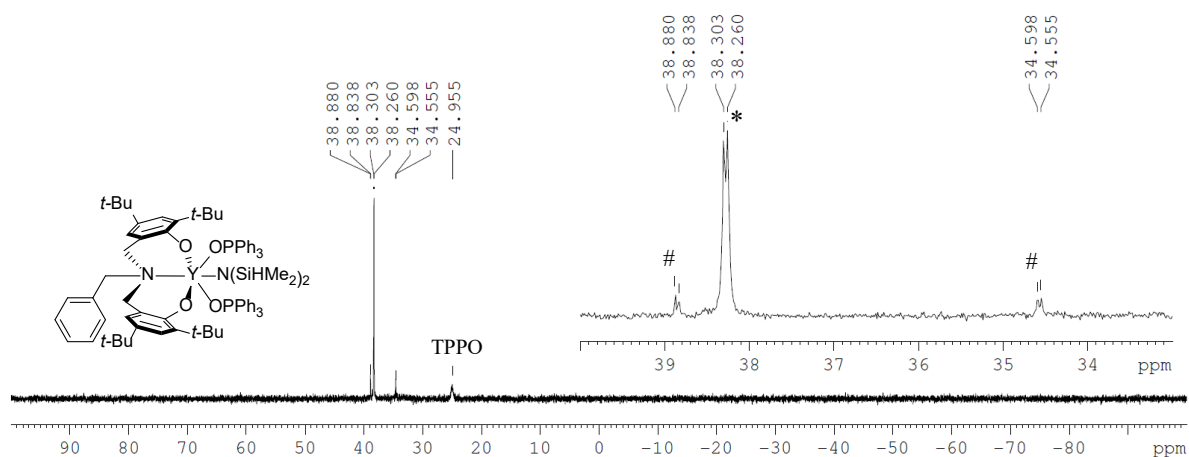
Figure 2.22e. $^{31}P\{^1H\}$-NMR (C$_6$D$_6$, 243 MHz, 75 mM) spectra of *in-situ* prepared **1-Y(TPPO)$_2$**. (**: **[1-Y(TPPO)$_2$]$_2$**; #: **1-Y(TPPO)**).
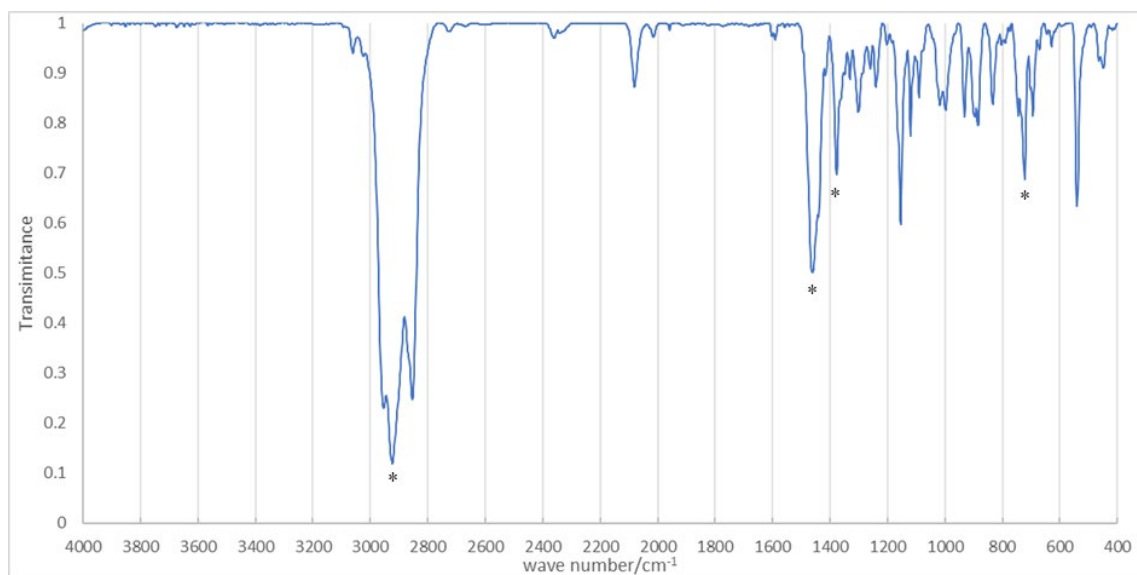
Figure 2.22f. IR (Nujol) spectra of **1-Y(TPPO)$_2$**. (*: Nujol).
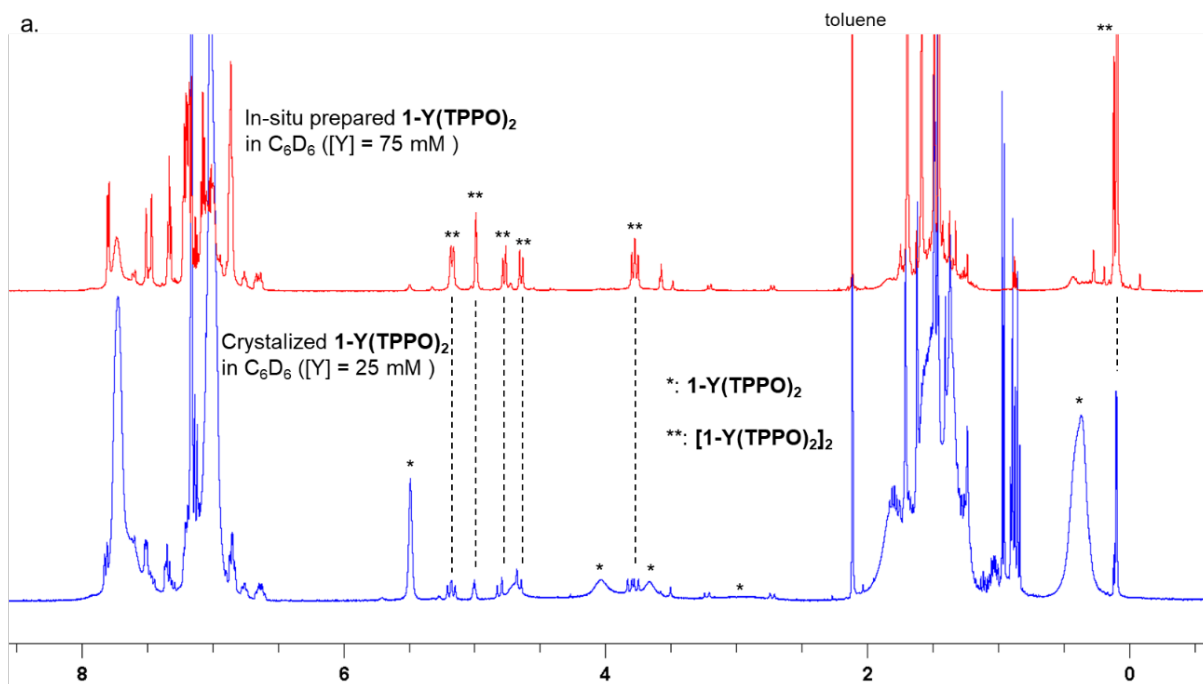
Figure 2.23a. ^{1}H-NMR (600 MHz, C$_6$D$_6$, 298 K) of **1-Y(TPPO)$_2$** prepared in-situ from **1-Y$_2$** and TPPO (75 mM [Y], 2 equiv TPPO / [Y]; red, top) and re-dissolved crystalline **1-Y(TPPO)$_2$** (25 mM, blue, bottom).
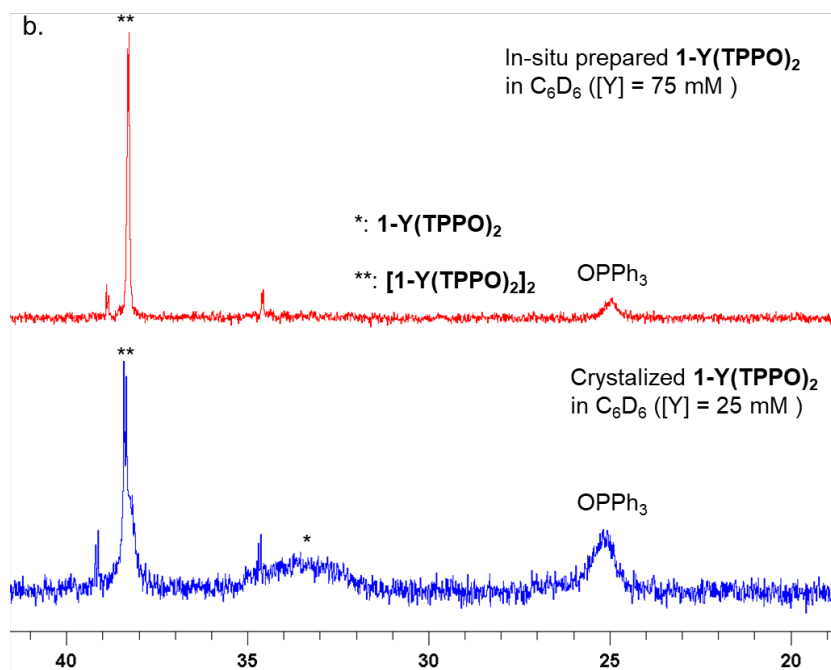
Figure 2.23b. ^{31}P{^{1}H}-NMR (243 MHz, C$_6$D$_6$, 298 K) of **1-Y(TPPO)$_2$** prepared in-situ from **1-Y$_2$** and TPPO (75 mM [Y], 2 equiv TPPO / [Y]; red, top) and re-dissolved crystalline **1-Y(TPPO)$_2$** (25 mM, blue, bottom).

Table 2.9. Diffusion coefficients, D, and estimated hydrodynamic radii, r_H, measured by ^{1}H DOSY NMR of **1-RE** complexes (**1-La, 1-La(TPPO)$_2$, 1-Y$_2$, 1-Y(TPPO)$_2$ and [1-Y(TPPO)$_2$]$_2$**)

Species	D_{Fc} (10^{-10} m^2/s)^a	D (10^{-10} m^2/s)	D_{Fc}/D	r_H(DOSY)^b (Å)	r_H(theo.)^c (Å)
Fc^d	-	-	-	-	2.166
1-La	13.2	5.10	2.59	5.61	6.011
1-La(TPPO)$_2$	12.8	4.13	3.10	6.71	6.764
1-Y$_2$	11.8	3.56	3.31	7.18	7.361^e
1-Y(TPPO)$_2$^{f}	11.1	3.54	3.14	6.79	6.791
[1-Y(TPPO)$_2$]$_2$^{f}	11.1	2.37	4.68	10.14	-

a – DOSY measured diffusion coefficient of ferrocene (Fc) in the experiment of the corresponding complex. DOSY measured diffusion coefficient of the sample *b* – $r_H = D_{Fc}/D_{sample} \cdot r_H$(Fc, theo.). *c* – r_H(theo.) is the average of half lengths of the principal axes of the homogeneous ellipsoid with the same principal moments of inertia of the molecule, which are determined from the crystal structure. *d* – Fc was added to each sample as an internal standard to cancel the fluctuation of temperature and viscosity, of which the diffusion coefficient varies. *e* – Estimated according to structure of **3-Y$_2$**,[12] due to the lack of X-ray structure of **1-Y$_2$**. *f* – Prepared *in-situ* with **1-Y$_2$** and addition of TPPO (2 equiv).
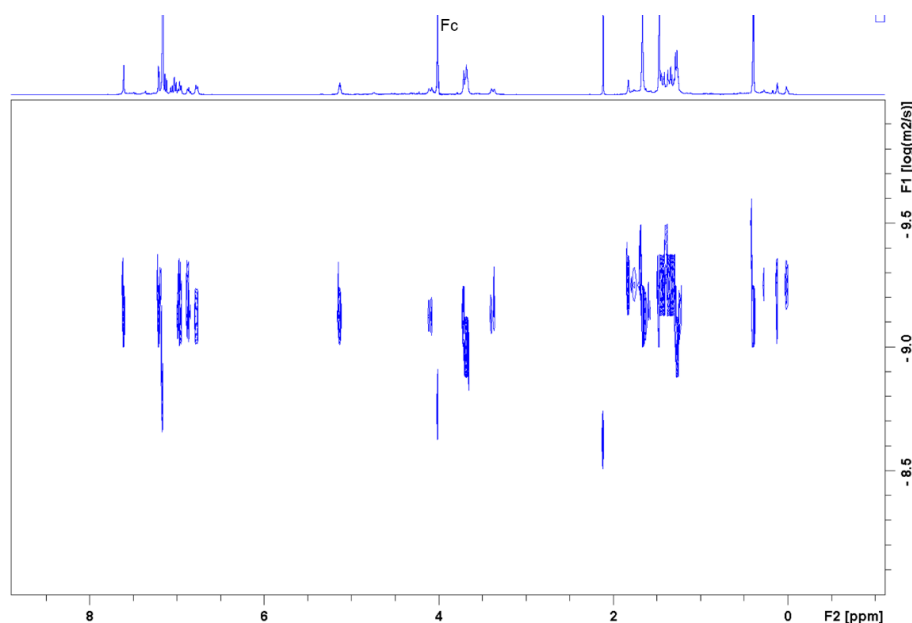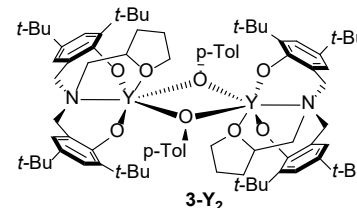
Figure 2.24. ^{1}H DOSY NMR (400 MHz, C$_6$D$_6$) of a mixture of **1-La** and ferrocene (Fc). In 0.5 mL C$_6$D$_6$, **1-La** (10 mg, 0.010 mmol, 1.0 equiv; MW: 957.27 g•mol^{-1}) and Fc (3.2 mg, 0.017 mmol, 1.7 equiv; MW: 186.04 g•mol^{-1}) were dissolved. Diffusion time was (Δ, d20) 100 ms, and the rectangular gradient pulse duration (δ, p30) was 1200 µs.
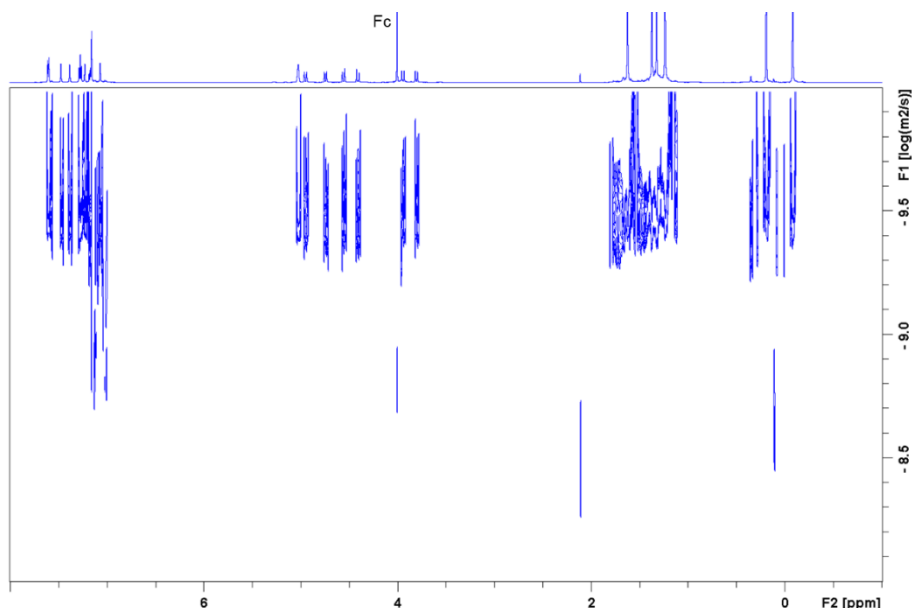
Figure 2.25. ^{1}H DOSY NMR (600 MHz, C$_6$D$_6$) of a mixture of **1-Y$_2$** and Fc. In 0.5 mL C$_6$D$_6$, **1-Y$_2$** (10 mg, 0.007 mmol, 1.0 equiv; MW: 1526.12 g•mol^{-1}) and Fc (0.4 mg, 0.002 mmol, 0.34 equiv; MW: 186.04 g•mol^{-1}) were dissolved. Diffusion time was (Δ, d20) 100 ms, and the rectangular gradient pulse duration (δ, p30) was 1000 µs.
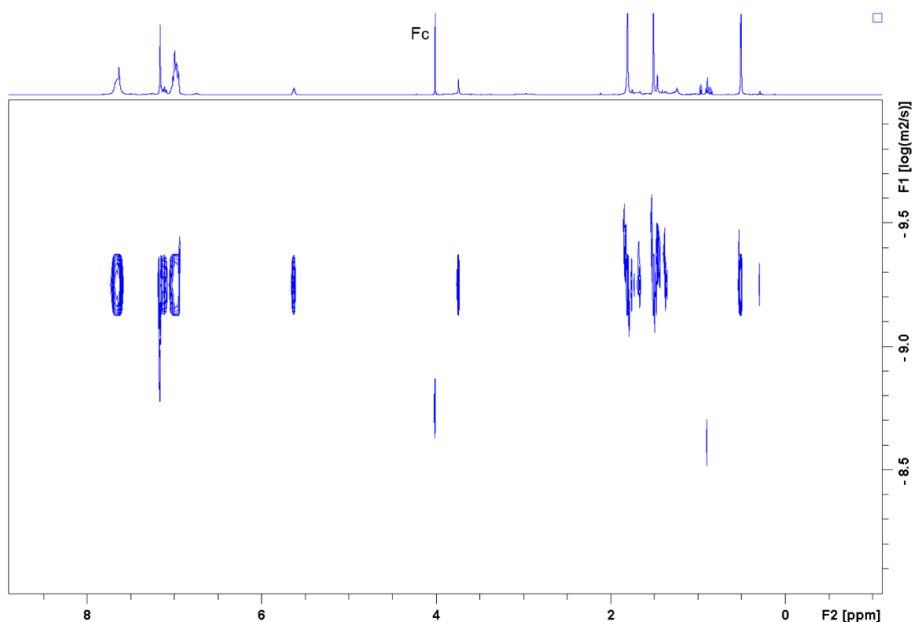
Figure 2.26. ^{1}H DOSY NMR (400 MHz, C$_6$D$_6$) of a mixture of **1-La(TPPO)$_2$** and Fc. In 0.5 mL C$_6$D$_6$, **1-La** (10 mg, 0.007 mmol, 1.0 equiv; MW: 1369.64 g•mol^{-1}) and Fc (0.5 mg, 0.003 mmol, 0.37 equiv; MW: 186.04 g•mol^{-1}) were dissolved. Diffusion time was (Δ, d20) 100 ms, and the rectangular gradient pulse duration (δ, p30) was 1200 µs.
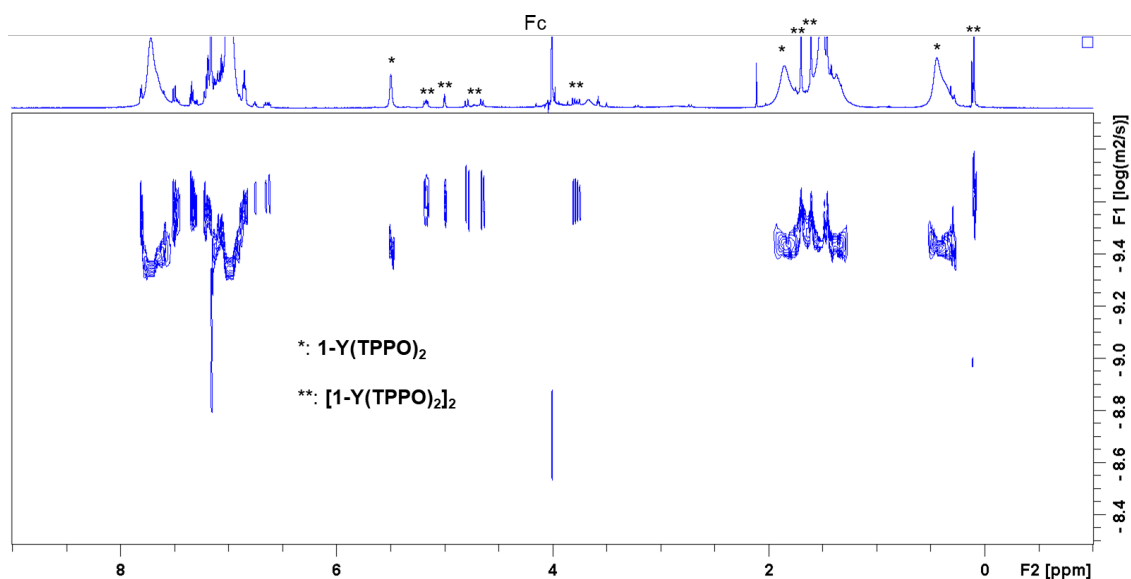
Figure 2.27. ^{1}H DOSY NMR (600 MHz, C$_6$D$_6$) of a mixture of **1-Y(TPPO)$_2$**, and Fc. In 0.5 mL C$_6$D$_6$, **1-Y(TPPO)$_2$** (16 mg, 0.012 mmol, 1.0 equiv; MW: 1319.64 g•mol^{-1}), and Fc (0.4 mg, 0.002 mmol, 0.17 equiv; MW: 186.04 g•mol^{-1}) were dissolved. 1 h later, DOSY was taken. Diffusion time was (Δ, d20) 100 ms, and the rectangular gradient pulse duration (δ, p30) was 1400 μs.
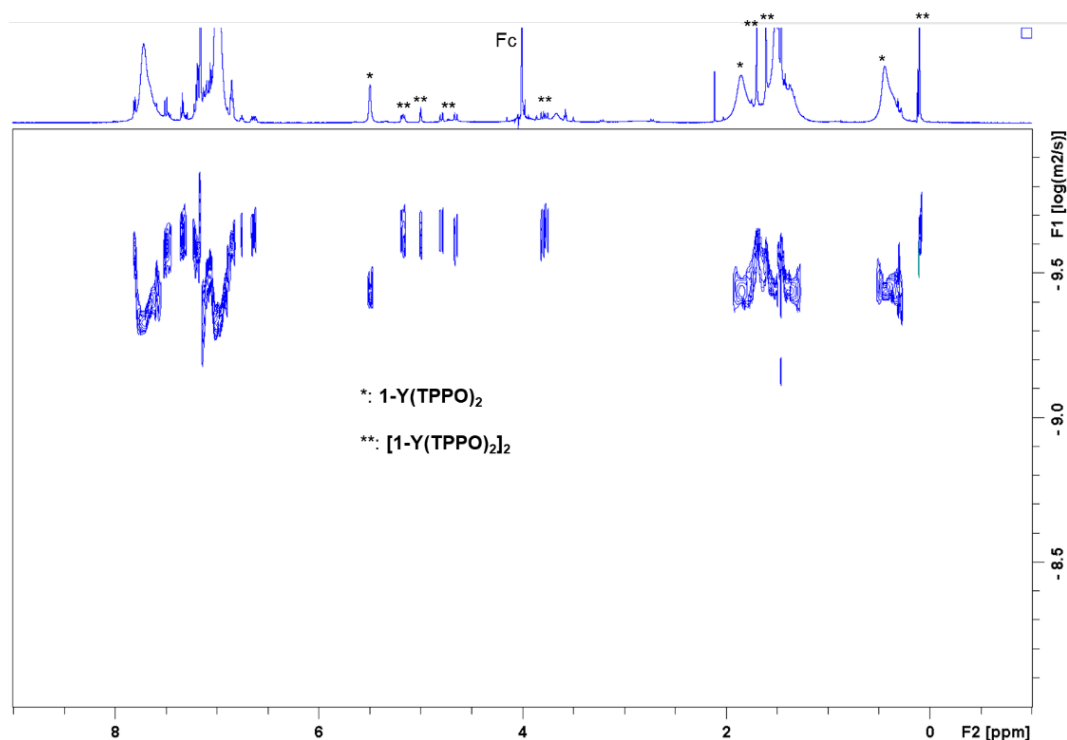
Figure 2.28. ^{1}H DOSY NMR (600 MHz, C$_6$D$_6$) of a mixture of **1-Y$_2$**, Fc, and TPPO. In 0.5 mL C$_6$D$_6$, **1-Y$_2$** (10 mg, 0.007 mmol, 1.0 equiv; MW: 1526.12 g•mol^{-1}), Fc (0.4 mg, 0.002 mmol, 0.34 equiv; MW: 186.04 g•mol^{-1}) and TPPO (7.3 mg, 0.007 mmol, 4.0 equiv; MW: 278.29 g•mol^{-1}) were dissolved. 7 h later, DOSY was taken. Diffusion time was (Δ, d20) 100 ms, and the rectangular gradient pulse duration (δ, p30) was 1400 μs. **Note:** Spectrum was nearly identical to authentic **1-Y(TPPO)$_2$** (Figure 2.27, nearly the same [Y] concentration).
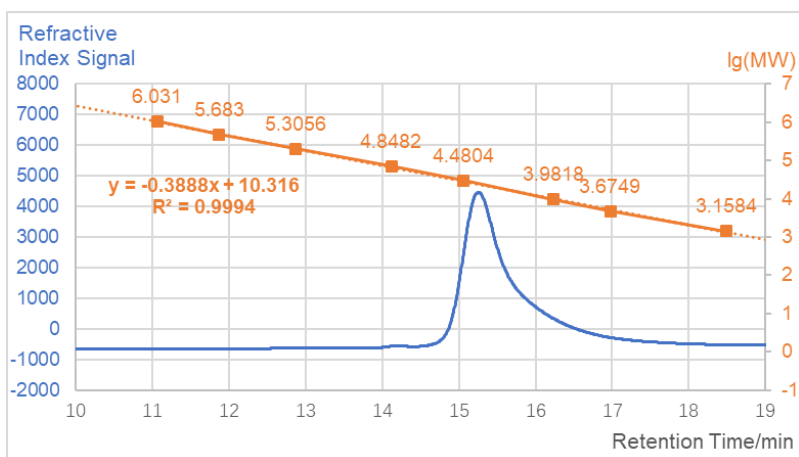
Figure 2.29. GPC calibration curve using polystyrene standards (orange) and GPC trace (blue) of Table 2.3, entry 6. Reaction was performed in toluene at ambient temperature with [BBL]/[**1-La**]/[TPPO]/[^{i}PrOH] = 200/1/2/1 and [BBL] = 2.4 M within 1 h. Conversion = 97%, M_n = 9.6 kg/mol (corrected by Mark-Houwink factor of 0.54), $Đ$ = 1.18
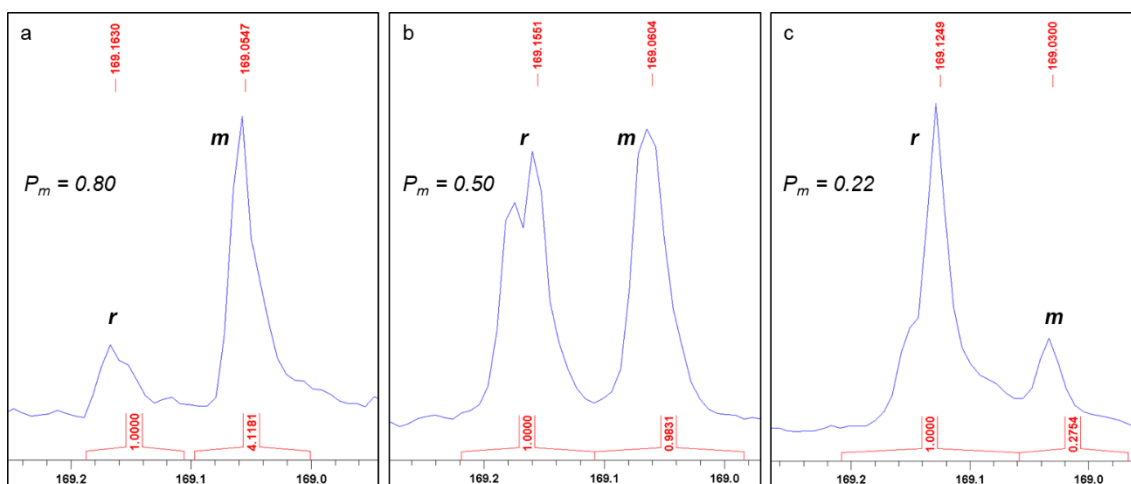
Figure 2.30. Carbonyl region of IG-^{13}C-NMR (152 MHz, CDCl$_3$) of P3HB with different P_m. (a) Table 2.5, entry 4 (**1-La** + 2 TPPO + ^{i}PrOH, –30 °C), (b) Table 2.8, entry 7 (0.5 **1-Y$_2$** + 2 TPPO + ^{i}PrOH), (c) Table 2.8, entry 8 (**2-Y** + ^{i}PrOH).

Table 2.10. Crystallographic parameters for compounds **1-La**, **1-La(TPPO)₂**, and **1-Y(TPPO)₂**

	1-La	1-La(TPPO)₂	1-Y(TPPO)2
Empirical formula	$C_{49}H_{83}LaN_2O_4Si_2$	$C_{91}H_{111}LaN_2O_4P_2Si_2$	$C_{91}H_{111}N_2O_4P_2Si_2Y$
Formula weight	959.26	1553.84	1503.84
Temperature/K	173.2	173.21	173.19
Crystal system	monoclinic	monoclinic	monoclinic
Space group	$P2_1/c$	$P2_1/n$	$P2_1/n$
a/Å	17.0458(16)	15.355(2)	15.2210(16)
b/Å	16.5877(16)	15.378(2)	15.3725(15)
c/Å	19.5942(17)	35.734(5)	35.552(4)
α/°	90	90	90
β/°	112.851(3)	94.563(5)	93.759(3)
γ/°	90	90	90
Volume/Å³	5105.5(8)	8411(2)	8300.7(15)
Z	4	4	4
ρ_{calc}g/cm³	1.248	1.227	1.203
μ/mm⁻¹	0.925	0.624	0.820
F(000)	2032.0	3272.0	3200.0
Crystal size/mm³	0.25 × 0.25 × 0.2	0.14 × 0.12 × 0.1	0.3 × 0.2 × 0.1
Radiation	MoKα (λ = 0.71073)	MoKα (λ = 0.71073)	MoKα (λ = 0.71073)
2Θ range for data collection/°	3.57 to 55.872	3.862 to 55.2	3.992 to 55.156
Index ranges	-22 ≤ h ≤ 22, -21 ≤ k ≤ 21, -25 ≤ l ≤ 25	-19 ≤ h ≤ 20, -20 ≤ k ≤ 19, -46 ≤ l ≤ 44	-19 ≤ h ≤ 19, -19 ≤ k ≤ 19, -46 ≤ l ≤ 46
Reflections collected	192582	152196	166733
Independent reflections	11709 [R_{int} = 0.1329, R_{sigma} = 0.0585]	19424 [R_{int} = 0.1040, R_{sigma} = 0.0594]	19123 [R_{int} = 0.0829, R_{sigma} = 0.0489]
Data/restraints/parameters	11709/0/549	19424/175/886	19123/164/875
Goodness-of-fit on F²	1.022	1.046	1.018
Final R indexes [I>=2σ (I)]	R_1 = 0.0527, wR_2 = 0.0906	R_1 = 0.0528, wR_2 = 0.1315	R_1 = 0.0477, wR_2 = 0.1238
Final R indexes [all data]	R_1 = 0.0847, wR_2 = 0.1021	R_1 = 0.0659, wR_2 = 0.1399	R_1 = 0.0615, wR_2 = 0.1332
Largest diff. peak/hole / e Å⁻³	1.17/-0.83	0.48/-0.89	0.94/-0.81
CCDC Dep. #	1980000	1980001	1980002
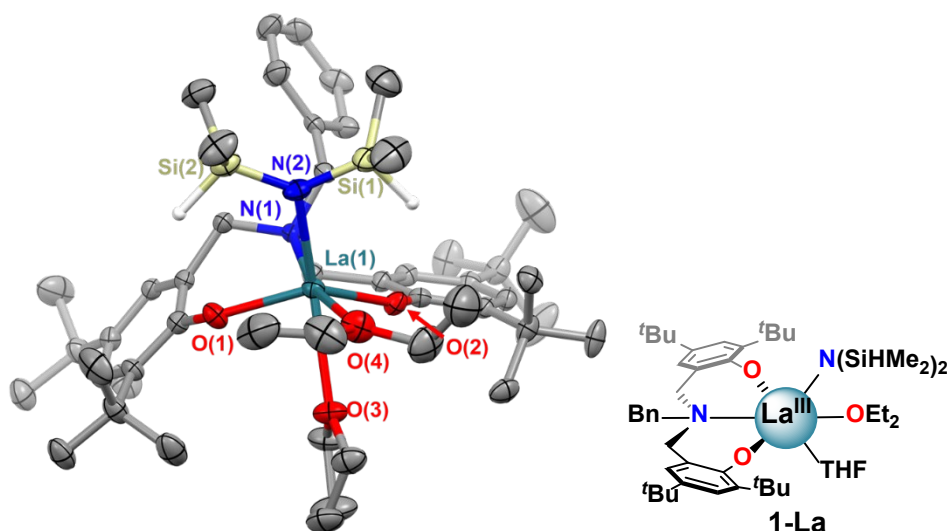
Figure 2.31. Thermal ellipsoid plot of **1-La** ([La(^{1}L)(N(SiHMe$_2$)$_2$)(Et$_2$O)(THF)]) shown at 50% probability. Hydrogen atoms other than those attached to Si(1) and Si(2) have been removed for clarity. Crystallographic data are available on Cambridge Crystallographic Data Centre. CCDC ID: LUSFUD.
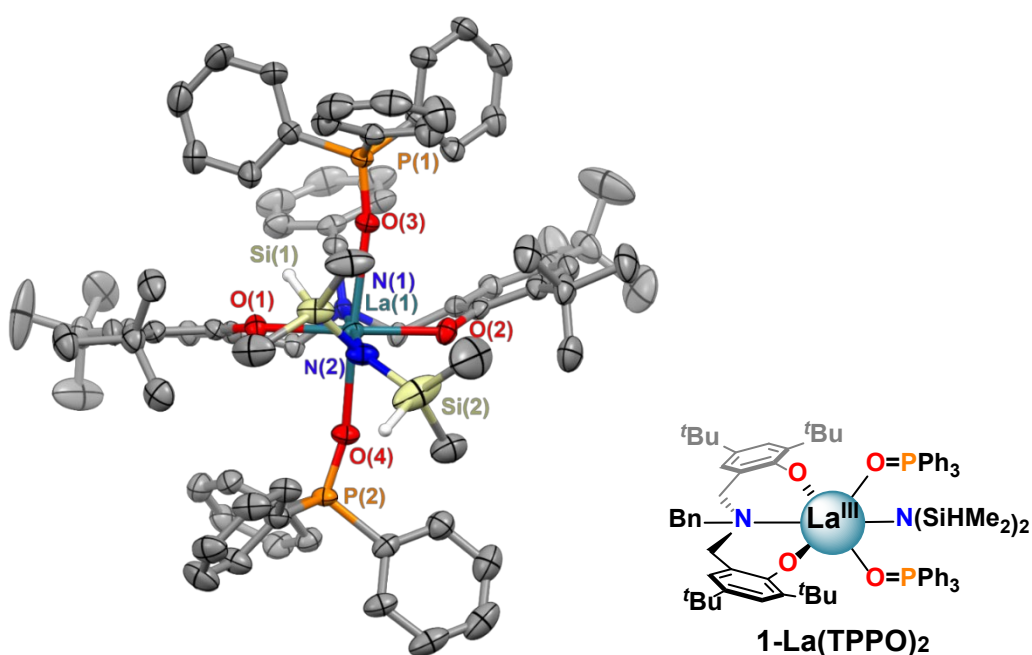
Figure 2.32. Thermal ellipsoid plot of **1-La(TPPO)$_2$** ([La(^{1}L)(N(SiHMe$_2$)$_2$)(TPPO)$_2$]) shown at 50% probability. Second components of the two disordered tert-butyl groups and the (Me$_2$H) unit on Si(2) have been removed for clarity. Hydrogen atoms other than those attached to Si(1) and Si(2) have been removed for clarity. Crystallographic data are available on Cambridge Crystallographic Data Centre. CCDC ID: LUSGAK.
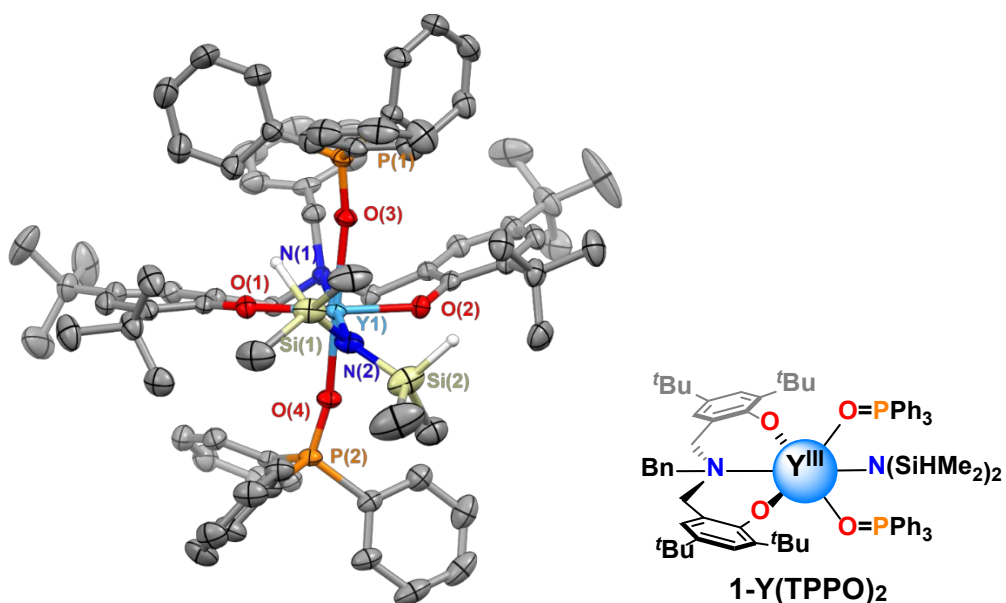
Figure 2.33. Thermal ellipsoid plot of **1-Y(TPPO)₂** ([Y(¹L)(N(SiHMe₂)₂)(TPPO)₂]) shown at 50% probability. Second components of the two disordered tert-butyl groups have been removed for clarity. Hydrogen atoms other than those attached to Si(1) and Si(2) have been removed for clarity. Crystallographic data are available on Cambridge Crystallographic Data Centre. CCDC ID: LUSGEO.

2.5. References

1. Carpentier, J.-F., Rare-Earth Complexes Supported by Tripodal Tetradentate Bis(phenolate) Ligands: A Privileged Class of Catalysts for Ring-Opening Polymerization of Cyclic Esters. *Organometallics* **2015,** *34* (17), 4175-4189.

2. Ajellal, N.; Bouyahyi, M.; Amgoune, A.; Thomas, C. M.; Bondon, A.; Pillin, I.; Grohens, Y.; Carpentier, J.-F., Syndiotactic-Enriched Poly(3-hydroxybutyrate)s via Stereoselective Ring-Opening Polymerization of Racemic β-Butyrolactone with Discrete Yttrium Catalysts. *Macromolecules* **2009,** *42* (4), 987-993.

3. Amgoune, A.; Thomas, C. M.; Ilinca, S.; Roisnel, T.; Carpentier, J.-F., Highly active, productive, and syndiospecific yttrium initiators for the polymerization of racemic β-butyrolactone. *Angew. Chem., Int. Ed.* **2006,** *45* (17), 2782-2784.

4. Dyer, H. E.; Huijser, S.; Susperregui, N.; Bonnet, F.; Schwarz, A. D.; Duchateau, R.; Maron, L.; Mountford, P., Ring-Opening Polymerization of rac-Lactide by Bis(phenolate)amine-Supported Samarium Borohydride Complexes: An Experimental and DFT Study. *Organometallics* **2010,** *29* (16), 3602-3621.

5. Platt, A. W. G., Lanthanide phosphine oxide complexes. *Coord. Chem. Rev.* **2017,** *340*, 62-78.

6. Smith, M. B., Phosphorus Ligands☆. In *Reference Module in Chemistry, Molecular Sciences and Chemical Engineering*, Elsevier: 2013.

7. Anwander, R.; Runte, O.; Eppinger, J.; Gerstberger, G.; Herdtweck, E.; Spiegler, M., Synthesis and structural characterisation of rare-earth bis(dimethylsilyl)amides and their surface organometallic chemistry on mesoporous MCM-41†. *J. Chem. Soc., Dalton Trans.*

1998, (5), 847-858.

8. Dietrich, H. M.; Meermann, C.; Törnroos, K. W.; Anwander, R., Sounding out the Reactivity of Trimethylyttrium. *Organometallics* **2006,** *25* (18), 4316-4321.

9. Yuen, H. F.; Marks, T. J., Synthesis and Catalytic Properties of Phenylene-Bridged Binuclear Organolanthanide Complexes. *Organometallics* **2008,** *27* (2), 155-158.

10. Meermann, C.; Gerstberger, G.; Spiegler, M.; Törnroos, K. W.; Anwander, R., Donor and ate-Coordination in Rare-Earth Metal Bis(dimethylsilyl)amide Complexes. *Eur. J. Inorg. Chem.* **2008,** *2008* (12), 2014-2023.

11. Chapurina, Y.; Klitzke, J.; Casagrande Jr, O. d. L.; Awada, M.; Dorcet, V.; Kirillov, E.; Carpentier, J.-F., Scandium versus yttrium{amino-alkoxy-bis(phenolate)} complexes for the stereoselective ring-opening polymerization of racemic lactide and β-butyrolactone. *Dalton Trans.* **2014,** *43* (38), 14322-14333.

12. Ouyang, H.; Nie, K.; Yuan, D.; Yao, Y., Synthesis of amine-bridged bis (phenolate) rare-earth metal aryloxides and their catalytic performances for the ring-opening polymerization of l-lactic acid O-carboxyanhydride and l-lactide. *Dalton Transactions* **2017,** *46* (45), 15928-15938.

13. Ajellal, N.; Bouyahyi, M.; Amgoune, A.; Thomas, C. M.; Bondon, A.; Pillin, I.; Grohens, Y.; Carpentier, J.-F., Syndiotactic-Enriched Poly(3-hydroxybutyrate)s via Stereoselective Ring-Opening Polymerization of Racemic β-Butyrolactone with Discrete Yttrium Catalysts. *Macromolecules* **2009,** *42* (4), 987-993.

14. Ma, H.; Okuda, J., Kinetics and Mechanism of l-Lactide Polymerization by Rare Earth Metal Silylamido Complexes: Effect of Alcohol Addition. *Macromolecules* **2005,** *38* (7), 2665-

2673.

15. Nie, K.; Fang, L.; Yao, Y.; Zhang, Y.; Shen, Q.; Wang, Y., Synthesis and Characterization of Amine-Bridged Bis(phenolate)lanthanide Alkoxides and Their Application in the Controlled Polymerization of rac-Lactide and rac-β-Butyrolactone. *Inorganic Chemistry* **2012,** *51* (20), 11133-11143.

16. Altenbuchner, P. T.; Kronast, A.; Kissling, S.; Vagin, S. I.; Herdtweck, E.; Pöthig, A.; Deglmann, P.; Loos, R.; Rieger, B., Mechanistic Investigations of the Stereoselective Rare Earth Metal-Mediated Ring-Opening Polymerization of β-Butyrolactone. *Chemistry − A European Journal* **2015,** *21* (39), 13609-13617.

17. Zhuo, Z.; Zhang, C.; Luo, Y.; Wang, Y.; Yao, Y.; Yuan, D.; Cui, D., Stereo-selectivity switchable ROP of rac-β-butyrolactone initiated by salan-ligated rare-earth metal amide complexes: the key role of the substituents on ligand frameworks. *Chemical Communications* **2018,** *54* (85), 11998-12001.

18. Save, M.; Schappacher, M.; Soum, A., Controlled Ring-Opening Polymerization of Lactones and Lactides Initiated by Lanthanum Isopropoxide, 1. General Aspects and Kinetics. *Macromolecular Chemistry and Physics* **2002,** *203* (5-6), 889-899.

19. Dubois, P.; Barakat, I.; Jerome, R.; Teyssie, P., Macromolecular engineering of polyactones and polyactides. 12. Study of the depolymerization reactions of poly(.epsilon.-caprolactone) with functional aluminum alkoxide end groups. *Macromolecules* **1993,** *26* (17), 4407-4412.

20. Dubois, P., Jérôme, R. Teyssié, P., Effect of Lewis bases on the ring-opening polymerization of ε-caprolactone and lactides initiated by aluminum alkoxides. *Polym. Prepr. (Am. Chem. Soc., Div. Polym. Chem.)* **1994,** *35* (2), 536-537.

21. Dubois, P.; Ropson, N.; Jérôme, R.; Teyssié, P., Macromolecular Engineering of Polylactones and Polylactides. 19. Kinetics of Ring-Opening Polymerization of ε-Caprolactone Initiated with Functional Aluminum Alkoxides. *Macromolecules* **1996,** *29* (6), 1965-1975.

22. Boffa, L. S.; Novak, B. M., "Link-Functionalized" Polymers: An Unusual Macromolecular Architecture through Bifunctional Initiation. *Macromolecules* **1997,** *30* (12), 3494-3506.

23. Degée, P.; Dubois, P.; Jacobsen, S.; Fritz, H.-G.; Jérôme, R., Beneficial effect of triphenylphosphine on the bulk polymerization of L,L-lactide promoted by 2-ethylhexanoic acid tin (II) salt. *Journal of Polymer Science Part A: Polymer Chemistry* **1999,** *37* (14), 2413-2420.

24. Ravi, P.; Gröb, T.; Dehnicke, K.; Greiner, A., Novel [Sm2I(NPPh3)5(DME)] Initiator for the Living Ring-Opening Polymerization of ε-Caprolactone and δ-Valerolactone. *Macromolecules* **2001,** *34* (25), 8649-8653.

25. Chisholm, M. H.; Gallucci, J. C.; Phomphrai, K., Well-Defined Calcium Initiators for Lactide Polymerization. *Inorganic Chemistry* **2004,** *43* (21), 6717-6725.

26. Horeglad, P.; Kruk, P.; Pécaut, J., Heteroselective Polymerization of rac-Lactide in the Presence of Dialkylgallium Alkoxides: The Effect of Lewis Base on Polymerization Stereoselectivity. *Organometallics* **2010,** *29* (17), 3729-3734.

27. Chisholm, M. H.; Choojun, K.; Chow, A. S.; Fraenkel, G., Molecular Dynamics and Ligand Exchange in Magnesium Complexes: Evidence for both Dissociative and Associative Ligand Exchange. *Angewandte Chemie International Edition* **2013,** *52* (11), 3264-3266.

28. Klitzke, J. S.; Roisnel, T.; Kirillov, E.; Casagrande, O. d. L.; Carpentier, J.-F., Yttrium–

and Aluminum–Bis(phenolate)pyridine Complexes: Catalysts and Model Compounds of the Intermediates for the Stereoselective Ring-Opening Polymerization of Racemic Lactide and β-Butyrolactone. *Organometallics* **2014,** *33* (1), 309-321.

29. Nemoto, T.; Ohshima, T.; Yamaguchi, K.; Shibasaki, M., Catalytic Asymmetric Epoxidation of Enones Using La−BINOL−Triphenylarsine Oxide Complex: Structural Determination of the Asymmetric Catalyst. *J. Am. Chem. Soc.* **2001,** *123* (12), 2725-2732.

30. Kakei, H.; Tsuji, R.; Ohshima, T.; Morimoto, H.; Matsunaga, S.; Shibasaki, M., Catalytic Asymmetric Epoxidation of α,β-Unsaturated Esters with Chiral Yttrium–Biaryldiol Complexes. *Chem. Asian J.* **2007,** *2* (2), 257-264.

31. Kakei, H.; Tsuji, R.; Ohshima, T.; Shibasaki, M., Catalytic Asymmetric Epoxidation of α,β-Unsaturated Esters Using an Yttrium-Biphenyldiol Complex. *J. Am. Chem. Soc.* **2005,** *127* (25), 8962-8963.

32. Hara, K.; Park, S.-Y.; Yamagiwa, N.; Matsunaga, S.; Shibasaki, M., Catalytic Asymmetric Epoxidation of α,β-Unsaturated Phosphane Oxides with a Y(O-iPr)3/Biphenyldiol Complex. *Chem. Asian J.* **2008,** *3* (8-9), 1500-1504.

33. Wang, L.; Yang, D.; Li, D.; Liu, X.; Wang, P.; Wang, K.; Zhu, H.; Bai, L.; Wang, R., The Important Role of the Byproduct Triphenylphosphine Oxide in the Magnesium(II)-Catalyzed Enantioselective Reaction of Hemiacetals and Phosphorus Ylides. *Angew. Chem. Int. Edit.* **2018,** *57* (29), 9088-9092.

34. Arnold, P. L.; Buffet, J.-C.; Blaudeck, R. P.; Sujecki, S.; Blake, A. J.; Wilson, C., C3-Symmetric Lanthanide Tris(alkoxide) Complexes Formed by Preferential Complexation and Their Stereoselective Polymerization of rac-Lactide. *Angew. Chem. Int. Edit.* **2008,** *47* (32),

6033-6036.

35. Arnold, P. L.; Buffet, J. C.; Blaudeck, R.; Sujecki, S.; Wilson, C., Ligand Recognition Processes in the Formation of Homochiral C3-Symmetric LnL3 Complexes of a Chiral Alkoxide. *Chem. Eur. J.* **2009,** *15* (33), 8241-8250.

36. Buffet, J.-C.; Okuda, J.; Arnold, P. L., Chiral Indium Alkoxide Complexes as Initiators for the Stereoselective Ring-Opening Polymerization of rac-Lactide. *Inorg. Chem.* **2010,** *49* (2), 419-426.

37. Platel, R. H.; White, A. J. P.; Williams, C. K., Stereocontrolled lactide polymerisation determined by the nuclearity of the yttrium initiator. *Chem. Commun.* **2009,** (27), 4115-4117.

38. Platel, R. H.; White, A. J. P.; Williams, C. K., Bis(phosphinic)diamido Yttrium Amide, Alkoxide, and Aryloxide Complexes: An Evaluation of Lactide Ring-Opening Polymerization Initiator Efficiency. *Inorg. Chem.* **2011,** *50* (16), 7718-7728.

39. Zhang, Z.; Cui, D., Heteroscorpionate Rare-Earth Metal Zwitterionic Complexes: Syntheses, Characterization, and Heteroselective Catalysis on the Ring-Opening Polymerization of rac-Lactide. *Chem. Eur. J.* **2011,** *17* (41), 11520-11526.

40. Mou, Z.; Liu, B.; Liu, X.; Xie, H.; Rong, W.; Li, L.; Li, S.; Cui, D., Efficient and Heteroselective Heteroscorpionate Rare-Earth-Metal Zwitterionic Initiators for ROP of rac-Lactide: Role of σ-Ligand. *Macromolecules* **2014,** *47* (7), 2233-2241.

41. Ajellal, N.; Durieux, G.; Delevoye, L.; Tricot, G.; Dujardin, C.; Thomas, C. M.; Gauvin, R. M., Polymerization of racemic β-butyrolactone using supported catalysts: a simple access to isotactic polymers. *Chem. Commun. (Cambridge, U. K.)* **2010,** *46* (7), 1032-1034.

42. Asano, S.; Aida, T.; Inoue, S., 'Immortal' polymerization. Polymerization of epoxide

catalysed by an aluminium porphyrin–alcohol system. *Journal of the Chemical Society, Chemical Communications* **1985,** (17), 1148-1149.

43. Ajellal, N.; Carpentier, J.-F.; Guillaume, C.; Guillaume, S. M.; Helou, M.; Poirier, V.; Sarazin, Y.; Trifonov, A., Metal-catalyzed immortal ring-opening polymerization of lactones, lactides and cyclic carbonates. *Dalton Transactions* **2010,** *39* (36), 8363-8376.

44. Shaik, M.; Peterson, J.; Du, G., Cyclic and Linear Polyhydroxylbutyrates from Ring-Opening Polymerization of β-Butyrolactone with Amido-Oxazolinate Zinc Catalysts. *Macromolecules* **2019,** *52* (1), 157-166.

45. Cai, C.-X.; Toupet, L.; Lehmann, C. W.; Carpentier, J.-F., Synthesis, structure and reactivity of new yttrium bis(dimethylsilyl)amido and bis(trimethylsilyl)methyl complexes of a tetradentate bis(phenoxide) ligand. *J. Organometallic Chem.* **2003,** *683* (1), 131-136.

46. Friebolin, H., Basic One- and Two-Dimensional NMR Spectroscopy. 4th Ed. ed.; WILEY-VCH: Weinheim :, 2005.

47. Pawlikowski, A. V.; Ellern, A.; Sadow, A. D., Ligand Exchange Reactions and Hydroamination with Tris(oxazolinyl)borato Yttrium Compounds. *Inorg. Chem.* **2009,** *48* (16), 8020-8029.

48. Robinson, J. R.; Gordon, Z.; Booth, C. H.; Carroll, P. J.; Walsh, P. J.; Schelter, E. J., Tuning Reactivity and Electronic Properties through Ligand Reorganization within a Cerium Heterobimetallic Framework. *J. Am. Chem. Soc.* **2013,** *135* (50), 19016-19024.

49. Ajellal, N.; Lyubov, D. M.; Sinenkov, M. A.; Fukin, G. K.; Cherkasov, A. V.; Thomas, C. M.; Carpentier, J.-F.; Trifonov, A. A., Bis(guanidinate) Alkoxide Complexes of Lanthanides: Synthesis, Structures and Use in Immortal and Stereoselective Ring-Opening Polymerization

of Cyclic Esters. *Chemistry – A European Journal* **2008,** *14* (18), 5440-5448.

50. Bouyahyi, M.; Ajellal, N.; Kirillov, E.; Thomas, C. M.; Carpentier, J.-F., Exploring Electronic versus Steric Effects in Stereoselective Ring-Opening Polymerization of Lactide and β-Butyrolactone with Amino-alkoxy-bis(phenolate)-Yttrium Complexes. *Chem. - Eur. J.* **2011,** *17* (6), 1872-1883, S1872/1-S1872/82.

51. Pappalardo, D.; Bruno, M.; Lamberti, M.; Pellecchia, C., Ring-Opening Polymerization of Racemic β-Butyrolactone Promoted by Salan- and Salen-Type Yttrium Amido Complexes. *Macromolecular Chemistry and Physics* **2013,** *214* (17), 1965-1972.

52. Hori, Y.; Hagiwara, T., Ring-opening polymerisation of β-butyrolactone catalysed by distannoxane complexes: study of the mechanism. *Int. J. Biol. Macromol.* **1999,** *25* (1), 237-245.

53. Tang, X.; Chen, E. Y. X., Chemical synthesis of perfectly isotactic and high melting bacterial poly(3-hydroxybutyrate) from bio-sourced racemic cyclic diolide. *Nat. Commun.* **2018,** *9* (1), 1-11.

54. Tang, X.; Westlie, A. H.; Watson, E. M.; Chen, E. Y.-X., Stereosequenced crystalline polyhydroxyalkanoates from diastereomeric monomer mixtures. *Science* **2019,** *366* (6466), 754-758.

55. Tang, X.; Westlie, A. H.; Caporaso, L.; Cavallo, L.; Falivene, L.; Chen, E. Y., Biodegradable Polyhydroxyalkanoates by Stereoselective Copolymerization of Racemic Diolides: Stereocontrol and Polyolefin-Like Properties. *Angew. Chem. Int. Edit.* **2020,** *59* (20), 7881-7890.

56. Albertsson, A.-C.; Varma, I. K., Recent Developments in Ring Opening Polymerization of

Lactones for Biomedical Applications. *Biomacromolecules* **2003,** *4* (6), 1466-1486.

57. Han, F.; Yang, L.; Li, Z.; Xia, C., Acidic-functionalized ionic liquid as an efficient, green and reusable catalyst for hetero-Michael addition of nitrogen, sulfur and oxygen nucleophiles to α, β-unsaturated ketones. *Organic & biomolecular chemistry* **2012,** *10* (2), 346-354.

58. Kurcok, P.; Jedlinski, Z.; Kowalczuk, M., Reactions of β-lactones with potassium alkoxides and their complexes with 18-crown-6 in aprotic solvents. *J. Org. Chem.* **1993,** *58* (16), 4219-4220.

59. Kurcok, P.; Dubois, P.; Jèrôme, R., Polymerization of β-butyrolactone initiated with Al(OiPr)3. *Polym. Int.* **1996,** *41* (4), 479-485.

60. Dominski, A.; Konieczny, T.; Zieba, M.; Klim, M.; Kurcok, P., Anionic Polymerization of beta-Butyrolactone Initiated with Sodium Phenoxides. The Effect of the Initiator Basicity/Nucleophilicity on the ROP Mechanism. *Polymers* **2019,** *11* (7).

61. Morikawa, H.; Marchessault, R. H., Pyrolysis of bacterial polyalkanoates. *Can. J. Chem.* **1981,** *59* (15), 2306-2313.

62. Ballistreri, A.; Garozzo, D.; Giuffrida, M.; Impallomeni, G.; Montaudo, G., Analytical degradation: An approach to the structural analysis of microbial polyesters by different methods. *J. Anal. Appl. Pyrolysis* **1989,** *16* (3), 239-253.

63. Kunioka, M.; Doi, Y., Thermal degradation of microbial copolyesters: poly(3-hydroxybutyrate-co-3-hydroxyvalerate) and poly(3-hydroxybutyrate-co-4-hydroxybutyrate). *Macromolecules* **1990,** *23* (7), 1933-1936.

64. Ariffin, H.; Nishida, H.; Shirai, Y.; Hassan, M. A., Determination of multiple thermal degradation mechanisms of poly(3-hydroxybutyrate). *Polym. Degrad. Stab.* **2008,** *93* (8),

1433-1439.

65. Rieth, L. R.; Moore, D. R.; Lobkovsky, E. B.; Coates, G. W., Single-Site β-Diiminate Zinc Catalysts for the Ring-Opening Polymerization of β-Butyrolactone and β-Valerolactone to Poly(3-hydroxyalkanoates). *Journal of the American Chemical Society* **2002,** *124* (51), 15239-15248.

66. Kricheldorf, H. R.; Scharnagl, N.; Jedlinski, Z., Polylactones 33. The role of deprotonation in the anionic polymerization of β-propiolactone. *Polymer* **1996,** *37* (8), 1405-1411.

67. Kawalec, M.; Adamus, G.; Kurcok, P.; Kowalczuk, M.; Foltran, I.; Focarete, M. L.; Scandola, M., Carboxylate-Induced Degradation of Poly(3-hydroxybutyrate)s. *Biomacromolecules* **2007,** *8* (4), 1053-1058.

68. Bachmann, B. M.; Seebach, D., Synthesis and Structure of Linear and Cyclic Oligomers of 3-Hydroxybutanoic Acid with Specific Sequences of (R)- and (S)-Configurations. *Helv. Chim. Ata* **1998,** *81* (12), 2430-2461.

69. Kricheldorf, H. R.; Scharnagl, N., Polyactones. 17. Anionic Polymerization of β-D,L-Butyrolactone. *Journal of Macromolecular Science, Part A* **1989,** *26* (7), 951-968.

70. Kurcok, P.; Kowalczuk, M.; Hennek, K.; Jedlinski, Z., Anionic polymerization of .beta.-lactones initiated with alkali-metal alkoxides: reinvestigation of the polymerization mechanism. *Macromolecules* **1992,** *25* (7), 2017-2020.

71. Jedliński, Z.; Kurcok, P.; Lenz, R. W., Synthesis of Potentially Biodegradable Polymers. *J. Macromol. Sci. A* **1995,** *32* (4), 797-810.

72. Zeng, T.; Qian, Q.; Zhao, B.; Yuan, D.; Yao, Y.; Shen, Q., Synthesis and characterization of rare-earth metal guanidinates stabilized by amine-bridged bis(phenolate) ligands and their

application in the controlled polymerization of rac-lactide and rac-β-butyrolactone. *RSC Adv.* **2015,** *5* (65), 53161-53171.

73. Nie, K.; Feng, T.; Song, F.; Zhang, Y.; Sun, H.; Yuan, D.; Yao, Y.; Shen, Q., Bimetallic amine-bridged bis(phenolate) lanthanide aryloxides and alkoxides: synthesis, characterization, and application in the ring-opening polymerization of rac-lactide and rac-β-butyrolactone. *Sci. China Chem.* **2014,** *57* (8), 1106-1116.

74. Grunova, E.; Kirillov, E.; Roisnel, T.; Carpentier, J.-F., Group 3 metal complexes supported by tridentate pyridine- and thiophene-linked bis(naphtholate) ligands: synthesis, structure, and use in stereoselective ring-opening polymerization of racemic lactide and β-butyrolactone. *Dalton Transactions* **2010,** *39* (29), 6739-6752.

75. Sinenkov, M. A.; Fukin, G. K.; Cherkasov, A. V.; Ajellal, N.; Roisnel, T.; Kerton, F. M.; Carpentier, J.-F.; Trifonov, A. A., Neodymium borohydride complexes supported by diamino-bis(phenoxide) ligands: diversity of synthetic and structural chemistry, and catalytic activity in ring-opening polymerization of cyclic esters. *New J. Chem.* **2011,** *35* (1), 204-212.

76. D'auria, I.; Mazzeo, M.; Pappalardo, D.; Lamberti, M.; Pellecchia, C., Ring-opening polymerization of cyclic esters promoted by phosphido-diphosphine pincer group 3 complexes. *J. Polym. Sci. A* **2011,** *49* (2), 403-413.

77. Griesbaum, K.; Zwick, G., Diozonolysen von acyclischen konjugierten Dienen in Methanol. *Chemische Berichte* **1986,** *119* (1), 229-243.

78. Neverov, A. A.; McDonald, T.; Gibson, G.; Brown, R. S., Catalysis of transesterification reactions by lanthanides □ Unprecedented acceleration of methanolysis of aryl and alkyl esters promoted by La(OTf)3 at neutral sspH and ambient temperatures. *Can. J. Chem.* **2001,** *79* (11),

1704-1710.

79. Hatano, M.; Ishihara, K., Lanthanum(iii) catalysts for highly efficient and chemoselective transesterification. *Chem. Commun.* **2013,** *49* (20), 1983-1997.

80. Zeng, R.; Sheng, H.; Zhang, Y.; Feng, Y.; Chen, Z.; Wang, J.; Chen, M.; Zhu, M.; Guo, Q., Heterobimetallic Dinuclear Lanthanide Alkoxide Complexes as Acid–Base Difunctional Catalysts for Transesterification. *J. Org. Chem.* **2014,** *79* (19), 9246-9252.

81. Shibasaki, M.; Kanai, M.; Matsunaga, S.; Kumagai, N., Recent Progress in Asymmetric Bifunctional Catalysis Using Multimetallic Systems. *Acc. Chem. Res.* **2009,** *42* (8), 1117-1127.

82. Robinson, J. R.; Gu, J.; Carroll, P. J.; Schelter, E. J.; Walsh, P. J., Exchange Processes in Shibasaki's Rare Earth Alkali Metal BINOLate Frameworks and Their Relevance in Multifunctional Asymmetric Catalysis. *J. Am. Chem. Soc.* **2015,** *137* (22), 7135-7144.

83. Kumagai, N.; Kanai, M.; Sasai, H., A Career in Catalysis: Masakatsu Shibasaki. *ACS Catal.* **2016,** *6* (7), 4699-4709.

84. Zhu, J.-B.; Chen, E. Y.-X., Catalyst-Sidearm-Induced Stereoselectivity Switching in Polymerization of a Racemic Lactone for Stereocomplexed Crystalline Polymer with a Circular Life Cycle. *Angewandte Chemie International Edition* **2019,** *58* (4), 1178-1182.

85. Ropson, N.; Dubois, P.; Jerome, R.; Teyssie, P., Macromolecular Engineering of Polylactones and Polylactides. 20. Effect of Monomer, Solvent, and Initiator on the Ring-Opening Polymerization As Initiated with Aluminum Alkoxides. *Macromolecules* **1995,** *28* (23), 7589-7598.

86. Montaudo, G.; Montaudo, M. S.; Puglisi, C.; Samperi, F.; Spassky, N.; LeBorgne, A.; Wisniewski, M., Evidence for Ester-Exchange Reactions and Cyclic Oligomer Formation in

the Ring-Opening Polymerization of Lactide with Aluminum Complex Initiators. *Macromolecules* **1996,** *29* (20), 6461-6465.

87. Horeglad, P.; Szczepaniak, G.; Dranka, M.; Zachara, J., The first facile stereoselectivity switch in the polymerization of rac-lactide—from heteroselective to isoselective dialkylgallium alkoxides with the help of N-heterocyclic carbenes. *Chemical Communications* **2012,** *48* (8), 1171-1173.

88. Horeglad, P.; Cybularczyk, M.; Litwińska, A.; Dąbrowska, A. M.; Dranka, M.; Żukowska, G. Z.; Urbańczyk, M.; Michalak, M., Controlling the stereoselectivity of rac-LA polymerization by chiral recognition induced the formation of homochiral dimeric metal alkoxides. *Polym. Chem.* **2016,** *7* (11), 2022-2036.

89. Horeglad, P.; Cybularczyk, M.; Trzaskowski, B.; Żukowska, G. Z.; Dranka, M.; Zachara, J., Dialkylgallium Alkoxides Stabilized with N-Heterocyclic Carbenes: Opportunities and Limitations for the Controlled and Stereoselective Polymerization of rac-Lactide. *Organometallics* **2015,** *34* (14), 3480-3496.

90. Sandström, J.; Sandström, J. S., *Dynamic NMR spectroscopy*. Academic Press: 1982.

91. Bradley, D. C.; Ghotra, J. S.; Hart, F. A., Low co-ordination numbers in lanthanide and actinide compounds. Part I. The preparation and characterization of tris {bis (trimethylsilyl)-amido} lanthanides. *Journal of the Chemical Society, Dalton Transactions* **1973,** (10), 1021-1023.

92. Smith, A. R.; Livinghouse, T., Rapid and Efficient Procedure for the Synthesis of Group 3 Metal Tris [bis (dimethylsilyl) amide] THF Complexes. *Organometallics* **2013,** *32* (5), 1528-1530.

93. Amgoune, A.; Thomas, C. M.; Roisnel, T.; Carpentier, J. F., Ring-opening polymerization of lactide with group 3 metal complexes supported by dianionic alkoxy-amino-bisphenolate ligands: combining high activity, productivity, and selectivity. *Chemistry–A European Journal* **2006,** *12* (1), 169-179.

94. Cai, C.-X.; Amgoune, A.; Lehmann, C. W.; Carpentier, J.-F., Stereoselective ring-opening polymerization of racemic lactide using alkoxy-amino-bis (phenolate) group 3 metal complexes. *Chemical communications* **2004,** (3), 330-331.

95. SAINT, B., v8. 37a. *Bruker AXS Inc.: Madison, WI, USA* **2012**.

96. Sheldrick, G.; Shelxs97, A. C., Sect. A: Found. Crystallogr., 2008, 64, 112 CrossRef CAS;(b) GM Sheldrick, Shelxl 2014, Crystal structure refinement with SHELXL. *Acta Crystallogr., Sect. C: Struct. Chem* **2015,** *71*, 3-8.

97. Sheldrick, G., SADABS, v2014/5; Bruker AXS Inc. *Madison, WI* **2001**.

98. Herbst-Irmer, R.; Spek, A.; Schneider, T.; Sawaya, M., *Crystal Structure Refinement: A Crystallographer's Guide to SHELXL*. Oxford University Press: 2006; Vol. 8.

99. Thorn, A.; Dittrich, B.; Sheldrick, G. M., Enhanced rigid-bond restraints. *Acta Crystallographica Section A: Foundations of Crystallography* **2012,** *68* (4), 448-451.

100. Spek, A. L., PLATON SQUEEZE: a tool for the calculation of the disordered solvent contribution to the calculated structure factors. *Acta Crystallographica Section C: Structural Chemistry* **2015,** *71* (1), 9-18.

101. Fleming, W. J.; Müller-Bunz, H.; Lillo, V.; Fernández, E.; Guiry, P. J., Axially chiral PN ligands for the copper catalyzed β-borylation of α, β-unsaturated esters. *Organic & biomolecular chemistry* **2009,** *7* (12), 2520-2524.

Chapter 3: *N*-Oxides Amplify Catalyst Reactivity and Iso-selectivity in the Ring-Opening Polymerization of *rac-β*-BBL

Abstract

N-oxides can amplify the performance of a lanthanum aminobisphenolate catalyst in the ring-opening polymerization (ROP) of *rac-β*-butyrolactone (*rac*-BBL) to unprecedented levels (TOF up to 1,900 h^{-1}, P_m up to 0.82). Experiments and computations establish that donor electronics control catalyst activity, while donor steric bulk in the primary coordination-sphere is crucial to suppressing catalyst deactivation.

3.1. Introduction

In Chapter 2, we have discovered that embedding increased coordinative unsaturation and ligand flexibility into rare-earth complexes can generate catalysts whose performance in the stereospecific ROP of *rac*-BBL can be amplified by addition of simple and inexpensive monodentate neutral donor ligands.[1-2] In the case of a lanthanum *N*-benzyl aminobisphenolate catalyst, $[La(^{Bn}L)(N(SiHMe_2)_2)(THF)_2]$ ($^{Bn}L: BnN(CH_2^{2,6-tBu}ArO)_2$), **1-La**, addition of hard phosphine oxide donors (OPR_3; R = $^nC_8H_{17}$, Ph, NMe_2) generated the most isoselective and reactive homogeneous catalysts for the ROP of *rac*-BBL reported to date (e.g. $OP(^nC_8H_{17})_3$, 0 °C: TOF = ~200 h^{-1}, P_m = 0.80).[1] Our initial mechanistic studies with $OPPh_3$ revealed that these dynamic, strong neutral donors influenced several key catalyst equilibria associated with propagation, stereocontrol, and catalyst deactivation. We posited that each of these equilibria, and therefore catalyst performance, might be uniquely attenuated by donor structure and strength, and motivates our current study.

Heteroaromatic *N*-oxides are a versatile class of neutral donor ligands with exceptional structural and electronic diversity,[3-5] and can display donor strength comparable to phosphine-oxides.[6-7] Alkyl and heteroaromatic *N*-oxides have been employed with great success as additives and ligands in asymmetric catalysis,[8-14]

Herein, we report that *N*-oxides can promote unprecedented catalyst activity (RT: TOF up to 1,900 h^{-1}) and isoselectivity (–30 °C: P_m = 0.82) for the ROP of *rac*-BBL catalyzed by **1-La**. This marks their first use in ROP. Our combined experimental and computational studies

clearly establish that donor electronics control catalyst activity, while donor steric bulk in the

primary coordination-sphere is crucial to suppressing catalyst deactivation.

3.2. Results and Discussion

1-La was evaluated as a catalyst for the ROP of *rac*-BBL in the presence of diphenylmethanol (HOCHPh$_2$) and pyridine *N*-oxide derivatives (Table 3.1). In the absence of a strong neutral donor ligand, the lanthanum alkoxide formed *in situ* from 0.5 mol% **1-La** and HOCHPh$_2$ was modestly active with a slight preference towards formation of isoenriched P3HB (Entry 1, P_m = 0.57). Encouragingly, addition of pyridine *N*-oxide (PyO, 1 mol%) led to increased rates and isoselectivity (entry 3, P_m = 0.68), but performance fell short of monodentate phosphine-oxides such as OPPh$_3$ (entry 2).

Table 3.1. ROP of *rac*-BBL (2.4 M) catalyzed by **1-La** (0.5 mol%) in the presence of HOCHPh$_2$ (0.5 mol%) and neutral donor ligands (1 mol%).
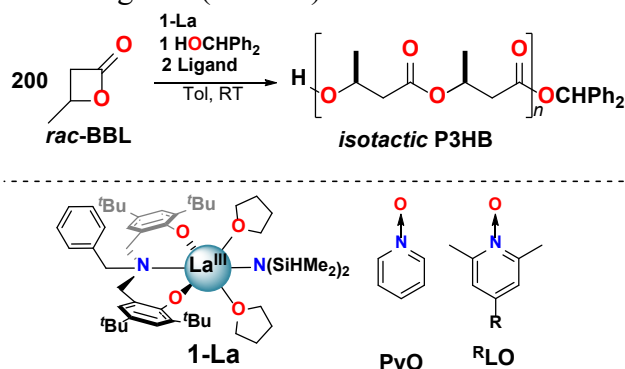
Entry	Ligand	Time (h)[a]	Conv. (%)[b]	$M_{n, calc}$[c] (kg/mol)	$M_{n, exp}$[d] (kg/mol)	$Đ$[d] (M_w/M_n)	P_m[f]
1	-	1	20	3.4	2.8	1.05	0.57
2	OPPh$_3$	1	95	16.3	9.4	1.19	0.71
3	PyO	3	55	9.5	7.1	1.14	0.68
4	^{NMe2}LO	10	22	3.8	2.2	1.23	0.72
5	^{OMe}LO	0.1	95	16.3	12.5	1.16	0.73
6	LO	0.3	92	15.8	11.4	1.18	0.73
7	^{Cl}LO	0.5	93	16.0	11.7	1.16	0.73
8	^{NO2}LO	5	31	5.3	2.2	1.28	0.69
9	^{OMe}LO[g]	1	99	17.0	15.1	1.08	0.82

a – Reaction times not optimized. *b* – Determined by ^{1}H NMR integration of BBL and P3HB methine resonances in the crude reaction mixture. *c* – [BBL]/[RE] × Conv. × 0.08609 + 0.18323 kg/mol. *d* – Determined by gel permeation chromatography (GPC) at 30 °C in THF using polystyrene standards and corrected by a Mark-Houwink factor of 0.54.[15] *e* – M_w/M_n. *f* – Probability of *meso* linkages between repeat units. Determined by integration of P3HB <u>C</u>=O resonances using inverse gated (IG) ^{13}C{^{1}H} NMR. *g* – At –30 °C.

We hypothesized this was due to electronic and steric effects. Electronically, PyO is a weaker donor than OPPh3 by the 4-fluorophenol hydrogen-bond basicity scale,[16] while buried volume calculations ($\%V_{bur}$) support a significantly reduced steric profile for PyO relative to OPPh3 ($\%V_{bur}$(PyO): 12.4%, $\%V_{bur}$(OPPh3): 16.3%; Table 3.2 and 3.3). Alternatively, 4-substituted 2,6-dimethylpyridine (lutidine) N-oxide derivatives, ^{R}**LO** (R = NO2, Cl, H, OMe, NMe2), were identified as attractive candidates. The steric profile of ^{R}**LO** (Table 3.2; $\%V_{bur}$: 15.9%) are comparable to OPPh3, while experimental aqueous pK_a values (pK_a^{W}(^{NO2}**LO**): 1.01, pK_a^{W}(^{NMe2}**LO**): 4.75)[17-18] and calculated natural charges of the N-oxide oxygen (q_O(^{NO2}**LO**): –0.541, q_O(^{NMe2}**LO**): –0.658; Figure 3.1 and Table 3.4) suggested that Lewis basicity could be systematically tuned within a sterically conserved environment.

Table 3.2. $\%V_{bur}(r_{3.5})$ of OPPh3 (CSD: TPEPHO)

Quadrant	V_{free}	V_{bur}	V_{total}	$\%V_{free}$	$\%V_{bur}$
SW	36.2	8.7	44.9	80.7	19.3
NW	36.4	8.4	44.9	81.2	18.8
NE	38.5	6.3	44.9	85.9	14.1
SE	39	5.9	44.9	86.9	13.1

$\%V_{free}$ = 83.7% // $\%V_{bur}$ = 16.3%
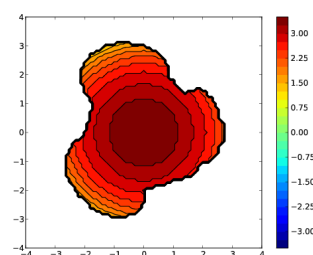
Table 3.3. $\%V_{bur}(r_{3.5})$ of PyO (CSD: ACOHAC)

Quadrant	V_{free}	V_{bur}	V_{total}	$\%V_{free}$	$\%V_{bur}$
SW	39.3	5.5	44.9	87.7	12.3
NW	39.2	5.6	44.9	87.4	12.6
NE	39.3	5.5	44.9	87.7	12.3
SE	39.2	5.6	44.9	87.4	12.6

$\%V_{free}$ = 87.6% // $\%V_{bur}$ = 12.4%
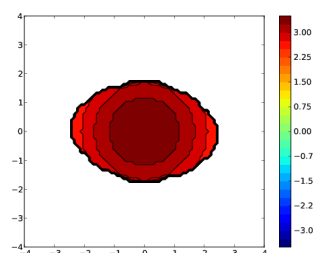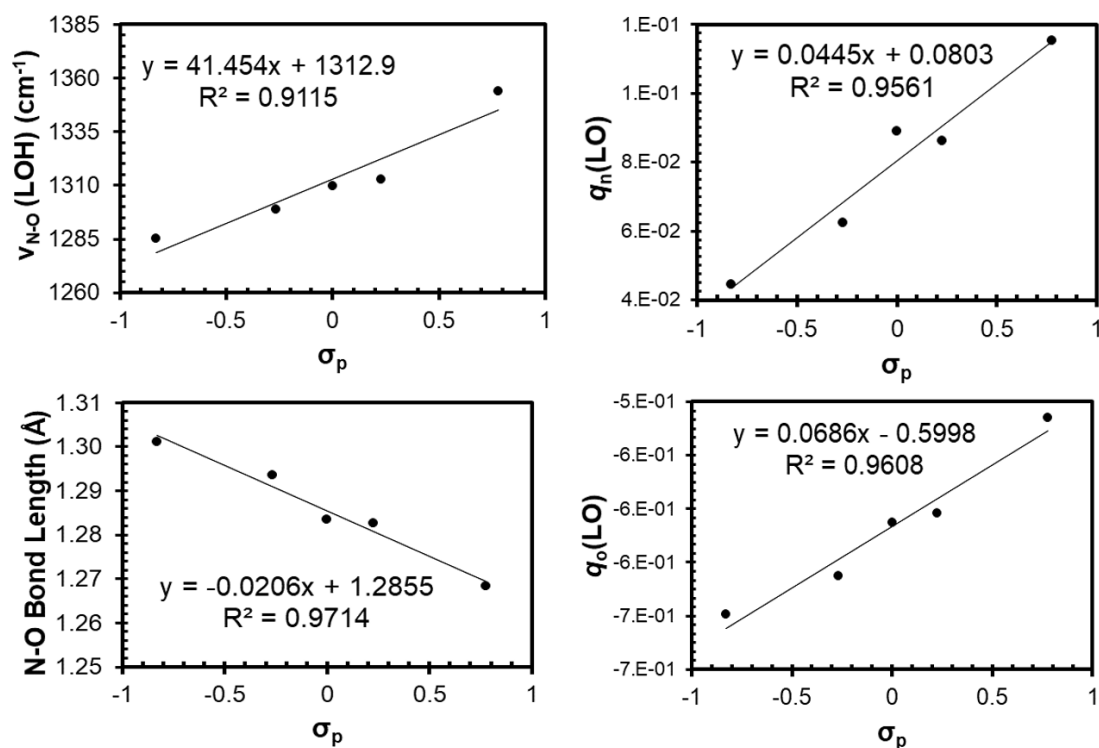
Figure 3.1. Graphs illustrating N-O Bond length, v_{N-O}, q_N, and q_O as a function of σ_p for lutidine N-oxide structures.

Table 3.4. N-O Bond length, v_{N-O}, q_N, and q_O as a function of σ_p for lutidine N-oxide structures. Frequency calculations were performed in Gaussian09 while natural charges were calculated using NBO 3.1 (see Section 3.5).

R	σ_p	N-O Bond Length (Å)	v_{N-O} (cm^{-1})	Natural Charge (q_N)	Natural Charge (q_O)
NMe$_2$	-0.83	1.30116	1285.26	0.04481	-0.65764
OMe	-0.268	1.29356	1298.77	0.06075	-0.62840
H	0	1.28346	1309.54	0.08642	-0.60003
Cl	0.227	1.28273	1312.83	0.08406	-0.59850
NO$_2$	0.778	1.26381	1354.10	0.11326	-0.54126

Although catalyst isoselectivity was largely invariant with respect to donor strength (Table 3.1, entries 4–8; P_m = 0.69–0.73), catalyst activity was extremely sensitive to the electronics of **^{R}LO**. Catalyst turnover frequency varied ~430-fold, where peak values occurred with an *N*-oxide of *intermediate* donor strength, **^{OMe}LO** (Figure 3.2). The overall trend in activity was reminiscent of volcano plots[19-20] following Sabatier's principle.[21] Such effects are frequently

encountered in heterogeneous systems, but have only recently been observed in homogeneous catalysis.[22-24] At RT, exogenous ^{OMe}LO promoted a remarkable 10-fold increase in catalyst activity compared to the previous champion system (**1-La** / L; TOF(^{OMe}LO) ~1,900 h^{-1} *vs* TOF(OPPh$_3$) ~200 h^{-1}). Lowering the reaction temperature to –30 °C led to significant improvements in isoselectivity, while maintaining high catalyst activity (entry 9: P_m = 0.82, TOF ~200 h^{-1}). The **1-La** / ^{OMe}LO system is the most active isoselective catalyst for the ROP of *rac*-BBL reported to date, and marks the first report of using *N*-oxides as ligands in ROP.
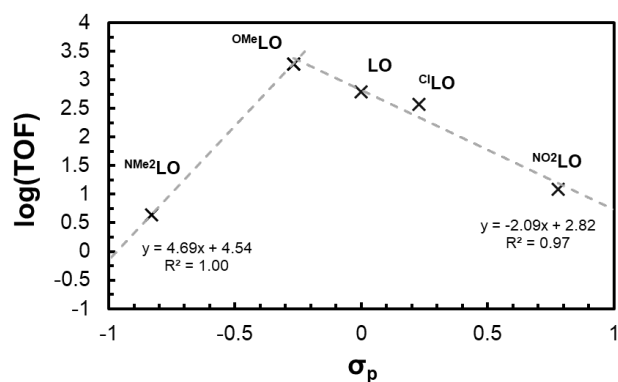
Figure 3.2. Turnover frequencies (TOF, min^{-1}) plotted versus σ_p (Hammett para-substituent constant) for the ROP of *rac*-BBL with **1-La** + HOCHPh$_2$ + ^{R}**LO**. Reactions were performed in toluene at ambient temperature with [BBL]:[**1-La**]:[^{R}**LO**]:[HOCHPh$_2$] = 200:1:2:1 and [BBL] = 2.4 M.
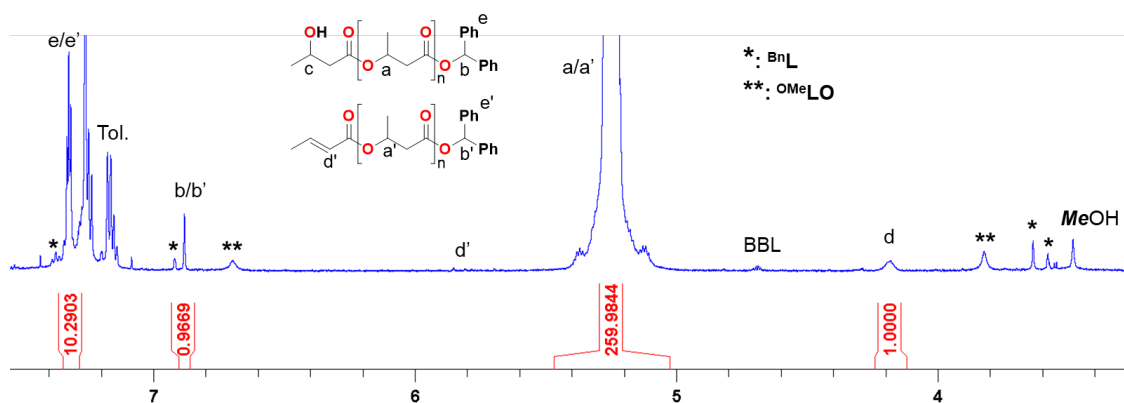
Figure 3.3. ^{1}H-NMR (600 MHz, CDCl$_3$) of P3HB (Table 3.1, entry 5). Reaction was performed in toluene at ambient temperature with [BBL]:[**1-La**]:[^{OMe}**LO**]:[Ph$_2$CHOH] = 200:1:2:1 and [BBL] = 2.4 M within 0.1 h. The polymer was precipitated from and washed with MeOH. Peaks of Ph$_2$CH and CH-OH are consistent with those of benzhydryl-3-oxobutanoate.[25]

Insight into the mechanism of catalyst initiation and propagation was provided by end-group analysis of P3HB generated from **1-La** in the presence of HOCHPh$_2$ and ^{OMe}**LO** at –30 °C ([**1-La**]:[HOCHPh$_2$]:[^{OMe}**LO**]:[BBL], 1:1:2:200). ^{1}H NMR spectroscopy revealed the presence of ester and alcohol end-groups in a ~1:1 ratio (Figure 3.3), which unambiguously established that the ROP of *rac*-BBL proceeded through a coordination-insertion mechanism (i.e. acyl cleavage).[26-27] Following a coordination-insertion mechanism, formation of crotyl end-groups can be symptomatic of a common catalyst deactivation pathway for the ROP of BBL, polymer chain-scission via base-promoted elimination.[1, 28-29] Gratifyingly, crotyl end-groups were nearly undetectable in these P3HB samples (< ~0.02 equiv / **1-La**), indicative that *N*-oxide binding suppressed base-promoted elimination to a much greater extent than *P*-oxide donors (e.g. OPPh$_3$: 1 equiv / **1-La**).[1] This was further corroborated by the excellent agreement between experimental and calculated M_n and narrow $Đ$ maintained over the course of the reaction (Figure 3.4 and Table 3.5).
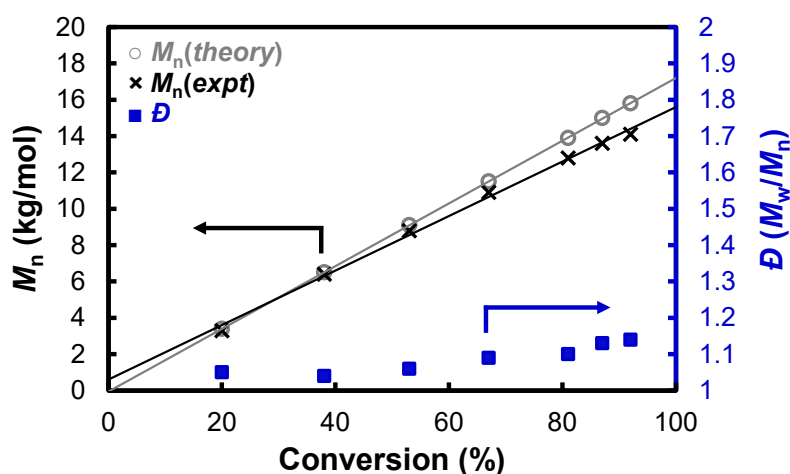
Figure 3.4. Plot of P3HB M_n and molecular weight dispersity, $Đ$ (M_w/M_n), as a function of conversion. **1-La** = 0.5 mol%, HOCHPh$_2$ = 0.5 mol%, ^{OMe}**LO** = 1 mol%. [*rac*-BBL] = 2.4 M, Tol, –30 °C.

Table 3.5. ROP of *rac*-BBL with **1-La** + HOCHPh$_2$ + 2 $^{\mathbf{OMe}}$**LO** quenched at different times.

Entry	Time (min)	Conv. (%)[a]	$M_{n,\,calc}$[c] (kg/mol)	$M_{n,\,exp}$[c] (kg/mol)	Đ[c,d]
1	1	1	0.17	n.d.	n.d.
2	2	3	0.51	n.d.	n.d.
3	3	6	1.0	n.d.	n.d.
4	5	13	2.3	2.3	1.04
5	10	33	5.6	5.5	1.05
6	15	51	8.8	8.3	1.05
7	20	65	11.1	10.2	1.06
8	25	76	13.1	12.4	1.07
9	30	87	14.9	13.8	1.08
10	40	95	16.3	15.0	1.08

a – Determined by ^{1}H-NMR integration of BBL and PHB methine resonances in the crude reaction mixture. *b* – [BBL]/[La]/[^{i}PrOH] × Conv. × 0.08609 kg•mol^{-1}. *c* – Determined by gel permeation chromatography (GPC) at 30 °C in THF using polystyrene standards and corrected by Mark-Houwink factor of 0.54. d – M_w/M_n.

Previously, we discovered that strong neutral donor ligands could amplify catalyst performance in the ROP of *rac*-BBL by (i) suppressing catalyst deactivation and (ii) increasing propagation rates.[1-2] These observations were largely qualitative in nature, and we were unable to fully decouple the influence of donors on each of these steps. Propagation rates (k_p) devoid of contributions from catalyst deactivation and uncontrolled reaction exotherms were obtained from kinetic studies performed with **1-La** (1 mol%) and $^{\mathbf{R}}$**LO** or OPPh$_3$ (2 mol%) at RT under more dilute conditions (0.3 M *vs* 2.4 M; see Experiment Section). A Hammett plot of log(k_p) values revealed a strong rate dependence on donor electronics, where k_p varied by ~290-fold moving from $^{\mathbf{NO2}}$**LO** to $^{\mathbf{OMe}}$**LO** (Figure 3.5). A ρ value of ~−2.4 was obtained from the slope of log(k_p) values containing $^{\mathbf{NO2}}$**LO** to $^{\mathbf{OMe}}$**LO**, and indicated a significant build-up of positive charge in the transition-state of the turnover limiting step. A dramatic drop-off in k_p was observed moving to the most electron-rich $^{\mathbf{R}}$**LO** of the series, $^{\mathbf{NMe2}}$**LO**, implying donor strength

and ligand exchange play a crucial role in the turnover limiting step.
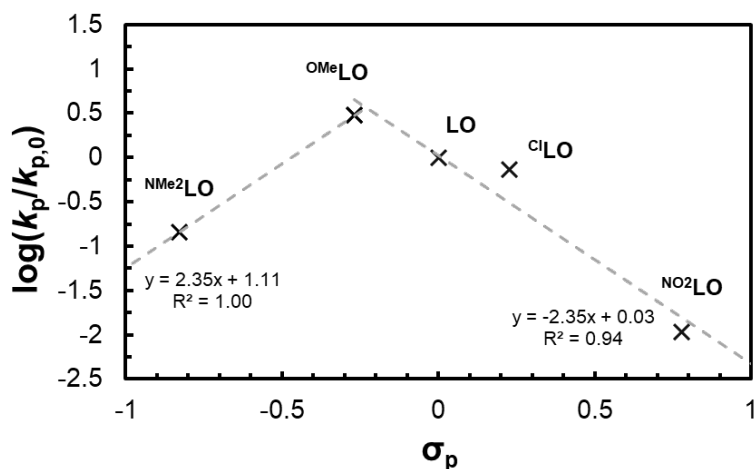
Figure 3.5. Hammett plot of $\log(k_p/k_{p,0})$ *vs* σ_p for the ROP of *rac*-BBL (0.3 M) catalyzed by **1-La** (1 mol%) in the presence of HOCHPh$_2$ (1 mol%) and **^{R}LO** (2 mol%) in toluene at RT. k_p: propagation rate of **^{R}LO** (calculated from Table 3.6 and Figure 3.6). $k_{p,0}$: k_p of **LO**. σ_p: Hammett para-substituent constant.
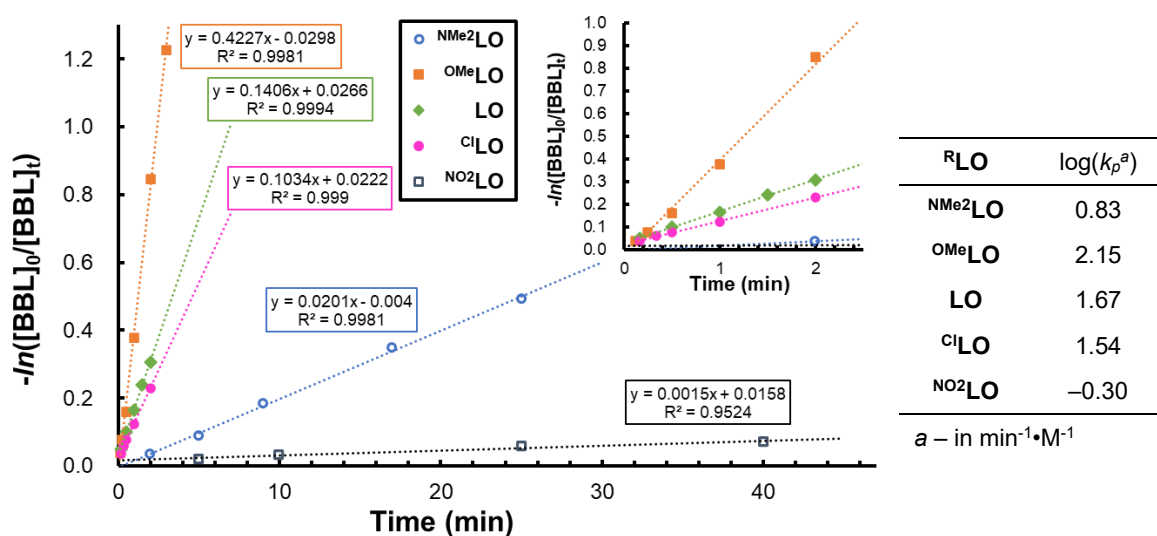
Figure 3.6. Propagation rate constants (k_p) for the ROP of *rac*-BBL with **1-La** + Ph$_2$CHOH + **^{R}LO**. Reactions were performed in toluene at ambient temperature with [BBL]:[**1-La**]:[**^{R}LO**]:[HOCHPh$_2$] = 100:1:2:1 and [BBL] = 0.3 M.

Table 3.6. Conversions in early stage of ROP of *rac*-BBL with **1-La** + HOCHPh₂ + ^{R}LO
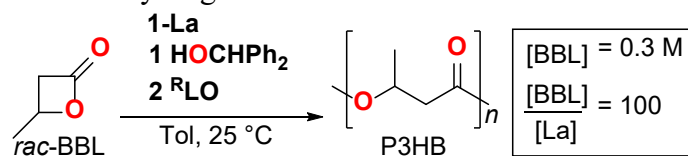
^{NMe2}LO		^{OMe}LO		LO		^{Cl}LO		^{NO2}LO	
Time (min)	Conv. (%)[a]	Time (min)	Conv. (%)[a]	Time (min)	Conv. (%)[a]	Time (min)	Conv. (%)[a]	Time (min)	Conv. (%)[a]
2	3.4	0.12	3.7	0.17	4.7	0.17	3.6	5	1.8
5	8.5	0.25	7.4	0.5	9.5	0.33	5.7	10	3.3
9	16.8	0.5	14.7	1	15.2	0.5	7.3	25	5.7
17	29.4	1	31.5	1.5	21.3	1	11.6	40	6.9
25	38.8	2	57.1	2	26.4	2	20.5		
		3	70.6						

a – Determined by ¹H-NMR integration of BBL and P3HB methine resonances in the crude reaction mixture.
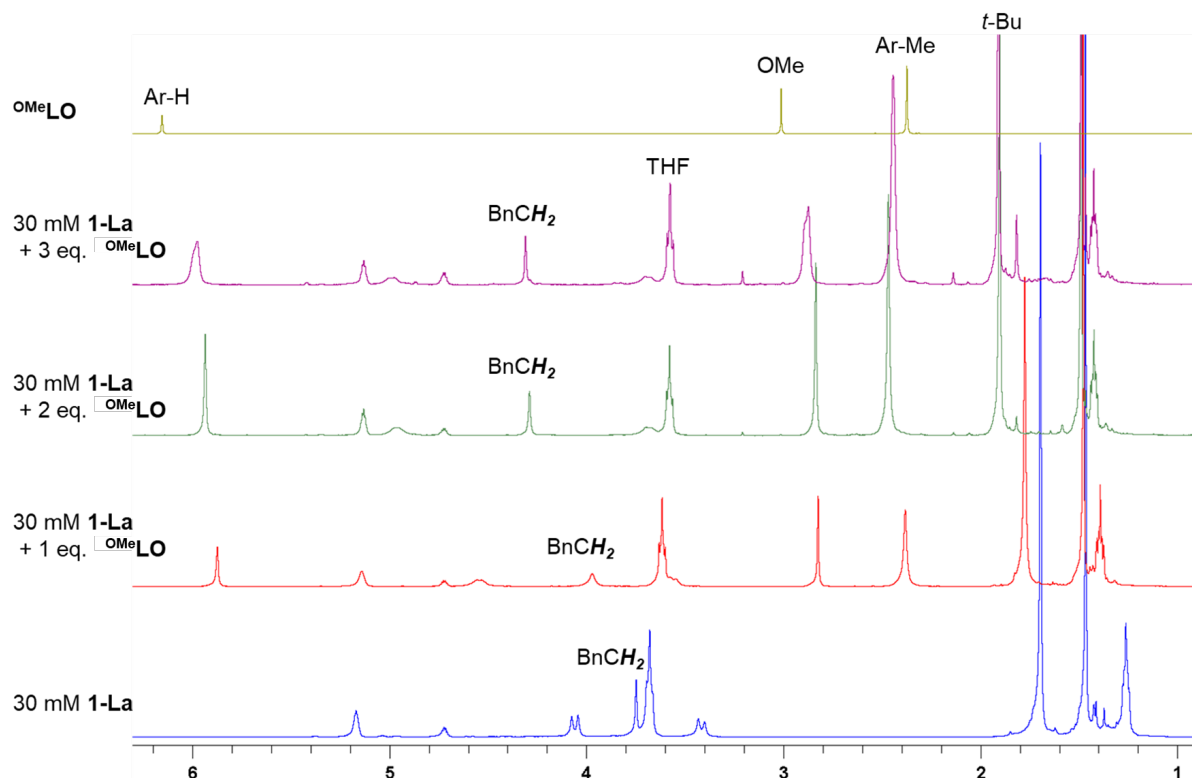
Figure 3.7. ¹H-NMR (400 MHz, C₆D₆, 298 K) of **1-La** (30 mM) in the presence of 0, 1, 2 and 3 equiv. of ^{OMe}LO.

Given the unprecedented reactivity of **1-La** in the presence of HOCHPh₂ and ^{R}LO, we set out to characterize the metal-ligand adducts to better understand the origin for the donor-amplified catalyst performance. A 1:2 binding stoichiometry between [**La**]:[^{OMe}LO] was determined

following the titration of **1-La** + HOCHPh$_2$ with varying equivalents of ^{OMe}**LO** (0 – 3 equiv) using ^{1}H NMR spectroscopy (Figure 3.7).
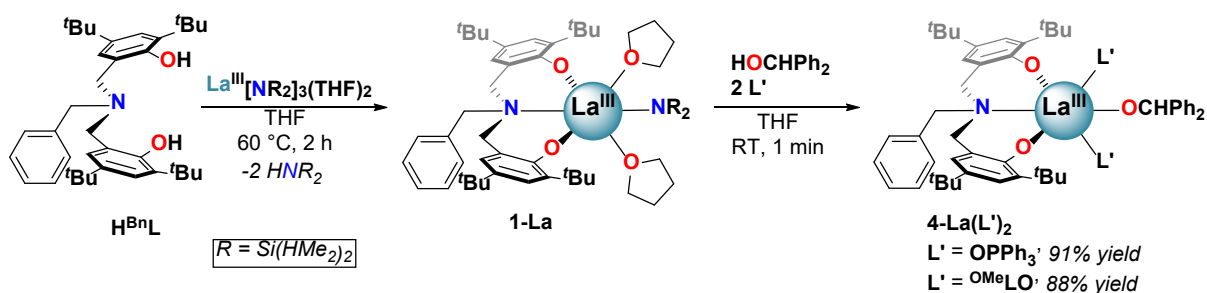
Scheme 3.1. Synthesis of **4-La(OPPh$_3$)$_2$** and **4-La(^{OMe}LO)$_2$**

Isolation of the 1:2 adducts, [La(^{Bn}L)(OCHPh$_2$)(^{OMe}LO)$_2$] (**4-La(^{OMe}LO)$_2$**) and [La(^{Bn}L)(OCHPh$_2$)(OPPh$_3$)$_2$] (**4-La(OPPh$_3$)$_2$**), were achieved in 91% and 88% yield, respectively, from the protonolysis of H^{Bn}L by La[N(SiHMe$_2$)$_2$]$_3$(THF)$_2$ followed by two equivalents ^{OMe}**LO** or OPPh$_3$ (Scheme 3.1). Similar to **1-La(OPPh$_3$)**, ^{1}H Diffusion-ordered NMR spectroscopy (DOSY)[30-32] supported monomeric formulations of **4-La(^{OMe}LO)$_2$** and **4-La(OPPh$_3$)$_2$** in C$_6$D$_6$ (Table 3.7).

Table 3.7. Diffusion coefficients, *D*, and estimated hydrodynamic radii, r$_H$, measured by ^{1}H DOSY NMR of complexes (**1-La(OPPh$_3$)$_2$, 4-La(OPPh$_3$)$_2$,** and **4-La(^{OMe}LO)$_2$**)

Species	D_{Fc} (10^{-10} m^2/s)^a	D (10^{-10} m^2/s)	D_{Fc}/D	r$_H$(DOSY)^b (Å)	r$_H$(theo.)^c (Å)
Fc^d	-	-	-	-	2.166
1-La(OPPh$_3$)$_2$^{e}	12.8	4.13	3.10	6.71	6.764
4-La(OPPh$_3$)$_2$	15.3	5.07	3.02	6.54	-
4-La(^{OMe}LO)$_2$	13.5	4.83	2.80	6.05	-

a – DOSY measured diffusion coefficient of ferrocene (Fc) in the experiment of the corresponding complex. DOSY measured diffusion coefficient of the sample *b* – r$_H$ = D_{Fc}/D_{sample}·r$_H$(Fc, theo.). *c* – r$_H$(theo.) is the average of half lengths of the principal axes of the homogeneous ellipsoid with the same principal moments of inertia of the molecule, which are determined from the crystal structure. *d* – Fc was added to each sample as an internal standard to cancel the fluctuation of temperature and viscosity, of which the diffusion coefficient varies. *e* – From Chapter 2. Previously proven to be monomeric in the solid (X-ray diffraction) and solution (DOSY).

At RT, both complexes displayed effective *C*$_s$ symmetry in solution, which was indicative of free rotation about the La–O$_{CHPh2}$ bond and rapid exchange of the axial neutral donor-ligands

on the NMR timescale. Ligand competition studies performed with **4-La(OPPh₃)₂** (40 mM, C₆D₆) in the presence of 1 equiv ^{R}**LO** enabled a qualitative ranking of donor strength.
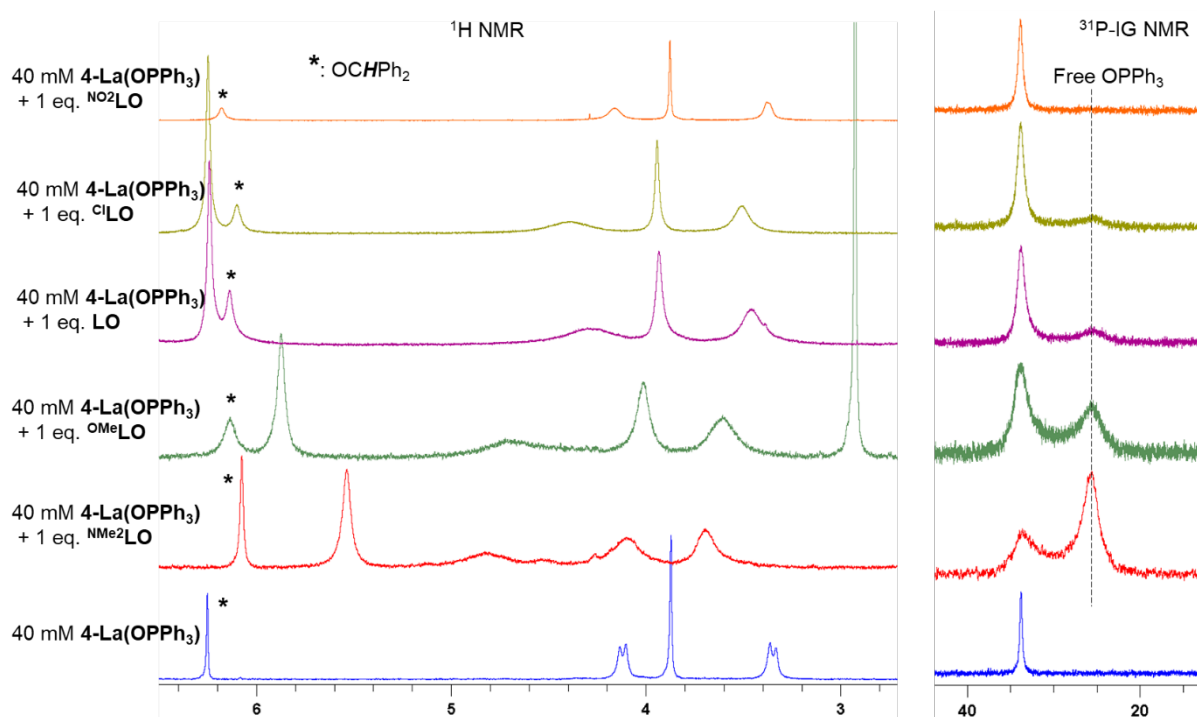
Figure 3.8. ^{1}H-NMR (400 MHz, C₆D₆, 298 K) and IG-^{31}P-NMR (162 MHz, C₆D₆, 298 K) of **4-La(OPPh₃)₂** (40 mM) and **4-La(OPPh₃)₂** (40 mM) in the presence of 1 equiv. of ^{R}**LO**.

Table 3.8. Equivalents of free OPPh₃ generated upon addition of 1 equiv ^{R}**LO** to **4-La(OPPh₃)₂** (C₆D₆ solution, RT, 40 mM).

^{R}**LO**	^{NMe2}**LO**	^{OMe}**LO**	**LO**	^{Cl}**LO**	^{NO2}**LO**
Equiv. of free OPPh₃[a]	1.32[b]	0.89	0.47	0.37	n.d.[c] (< 0.05)

a – Determined by integration of inverse-gated (IG) ^{31}P-NMR of free (26 ppm) and coordinated (34 ppm) OPPh₃ resonances. *b* – The generation of more than one equiv OPPh₃ from only one equiv ^{NMe2}**LO** suggests that a significant amount of another adduct, [La(^{Bn}L)(OCHPh₂)(^{NMe2}**LO**)], must also be formed with this strong donor. *c* – Not determined; no signal for free OPPh₃ was observed.

Quantification of free- and bound-OPPh₃ using inverse-gated ^{31}P NMR generated the following series: ^{NMe2}**LO** > ^{OMe}**LO** > OPPh₃ ~ **LO** > ^{Cl}**LO** >> ^{NO2}**LO** (Figure 3.8, Table 3.8), where donor

order followed expectations based on pK_a, σ_p, and natural charge of free ^{R}**LO** (*vide supra*). Furthermore, OPPh$_3$ and **LO** displayed comparable binding affinities, which made these ideal pairs to delineate the effects of donor sterics on catalyst performance.

Further insight into the structure of these adducts and the origins for enhanced reactivity and selectivity in the ROP of *rac*-BBL were provided by DFT modelling studies for the OPPh$_3$ and **LO** adducts of amide and alkoxide precatalysts (**1-La(L)$_2$** and **4-La(L)$_2$**; L = OPPh$_3$ and **LO**). For brevity, the discussion will focus on **1-La(L)$_2$**, as similar trends were observed for **1-La(L)$_2$** and **4-La(L)$_2$** (see Computational Section). The optimized structure of **1-La(OPPh$_3$)$_2$** obtained at the rM06-L[33] level of theory with Grimme's D3 dispersion correction[34] using Stuttgart-Dresden effective core-potentials on La[35-36] and 6-31G*[37-39] as a basis set for all other atoms was in good agreement with the previously reported X-ray structure (mean unsigned error, MUE: 0.0465). Qualitatively, partial space-filling models of **1-La(L)$_2$** revealed that **LO** and OPPh$_3$ exert significant axial steric pressure at the catalyst reaction site (Figure 3.9), and perhaps unexpectedly, the planar **LO** donor can adopt similar conformations to the phenyl rings of OPPh$_3$ positioned closest to the reaction site. Natural population analysis performed with NBO 3.1[40] revealed negligible differences in the natural charge of the amido nitrogens ($q_{\underline{N}(\text{SiHMe2})2}$: **1-La(OPPh$_3$)$_2$** = –1.84, **1-La(LO)$_2$** = –1.85), which implied steric origins for the differing performance of these pairs.

Buried volumes calculated from radii drawn to 3.5 Å, %$V_{bur}(r_{3.5})$, and 6.5 Å, %$V_{bur}(r_{6.5})$, using Samb$V$ca 2.1[41] revealed distinct and opposite crowding effects for **LO** and OPPh$_3$ in the primary and secondary coordination spheres (Figure 3.9 and Tables 3.9-3.12).
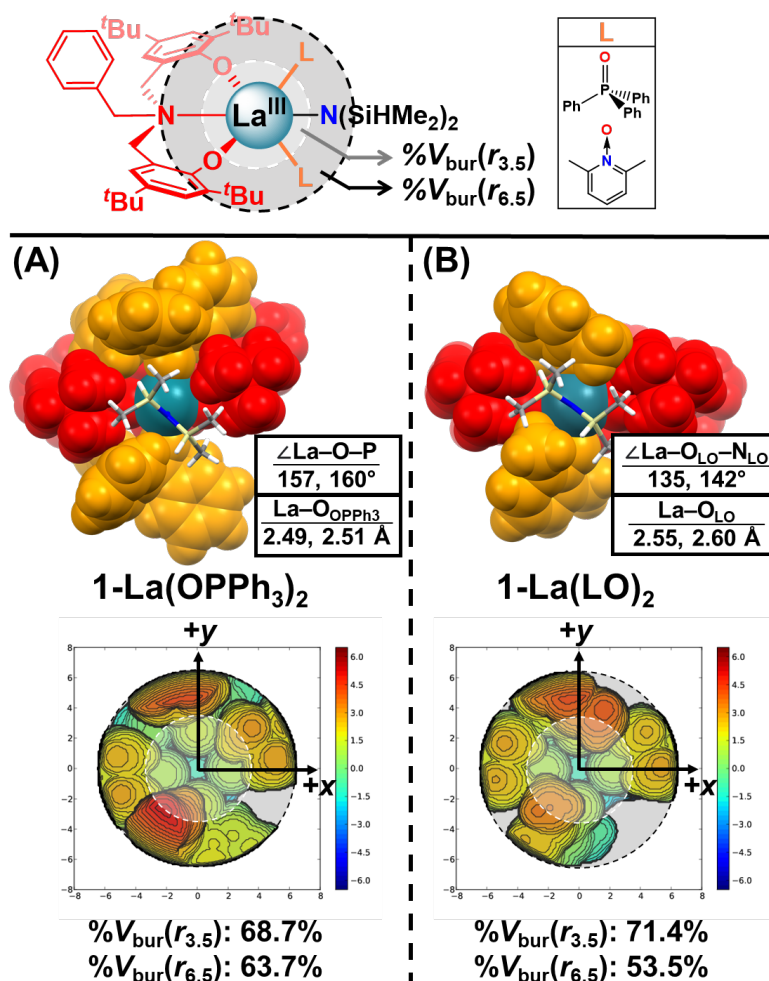
Figure 3.9. Comparison of DFT-optimized structures of (A) **1-La(OPPh₃)₂** and (B) **1-La(LO)₂**. Space-filling diagram: Neutral donors (OPPh₃, **LO**; orange), ^{Bn}L (red), La^{III} (teal). Capped sticks: N(SiHMe₂)₂. Buried volume (%V_{bur}) calculated at a radius (r) of 3.5 (white) and 6.5 Å (gray). La and N(SiHMe₂)₂ were excluded from the %V_{bur} calculations.

For **LO**, the ortho methyl groups and shallow La–O$_{LO}$–N$_{LO}$ bond-angles increased steric pressure within the primary coordination sphere (%$V_{bur}(r_{3.5})$): **1-La(OPPh₃)₂** = 63.7%, **1-La(LO)₂** = 68.7%), which should further disfavor coordination of P3HB ester linkages and therefore limit/suppress base-promoted elimination. The aryl groups of OPPh₃ led to significant steric crowding in the secondary coordination sphere (%$V_{bur}(r_{6.5})$): **1-La(OPPh₃)₂** = 71.4%, **1-La(LO)₂** = 53.5%); however, these larger structural changes seem to contribute very little, if at all, to catalyst isoselectivity and rates

Table 3.9. %V_{bur}($r_{3.5}$) of **1-La(OPPh₃)₂**

Quadrant	V_{free}	V_{bur}	V_{total}	%V_{free}	%V_{bur}
SW	10.8	34.0	44.9	24.2	75.8
NW	16.5	28.4	44.9	36.8	63.2
NE	11.8	33.0	44.9	26.4	73.6
SE	16.9	27.9	44.9	37.7	62.3

%V_{free} = 31.3% // %V_{bur} = 68.7%
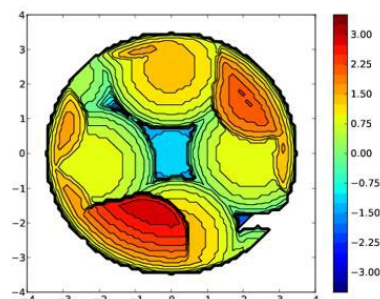
Table 3.10. %V_{bur}($r_{6.5}$) of **1-La(OPPh₃)₂**

Quadrant	V_{free}	V_{bur}	V_{total}	%V_{free}	%V_{bur}
SW	63.4	223.9	287.4	22.1	77.9
NW	91.5	195.8	287.4	31.9	68.1
NE	87.7	199.6	287.4	30.5	69.5
SE	174.2	113.2	287.4	60.6	39.4

%V_{free} = 36.3% // %V_{bur} = 63.7%
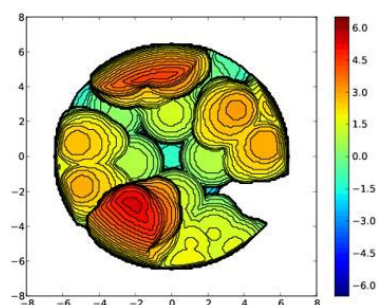
Table 3.11. %V_{bur}($r_{3.5}$) of **1-La(LO)₂**

Quadrant	V_{free}	V_{bur}	V_{total}	%V_{free}	%V_{bur}
SW	8.1	36.8	44.9	18.0	82.0
NW	13.5	31.4	44.9	30.1	69.9
NE	11.1	33.8	44.9	24.7	75.3
SE	18.7	26.2	44.9	41.6	58.4

%V_{free} = 28.6% // %V_{bur} = 71.4%
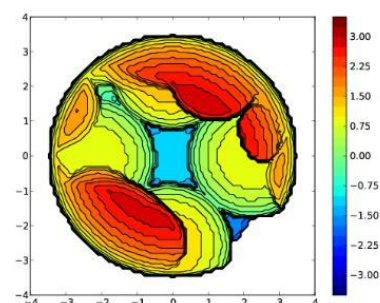
Table 3.12. %V_{bur}($r_{6.5}$) of **1-La(LO)₂**

Quadrant	V_{free}	V_{bur}	V_{total}	%V_{free}	%V_{bur}
SW	117.4	169.9	287.4	40.9	59.1
NW	106.1	181.3	287.4	36.9	63.1
NE	125.9	161.4	287.4	43.8	56.2
SE	185.6	101.7	287.4	64.6	35.4

%V_{free} = 46.5% // %V_{bur} = 53.5%
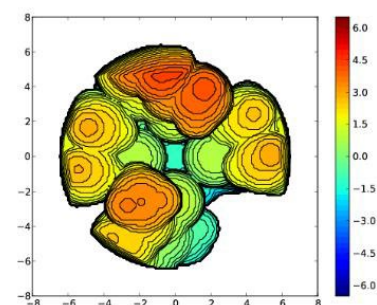
3.3. Conclusions

In closing, *N*-oxides can amplify catalyst performance in stereospecific ROP to unprecedented levels, where addition of ^{OMe}**LO** to **1-La** generates the most active isoselective catalyst for the ROP of *rac*-BBL reported to date. Our experimental and computational studies begin to establish clear connections between donor structure and strength on catalyst performance. Donor strength is clearly the presiding factor controlling catalyst activity in these systems, where the turnover limiting step is highly dependent on donor binding equilibria. Alternatively, the donor's steric profile in the primary coordination sphere plays a large role in suppressing catalyst deactivation. While the presence of a donor is crucial to the observed stereoselectivity, P_m were found to be nearly independent of donor strength and steric profile. Our results suggest that further improvements in catalyst performance might be realized by varying the donor steric profile in the primary coordination sphere, and optimizing binding affinity via attenuated donor electronics.

3.4. Experimental Section

3.4.1. General Methods

Instruments and measurements: Unless specified, all reactions were performed under inert conditions (N_2) using standard Schlenk techniques or in a MBraun drybox equipped with a standard catalyst purifier and solvent trap. Glassware was oven-dried for at least 2 h at 150 °C prior to use. Celite and 3 Å molecular sieves were heated under reduced pressure at 300 °C for at least 24 h and then cooled under vacuum prior to use. The following spectrometers were used for NMR characterization: Bruker Avance III HD Ascend (^{1}H: 600 MHz, ^{13}C: 151 MHz, ^{31}P: 243 MHz) and a Bruker DRX (^{1}H: 400 MHz, ^{13}C: 101 MHz, ^{31}P: 162 MHz). ^{1}H- and ^{13}C-NMR shifts are referenced relative to the solvent signal (CDCl$_3$: ^{1}H: 7.26 ppm, ^{13}C: 77.16 ppm; C$_6$D$_6$: ^{1}H: 7.16 ppm, ^{13}C: 128.06 ppm), while ^{31}P-NMR shifts are referenced relative to external solution standards (H$_3$PO$_4$, 0 ppm). Both instruments were equipped with Z-gradient BBFO probes. Polymer tacticity (P_m, percentage of *meso* diads) was measured using a ^{13}C inverse-gated pulse sequence, followed by integration of the *C*=O resonances (Figure 3.15).

Gel permeation chromatography (GPC) measurements were performed using an Agilent 1260 equipped with two Poroshell 120 EC-C18 columns heated at 35 °C (4.6 x 100 mm, 2.7 μm) and a UV-vis diode-array detector and refractive detector. The eluent was inhibitor-free THF, and the system was calibrated with standard polystyrene standards ranging from 580 to 1,500,000 Da. Reported molecular weights are those obtained from GPC corrected by a Mark-Houwink factor of 0.54.[15] Unless stated otherwise, all GPC samples were of the quenched crude reaction mixtures (not precipitated or purified polymers). Elemental analyses were performed

by CENTC Elemental Analysis Facility at University of Rochester (Rochester, NY) for air-sensitive compounds (**1-RE** and **1-RE(OPPh$_3$)$_2$**) respectively. Samples were shipped in a sealed 2 mL vial that was placed in a 20 mL scintillation vial and sealed, which were then placed in a vacuum-sealed plastic bag.

Materials: Tetrahydrofuran, diethyl ether, toluene, hexanes, and pentane were purchased from Fisher Scientific. Solvents were sparged for 20 min with dry Ar and dried using a commercial two-column solvent purification system (LC Technologies). Solvents were further dried by storing them over 3 Å molecular sieves for at least 48 h prior to use. Ultrapure, deionized water (18.2 MΩ) was obtained from a Millipore Direct-Q 3 UV Water Purification System. Deuterated solvents were purchased from Cambridge Isotope Laboratories, Inc. C$_6$D$_6$ was degassed with 3 freeze-pump-thaw cycles and stored over 3 Å molecular sieves for at least 48 h prior to use. Qualitative assessment of moisture-content in these solvents was performed by adding 1 drop of a concentrated solution of a sodium benzophenone radical anion (purple) to 10 mL of solvent where maintenance of a dark blue color for at least 5 minutes was sufficient for use.

2,6-ditertbutyl phenol (Oakwood Chemical; 99% purity), para-formaldehyde (Alfa Aesar; 97% purity), benzylamine (TCI; 99% purity), triphenylphosphine oxide (Acros; 99% purity), hexamethylphosphoramide (TCI; 98% purity), triphenylphosphate (Sigma-Aldrich; 99% purity), potassium hexamethyldisilazide (Sigma-Aldrich; 95% purity), 1,1,3,3-tetramethyldisilazane (TCI, 97% purity), LaCl$_3$ (Strem; RE = La; 99.9% purity), and acetyl

chloride (Acros; 99% purity) were purchased and used as received. Racemic butyrolactone (Sigma-Aldrich; 98% purity) was freshly distilled from CaH_2 under nitrogen and degassed by freeze-pump-thaw cycles prior to use. $La[N(SiMe_3)_2]_3$,[42] $La[N(SiHMe_2)_2]_3(THF)_2$,[43] **BnL**, **1-La**, **1-La(OPPh$_3$)$_2$**,[1] were prepared according to reported procedures.

3.4.2. Synthetic Details and Characterization.
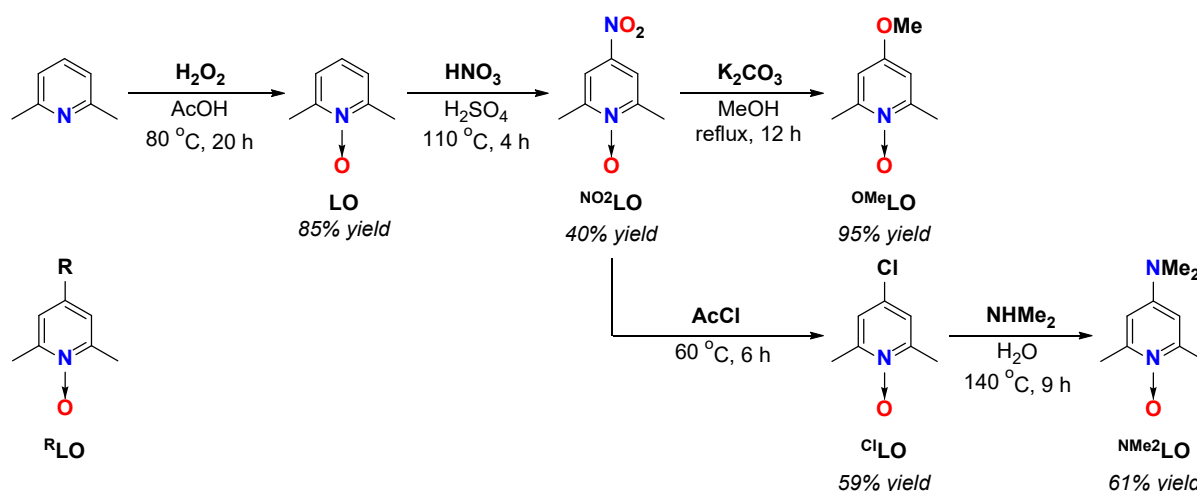
Scheme 3.2. Synthesis of 4-substituted lutidine-oxides (**^{R}LO**)

2,6-Lutidine-1-oxide (LO)
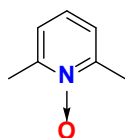
H_2O_2 (20 mL, 174 mmol, 2.0 equiv., 27% in H_2O, 1.10 g/mL; MW = 34.01 g•mol^{-1}) was added to a stirring solution of 2,6-lutidine (9.30 g, 86.8 mmol, 1.0 equiv.; MW = 107.16 g•mol^{-1}) in AcOH (25 mL, 434 mmol, 5.0 equiv., 1.05 g/mL; MW = 60.05 g•mol^{-1}) in a 250 mL round-bottomed flask equipped with a Vigreux condenser. The reaction was heated at 80 °C for 20 h. A saturated $Na_2S_2O_5$ solution (10 mL) was added to the reaction to quench residual peroxide. The reaction was concentrated to ca. 25 mL at 60 °C under reduced pressure (ca. 0.5 Torr). The pH of the mixture was adjusted to 12 with a 25% NaOH solution. The mixture was extracted

with CH$_2$Cl$_2$ (6 x 20 mL). The combined extraction was dried with Na$_2$SO$_4$, filtered, and evaporated under reduced pressure. **2,6-Lutidine-1-oxide** was obtained as a colorless oil. Yield: 9.10 g (20.3 mmol, 85% yield; MW: 123.16 g•mol^{-1}). The ^{1}H-NMR spectrum agrees with the previous report.[44]

^{1}H-NMR (400 MHz, CDCl$_3$, 298 K): δ (ppm) = 2.52 (s, 6H; Me), 7.05 (dd, J = 8.4, 7.6 Hz, 2H; 3,5-H), 7.12 (d, J = 7.6 Hz, 1H; 4-H);

^{1}H-NMR (400 MHz, C$_6$D$_6$, 298 K): δ (ppm) = 2.31 (s, 6H; Me), 6.28 (t, J = 7.6 Hz, 2H; 3,5-H), 6.39 (d, J = 7.6 Hz, 1H; 4-H).

4-Nitro-2,6-lutidine-1-oxide (^{NO2}LO)

H$_2$SO$_4$ (6.2 mL 114 mmol, 3.0 equiv., 98%, 1.84 g/mL; MW = 98.07 g•mol^{-1}) was added to 2,6-lutidine-1-oxide (4.66 g 37.8 mmol, 1.0 equiv.; MW = 123.16 g•mol^{-1}) in a 250 mL round-bottomed flask equipped with a Vigreux condenser. HNO$_3$ (4.8 mL 76 mmol, 2.0 equiv., 70% in water, 1.41 g/mL; MW = 63.01 g•mol^{-1}) was added dropwise. The reaction was heated at 110 °C for 4 h and allowed to warm to RT. The flask was then cooled in an ice bath, and water (50 mL) was added. The mixture was extracted with CH$_2$Cl$_2$ (3 x 25 mL). The combined organic layer was washed with saturated Na$_2$CO$_3$ solution (2 x 25 mL) and water (2 x 25 mL), dried with Na$_2$SO$_4$, filtered, and dried under reduced pressure. The resulting solid was washed with pentane (3 x 20 mL) and dried under reduced pressure. **4-Nitro-2,6-lutidine-1-oxide** was

obtained as a light-yellow solid. Yield: 2.53 g (15.1 mmol, 40% yield; MW: 168.15 g•mol^{-1}).

The ^{1}H-NMR spectrum agrees with the previous report.[44]

^{1}H-NMR (400 MHz, CDCl$_3$, 298 K): δ (ppm) = 2.58 (s, 6H; Me), 8.03 (s, 2H; 3,5-H);

^{1}H-NMR (400 MHz, C$_6$D$_6$, 298 K): δ (ppm) = 1.92 (s, 6H; Me), 7.14 (s, 2H; 3,5-H).

4-Methoxy-2,6-lutidine-1-oxide (^{OMe}LO)
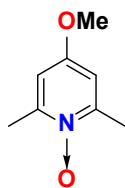
K$_2$CO$_3$ (2.38 g 17.3 mmol, 2.0 equiv.; MW = 138.20 g•mol^{-1}) was added to a suspension of 4-nitro-2,6-lutidine-1-oxide (1.45 g 8.62 mmol, 1.0 equiv.; MW = 168.15 g•mol^{-1}) in 15 mL MeOH in a 250 mL round-bottomed flask equipped with a Vigreux condenser. The reaction was heated in an oil bath at 70 °C for 12 h and allowed to reflux. The mixture was cooled and concentrated to ca. 10 mL under reduced pressure. Water (20 mL) was added and the mixture was extracted with CH$_2$Cl$_2$ (3 x 15 mL). The combined extraction was dried with Na$_2$SO$_4$, filtered, and dried under reduced pressure. **4-Methoxy-2,6-lutidine-1-oxide** was obtained as a white solid. Yield: 1.25 g (8.16 mmol, 95% yield; MW: 153.18 g•mol^{-1}). The ^{1}H-NMR spectrum agrees with the previous report.[44]

^{1}H-NMR (400 MHz, CDCl$_3$, 298 K): δ (ppm) = 2.53 (s, 6H; ArMe), 3.81 (s, 3H; OMe), 6.69 (s, 2H; 3,5-H);

^{1}H-NMR (400 MHz, C$_6$D$_6$, 298 K): δ (ppm) = 2.37 (s, 6H; ArMe), 3.01 (s, 3H; OMe), 6.15 (s, 2H; 3,5-H).

4-Chloro-2,6-lutidine-1-oxide (^{Cl}LO)
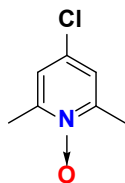
A 250 mL round-bottomed flask was charged with 4-nitro-2,6-lutidine-1-oxide (3.33 g 19.8 mmol, 1.0 equiv.; MW = 168.15 g•mol^{-1}) and AcCl (21 mL, 297 mmol, 15 equiv., 1.10 g/mL; MW = 78.50 g•mol^{-1}) and equipped with a Vigreux condenser. The suspension was heated for 6 h in an oil bath at 60 °C and allowed to reflux. The precipitated solid was isolated by vacuum filtration, washed with acetone (3 x 5 mL), and then dissolved in CH$_2$Cl$_2$ (15 mL). The solution was washed with 10% NaOH solution (15 mL) and water (15 mL). The organic layer was dried with Na$_2$SO$_4$, filtered, and dried under reduced pressure. **4-Chloro-2,6-lutidine-1-oxide** was obtained as a white solid. Yield: 1.85 g (11.7 mmol, 59% yield; MW: 157.60 g•mol^{-1}). The ^{1}H-NMR spectrum agrees with the previous report.[44]

^{1}H-NMR (400 MHz, CDCl$_3$, 298 K): δ (ppm) = 2.49 (s, 6H; ArMe), 7.14 (s, 2H; 3,5-H);

^{1}H-NMR (400 MHz, C$_6$D$_6$, 298 K): δ (ppm) = 2.10 (s, 6H; ArMe), 6.32 (s, 2H; 3,5-H).

4-Dimethylamino-2,6-lutidine-1-oxide (^{NMe2}LO)
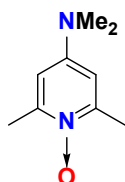
4-Chloro-2,6-lutidine-1-oxide (400 mg, 2.54 mmol, 1.0 equiv.; MW = 157.60 g•mol^{-1}) was added to an aqueous solution of NHMe$_2$ (4.8 mL, 38.1 mmol, 15 equiv., 40% in H$_2$O, 0.89

g/mL; MW = 45.09 g•mol^{-1}) in a 50 mL sealed vessel. The reaction vessel was heated for 9 h at 140 °C, and then allowed to cool to RT prior to opening. Water (5 mL) was added and the reaction mixture and was extracted with CH$_2$Cl$_2$ (9 x 10 mL). The combined extraction was dried with Na$_2$SO$_4$, filtered, and evaporated under reduced pressure to yield the crude product as a brown oil. Toluene (5 mL) was added to the crude product, then dried under reduced pressure, followed by CH$_2$Cl$_2$ (5 mL). Volatiles were removed under reduced pressure. **4-Dimethylamino-2,6-lutidine-1-oxide** was obtained as a white solid. Yield: 256 mg (1.54 mmol, 61% yield; MW: 166.22 g•mol^{-1}).

^{1}H-NMR (400 MHz, CDCl$_3$, 298 K): δ (ppm) = 2.43 (s, 3H; ArMe), 2.92 (s, 6H; NMe$_2$), 6.30 (s, 2H; 3,5-H);

^{1}H-NMR (400 MHz, C$_6$D$_6$, 298 K): δ (ppm) = 2.18 (s, 3H; NMe$_2$), 2.53 (s, 6H; ArMe), 5.93 (s, 2H; 3,5-H).

La(^{Bn}L)(OCHPh$_2$)(OPPh$_3$)$_2$ [4-La(OPPh$_3$)$_2$]

4-La(OPPh₃)₂
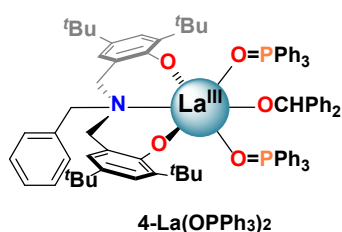
A 20 mL scintillation vial was charged with **H^{Bn}L** (304 mg, 0.56 mmol, 1.0 equiv.; MW: 543.84 g•mol^{-1}), a Teflon-coated stir-bar, and THF (2 mL). To the stirring, clear, and colorless solution, La[N(SiHMe$_2$)$_2$]$_3$(THF)$_2$ (380 mg, 0.56 mmol, 1.0 equiv.; MW: 680.12 g•mol^{-1}) was added. The solution was heated at 60 °C for 2 h and conversion to **1-La** was confirmed by H-NMR analysis of a reaction aliquot. After the solution was cooled to RT, HOCHPh$_2$ (103 mg, 0.56

mmol, 1.0 equiv.; MW: 184.24 g•mol^{-1}) and OPPh$_3$ (311 mg, 1.12 mmol, 2.0 equiv.; MW: 278.29 g•mol^{-1}) was added. The solution was stirred for 1 min, and then all volatiles were removed under reduced pressure. The resulting solid was triturated with toluene (2 x 2 mL), washed with pentane (2 x 3 mL), and dried under reduced pressure to afford **4-La(OPPh$_3$)$_2$** as a white solid. Yield: 725 mg (0.51 mmol, 91% yield; MW: 1420.54 g•mol^{-1}).

^{1}H-NMR (400 MHz, C$_6$D$_6$, 298 K): δ (ppm) = 1.58 (s, 18H; 4-^{t}Bu), 1.71 (s, 18H; 2-^{t}Bu), 3.35 (d, ^2J = 12.3 Hz, 2H; NCH_2ArO), 3.87 (s, 2H; NCH_2Bn), 4.12 (d, ^2J = 12.3 Hz, 2H; NCH_2ArO), 6.25 (s, 1H; OCHPh$_2$), 6.86-6.91 (m, 12H; m-H$_{OPPh3}$), 6.97-7.09 (m, 13H; p- H$_{OPPh3}$, 5-H$_{ArO}$, H$_{Ph}$), 7.11-7.17 (m, 4H; H$_{Ph}$), 7.21 (d, J = 7.3 Hz, H$_{Bn}$), 7.56-7.61 (m, 14H; o-H$_{OPPh3}$, 3-H$_{ArO}$), 7.76 (d, J = 7.4 Hz, 4H; o-H$_{OCHPh2}$);

^{13}C{^{1}H}-NMR (101 MHz, C$_6$D$_6$, 298 K): δ (ppm) = 30.6 (C$\underline{Me}_3$), 32.5 (C$\underline{Me}_3$), 34.3 ($\underline{C}$Me$_3$), 35.8 ($\underline{C}$Me$_3$), 51.4 (N$\underline{C}$H$_2$Bn), 59.9 (N$\underline{C}$H$_2$ArO), 82.4 (O$\underline{C}$HPh$_2$), 123.2, 125.2, 125.5, 126.8, 127.5, 127.8, 127.9 128.2, 128.9 (d, $J_{P(31)-C(13)}$ = 12.6 Hz; m-C$_{OPPh3}$), 130.6 (d, $J_{P(31)-C(13)}$ = 106 Hz; C–P), 132.0, 132.3 (d, $J_{P(31)-C(13)}$ = 2.2 Hz; p-C$_{OPPh3}$), 132.8 (d, $J_{P(31)-C(13)}$ = 10.6 Hz; o-C$_{OPPh3}$, 133.8, 135.6, 136.7, 151.9 (O-CH-$\underline{C}$$_{OCHPh2}$), 164.3 (C$_{Ar}$–O);

^{31}P{^{1}H}-NMR (162 MHz, C$_6$D$_6$, 298 K): δ (ppm) = 33.8 (br);

Elemental Analysis calcd. (%) for C$_{89}$H$_{92}$LaN$_2$O$_5$P$_2$: C 72.72, H 6.53, N 0.99; found: C 72.55, H 6.87, N 1.00.
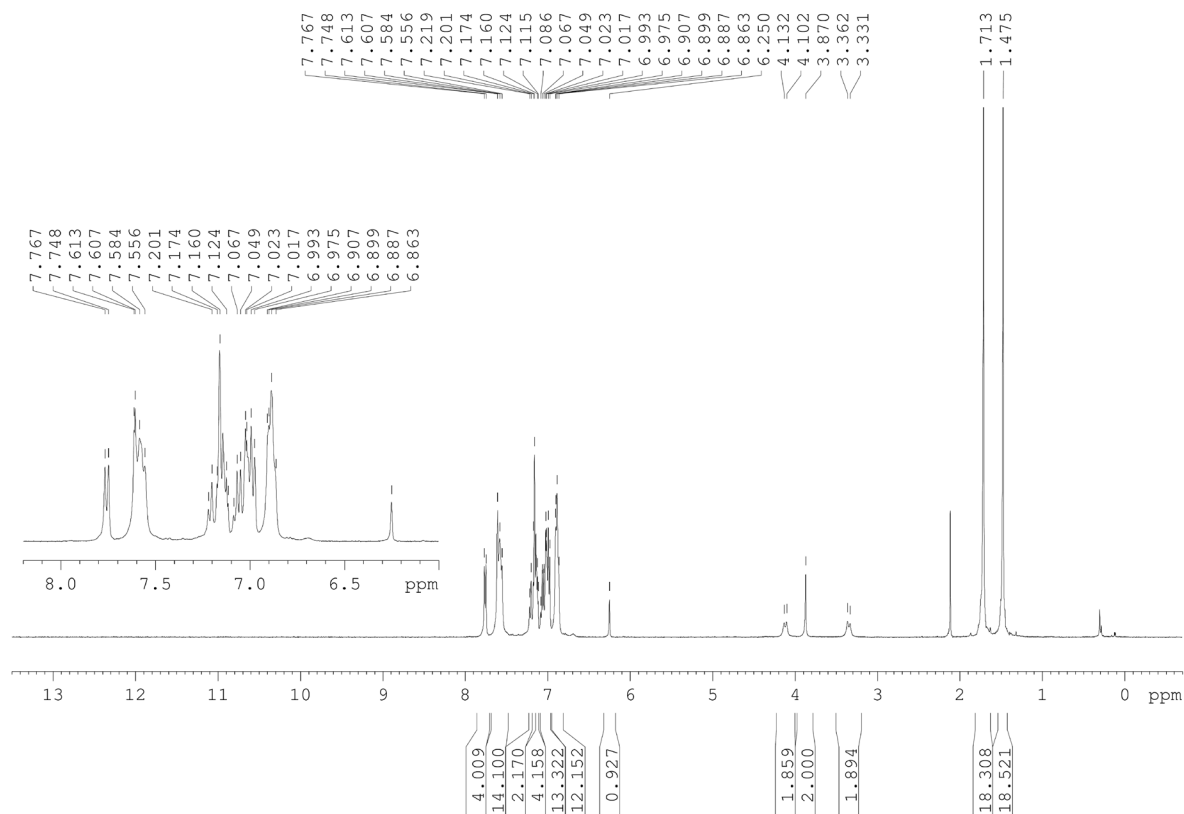
Figure 3.10a. ^{1}H-NMR (C$_6$D$_6$, 400 MHz) spectra of **4-La(OPPh$_3$)$_2$**.
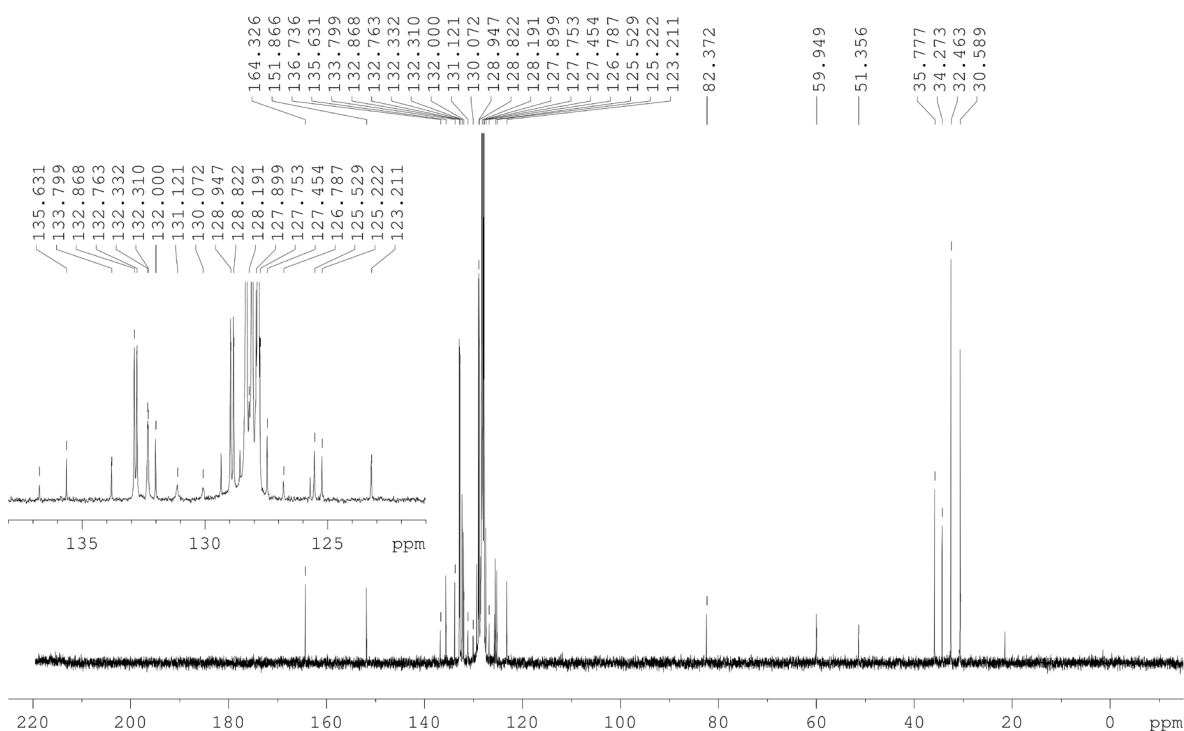
Figure 3.10b. ^{13}C{^{1}H}- NMR (C$_6$D$_6$, 101 MHz) spectra of **4-La(OPPh$_3$)$_2$.**
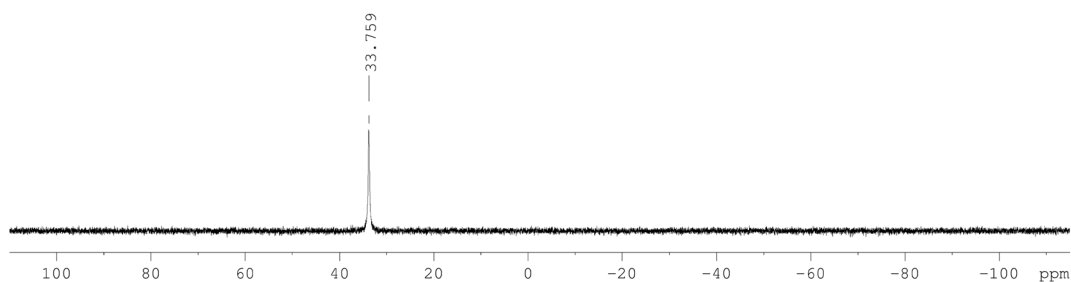
Figure 3.10c. $^{31}P\{^1H\}$-NMR (C6D6, 162 MHz) spectra of **4-La(OPPh3)2.**

La(^{Bn}L)(OCHPh2)(^{OMe}LO)2 [4-La(^{OMe}LO)2]

2-La(^{OMe}LO-LO)2
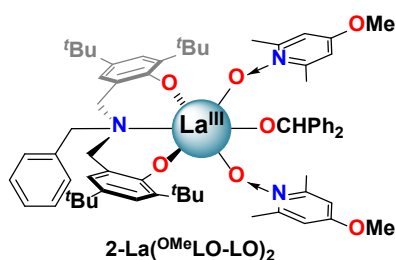
A 20 mL scintillation vial was charged with **H^{Bn}L** (139 mg, 0.26 mmol, 1.0 equiv.; MW: 543.84 g•mol^{-1}), a Teflon-coated stir-bar, and THF (2 mL). To the stirring, clear, and colorless solution, La[N(SiHMe2)2]3(THF)2 (174 mg, 0.26 mmol, 1.0 equiv.; MW: 680.12 g•mol^{-1}) was added. The solution was heated at 60 °C for 2 h and conversion to **1-La** was confirmed by H-NMR analysis of a reaction aliquot. After the solution was cooled to RT, Ph2CHOH (47 mg, 0.26 mmol, 1.0 equiv.; MW: 184.24 g•mol^{-1}) and 4-MeO-LO (78 mg, 10.51 mmol, 2.0 equiv.; MW: 153.18 g•mol^{-1}) was added. The solution was stirred for 1 min, and then all volatiles were removed under reduced pressure. The resulting solid was washed with cold pentane (2 x 2 mL) and dried under reduced pressure to afford **4-La(^{OMe}LO)2** as a white solid. Yield: 264 mg (0.23 mmol, 88% yield; MW: 1170.32 g•mol^{-1}). **Note**: The product was consistently found to contain ca. 1 equiv. pentane even after drying under reduced pressure (ca. 1 Torr) at RT.

^{1}H-NMR (600 MHz, C6D6, 298 K): δ (ppm) = 1.49 (s, 18H; 4-^{t}Bu), 1.91 (s, 18H; 2-^{t}Bu), 2.31

(s, 12H; ArMe$_{OMe-LO}$), 2.85 (s, 6H; OMe), 3.75 (d, ^2J = 12.7 Hz, 2H; NC$\underline{H_2}$ArO), 4.26 (s, 2H; NC$\underline{H_2}$Bn), 5.05 (d, br, ^2J = 12.7 Hz, 2H; NC$\underline{H_2}$ArO), 5.75 (s, 1H; OC$\underline{H}$Ph$_2$), 5.78 (s, 4H; 3,5-H$_{OMe-LO}$), 6.96 (t, J = 7.2 Hz, 2H; p-H$_{OCHPh2}$), 7.10 (t, J = 7.4 Hz, 4H; m-H$_{OCHPh2}$), 7.17 (heavily overlapped with C$_6$D$_5$H, 1H; p-H$_{Bn}$), 7.27 (d, J = 2.4 Hz, 2H; 5-H$_{ArO}$), 7.30 (t, J = 7.2 Hz, 2H; m-H$_{Bn}$), 7.45 (d, J = 7.4 Hz, 4H; o-H$_{OCHPh2}$), 7.56 (br, 2H; o-H$_{Bn}$), 7.67 (d, J = 2.4 Hz, 2H; 3-H$_{ArO}$);

^{13}C{^{1}H}-NMR (151 MHz, C$_6$D$_6$, 298 K): δ (ppm) = 19.38 (Ar$\underline{Me}_{OMe-LO}$), 30.6 (C$\underline{Me}_3$), 32.4 (C$\underline{Me}_3$), 34.3 ($\underline{C}$Me$_3$), 35.8 ($\underline{C}$Me$_3$), 50.8 (N$\underline{C}$H$_2$Bn), 55.0 (OMe), 60.6 (N$\underline{C}$H$_2$ArO), 81.4 (O$\underline{C}$HPh$_2$), 109.4 (3,5-C$_{OMe-LO}$), 123.3, 125.3, 125.7, 127.2, 127.3, 127.78 127.81, 128.3, 128.4, 132.5 (2,6-C$_{OMe-LO}$), 134.3, 135.4, 136.6, 150.6 (O-CH-$\underline{C}_{OCHPh2}$), 158.6 (br, 4-C$_{OMe-LO}$), 164.0 (C$_{Ar}$–O);

Elemental Analysis calcd. (%) for (C$_{66}$H$_{84}$LaN$_3$O$_7$ + C$_5$H$_8$): C 68.86, H 7.49, N 3.39; found: C 68.59, H 7.67, N 3.35.
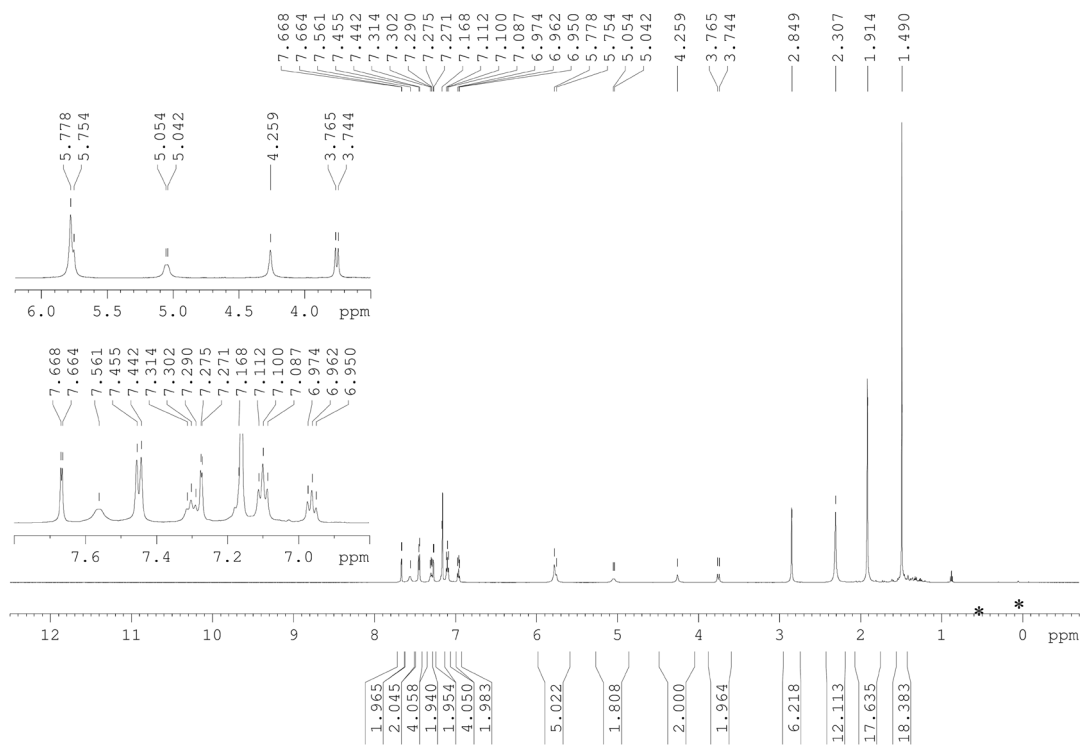
Figure 3.11a. ^{1}H-NMR (C$_6$D$_6$, 600 MHz) spectra of **4-La(^{OMe}LO)$_2$** (*: pentane).
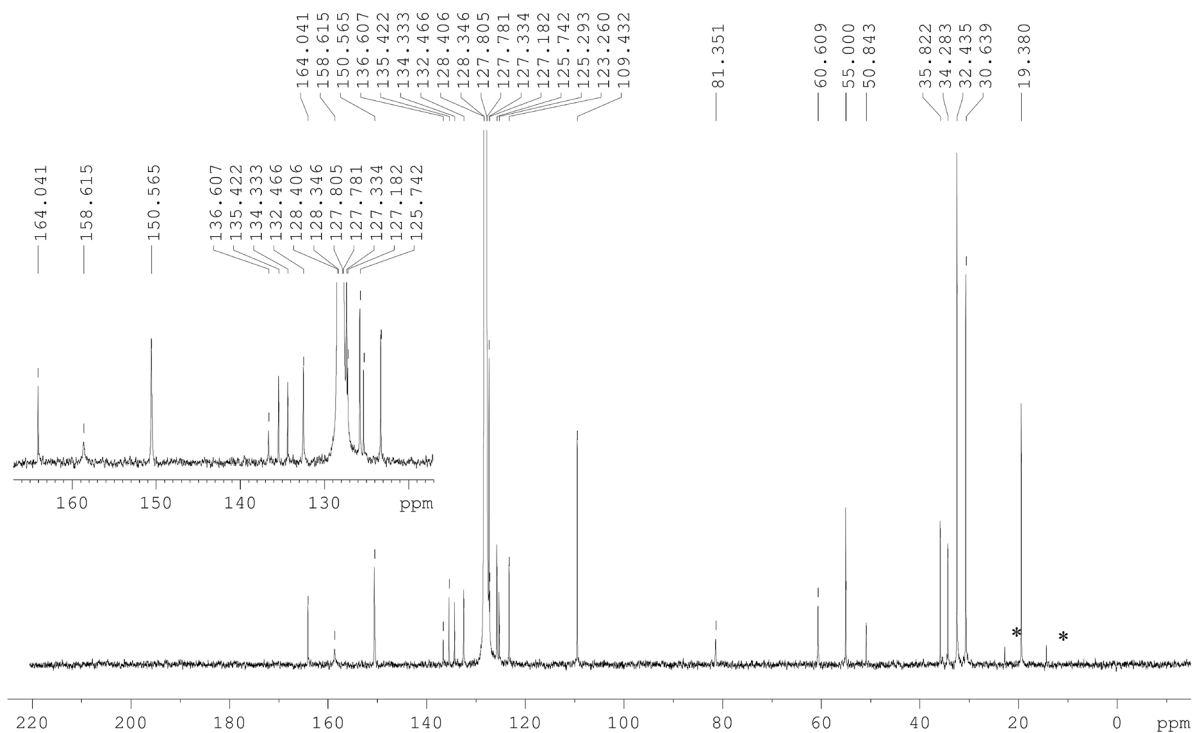
Figure 3.11b. ^{13}C{^{1}H}-NMR (C$_6$D$_6$, 151 MHz) spectra of **4-La(^{OMe}LO)$_2$** (*: pentane).
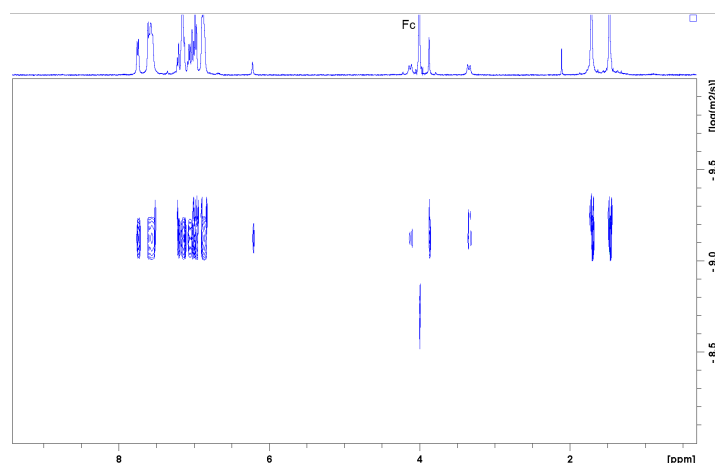
Figure 3.12. ^{1}H DOSY NMR (400 MHz, C$_6$D$_6$) of a mixture of **4-La(OPPh$_3$)$_2$** and ferrocene (Fc). **4-La(OPPh$_3$)$_2$** (14 mg, 0.010 mmol, 1.0 equiv; MW: 1420.54 g•mol^{-1}) and Fc (3.5 mg, 0.019 mmol, 1.9 equiv; MW: 186.04 g•mol^{-1}) were dissolved in 0.5 mL C$_6$D$_6$. Diffusion time was (Δ, d20) 100 ms, and the rectangular gradient pulse duration (δ, p30) was 1000 µs.
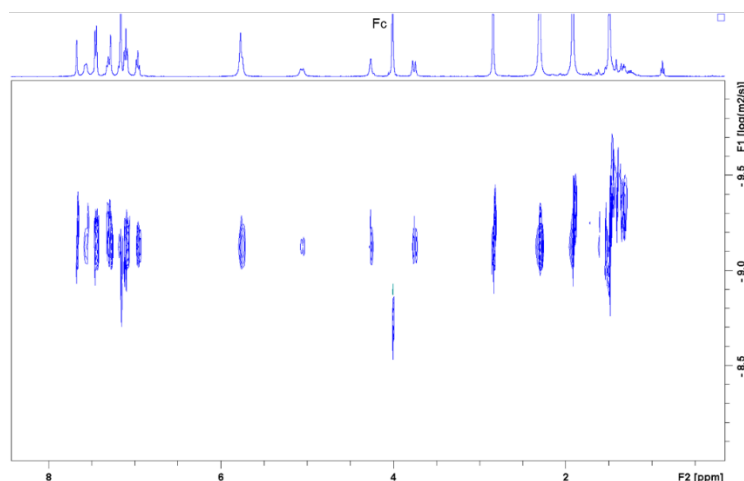
Figure 3.13. ^{1}H DOSY NMR (400 MHz, C$_6$D$_6$) of a mixture of **4-La(^{OMe}LO)$_2$** and ferrocene (Fc). **4-La(^{OMe}LO)$_2$** (12 mg, 0.010 mmol, 1.0 equiv; MW: 1170.32 g•mol^{-1}) and Fc (2.0 mg, 0.011 mmol, 1.1 equiv; MW: 186.04 g•mol^{-1}) were dissolved in 0.5 mL C$_6$D$_6$. Diffusion time was (Δ, d20) 100 ms, and the rectangular gradient pulse duration (δ, p30) was 1000 µs.

3.4.3. Experimental Procedures

Typical polymerization procedures

Reactions at ambient temperature:

In a glovebox, a 2 mL scintillation vial was charged with **1-La** (5.0 mg, 0.0052 mmol, 1.0 equiv.; MW: 957.27 g•mol^{-1}), and toluene (0.382 mL). A toluene solution of HOCHPh$_2$ (2% m/m, 0.055 mL, ρ = 0.867 g/mL; 0.96 mg, 0.0052 mmol, 1.0 equiv.; MW: 184.24 g•mol^{-1}) then

a toluene solution of ligand, e.g., ^{OMe}LO (5% m/m, 0.037 mL, $\rho = 0.867$ g/mL; 1.6 mg, 0.0105 mmol, 2.0 equiv.; MW: 153.18 g•mol^{-1}) were added to the clear, colorless solution. After approximately one minute, *rac*-BBL (0.085 mL, $\rho = 1.06$ g/mL, 90 mg, 1.04 mmol, 200 equiv.; MW: 86.09 g•mol^{-1}) was added to the catalyst solution. The conversion was checked by ^{1}H NMR by adding a reaction aliquot to a 0.02 mL of a ca. 5 wt% toluene solution of benzoic acid (BzOH), followed by addition of CDCl$_3$ (~0.5 mL). After the desired conversion and/or time was reached, the reaction was quenched by the addition of a toluene solution of BzOH (5% m/m, ca. 0.1 mL), and volatiles were removed under reduced pressure.

Note: The ROP of *rac*-BBL is exothermic ($\Delta G_p° = -14.1$ kcal•mol^{-1}),[45] and highly active catalysts under the concentrated reaction conditions (2.4 M) can produce a significant exotherm (i.e. reaction is warm to touch). In order to avoid unintended warming of the reaction for the kinetic studies, propagation rates (k_p) were measured under reaction conditions that were diluted 8-fold (0.3 M rather than 2.4 M). The higher solvent volume and slower rates allowed for efficient heat-transfer and stable reaction temperatures.

Reactions at –30 °C:

The following modifications to the procedure for the ambient temperature reaction were made: Before addition of *rac*-BBL, both catalyst solution and *rac*-BBL were chilled at –30 °C in the glovebox freezer. After the solution temperatures equilibrated, the *rac*-BBL was added to the catalyst solution and the reaction was run in the freezer.

Sample for end-group analysis:

The sample prepared for end-group analysis was isolated from the ROP of *rac*-BBL at –30 °C using [BBL]:[**1-La**]:[^{OMe}LO]:[Ph$_2$CHOH] = 200:1:2:1, [BBL] = 2.4 M. After quenching with

BzOH and removing the volatiles, the residue was washed with MeOH (3 x 1 mL) to remove

most of the residual free ligand and BzOH. The sample was then dried under reduced pressure

to afford the sample used for end-group analysis by NMR.

3.4.4. Supporting Data and Spectra

Table 3.13. Impact of ^{OMe}LO equivalents on the ROP of *rac*-BBL.
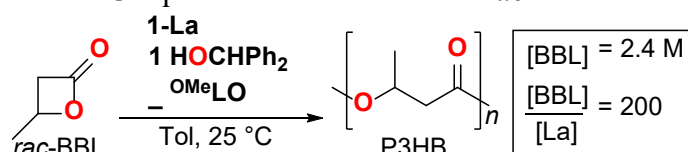
Entry	^{OMe}LO (equiv)	Time (h)	Conv. (%)[a]	$M_{n, calc}$[b] (kg/mol)	$M_{n, exp}$[c] (kg/mol)	$Đ$[c,d]	P_m[e]
1	0	1	20	3.4	2.8	1.05	0.57
2	1	0.1	54	9.3	n.d.	n.d.	n.d.
		1	95	16.5	10.8	1.20	0.67
3	2	0.1	95	16.5	12.5	1.16	0.73
4	3	0.1	96	16.5	12.8	1.14	0.73

a – Determined by ^{1}H-NMR integration of BBL and PHB methine resonances in the crude reaction mixture. *b* – [BBL]/[La]/[Ph$_2$CHOH] × Conv. × 0.08609 kg•mol^{-1}. *c* – Determined by gel permeation chromatography (GPC) at 30 °C in THF using polystyrene standards and corrected by Mark-Houwink factor of 0.54. *d* – M_w/M_n. *e* – Probability of *meso*-linkages between repeat units. Determined by integration of P3HB $\underline{C}$=O resonances using inverse gated (IG) ^{13}C-NMR.
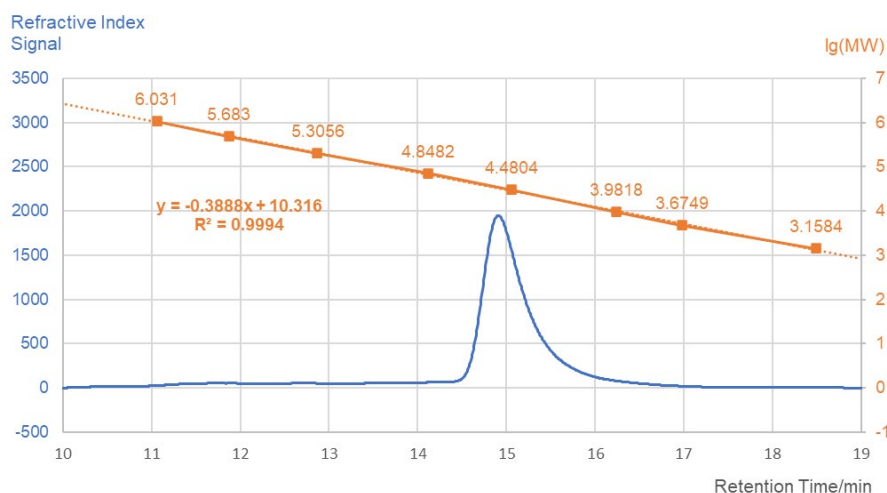
Figure 3.14. GPC calibration curve using polystyrene standards (orange) and GPC trace (blue) of Table 3.1, entry 5. The reaction was performed in toluene at ambient temperature for 0.1 h with [BBL]:[**1-La**]:[^{OMe}LO]:[HOCHPh$_2$] = 200:1:2:1 and [BBL] = 2.4 M. Conversion = 95%, M_n = 12.5 kg/mol (corrected by Mark-Houwink factor of 0.54), $Đ$ = 1.16
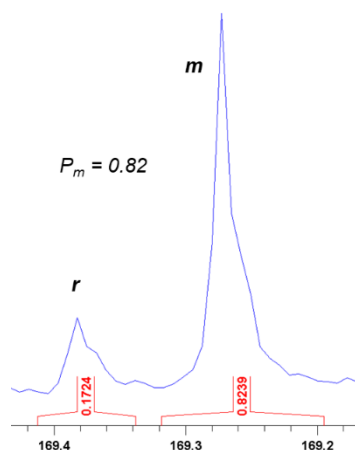
Figure 3.15. Carbonyl region of IG-^{13}C-NMR (151 MHz, CDCl$_3$) of P3HB (Table 3.1, entry 9). Reaction was performed in toluene at –30 °C for 1 h with [BBL]:[**1-La**]:[^{OMe}**LO**]: [HOCHPh$_2$] = 200:1:2:1 and [BBL] = 2.4 M . Conversion = 99%.

3.5. Computational Section

3.5.1. Methods

All calculations were performed employing the Gaussian 09 package (revision D.01).[46]

La complexes: Complexes were optimized at the M06-L level of theory[33] with Grimme's D3 dispersion correction[34] using the Stuttgart [7s6p5d|5s4p3d][36] ECP46MWB[35-36] contracted pseudopotential basis set on lanthanum and the 6-31G* basis set used on all other atoms.[37-39] The standard "fine" grid size was used for numerical integrations while a convergence criterion of 10^{-6} was used for all calculations. Optimized geometries were confirmed as minima by frequency analysis (the absence of negative frequencies). NBO[40] calculations were performed at the M06L level of theory using the def2-TZVP basis set.[47-48] Solvation effects associated with toluene were accounted for in the single point calculations using the SMD continuum solvation model.[49] Input geometries were generated from the crystallographic data or constructed using Avogadro.[50]

Free ligands (only): For 4-substituted lutidine *N*-oxide (**RLO**) calculations, structures were optimized at the M06-2X level of theory[51] employing the def2-TZVP basis set.[47-48] NBO calculations were performed with the same level of theory and basis set.

3.5.2. Structure

Table 3.14. Cartesian coordinates of **LO** optimized with M06-2X/Def2-TZVP.

Atom	X	Y	Z
N	0	-0.65882	0.00038
C	1.18731	0.01341	0.0001
C	1.18886	1.39543	-0.00005
C	0.00003	2.10448	-0.00003
C	-1.18883	1.39545	-0.00005
C	-1.18732	0.01344	0.00011
C	2.40848	-0.83405	-0.00004
H	2.14324	1.90408	-0.00016
C	-2.40849	-0.83401	-0.00004
H	0.00003	3.18541	-0.00014
H	-2.14319	1.90414	-0.00016
O	-0.00003	-1.94228	-0.00021
H	-3.2983	-0.20907	-0.00021
H	-2.41112	-1.48756	0.87333
H	-2.41087	-1.48761	-0.87338
H	3.2983	-0.20912	-0.00028
H	2.41082	-1.48771	-0.87333
H	2.41113	-1.48752	0.87339

Table 3.15. Cartesian coordinates of ^{NO2}**LO** optimized with M06-2X/Def2-TZVP.

Atom	X	Y	Z
N	-1.60028	-0.00001	0.00028
C	-1.06449	-1.13601	0.00012
C	0.4103	-1.25428	0.00001
C	1.14876	0.00001	0.00002
C	0.41029	1.25428	0.00002
C	-1.06452	1.13599	0.00009
C	-1.81718	-2.47395	0.00003
H	1.15676	-2.07871	-0.00003
C	-1.81722	2.47393	-0.00007
N	2.60567	0.00001	-0.00002
H	1.15673	2.07872	-0.00004
O	-2.90609	0.00001	-0.00025
O	3.07679	-1.02808	-0.00019
O	3.0768	1.02809	0.0001
H	-0.98448	-3.20718	-0.00004
H	-2.57445	-2.17403	-0.7993
H	-2.57448	-2.17414	0.79933
H	-0.98452	3.20716	-0.0001
H	-2.57459	2.17413	0.79918
H	-2.57442	2.174	-0.79946

Table 3.16. Cartesian coordinates of ^{MeO}LO optimized with M06-2X/Def2-TZVP.

Atom	X	Y	Z
N	-1.4199	0.19516	0.00019
C	-0.50413	1.19459	-0.00039
C	0.85161	0.90647	-0.00087
C	1.28111	-0.41235	-0.00082
C	0.32066	-1.41944	-0.00056
C	-1.01936	-1.1109	-0.00011
C	-1.0536	2.57609	-0.00033
H	1.54289	1.73545	-0.0014
C	-2.10957	-2.1215	0.00032
O	2.57218	-0.80163	-0.00127
H	0.63183	-2.45479	-0.00066
O	-2.68262	0.47596	0.00098
C	3.56264	0.20888	0.00181
H	4.5192	-0.30548	0.00348
H	3.48249	0.83315	0.895
H	3.48657	0.83479	-0.89058
H	-1.69194	-3.12538	-0.00168
H	-2.74943	-1.97892	-0.87138
H	-2.74658	-1.98141	0.87456
H	-0.24607	3.30409	-0.0024
H	-1.6894	2.72406	0.87369
H	-1.69286	2.72267	-0.87202

Table 3.17. Cartesian coordinates of ^{Cl}LO optimized with M06-2X/Def2-TZVP.

Atom	X	Y	Z
N	1.41199	0	0.00008
C	0.73885	-1.18669	0.00001
C	-0.64226	-1.19467	0.00001
C	-1.33725	0.00001	0.00002
C	-0.64226	1.19467	-0.00001
C	0.73886	1.18669	0
C	1.58295	-2.40941	-0.00001
H	-1.16398	-2.14099	-0.00002
C	1.58295	2.40941	0
Cl	-3.06503	0	-0.00001
H	-1.16398	2.141	-0.00004
O	2.69472	-0.00001	-0.00006
H	0.95797	-3.29883	-0.00018
H	2.23605	-2.41004	0.87363
H	2.2363	-2.40984	-0.87345
H	0.95797	3.29883	-0.00017
H	2.23632	2.40985	-0.87343
H	2.23604	2.41002	0.87365

Table 3.18. Cartesian coordinates of ^{NMe2}**LO** optimized with M06-2X/Def2-TZVP.

Atom	X	Y	Z
N	1.76028	0.00002	0.0001
C	1.0796	-1.17569	-0.00111
C	-0.29866	-1.19107	-0.00517
C	-1.04168	-0.00012	-0.00933
C	-0.29877	1.19091	-0.0052
C	1.07948	1.17566	-0.00116
C	1.9185	-2.40413	0.00247
H	-0.7835	-2.15517	-0.00525
C	1.91826	2.4042	0.00225
N	-2.40596	-0.00006	-0.01764
H	-0.78378	2.15493	-0.00489
O	3.06143	0.00009	0.00422
C	-3.12371	-1.25512	0.00814
C	-3.12333	1.25522	0.00851
H	-2.89351	-1.83362	0.90844
H	-2.88302	-1.87048	-0.86373
H	-4.19115	-1.05508	-0.00374
H	-2.883	1.87058	-0.86347
H	-2.8923	1.83351	0.90875
H	-4.19084	1.05548	-0.00246
H	1.29075	-3.29209	0.0026
H	2.57101	-2.40485	0.87622
H	2.57425	-2.40763	-0.86887
H	1.29042	3.29209	0.00212
H	2.57404	2.40752	-0.86907
H	2.57074	2.40522	0.87602

Table 3.19. Cartesian coordinates of **LO** optimized with M06L/6-31G*.
E_{M06L} = -402.0456974 Hartree

Atom	X	Y	Z
N	0	-0.66906	0.00033
C	-1.19973	0.01776	0.0001
C	-1.19289	1.40246	0.00006
C	-0.00001	2.1169	0.00013
C	1.19287	1.40246	0.00006
C	1.19974	0.01777	0.0001
C	-2.4095	-0.83747	-0.00007
H	-2.15341	1.91444	-0.00002
C	2.40949	-0.83746	-0.00007
H	-0.00002	3.20354	0.0001
H	2.15339	1.91446	-0.00002
O	0.00001	-1.94762	-0.00045
H	3.31681	-0.22691	-0.00036
H	2.41496	-1.5023	-0.87202

H	2.41535	-1.50206	0.87206
H	-3.31681	-0.22694	-0.00036
H	-2.41533	-1.50208	0.87206
H	-2.41494	-1.50231	-0.87202

Table 3.20. Cartesian coordinates of ^{NO2}LO optimized with M06L/6-31G*.
E_{M06L} = -606.5446496 Hartree.

Atom	X	Y	Z
N	1.65718	0	0.00002
C	0.97325	-1.20839	-0.00001
C	-0.40537	-1.20622	-0.00001
C	-1.096	0	0
C	-0.40537	1.20622	0.00002
C	0.97325	1.20839	0.00002
C	1.83056	-2.41573	-0.00003
H	-0.95126	-2.14467	-0.00003
C	1.83056	2.41573	0.00003
N	-2.54953	0	0
H	-0.95126	2.14467	0.00003
O	2.92724	0	-0.00001
O	-3.11804	-1.09357	-0.00004
O	-3.11804	1.09357	0
H	1.22061	-3.32228	-0.00006
H	2.49326	-2.42048	0.87307
H	2.49329	-2.42043	-0.87309
H	1.22061	3.32228	0.00001
H	2.49329	2.42045	-0.87303
H	2.49325	2.42046	0.87313

Table 3.21. Cartesian coordinates of ^{MeO}LO optimized with M06L/6-31G*.
E_{M06L} = -516.5547283 Hartree.

Atom	X	Y	Z
N	-1.43361	0.19497	-0.00008
C	-0.50093	1.20667	-0.00021
C	0.85517	0.91067	-0.00014
C	1.29095	-0.41287	0
C	0.32859	-1.42532	-0.00005
C	-1.01778	-1.12467	-0.00015
C	-1.06532	2.57637	-0.00038
H	1.55275	1.7437	-0.00022
C	-2.11226	-2.12265	-0.00024
O	2.59068	-0.80686	0.00009
H	0.64443	-2.46548	-0.00003
O	-2.68783	0.47091	0.00006
C	3.5636	0.2171	0.00089
H	4.5316	-0.28706	0.00145

137

Atom	X	Y	Z
H	3.48209	0.85076	0.89575
H	3.4833	0.85105	-0.89388
H	-1.71281	-3.1407	-0.00134
H	-2.76236	-1.9805	-0.87165
H	-2.76124	-1.98211	0.87228
H	-0.27085	3.32823	-0.00147
H	-1.71253	2.72711	0.87199
H	-1.71415	2.72608	-0.87172

Table 3.22. Cartesian coordinates of ^{Cl}LO optimized with M06L/6-31G*.
E_{rM06L} = -861.6255661 Hartree.

Atom	X	Y	Z
N	-1.42603	0	-0.00006
C	-0.73845	1.19928	-0.00002
C	0.64538	1.20072	-0.00003
C	1.34503	0	-0.00005
C	0.64538	-1.20072	-0.00003
C	-0.73845	-1.19927	-0.00002
C	-1.59072	2.41045	0.00003
H	1.17101	2.15217	-0.00002
C	-1.59072	-2.41044	0.00004
Cl	3.08174	0	-0.00004
H	1.171	-2.15217	-0.00001
O	-2.70421	0	0.00015
H	-0.98047	3.31746	0.00007
H	-2.25486	2.41404	0.8723
H	-2.25487	2.41412	-0.87223
H	-0.98048	-3.31746	0.00008
H	-2.25487	-2.41412	-0.87222
H	-2.25487	-2.41404	0.87231

Table 3.23. Cartesian coordinates of ^{NMe2}LO optimized with M06L/6-31G*.
E_{M06L} = -535.994177 Hartree

Atom	X	Y	Z
N	1.78921	0	-0.00003
C	1.08428	1.19443	-0.00013
C	-0.30417	1.1967	-0.00065
C	-1.04916	0	-0.00127
C	-0.30417	-1.1967	-0.00069
C	1.08428	-1.19443	-0.00016
C	1.92682	2.41535	0.00042
H	-0.79844	2.16441	-0.00047
C	1.92682	-2.41535	0.00035
N	-2.4317	0	-0.00252
H	-0.79844	-2.16441	-0.00057
O	3.09716	0	0.00043

C	-3.14672	1.25037	0.00104
C	-3.14672	-1.25037	0.00123
H	-2.91297	1.86034	-0.88551
H	-2.91526	1.85499	0.892
H	-4.22103	1.05245	-0.00114
H	-2.91499	-1.85498	0.89212
H	-2.91323	-1.86035	-0.88538
H	-4.22103	-1.05245	-0.00063
H	1.3095	3.31841	0.00045
H	2.59247	2.42402	-0.87066
H	2.59198	2.42359	0.87188
H	1.3095	-3.31841	0.00036
H	2.59199	-2.42361	0.87181
H	2.59247	-2.424	-0.87074

Table 3.24. Cartesian coordinates of **OPPh₃** optimized with M06L/6-31G*.
E_{M06L} = -1111.44 Hartree

Atom	X	Y	Z
H	-4.59611	-2.69704	-1.09264
C	-3.70343	-2.19768	-0.71912
H	-2.56526	-2.56019	-2.51449
C	-2.56549	-2.1185	-1.51927
H	-4.58117	-1.71995	1.19041
C	-3.6958	-1.64867	0.56104
C	-1.42245	-1.48293	-1.04296
C	-2.55555	-1.01139	1.0392
H	-0.5261	-1.44357	-1.6633
C	-1.41346	-0.91632	0.23606
H	-2.52818	-0.59259	2.04448
H	-0.98064	1.11893	-1.6619
P	0.00388	-0.02159	0.9387
C	-0.57869	1.92612	-1.04764
H	1.39618	0.19076	-1.70771
O	0.01401	-0.02204	2.43696
H	-0.98122	3.43919	-2.52396
C	-0.07909	1.65082	0.22961
C	-0.58771	3.23155	-1.53027
C	1.93812	-0.51728	-1.07897
C	1.4922	-0.77869	0.221
C	3.08716	-1.13455	-1.56359
H	3.43127	-0.92364	-2.57474
C	0.39186	2.70078	1.02521
C	-0.10665	4.27074	-0.737
C	2.22096	-1.65067	1.03674
C	0.37875	4.00518	0.54128
H	1.88141	-1.82343	2.05725

H	0.75003	2.48003	2.02994
C	3.80356	-2.00863	-0.74882
H	-0.11904	5.29234	-1.11347
C	3.37226	-2.26299	0.55105
H	4.70735	-2.48485	-1.12561
H	3.93951	-2.93595	1.19186
H	0.74242	4.81895	1.16647

Table 3.25. Comparison of natural charges (q) across optimized **1-La(OPPh$_3$)$_2$**, **1-La(LO)$_2$**, **4-La(OPPh$_3$)$_2$**, and **4-La(LO)$_2$** structures. Natural charges were calculated with NBO 3.1 using the M06L functional and Def2-TZVP basis set (see computational methods).

	1-La(OPPh$_3$)$_2$	1-La(LO)$_2$	4-La(OPPh$_3$)$_2$	4-La(LO)$_2$
$q_{La(1)}$	1.98683	1.92241	2.08173	1.9921
$q_{O(1)}$	-0.91116	-0.92309	-0.90916	-0.88704
$q_{O(2)}$	-0.90204	-0.92832	-0.91293	-0.9271
$q_{O(3)}$	-1.15147	-0.63383	-1.15874	-0.64161
$q_{O(4)}$	-1.15244	-0.61308	-1.14579	-0.61556
$q_{O(5)}$	N/A	N/A	-0.99826	-1.00459
$q_{N(1)}$	-0.46224	-0.46834	-0.47775	-0.47773
$q_{N(2)}$	-1.83539	-1.85027	N/A	N/A
$q_{N(3)}$	N/A	0.06952	N/A	0.07744
$q_{N(4)}$	N/A	0.08294	N/A	0.06423
$q_{P(1)}$	1.98456	N/A	1.98832	N/A
$q_{P(2)}$	1.98683	N/A	1.98017	N/A

Table 3.26. Comparison of Wilberg bond indices across optimized **1-La(OPPh$_3$)$_2$**, **1-La(LO)$_2$**, **4-La(OPPh$_3$)$_2$**, and **4-La(LO)$_2$** structures. Bond indices were calculated with NBO 3.1 using the M06L functional and Def2-TZVP basis set (see computational methods).

Bond	1-La(OPPh$_3$)$_2$	1-La(LO)$_2$	4-La(OPPh$_3$)$_2$	4-La(LO)$_2$
O(3) - P(1)	1.0196	N/a	1.0272	N/A
O(4) - P(2)	1.0284	N/a	1.0345	N/A
O(3) - N(3)	N/A	1.1461	N/A	1.1485
O(4) - N(4)	N/A	1.1644	N/A	1.1541
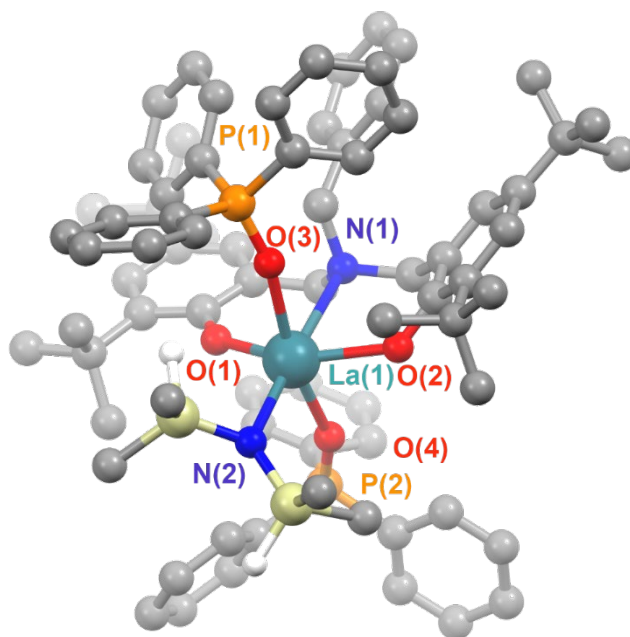
Figure 3.16. Labeled ball and stick image of **1-La(OPPh₃)₂**. H-atoms other than those of the NDMS Si-H were removed for clarity.

Table 3.27. Comparison of selected bond distances (Å) and metrical parameters of the X-ray / DFT calculated structures of **1-La(OPPh₃)₂**. The mean unsigned error (MUE) is 0.0465.

Distance (Å)	X-ray	DFT	Angle (°)	X-ray	DFT
La(1)–O(1)	2.276(2)	2.352	O(1)–La(1)–O(2)	144.92(8)	143.16
La(1)–O(2)	2.267(2)	2.340	O(1)–La(1)–O(3)	96.74(7)	96.49
La(1)–O(3)	2.482(2)	2.502	O(1)–La(1)–O(4)	84.02(7)	81.62
La(1)–O(4)	2.457(2)	2.490	O(1)–La(1)–N(1)	71.33(7)	71.57
La(1)–N(1)	2.828(2)	2.885	O(1)–La(1)–N(2)	109.07(8)	109.14
La(1)–N(2)	2.459(3)	2.479	O(2)–La(1)–O(3)	85.42(7)	86.13
			O(2)–La(1)–O(4)	87.84(7)	85.10
			O(2)–La(1)–N(1)	73.92(7)	72.90
			O(2)–La(1)–N(2)	105.42(8)	105.88
			O(3)–La(1)–O(4)	169.24(7)	165.65
			O(3)–La(1)–N(1)	85.97(7)	82.39
			O(3)–La(1)–N(2)	96.63(8)	100.31
			O(4)–La(1)–N(1)	84.11(7)	83.53
			O(4)–La(1)–N(2)	93.24(8)	93.71
			N(1)–La(1)–N(2)	177.28(8)	177.05
			P(1)–O(3)–La(1)	167.6(1)	160.24
			P(2)–O(4)–La(1)	163.0(1)	156.94

Table 3.28. Cartesian coordinates of **1-La(OPPh₃)₂**.

Atom	X	Y	Z
La	-0.29981	-1.12441	0.41677
P	-3.74097	-1.48595	-1.45500
P	2.86892	0.44494	2.21830
Si	-0.68865	-2.32960	3.51336
Si	-1.14850	-4.61708	1.53020
O	-1.53853	0.78492	1.01052
O	0.92655	-2.09454	-1.32405
O	1.86782	-0.37776	1.41819
O	-2.27603	-1.50307	-1.05007
N	0.29273	0.97205	-1.47470
N	-0.88206	-2.98133	1.95315
C	-1.90097	2.00475	0.69177
C	-2.68182	2.79876	1.58781
C	-3.21061	2.20371	2.90052
C	-2.06846	1.73578	3.81483
H	-1.48231	0.93847	3.34954
H	-2.47598	1.34691	4.75887
H	-1.39683	2.56965	4.06600
C	-4.12874	1.00989	2.59502
H	-5.01097	1.33205	2.02287
H	-4.49363	0.55516	3.52739
H	-3.60650	0.23436	2.02395
C	-4.03659	3.21514	3.69943
H	-3.44566	4.09286	3.99347
H	-4.40195	2.74214	4.61975
H	-4.91331	3.56853	3.14158
C	-2.98944	4.11350	1.22096
H	-3.55859	4.72400	1.91677
C	-2.60834	4.68217	0.00284
C	-2.91820	6.12510	-0.38782
C	-3.63497	6.88584	0.72586
H	-4.60251	6.43053	0.97328
H	-3.82733	7.92037	0.41444
H	-3.03676	6.92139	1.64535
C	-3.80695	6.14868	-1.63881
H	-3.33988	5.61227	-2.47483
H	-3.99682	7.17976	-1.96774
H	-4.77923	5.67757	-1.43997
C	-1.60302	6.85217	-0.70303
H	-0.92460	6.82899	0.16014
H	-1.78529	7.90346	-0.96541
H	-1.07976	6.38459	-1.54646

C	-1.91934	3.85626	-0.88488
H	-1.68055	4.23038	-1.88418
C	-1.55096	2.54916	-0.57846
C	-0.97878	1.70336	-1.69057
H	-1.71235	0.92442	-1.95735
H	-0.88262	2.34571	-2.58894
C	1.36692	1.80041	-0.89676
H	2.15273	1.10496	-0.57673
H	0.93211	2.23246	0.01047
C	2.02037	2.90614	-1.69463
C	1.37060	4.12081	-1.93938
H	0.35442	4.25854	-1.57668
C	2.02739	5.17353	-2.56952
H	1.50204	6.11228	-2.74321
C	3.35882	5.03836	-2.95459
H	3.87719	5.86387	-3.43991
C	4.02685	3.84392	-2.69802
H	5.07490	3.73169	-2.97403
C	3.36105	2.78997	-2.07716
H	3.89255	1.85886	-1.87022
C	0.67020	0.32745	-2.75881
H	0.75636	1.10505	-3.54257
H	-0.18979	-0.30738	-3.02934
C	1.93172	-0.48819	-2.74119
C	3.01788	-0.09908	-3.52018
H	2.92581	0.82287	-4.10000
C	4.19730	-0.84425	-3.58075
C	5.33998	-0.40032	-4.49338
C	5.73666	1.04749	-4.17858
H	6.07926	1.15358	-3.13887
H	4.89474	1.73610	-4.31860
H	6.55180	1.38091	-4.83621
C	4.87222	-0.47187	-5.95378
H	4.58563	-1.49575	-6.22435
H	5.66750	-0.14729	-6.63970
H	4.00037	0.17210	-6.12303
C	6.58057	-1.27971	-4.34331
H	6.97325	-1.26756	-3.31674
H	7.37903	-0.91846	-5.00394
H	6.37862	-2.32480	-4.60869
C	4.24825	-2.00662	-2.80388
H	5.16424	-2.59086	-2.82028
C	3.19434	-2.45659	-2.00425
C	3.32682	-3.73267	-1.16322
C	4.72751	-4.34167	-1.27227
H	4.97455	-4.63206	-2.30132
H	4.78334	-5.24658	-0.65423

H	5.50514	-3.64978	-0.91949
C	2.32024	-4.78818	-1.64169
H	1.29544	-4.41332	-1.57327
H	2.39773	-5.69940	-1.03110
H	2.51583	-5.06604	-2.68571
C	3.08852	-3.44184	0.32892
H	3.74144	-2.63436	0.68747
H	3.30576	-4.33859	0.92705
H	2.05257	-3.15402	0.53617
C	1.98587	-1.69963	-1.99767
C	0.62807	-3.16939	4.56618
H	1.54563	-3.32598	3.98374
H	0.28825	-4.15504	4.91108
H	0.89244	-2.58202	5.45447
C	-2.26719	-2.15239	4.52899
H	-2.08478	-1.64769	5.48676
H	-2.71239	-3.13102	4.75297
H	-3.01709	-1.56416	3.98423
C	-1.53446	-4.71530	-0.31498
H	-2.52682	-4.31158	-0.55461
H	-1.50155	-5.74646	-0.69006
H	-0.80510	-4.13601	-0.90068
C	0.32003	-5.75244	1.86761
H	1.19714	-5.41979	1.29713
H	0.10879	-6.78798	1.57064
H	0.60877	-5.76494	2.92551
C	-4.00040	-2.71936	-2.74725
C	-2.86971	-3.29317	-3.33878
H	-1.87934	-3.00260	-2.98969
C	-3.02270	-4.23846	-4.34918
H	-2.14189	-4.68758	-4.80379
C	-4.29655	-4.61193	-4.76905
H	-4.41359	-5.35515	-5.55577
C	-5.42497	-4.04182	-4.18097
H	-6.42028	-4.33897	-4.50593
C	-5.27895	-3.09699	-3.17194
H	-6.16263	-2.65867	-2.70671
C	-4.82869	-1.83621	-0.05986
C	-6.18823	-1.49780	-0.08521
H	-6.60729	-0.97653	-0.94669
C	-6.99975	-1.79660	1.00373
H	-8.05343	-1.52520	0.98377
C	-6.45976	-2.43020	2.12197
H	-7.09600	-2.66084	2.97462
C	-5.10725	-2.75796	2.15558
H	-4.67697	-3.24193	3.03033
C	-4.28838	-2.46021	1.06973

H	-3.22135	-2.68740	1.11786
C	-4.27478	0.10418	-2.11753
C	-4.29907	0.34785	-3.49606
H	-4.09539	-0.46261	-4.19579
C	-4.57801	1.62603	-3.96960
H	-4.59462	1.81359	-5.04160
C	-4.83126	2.66366	-3.07378
H	-5.04042	3.66511	-3.44732
C	-4.80995	2.42641	-1.70130
H	-4.97615	3.23708	-0.99323
C	-4.53043	1.15210	-1.22256
H	-4.48753	0.97593	-0.14730
C	2.98406	-0.08995	3.94054
C	3.73558	-1.23458	4.24179
H	4.26388	-1.76125	3.44643
C	3.81077	-1.69789	5.54974
H	4.39605	-2.58687	5.77620
C	3.13052	-1.02927	6.56560
H	3.19013	-1.39314	7.58984
C	2.36904	0.09918	6.27156
H	1.83311	0.61910	7.06299
C	2.29645	0.57123	4.96459
H	1.70652	1.45960	4.74194
C	2.43212	2.19679	2.18403
C	1.09343	2.54843	2.41586
H	0.36187	1.77692	2.66199
C	0.67522	3.86350	2.24034
H	-0.37540	4.11661	2.38307
C	1.58785	4.83315	1.82586
H	1.25505	5.85687	1.66346
C	2.91713	4.49065	1.59374
H	3.62229	5.24009	1.23880
C	3.34121	3.17713	1.77163
H	4.37362	2.91097	1.54973
C	4.52611	0.29168	1.52410
C	4.66537	-0.10391	0.18884
H	3.78866	-0.37614	-0.40197
C	5.93379	-0.18380	-0.38109
H	6.02315	-0.51030	-1.41646
C	7.06066	0.14027	0.36868
H	8.04951	0.07662	-0.08243
C	6.92658	0.53701	1.69894
H	7.80714	0.78405	2.28868
C	5.66426	0.60986	2.27718
H	5.56048	0.90881	3.32104
H	-0.21623	-0.91038	3.26421
H	-2.32449	-5.20212	2.26206
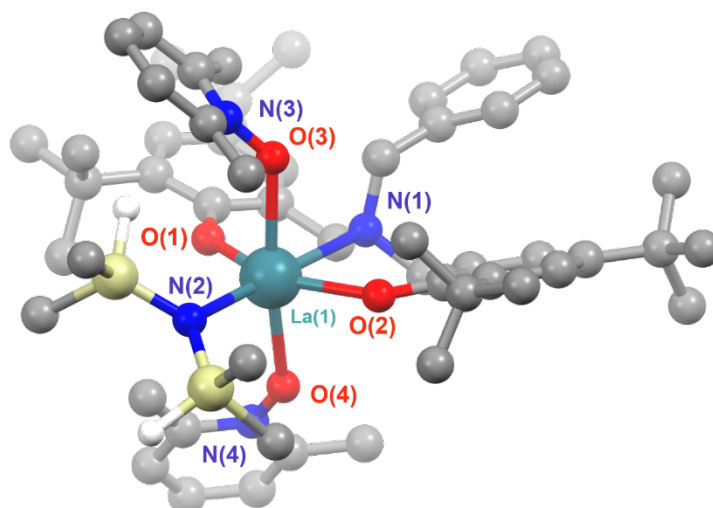
Figure 3.17. Labeled ball and stick image of **1-La(LO)₂**. H-atoms other than those of the NDMS Si-H were removed for clarity.

Table 3.29. Selected bond distances (Å) and metrical parameters of the DFT calculated structures of **1-La(LO)₂**.

Distance (Å)	DFT	Angle (°)	DFT
La(1)–O(1)	2.364	O(1)–La(1)–O(2)	90.30
La(1)–O(2)	2.321	O(1)–La(1)–O(3)	145.24
La(1)–O(3)	2.554	O(1)–La(1)–O(4)	82.97
La(1)–O(4)	2.600	O(1)–La(1)–N(1)	73.00
La(1)–N(1)	2.825	O(1)–La(1)–N(2)	108.28
La(1)–N(2)	2.488	O(2)–La(1)–O(3)	89.43
		O(2)–La(1)–O(4)	89.62
		O(2)–La(1)–N(1)	72.29
		O(2)–La(1)–N(2)	106.44
		O(3)–La(1)–O(4)	86.50
		O(3)–La(1)–N(1)	166.72
		O(3)–La(1)–N(2)	93.28
		O(4)–La(1)–N(1)	80.61
		O(4)–La(1)–N(2)	99.68
		N(1)–La(1)–N(2)	178.71
		P(1)–N(3)–La(1)	133.64
		P(2)–N(4)–La(1)	141.87

Table 3.30. Cartesian coordinates of **1-La(LO)₂**.

Atom	X	Y	Z
La	0.07843	-1.20463	0.32087
Si	1.94421	-4.12572	-0.59786
Si	-0.35345	-4.70646	1.27474
O	2.10945	-0.00116	0.20647

146

O	-2.23046	-1.03693	0.48729
O	-0.12494	-1.12983	-2.22397
O	0.28224	-0.68215	2.85979
N	-0.58880	1.54011	0.28184
N	0.61175	-3.63507	0.34972
C	2.64267	1.19912	0.03892
C	3.98987	1.37583	-0.40299
C	4.93021	0.17767	-0.59537
C	4.39014	-0.80937	-1.63679
H	3.38441	-1.15693	-1.38603
H	5.04287	-1.69175	-1.70468
H	4.36147	-0.34518	-2.63258
C	5.09708	-0.53665	0.75309
H	5.53718	0.13881	1.49890
H	5.75884	-1.40880	0.65189
H	4.13039	-0.87692	1.12935
C	6.32732	0.59521	-1.06037
H	6.30350	1.11568	-2.02668
H	6.95043	-0.29980	-1.18348
H	6.83085	1.24817	-0.33631
C	4.47034	2.67753	-0.57384
H	5.48838	2.80568	-0.92914
C	3.72628	3.82429	-0.29203
C	4.27317	5.24190	-0.44200
C	5.66599	5.25922	-1.06958
H	6.40058	4.72965	-0.44976
H	6.01580	6.29319	-1.18254
H	5.66935	4.79575	-2.06448
C	4.35441	5.90355	0.94056
H	3.36979	5.94170	1.42342
H	4.72860	6.93381	0.86218
H	5.02805	5.34725	1.60450
C	3.33407	6.06985	-1.33010
H	3.21557	5.61310	-2.32099
H	3.72582	7.08680	-1.46887
H	2.33526	6.16173	-0.88523
C	2.43206	3.62287	0.18170
H	1.82843	4.48498	0.47507
C	1.86679	2.35702	0.32258
C	0.50922	2.26817	0.96483
H	0.60408	1.75944	1.93923
H	0.17118	3.29887	1.19128
C	-0.82969	1.95383	-1.11883
H	-1.50067	1.19931	-1.55339
H	0.14277	1.85201	-1.61755

C	-1.38931	3.33063	-1.38977
C	-0.56956	4.46342	-1.33849
H	0.48643	4.33983	-1.10523
C	-1.07093	5.72866	-1.62841
H	-0.41243	6.59535	-1.58455
C	-2.40438	5.88151	-1.99864
H	-2.79914	6.86825	-2.23610
C	-3.22419	4.75952	-2.08622
H	-4.26067	4.86483	-2.40306
C	-2.72226	3.49707	-1.78063
H	-3.37045	2.62356	-1.85321
C	-1.77941	1.66867	1.16556
H	-1.90464	2.73420	1.43980
H	-1.49642	1.13505	2.08788
C	-3.09968	1.15190	0.67988
C	-4.19158	2.01543	0.65696
H	-4.01771	3.06677	0.90143
C	-5.47398	1.58423	0.32141
C	-6.64218	2.56830	0.33090
C	-6.35215	3.72190	-0.63636
H	-6.22506	3.35189	-1.66290
H	-5.43516	4.25801	-0.36130
H	-7.17677	4.44829	-0.63784
C	-6.81388	3.13986	1.74467
H	-7.03285	2.34378	2.46740
H	-7.63910	3.86489	1.77665
H	-5.90536	3.65369	2.08253
C	-7.95754	1.91237	-0.08582
H	-7.90400	1.50009	-1.10158
H	-8.76729	2.65305	-0.07123
H	-8.24240	1.09821	0.59275
C	-5.61624	0.23218	-0.00175
H	-6.60305	-0.12700	-0.27845
C	-4.56588	-0.68823	0.01911
C	-4.81044	-2.16047	-0.32136
C	-6.25351	-2.43155	-0.75180
H	-6.97364	-2.21246	0.04681
H	-6.36271	-3.49330	-1.00781
H	-6.53926	-1.84752	-1.63626
C	-4.52208	-3.03989	0.90268
H	-3.48106	-2.94655	1.22155
H	-4.71580	-4.09704	0.67053
H	-5.16543	-2.75743	1.74619
C	-3.90001	-2.58406	-1.47970
H	-4.11611	-1.99775	-2.38391
H	-4.04924	-3.64679	-1.72262
H	-2.85014	-2.43138	-1.21721

C	-3.27175	-0.22515	0.39014
C	1.67160	-5.70898	-1.59503
H	0.75052	-5.68363	-2.18976
H	1.59566	-6.57725	-0.92626
H	2.50656	-5.90237	-2.28131
C	3.57390	-4.35573	0.32949
H	4.33026	-4.82865	-0.31064
H	3.44843	-4.99224	1.21565
H	3.99073	-3.39741	0.66281
C	-1.18411	-3.74906	2.67779
H	-0.47915	-3.46681	3.47058
H	-1.98312	-4.33866	3.14606
H	-1.65655	-2.81851	2.32763
C	-1.70209	-5.53618	0.24938
H	-2.34506	-4.77821	-0.21946
H	-2.35177	-6.18357	0.85236
H	-1.27945	-6.14921	-0.55742
H	2.20239	-3.01558	-1.57518
H	0.45546	-5.80035	1.90947
H	-0.72042	-3.70375	-1.85188
H	-1.80665	-2.99018	-3.03958
C	-0.90151	-3.59742	-2.93255
H	-1.08141	-4.58969	-3.35633
C	0.24445	-2.94869	-3.60445
N	0.55795	-1.67483	-3.20380
H	0.80977	1.02183	-3.52588
H	0.75834	-4.55684	-4.89121
C	1.00866	-3.54004	-4.59891
C	1.55626	-0.94873	-3.80035
C	1.72660	0.44805	-3.34232
C	2.06330	-2.85752	-5.18916
C	2.31903	-1.55315	-4.78832
H	2.66815	-3.32969	-5.95888
H	2.55929	0.92658	-3.86478
H	1.91611	0.49205	-2.26314
H	3.11995	-0.97056	-5.23669
H	-1.23171	0.41083	4.53654
H	-0.60997	1.70374	5.60801
C	-0.42406	1.13413	4.69361
H	-0.46337	1.82577	3.84276
C	0.88831	0.45089	4.77268
N	1.16639	-0.47845	3.79856
H	1.64429	-2.95584	2.77069
H	1.59126	1.42736	6.52135
C	1.82905	0.68427	5.76428
C	2.32584	-1.21474	3.81940
C	2.48355	-2.25011	2.77864

C	3.03310	-0.00626	5.78719
C	3.26382	-0.96282	4.80875
H	3.77115	0.18749	6.56074
H	3.41380	-2.80488	2.92715
H	2.52155	-1.79704	1.77853
H	4.18084	-1.54639	4.79321
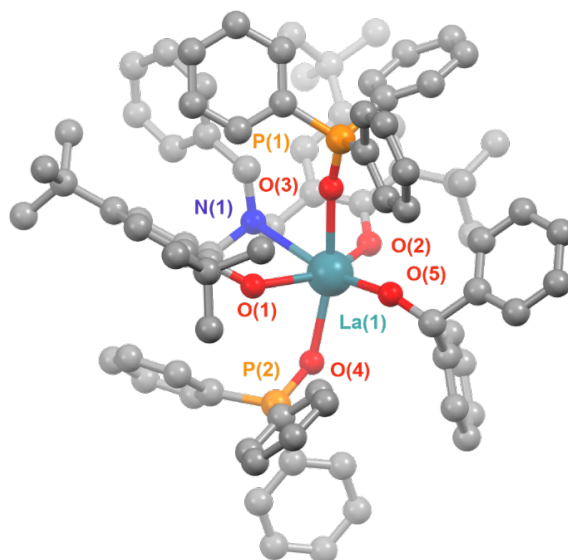
Figure 3.18. Labeled ball and stick image of **4-La(OPPh₃)₂**. H-atoms were removed for clarity.

Table 3.31. Selected bond distances (Å) and metrical parameters of the DFT calculated structures of **4-La(OPPh₃)₂**.

Distance (Å)	DFT	Angle (°)	DFT
La(1)–O(1)	2.383	O(1)–La(1)–O(2)	146.63
La(1)–O(2)	2.363	O(1)–La(1)–O(3)	85.63
La(1)–O(3)	2.494	O(1)–La(1)–O(4)	80.96
La(1)–O(4)	2.505	O(1)–La(1)–O(5)	102.29
La(1)–O(5)	2.323	O(1)–La(1)–N(1)	73.86
La(1)–N(1)	2.871	O(2)–La(1)–O(3)	93.01
		O(2)–La(1)–O(4)	99.13
		O(2)–La(1)–O(5)	110.83
		O(2)–La(1)–N(1)	73.21
		O(3)–La(1)–O(4)	166.51
		O(3)–La(1)–O(5)	85.16
		O(3)–La(1)–N(1)	78.52
		O(4)–La(1)–O(5)	95.91
		O(4)–La(1)–N(1)	99.30
		O(5)–La(1)–N(1)	163.44
		P(1)–O(3)–La(1)	169.67
		P(2)–O(4)–La(1)	136.72

Table 3.32. Cartesian coordinates of **4-La(OPPh₃)₂**.

Atom	X	Y	Z
La	-0.90356	-0.52548	-0.31549
P	-4.05013	1.32622	-1.23408
P	2.21106	-1.16708	2.10906
O	-1.15358	1.59828	0.73636
O	0.05659	-1.74404	-2.09802
O	1.11414	-0.79043	1.12600
O	-3.01434	0.22335	-1.43736
N	0.95972	1.23156	-1.61241
C	-0.40272	2.66937	0.89858
C	-0.27967	3.34613	2.14928
C	-1.06053	2.87147	3.38076
C	-0.74748	1.40636	3.72401
H	-0.90580	0.74166	2.86939
H	-1.39485	1.06329	4.54415
H	0.29065	1.29155	4.06712
C	-2.56274	3.01465	3.10349
H	-2.81766	4.05806	2.86663
H	-3.15122	2.71808	3.98322
H	-2.86772	2.37953	2.26593
C	-0.73594	3.69877	4.62608
H	0.33061	3.64701	4.88539
H	-1.30198	3.30940	5.48190
H	-1.00545	4.75616	4.50674
C	0.55454	4.47034	2.21461
H	0.65789	4.97388	3.17252
C	1.27146	4.97713	1.12531
C	2.18046	6.20085	1.20040
C	2.34833	6.71440	2.62958
H	1.39539	7.03877	3.06672
H	3.02710	7.57669	2.64391
H	2.77505	5.94866	3.29237
C	1.57525	7.32543	0.34804
H	1.45076	7.00897	-0.69574
H	2.21755	8.21723	0.35365
H	0.58693	7.61758	0.72751
C	3.57069	5.85223	0.64737
H	4.03861	5.04015	1.22023
H	4.23638	6.72556	0.69198
H	3.53136	5.51867	-0.39696
C	1.11312	4.31409	-0.09093
H	1.63200	4.67572	-0.98175
C	0.31020	3.18964	-0.21619
C	0.20203	2.50445	-1.53936

H	-0.84998	2.25150	-1.75950
H	0.52279	3.19388	-2.34123
C	2.26341	1.25017	-0.94971
H	2.62372	0.21322	-0.95706
H	2.06684	1.47726	0.10338
C	3.38705	2.14900	-1.41057
C	3.34644	3.02209	-2.50073
H	2.45168	3.08766	-3.11528
C	4.44328	3.82556	-2.81540
H	4.38740	4.49615	-3.67185
C	5.59939	3.77657	-2.04348
H	6.45153	4.40799	-2.28872
C	5.65452	2.90856	-0.95364
H	6.55086	2.85817	-0.33568
C	4.56298	2.10539	-0.64955
H	4.61132	1.42672	0.20490
C	0.97062	0.71827	-3.00430
H	1.33437	1.49358	-3.70158
H	-0.08498	0.53188	-3.26782
C	1.77942	-0.52764	-3.15872
C	3.06272	-0.46861	-3.68764
H	3.44631	0.50552	-4.00331
C	3.86997	-1.60258	-3.78682
C	5.31044	-1.46504	-4.27320
C	6.07145	-0.53956	-3.31133
H	6.06841	-0.94073	-2.28742
H	5.61866	0.45900	-3.26886
H	7.11866	-0.42040	-3.62356
C	5.33490	-0.84718	-5.67703
H	4.80262	-1.48203	-6.39648
H	6.36725	-0.72215	-6.03257
H	4.85877	0.14054	-5.68947
C	6.03733	-2.80755	-4.32935
H	6.09804	-3.28392	-3.34096
H	7.06511	-2.66518	-4.68711
H	5.54252	-3.51318	-5.00875
C	3.30198	-2.81571	-3.38265
H	3.89946	-3.71912	-3.48096
C	2.01647	-2.93584	-2.84594
C	1.44150	-4.29686	-2.44864
C	2.39846	-5.45122	-2.74879
H	2.65221	-5.51389	-3.81492
H	1.92707	-6.40050	-2.46288
H	3.33483	-5.36581	-2.17984
C	0.14951	-4.54480	-3.24064
H	-0.56455	-3.73261	-3.07995
H	-0.31912	-5.48996	-2.93056

H	0.36046	-4.60722	-4.31631
C	1.14279	-4.33872	-0.94449
H	2.07046	-4.31667	-0.35828
H	0.59676	-5.25594	-0.68014
H	0.53122	-3.48340	-0.64124
C	1.24387	-1.75043	-2.67980
C	-5.43415	1.04171	-2.35772
C	-5.63911	-0.25935	-2.82786
H	-4.93536	-1.04584	-2.55742
C	-6.73311	-0.53505	-3.64259
H	-6.88935	-1.54853	-4.00884
C	-7.61996	0.48069	-3.99100
H	-8.47369	0.26154	-4.63001
C	-7.41509	1.77927	-3.52794
H	-8.10271	2.57513	-3.80834
C	-6.32476	2.06132	-2.71202
H	-6.15568	3.08067	-2.36275
C	-4.70479	1.31996	0.44855
C	-5.58907	2.30919	0.89693
H	-5.87614	3.12832	0.23589
C	-6.08983	2.25868	2.19264
H	-6.77070	3.03329	2.54034
C	-5.71353	1.22161	3.04637
H	-6.10149	1.18999	4.06324
C	-4.83573	0.23733	2.60384
H	-4.52256	-0.56571	3.27005
C	-4.33447	0.28076	1.30611
H	-3.63709	-0.48886	0.97709
C	-3.43448	2.98513	-1.58417
C	-3.21488	3.35817	-2.91923
H	-3.53367	2.70020	-3.72823
C	-2.57569	4.55760	-3.21021
H	-2.40029	4.83913	-4.24689
C	-2.14696	5.38999	-2.17558
H	-1.62416	6.31779	-2.40420
C	-2.37208	5.03013	-0.84999
H	-2.01260	5.66014	-0.03725
C	-3.01496	3.83226	-0.55332
H	-3.15842	3.53657	0.48361
C	1.52444	-1.68654	3.69076
C	0.17690	-2.05775	3.74482
H	-0.45191	-2.00278	2.85277
C	-0.36418	-2.49394	4.95221
H	-1.40934	-2.79898	4.98674
C	0.42512	-2.54761	6.09716
H	-0.00325	-2.88848	7.03835
C	1.76586	-2.16471	6.04573

H	2.37983	-2.19757	6.94370
C	2.31734	-1.73464	4.84487
H	3.36345	-1.42728	4.80373
C	3.31162	0.22930	2.43671
C	2.73793	1.50510	2.51644
H	1.67039	1.63866	2.34011
C	3.53121	2.61301	2.78941
H	3.06679	3.59787	2.82806
C	4.90182	2.45677	2.98767
H	5.52364	3.32786	3.19000
C	5.47903	1.19052	2.91543
H	6.55059	1.06805	3.06295
C	4.68809	0.07664	2.63988
H	5.14370	-0.91090	2.56427
C	3.25454	-2.49818	1.47580
C	3.91499	-2.29784	0.25470
H	3.81561	-1.35167	-0.28189
C	4.68481	-3.31452	-0.29656
H	5.17703	-3.15366	-1.25470
C	4.79800	-4.53831	0.36085
H	5.39446	-5.33636	-0.07845
C	4.13737	-4.74716	1.56912
H	4.21595	-5.70689	2.07662
C	3.36662	-3.73074	2.12797
H	2.84274	-3.89708	3.06909
H	-6.66346	-3.56808	-1.35573
H	-4.16901	-4.87773	2.80138
H	-3.21719	-6.93366	3.80917
C	-3.10504	-5.09798	2.69052
C	-2.57226	-6.25348	3.25395
C	-1.21482	-6.53788	3.11280
H	-0.79627	-7.44164	3.55340
C	-0.93696	-4.49844	1.85320
C	-0.39959	-5.65749	2.40623
H	0.66378	-5.86813	2.28585
H	-5.57050	-3.08039	0.82049
C	-5.57590	-3.55584	-1.28579
C	-4.96239	-3.28333	-0.06354
H	-3.68199	-2.59861	2.06544
C	-2.87781	-2.93774	1.37089
C	-4.80028	-3.79468	-2.41740
C	-3.57190	-3.25468	0.04797
H	-5.27541	-4.00894	-3.37426
C	-2.29397	-4.20509	1.98635
C	-2.80252	-3.48745	-1.09806
C	-3.40915	-3.75157	-2.32122
H	-1.71092	-3.47383	-1.03103

H	-2.79263	-3.93354	-3.20038
H	-0.30079	-3.79125	1.32277
O	-1.93245	-1.95287	1.20148
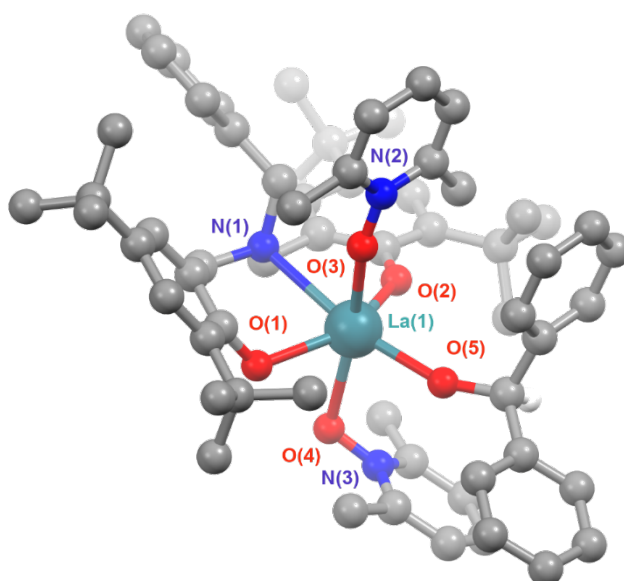
Figure 3.19. Labeled ball and stick image of **4-La(LO)₂**. H-atoms were removed for clarity.

Table 3.33. Selected bond distances (Å) and metrical parameters of the DFT calculated structures of **4-La(LO)₂**.

Distance (Å)	DFT	Angle (°)	DFT
La(1)–O(1)	2.365	O(1)–La(1)–O(2)	141.86
La(1)–O(2)	2.350	O(1)–La(1)–O(3)	91.03
La(1)–O(3)	2.509	O(1)–La(1)–O(4)	76.48
La(1)–O(4)	2.577	O(1)–La(1)–O(5)	116.54
La(1)–O(5)	2.293	O(1)–La(1)–N(1)	75.58
La(1)–N(1)	2.775	O(2)–La(1)–O(3)	104.35
		O(2)–La(1)–O(4)	89.74
		O(2)–La(1)–O(5)	96.93
		O(2)–La(1)–N(1)	72.06
		O(3)–La(1)–O(4)	165.81
		O(3)–La(1)–O(5)	95.09
		O(3)–La(1)–N(1)	82.98
		O(4)–La(1)–O(5)	84.76
		O(4)–La(1)–N(1)	100.07
		O(5)–La(1)–N(1)	167.82
		P(1)–N(3)–La(1)	156.11
		P(2)–N(4)–La(1)	114.07

Table 3.34. Cartesian coordinates of **4-La(LO)₂**.

Atom	X	Y	Z
La	0.62347	-0.26391	-0.56337
O	-0.37311	-1.84327	-2.01453
O	0.61844	2.02761	-0.04118
O	-0.43770	-1.35820	1.42989
O	1.67753	0.27209	-2.85264
N	-1.94566	0.70056	-0.97457
C	-1.49352	-2.44740	-1.67503
C	-1.56073	-3.85496	-1.46217
C	-0.30117	-4.71766	-1.61175
C	0.80530	-4.27831	-0.63733
H	1.10466	-3.23734	-0.80066
H	1.70025	-4.90318	-0.77469
H	0.49370	-4.37992	0.41127
C	0.23022	-4.60860	-3.04893
H	-0.50150	-5.00745	-3.76290
H	1.15883	-5.18772	-3.15982
H	0.43241	-3.56693	-3.31126
C	-0.57710	-6.19496	-1.32451
H	-0.94463	-6.35561	-0.30137
H	0.34955	-6.77215	-1.43738
H	-1.31441	-6.61897	-2.01747
C	-2.80138	-4.41834	-1.15239
H	-2.85073	-5.49168	-0.98752
C	-3.98290	-3.67749	-1.02633
C	-5.33262	-4.30868	-0.68824
C	-5.20444	-5.78605	-0.31969
H	-4.81677	-6.38488	-1.15307
H	-6.18685	-6.19481	-0.05091
H	-4.53503	-5.93476	0.53867
C	-6.26819	-4.18626	-1.89845
H	-6.41138	-3.13690	-2.18531
H	-7.25699	-4.61301	-1.67872
H	-5.85610	-4.71382	-2.76768
C	-5.96990	-3.57477	0.50015
H	-5.32199	-3.61119	1.38718
H	-6.93358	-4.02977	0.76787
H	-6.15769	-2.51886	0.26889
C	-3.89171	-2.30010	-1.24167
H	-4.79093	-1.68091	-1.19700
C	-2.68402	-1.67695	-1.54206
C	-2.64451	-0.22295	-1.91269
H	-2.09945	-0.12632	-2.86301
H	-3.67072	0.14916	-2.08329

C	-2.62544	0.83013	0.33185
H	-2.07151	1.60391	0.88477
H	-2.46887	-0.12521	0.85242
C	-4.10347	1.13124	0.34504
C	-4.99682	0.15842	0.80464
H	-4.60348	-0.80516	1.13601
C	-6.36696	0.40042	0.84506
H	-7.04342	-0.36975	1.21421
C	-6.86802	1.62803	0.41930
H	-7.93910	1.82160	0.44586
C	-5.98869	2.61174	-0.02772
H	-6.37072	3.58118	-0.34514
C	-4.61886	2.36746	-0.05924
H	-3.93440	3.15466	-0.37140
C	-1.71896	1.97983	-1.70385
H	-2.64443	2.25935	-2.24182
H	-0.98815	1.72281	-2.49470
C	-1.23458	3.18942	-0.95104
C	-1.91801	4.38950	-1.13113
H	-2.82126	4.37753	-1.74717
C	-1.48366	5.59100	-0.57400
C	-2.29762	6.86567	-0.78527
C	-3.73680	6.64222	-0.29960
H	-3.75876	6.36130	0.76100
H	-4.23480	5.84383	-0.86430
H	-4.33566	7.55481	-0.42365
C	-2.32778	7.21263	-2.27993
H	-1.31587	7.39336	-2.66387
H	-2.92620	8.11624	-2.46114
H	-2.76588	6.39940	-2.87214
C	-1.71525	8.05571	-0.02465
H	-1.67308	7.86746	1.05578
H	-2.33848	8.94478	-0.18351
H	-0.70056	8.30105	-0.36303
C	-0.29092	5.55093	0.15221
H	0.07399	6.47853	0.58255
C	0.46106	4.38886	0.35043
C	1.78460	4.43674	1.12825
C	2.12348	5.85207	1.60149
H	2.22702	6.55625	0.76600
H	3.08023	5.83680	2.13895
H	1.36713	6.25233	2.28879
C	2.95293	3.95028	0.25777
H	2.79899	2.91326	-0.05809
H	3.89352	3.99790	0.82604
H	3.07028	4.57798	-0.63576
C	1.71616	3.53587	2.36733

H	0.83501	3.76623	2.98126
H	2.60973	3.67580	2.99288
H	1.67254	2.48598	2.07064
C	-0.03056	3.16811	-0.19529
H	1.21151	0.29679	2.64334
H	-0.24030	1.20238	2.22588
C	0.25725	0.66502	3.04605
H	0.47528	1.37654	3.84562
C	-0.57076	-0.44620	3.55003
N	-0.89962	-1.42691	2.64950
H	-2.55829	-2.84843	1.06063
H	-0.75136	0.22323	5.55620
C	-1.03459	-0.55605	4.85290
C	-1.72166	-2.47609	2.98055
C	-2.08498	-3.39734	1.88603
C	-1.83216	-1.62443	5.23825
C	-2.17834	-2.57416	4.28594
H	-2.19120	-1.70818	6.26072
H	-2.77026	-4.17186	2.24232
H	-1.20318	-3.87282	1.44176
H	-2.82215	-3.41417	4.53402
H	1.71388	2.80531	-2.07666
H	2.89775	3.80911	-2.95174
C	2.42209	2.82564	-2.91375
H	1.82969	2.66865	-3.82305
C	3.44267	1.75975	-2.77698
N	2.97556	0.47281	-2.81117
H	2.47715	-2.15995	-2.15705
H	5.16752	2.98679	-2.57526
C	4.80770	1.96186	-2.63094
C	3.80831	-0.61571	-2.81344
C	3.16347	-1.93845	-2.98392
C	5.67967	0.88259	-2.55479
C	5.17090	-0.40490	-2.67228
H	6.74649	1.04026	-2.41527
H	3.91923	-2.72817	-3.02214
H	2.55087	-1.95695	-3.89302
H	5.82014	-1.27638	-2.62366
O	2.77877	-0.69251	0.09284
C	3.93752	-0.51099	0.81075
C	5.01412	-1.51538	0.42516
C	6.36684	-1.20886	0.58739
H	6.64423	-0.23944	1.00752
C	7.35417	-2.10999	0.20092
H	8.40540	-1.85141	0.32371
C	6.99798	-3.34058	-0.35059
H	7.76797	-4.04629	-0.65891

C	5.65025	-3.66040	-0.50340
H	5.36209	-4.62163	-0.92956
C	4.66680	-2.75266	-0.11758
H	3.60990	-2.97847	-0.25599
C	3.63231	-0.57969	2.30162
C	3.92059	0.48541	3.15366
H	4.42368	1.36636	2.74948
C	3.54231	0.44945	4.49633
H	3.76221	1.29780	5.14374
C	2.87011	-0.65967	4.99986
H	2.56645	-0.68924	6.04572
C	2.58230	-1.73556	4.15578
H	2.05148	-2.60572	4.54406
C	2.96225	-1.69482	2.81962
H	2.72120	-2.52199	2.14990
H	4.36938	0.49877	0.62280

3.5.3. Buried Volume (%V_{bur}) Calculations

All buried volume calculations of the free ligands and metal complexes were performed using SambVca 2.1.[41] Abbreviations for tabulated values are provided within SambVca 2.1, but several are provided again below for convenience.

Free ligands: Structures of the free ligands, OPPh$_3$, PyO, and **LO**, were obtained from the deposited X-ray structures found in the Cambridge Structural Database (CSD; Structure codes: OPPh$_3$ = TPEPHO,[52] PyO = PYRDNO11,[53] **LO** = ACOHAC[54]). In the case of **LO**, the interstitial water molecule was removed. These coordinates were then uploaded via the web applet, and the oxygen of the oxide donor was selected as the center of the sphere. The *z*-axis and *xz*-plane were defined as follows: *z*-axis = O$_{PyO}$ & N$_{PyO}$, O$_{LO}$ & N$_{LO}$, O$_{OPPh3}$ & P$_{OPPh3}$ // *xz*-plane = OPPh$_3$: P & C$_{OPPh3}$ (2-Ar), PyO: C (2,6-Ar), **LO**: C (2,6-Me$_2$). The distance of the coordination point from the center of the sphere was chosen to be 2.28 Å, with a scaling of 1.17 for all bond radii, and a sphere radius of 3.5 Å.

Metal complexes: Structures of the metal complexes, **1-La(OPPh$_3$)$_2$**, **1-La(LO)$_2$**, **4-La(OPPh$_3$)$_2$**, **4-La(LO)$_2$**, were obtained from the DFT optimized structures (SI, section 5). La was selected as the center of the sphere, and the *z*-axis and *xz*-plane were defined as follows: *z*-axis = La & ^{Bn}N // *xz*-plane = O$_{Ar}$ & O$_{Ar}$. Bond radii were scaled to 1.17 and two sphere radii were used to capture the %V_{bur} related to the primary (3.5 Å) and secondary (6.5 Å) coordination spheres. **Note**: La and the N(SiHMe$_2$)$_2$ / OCHPh$_2$ groups were excluded from the volume calculations.

3.6. References

1.	Dong, X.; Robinson, J. R., The role of neutral donor ligands in the isoselective ring-opening polymerization of rac-β-butyrolactone. *Chem. Sci.* **2020,** *11* (31), 8184-8195.

2.	Casey, K. C.; Appiah, J. K.; Robinson, J. R., Low-Symmetry β-Diketimine Aryloxide Rare-Earth Complexes: Flexible, Reactive, and Selective. *Inorg. Chem.* **2020,** *59* (20), 14827-14837.

3.	Karayannis, N. M.; Pytlewski, L. L.; Mikulski, C. M., Metal complexes of aromatic amine n-oxides. *Coord. Chem. Rev.* **1973,** *11* (2), 93-159.

4.	Karayannis, N. M.; Speca, A. N.; Chasan, D. E.; Pytlewski, L. L., Coordination complexes of the n-oxides of aromatic diimines and diazines. *Coord. Chem. Rev.* **1976,** *20* (1), 37-80.

5.	Wang, Y.; Zhang, L., Recent Developments in the Chemistry of Heteroaromatic N-Oxides. *Synthesis* **2015,** *47* (03), 289-305.

6.	Buchikhin, E. P.; Chekmarev, A. M.; Agafonov, Y. A.; Ulanov, A. V.; Kuznetsov, A. Y., Solvent Effect on the Efficiency of Donor-Acceptor Interaction. *Russian Journal of General Chemistry* **2002,** *72* (7), 1049-1052.

7.	Laurence, C.; Gal, J.-F., The Donor Number or SbCl5 Affinity Scale. In *Lewis Basicity and Affinity Scales*, 2009; pp 71-83.

8.	Irie, R.; Ito, Y.; Katsuki, T., Donor Ligand Effect in Asymmetric Epoxidation of Unfunctionalized Olefins with Chiral Salen Complexes. *Synlett* **1991,** *1991* (04), 265-266.

9.	Jacobsen, E. N.; Zhang, W.; Muci, A. R.; Ecker, J. R.; Deng, L., Highly enantioselective epoxidation catalysts derived from 1,2-diaminocyclohexane. *J. Am. Chem. Soc.* **1991,** *113* (18), 7063-7064.

10. Kureshy, R. I.; Khan, N. H.; Abdi, S. H. R.; Bhatt, A. K.; Iyer, P., Synthesis, physicochemical studies and aerobic enantioselective epoxidation of non functionalized olefins catalyzed by new Co(II) chiral salen complexes. *Journal of Molecular Catalysis A: Chemical* **1997,** *121* (1), 25-31.

11. Adam, W.; Mock-Knoblauch, C.; Saha-Möller, C. R.; Herderich, M., Are MnIV Species Involved in Mn(Salen)-Catalyzed Jacobsen−Katsuki Epoxidations? A Mechanistic Elucidation of Their Formation and Reaction Modes by EPR Spectroscopy, Mass-Spectral Analysis, and Product Studies: Chlorination versus Oxygen Transfer. *J. Am. Chem. Soc.* **2000,** *122* (40), 9685-9691.

12. Chen, F.-X.; Zhou, H.; Liu, X.; Qin, B.; Feng, X.; Zhang, G.; Jiang, Y., Enantioselective Cyanosilylation of Ketones by a Catalytic Double-Activation Method with an Aluminium Complex and an N-Oxide. *Chem. Eur. J.* **2004,** *10* (19), 4790-4797.

13. Liu, X.; Zheng, H.; Xia, Y.; Lin, L.; Feng, X., Asymmetric Cycloaddition and Cyclization Reactions Catalyzed by Chiral N,N′-Dioxide–Metal Complexes. *Acc. Chem. Res.* **2017,** *50* (10), 2621-2631.

14. Liu, X.; Lin, L.; Feng, X., Chiral N,N′-Dioxides: New Ligands and Organocatalysts for Catalytic Asymmetric Reactions. *Acc. Chem. Res.* **2011,** *44* (8), 574-587.

15. Save, M.; Schappacher, M.; Soum, A., Controlled Ring-Opening Polymerization of Lactones and Lactides Initiated by Lanthanum Isopropoxide, 1. General Aspects and Kinetics. *Macromolecular Chemistry and Physics* **2002,** *203* (5-6), 889-899.

16. Laurence, C.; Gal, J.-F., Thermodynamic and Spectroscopic Scales of Hydrogen-Bond Basicity and Affinity. In *Lewis Basicity and Affinity Scales*, 2009; pp 111-227.

17. Dega-Szafran, Z.; Grundwald-Wyspiańska, M.; Kania, A.; Kosturkiewicz, Z.; Tykarska, E.; Szafran, M., FT-IR, UV—visible and X-ray studies of complexes of pyridine N-oxides with pentachlorophenol. *Journal of Molecular Structure* **1995,** *356* (3), 169-182.

18. Gurzyński, Ł.; Puszko, A.; Makowski, M.; Chmurzyński, L., A potentiometric study of (acid+base) equilibria in substituted 4-nitropyridine N-oxide systems in methanol and dimethyl sulfoxide. *The Journal of Chemical Thermodynamics* **2007,** *39* (2), 309-315.

19. Parsons, R., The rate of electrolytic hydrogen evolution and the heat of adsorption of hydrogen. *Transactions of the Faraday Society* **1958,** *54* (0), 1053-1063.

20. Gerischer, H., Mechanismus der Elektrolytischen Wasserstoffabscheidung und Adsorptionsenergie von Atomarem Wasserstoff. *Bulletin des Sociétés Chimiques Belges* **1958,** *67* (7-8), 506-527.

21. Sabatier, P., Hydrogénations et déshydrogénations par catalyse. *Berichte der deutschen chemischen Gesellschaft* **1911,** *44* (3), 1984-2001.

22. Swiegers, G. F., *Mechanical Catalysis: Methods of Enzymatic, Homogeneous, and Heterogeneous Catalysis*. John Wiley & Sons: Hoboken, NJ, 2008.

23. Busch, M.; Wodrich, M. D.; Corminboeuf, C., Linear scaling relationships and volcano plots in homogeneous catalysis – revisiting the Suzuki reaction. *Chemical Science* **2015,** *6* (12), 6754-6761.

24. Wodrich, M. D.; Sawatlon, B.; Busch, M.; Corminboeuf, C., The Genesis of Molecular Volcano Plots. *Accounts of Chemical Research* **2021,** *54* (5), 1107-1117.

25. Li, W.; Ma, X.; Fan, W.; Tao, X.; Li, X.; Xie, X.; Zhang, Z., Ru-Catalyzed Asymmetric Hydrogenation of 3-Oxoglutaric Acid Derivatives via Solvent-Assisted Pinpoint Recognition

of Carbonyls in Close Chemical Propinquity. *Organic Letters* **2011,** *13* (15), 3876-3879.

26. Lavallee, C.; Grenier, D.; Prud'homme, R. E.; Leborgne, A.; Spassky, N., Synthesis and Properties of Racemic and Optically Active Substituted Poly(β-Propiolactones). In *Advances in Polymer Synthesis*, Culbertson, B. M.; McGrath, J. E., Eds. Springer US: Boston, MA, 1985; pp 441-460.

27. Zhang, Y.; Gross, R. A.; Lenz, R. W., Stereochemistry of the ring-opening polymerization of (S)-.beta.-butyrolactone. *Macromolecules* **1990,** *23* (13), 3206-3212.

28. Kricheldorf, H. R.; Scharnagl, N.; Jedlinski, Z., Polylactones 33. The role of deprotonation in the anionic polymerization of β-propiolactone. *Polymer* **1996,** *37* (8), 1405-1411.

29. Rieth, L. R.; Moore, D. R.; Lobkovsky, E. B.; Coates, G. W., Single-Site β-Diiminate Zinc Catalysts for the Ring-Opening Polymerization of β-Butyrolactone and β-Valerolactone to Poly(3-hydroxyalkanoates). *Journal of the American Chemical Society* **2002,** *124* (51), 15239-15248.

30. Morris, K. F.; Johnson, C. S., Diffusion-ordered two-dimensional nuclear magnetic resonance spectroscopy. *J. Am. Chem. Soc.* **1992,** *114* (8), 3139-3141.

31. Keresztes, I.; Williard, P. G., Diffusion-Ordered NMR Spectroscopy (DOSY) of THF Solvated n-Butyllithium Aggregates. *J. Am. Chem. Soc.* **2000,** *122* (41), 10228-10229.

32. Pregosin, P. S., NMR diffusion methods in inorganic and organometallic chemistry. In *Spectroscopic Properties of Inorganic and Organometallic Compounds: Techniques, Materials and Applications, Volume 42*, The Royal Society of Chemistry: 2012; Vol. 42, pp 248-268.

33. Zhao, Y.; Truhlar, D. G., A new local density functional for main-group thermochemistry, transition metal bonding, thermochemical kinetics, and noncovalent interactions. *J. Chem.*

Phys. **2006,** *125* (19), 194101.

34. Grimme, S.; Antony, J.; Ehrlich, S.; Krieg, H., A consistent and accurate ab initio parametrization of density functional dispersion correction (DFT-D) for the 94 elements H-Pu. *J. Chem. Phys.* **2010,** *132* (15), 154104.

35. Dolg, M.; Stoll, H.; Preuss, H., A combination of quasirelativistic pseudopotential and ligand field calculations for lanthanoid compounds. *Theoret. Chim. Acta* **1993,** *85* (6), 441-450.

36. Dolg, M.; Stoll, H.; Savin, A.; Preuss, H., Energy-adjusted pseudopotentials for the rare earth elements. *Theoret. Chim. Acta* **1989,** *75* (3), 173-194.

37. Rassolov, V. A.; Pople, J. A.; Ratner, M. A.; Windus, T. L., 6-31G* basis set for atoms K through Zn. *J. Chem. Phys.* **1998,** *109* (4), 1223-1229.

38. Petersson, G. A.; Al-Laham, M. A., A complete basis set model chemistry. II. Open-shell systems and the total energies of the first-row atoms. *J. Chem. Phys.* **1991,** *94* (9), 6081-6090.

39. Petersson, G. A.; Bennett, A.; Tensfeldt, T. G.; Al-Laham, M. A.; Shirley, W. A.; Mantzaris, J., A complete basis set model chemistry. I. The total energies of closed-shell atoms and hydrides of the first-row elements. *J. Chem. Phys.* **1988,** *89* (4), 2193-2218.

40. E.D. Glendening, A. E. R., J.E. Carpenter, F. Weinhold, , NBO Version 3.1. *TCI ,University of Wisconsin, Madison,* **1998**.

41. Falivene, L.; Cao, Z.; Petta, A.; Serra, L.; Poater, A.; Oliva, R.; Scarano, V.; Cavallo, L., Towards the online computer-aided design of catalytic pockets. *Nature Chemistry* **2019,** *11* (10), 872-879.

42. Bradley, D. C.; Ghotra, J. S.; Hart, F. A., Low co-ordination numbers in lanthanide and actinide compounds. Part I. The preparation and characterization of tris{bis(trimethylsilyl)-

amido}lanthanides. *Journal of the Chemical Society, Dalton Transactions* **1973,** (10), 1021-1023.

43. Smith, A. R.; Livinghouse, T., Rapid and Efficient Procedure for the Synthesis of Group 3 Metal Tris[bis(dimethylsilyl)amide] THF Complexes. *Organometallics* **2013,** *32* (5), 1528-1530.

44. Zohuri, G. H.; Seyedi, S. M.; Sandaroos, R.; Damavandi, S.; Mohammadi, A., Novel Late Transition Metal Catalysts Based on Iron: Synthesis, Structures and Ethylene Polymerization. *Catalysis Letters* **2010,** *140* (3), 160-166.

45. Duda, A.; Penczek, S., Mechanisms of Aliphatic Polyester Formation. In *Biopolymers Online*, Wiley VCH: 2002; Vol. 3b, pp 371-429.

46. Frisch, M. J. T., G. W.; Schlegel, H. B.; Scuseria, G. E.; Robb, M. A.; Cheeseman, J. R.; Scalmani, G.; Barone, V.; Mennucci, B.; Pe-tersson, G. A.; Nakatsuji, H.; Caricato, M.; Li, X.; Hratchian, H.; P.; Izmaylov, A. F. B., J.; Zheng, G.; Sonnenberg, J. L.; Hada, M.; Ehara, M.; Toyota, K.; Fukuda, R.; Hasegawa, J.; Ishida, M.; Nakajima, T.; Honda, Y.; Kitao, O.; Nakai, H.; Vreven, T.; Montgomery, J. A., Jr.; Peralta, J. E.; Ogliaro, F.; Bearpark, M.; Heyd, J. J.; Brothers, E.; Kudin, K. N.; Staroverov, V. N.; Kobayashi, R.; Normand, J.; Raghavachari, K.;; Rendell, A. B., J. C.; Iyengar, S. S.; Tomasi, J.; Cossi, M.; Rega, N.; Millam, N. J.; Klene, M.; Knox, J. E.; Cross, J. B.; Bakken, V.; Adamo, C.; Jaramillo, J.; Gomperts, R.; Stratmann, R. E.; Yazyev, O.; Austin, A. J.; Cammi, R.; Pomelli, C.; Ochterski, J. W.; Martin, R. L.; Morokuma, K.; Zakrzewski, V. G.; Voth, G. A.; Salvador, P.; Dannenberg, J. J.; Dapprich, S.; Daniels, A. D.; Farkas, Ö.; Foresman, J. B.; Ortiz, J. V.; Cioslowski, J.; Fox, D. J. *Gaussian 09, Revision D.01*, G09, Revision D.01; Wallingford, CT, 2009.

47. Weigend, F.; Ahlrichs, R., Balanced basis sets of split valence, triple zeta valence and quadruple zeta valence quality for H to Rn: Design and assessment of accuracy. *Phys Chem Chem Phys* **2005,** *7* (18), 3297-305.

48. Weigend, F., Accurate Coulomb-fitting basis sets for H to Rn. *Phys. Chem. Chem. Phys.* **2006,** *8* (9), 1057-1065.

49. Marenich, A. V.; Cramer, C. J.; Truhlar, D. G., Universal Solvation Model Based on Solute Electron Density and on a Continuum Model of the Solvent Defined by the Bulk Dielectric Constant and Atomic Surface Tensions. *J. Phys. Chem. B* **2009,** *113* (18), 6378-6396.

50. Hanwell, M.; Curtis, D.; Lonie, D. C.; Vandermeersch, T.; Zurek, E.; Hutchison, G., Avogadro: an advanced semantic chemical editor, visualization, and analysis platform. *Journal of Cheminformatics* **2012,** *4*, 17 - 17.

51. Zhao, Y.; Truhlar, D. G., The M06 suite of density functionals for main group thermochemistry, thermochemical kinetics, noncovalent interactions, excited states, and transition elements: two new functionals and systematic testing of four M06-class functionals and 12 other functionals. *Theoretical Chemistry Accounts* **2008,** *120* (1), 215-241.

52. Bandoli, G.; Bortolozzo, G.; Clemente, D. A.; Croatto, U.; Panattoni, C., Crystal and molecular structure of triphenylphosphine oxide. *Journal of the Chemical Society A: Inorganic, Physical, Theoretical* **1970,** (0), 2778-2780.

53. Marsh, R. E.; Kapon, M.; Hu, S.; Herbstein, F. H., Some 60 new space-group corrections. *Acta Crystallographica Section B* **2002,** *58* (1), 62-77.

54. Planas, J. G.; Mohamed, G. G.; Sillanpää, R.; Kivekäs, R.; Teixidor, F.; Viñas, C., Interplay of hydrogen bonding and π–π interactions in the molecular complex of 2,6-lutidine N-oxide

and water. *Journal of Molecular Structure* **2006,** *787* (1), 121-126.

Chapter 4: Quantitative Study of Kinetic of Polymerization of *rac-β*-BBL Accompanied by Time-dependent Concentration of Catalyst

Abstract

During polymerization of BBL, the simultaneous elimination discussed in previous chapters not only cleaves macromolecular chains, but also deactivates the catalyst. Despite the importance of tracking such processes, the evolution of active catalytic species is challenging to detect and measure directly. In this chapter, I describe how we can indirectly track the active catalyst profile by analyzing the time function of monomer conversion within the lanthanum catalyst we've developed. Through this analysis, we have found that the elimination is second order in the catalytic species in the OPPh3-assisted ROP of BBL, and determined rate constants for propagation and elimination under various conditions. Further application of this method in reactions with various equivalents of OPPh3 or different lutidine-oxides helps refine the role of these exogenous ligands in the donor-amplified ROP of rac-BBL. These results may direct further developments of this catalytic system.

4.1. Introduction

In previous studies of metal alkoxide catalyzed ROP of BBL, generation of crotyl end-groups after polymerization has been noticed and found to proceed through several possible pathways: (*i*) elimination of water, hydroxide, or oxide from the alcohol end-group under acidic or basic conditions respectively,[1-4] (*ii*) thermal scission,[5-8] or (*iii*) base-induced elimination of internal ester units.[9-11] Regardless of the different elimination pathways, the eventual outcome leads to the formation of a crotyl end-group and elimination of active catalytic species (i.e. formation of a metal carboxylate). The effect of such side reaction affects not only the average and distribution of molecular weights of the macromolecular product, but also the kinetics of the polymerization. While the former has received some limited attention, the latter has been largely overlooked. The low concentration of catalyst employed in these reactions can make the time-dependent quantification of catalyst speciation extremely challenging, which has led to significant difficulties in quantifying the active catalytic species and disentangling rates of propagation and elimination.

For example, we measured the conversion **1-La(TPPO)$_2$** catalyzed ROP of BBL at different time, where the conversion varied from 20% to 90%, in Chapter 2. Notably, the polymerization of BBL catalyzed by **1-La(TPPO)$_2$** didn't show simple, pseudo first-order behavior. As reflected by the conversion-time plots (Figure 4.1), the reaction rate was very fast at the beginning and drastically dropped when the conversion was above 50%. The lack of linearity in plots of -*ln*(1-conversion) *vs* time further discounts pseudo first-order behavior, while other attempts of fitting the reaction to a power law of [BBL] all failed.

4.2. Result and Discussion

4.2.1. General Analysis of the Kinetic Behavior

With the knowledge of the elimination side reaction during ROP of BBL, the deviation from pseudo-first order kinetic behavior in Figure 4.1 can be readily rationalized. As propagation proceeds, active species are converted to in-active La carboxylates. Therefore, the rate of propagation is no longer proptional to the concentration of BBL over time. While this qualitive explanation provides a clear motivation to design systems which suppress these deactivation pathways, a more quantative analysis which could decouple the influence of reaction conditions on propagation and elimination rates requires a more detailed and mathematical approach.
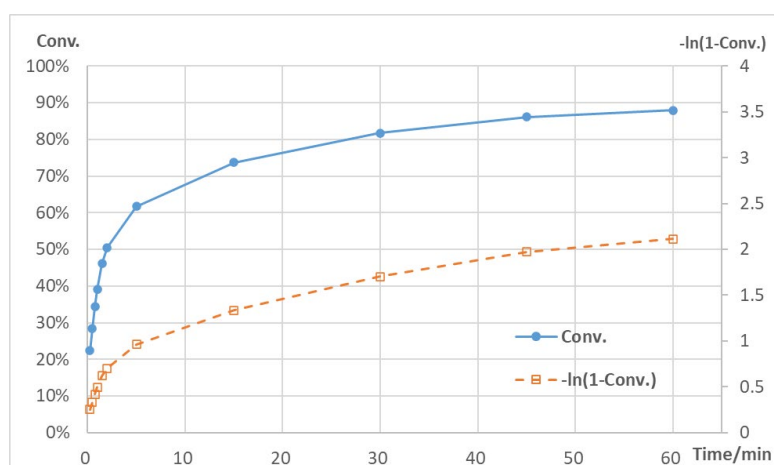
Figure 4.1. Conversion of BBL (blue circle), -*ln*(1-conversion) (orange squares) as functions of time. Reaction was performed in toluene at ambient temperature with [BBL]/[**1-La(TPPO)$_2$**]/[^{i}PrOH] = 200/1/1 and [BBL] = 2.4 M.

In order to comprehensively investigate the kinetic of this reaction, one must figure out the rate law of not only propagation, but also elimination. The propagation rate constant can be determined by measuring conversions at time points in the reaction where minimal catalyst degradation due to elimination has occurred (i.e. first-order behavior is maintained). In contrast, the direct determination of the elimination rate constant is not trivial, as the direct and accurate measurement of the degradation of catalyst is not as straightforward as following the

consumption of substrate. One approach could attempt quantitative detection of the active catalytic species during the reaction; however, this species is expected to be present in very ow concentrations and exists as undetermined, unstable, and variable states. Alternatively, one could follow the formation of the crotyl end-group, the byproduct of the degradation, but this is also challenging to quantify due to its low concentration.

Given the aforementioned difficulties in the direct measurement of catalyst evolution, we considered an alternative approach. Other than directly following the active catalyst or the byproduct of its degradation, one might indirectly extract the active catalyst concentration following monomer conversion. In principle, the rates of propagation and elimination could be extracted from the conversion-time relationship of the substrate, if a known or reasonably assumed reaction order of the substrate can be made. To avoid over-generalizing and complicating the problem, the following discussion will assume that, in the absence of catalyst deactivation, the consumption of substrate is first order in both substrate and catalyst. Such rate laws are commonly observed for the ROP of cyclic esters, including the ROP of BBL.[9, 12-16]

Relationship between the evolution of substrate and catalyst: A reaction which is first order in both substrate and catalyst can be defined as:

$$S' = \frac{dS}{dt} = -kCS \quad (1)$$

where S and C are functions of time and stand for the concentration of the substrate and catalyst respectively, k is the proportionality constant, or rate constant in chemistry, that doesn't change over time, and the prime notation means the time derivative.

Dividing both sides of (1) by $-S$ leads to the following:

$$-\frac{S'}{S} = -\left[\ln\left(\frac{S}{S_{t=0}}\right)\right]' = -[\ln(1 - Conv.)]' = kC \quad (2)$$

In eq. (2), S and C are now separated. The right-hand side is proportional to C, and one can know how C changes over time by plotting $-S/S'$, (i.e., $-[\ln(1\text{-}Conv.)]'$) and time. Although there is an undetermined number, k, this plot can help establish how the catalyst evolves during the reaction. Furthermore, one can postulate a reasonable time dependence (e.g., any power law of C) or a function containing S. Once the rate law of the catalyst is known and the numeric parameters determined, one can then plug the values back into the rate law of the substrate to compare with and validate against experimental data.

4.2.2. Kinetics of 4-La(OPPh$_3$)$_2$ Catalyzed ROP of BBL

Although essential to understanding and improving catalyst performance, the evolution of the active catalyst is not yet known. General approaches which can extract the rate of productive (propagation) and unproductive (deactivation) processes are unknown, despite significant interest, a non-power rate law, and the ability to follow reaction conversion (i.e., substrate concentration) at given points in time. This is surprising, as according to the above analysis, as long as we measure conversion accurately and frequently enough, there is a chance to discover how catalyst changes during reaction.

Before any experiment or analysis, it worth to pointing out that the polymerization of BBL is significantly exothermic ($\Delta G_p = -59.2$ kJ/mol).[17] Under typical ROP conditions (2.4 M BBL, 0.012 M La), this leads to a significant and immediate exotherm, which would lead to

uncontrolled temperature fluctuations and ruin kinetic measurements. The described, unwanted thermal effects can be avoided by performing the ROP of BBL under significantly more dilute conditions (e.g., 0.3 M BBL).

We initially conducted the reaction with 0.3 M BBL in toluene, 1 mol% **4-La(OPPh₃)₂** (see Chapter 3). To further avoid concentration fluctuations between kinetic runs, the actual concentrations of BBL and **4-La(OPPh₃)₂** were further determined using $O(SiMe_3)_2$ as an internal standard. The result is shown in Table 4.1. and Figure 4.2.a. Please note that key variables in eq. (2) such as S and k, have been replaced by M (monomer concentration) and k_p (propagation rate constant). Furthermore, for concision, we define

$$f(t) = \ln\big(1 - Conv.(t)\big) = \ln\big(\frac{M(t)}{M(0)}\big)$$

M is practically measurable, and thus so is f. Using eq. 2, we derived a time evolution of catalyst concentration (eq. 3), though with an undetermined constant factor, k_p. Eq. 3 gives a connection between the wondered C and the measurable f.

$$k_p C = -\frac{M'}{M} = -[\ln(1 - Conv.)]' = -f' \quad (3)$$

If the conversion is measured in a nearly continuous way, one can obtain f' at a certain time by differentiating f at adjacent times. In practice, the actual measurements conducted were fairly sparse. To keep the continuity and accuracy of f', we need to solve it in (at least) a 2nd order approximation. For the nth time point, t_n, we expand $f(t_{n\pm 1})$ to the term of 2nd derivative:

$$f(t_{n+i}) = f(t_n) + f'(t_n)(t_{n+i} - t_n) + \frac{1}{2}f''(t_n)(t_{n+i} - t_n)^2 + O\big((t_{n+i} - t_n)^3\big) \quad (4)$$

where $i = \pm 1$.

With the two equations of (4), $f'(t_n)$ is solved (see the procedures in 4.5.1):

$$f'(t_n) = \frac{1}{t_{n+1} - t_{n-1}}\left[(t_n - t_{n-1})\frac{f(t_{n+1}) - f(t_n)}{t_{n+1} - t_n} + (t_{n+1} - t_n)\frac{f(t_n) - f(t_{n-1})}{t_n - t_{n-1}}\right] \quad (5)$$

Table 4.1. ROP of *rac*-BBL (0.322 M) with **4-La(OPPh₃)₂** at different time points.
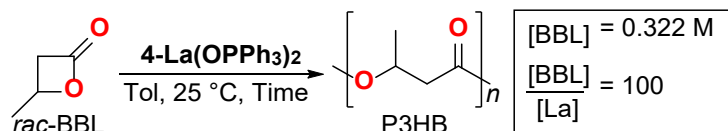
Entry	Time (min)	Conv. (%)[a]	$f = \ln(1\text{-Conv.})$	$-df/dt = k_pC$	$\ln(-df/dt)$	Sim. Conv. (%)[b]
0	0	0	0	-	-	0
1	2	14.1	-0.152	0.0544	-2.91	14.6
2	3	17.7	-0.195	0.0400	-3.22	18.3
3	5.5	23.9	-0.273	0.0268	-3.62	24.5
4	8	28.1	-0.329	0.0197	-3.93	28.5
5	12	32.2	-0.389	0.0133	-4.32	32.7
6	19	37.0	-0.462	0.00897	-4.71	37.4
7	30	41.5	-0.536	0.00551	-5.20	41.9
8	40	44.0	-0.580	0.00423	-5.47	44.7
9	55	47.3	-0.641	0.00336	-5.70	47.5
10	83	50.3	-0.699	-	-	51.1

a – Determined by ¹H-NMR integration of BBL and PHB methine resonances in the crude reaction mixture.
b – Simulated conversions are calculated with eq. (12). **k_p = 39.9 (M·min)⁻¹** and **k_e = 231 (M·min)⁻¹**, determined by linear regression of eq. (13).

The relative concentration of catalyst is shown in Figure 4.2.b. Although the actual concentration is veiled by the constant k_p, which stands for the rate constant of propagation, one can clearly notice the dramatic catalyst decay, which has been qualitatively represented in conversion-time plot in Figure 4.2.a.

Further investigation of the catalyst evolution with respect to time reveals the rate law for catalyst degradation. We found $1/(k_pC)$ can be represented as a linear function of reaction time (Figure 4.2.c), which supports a 2nd-order dependence on catalyst concentration (eq. 7) for

catalyst degradation (base-promoted elimination). Combined with the assumption that propagation is 1st order in monomer and catalyst (eq. 6), we solved the process of polymerization as a function of time and derived the rate constants from experimental data.

$$\frac{dM}{dt} = -k_p CM \quad (6)$$

$$\frac{dC}{dt} = -k_e C^2 \quad (7)$$

Where again C represents the catalyst concentration, M represents the monomer concentration, and k_p and k_e stand for the rate constants of propagation and elimination, respectively.
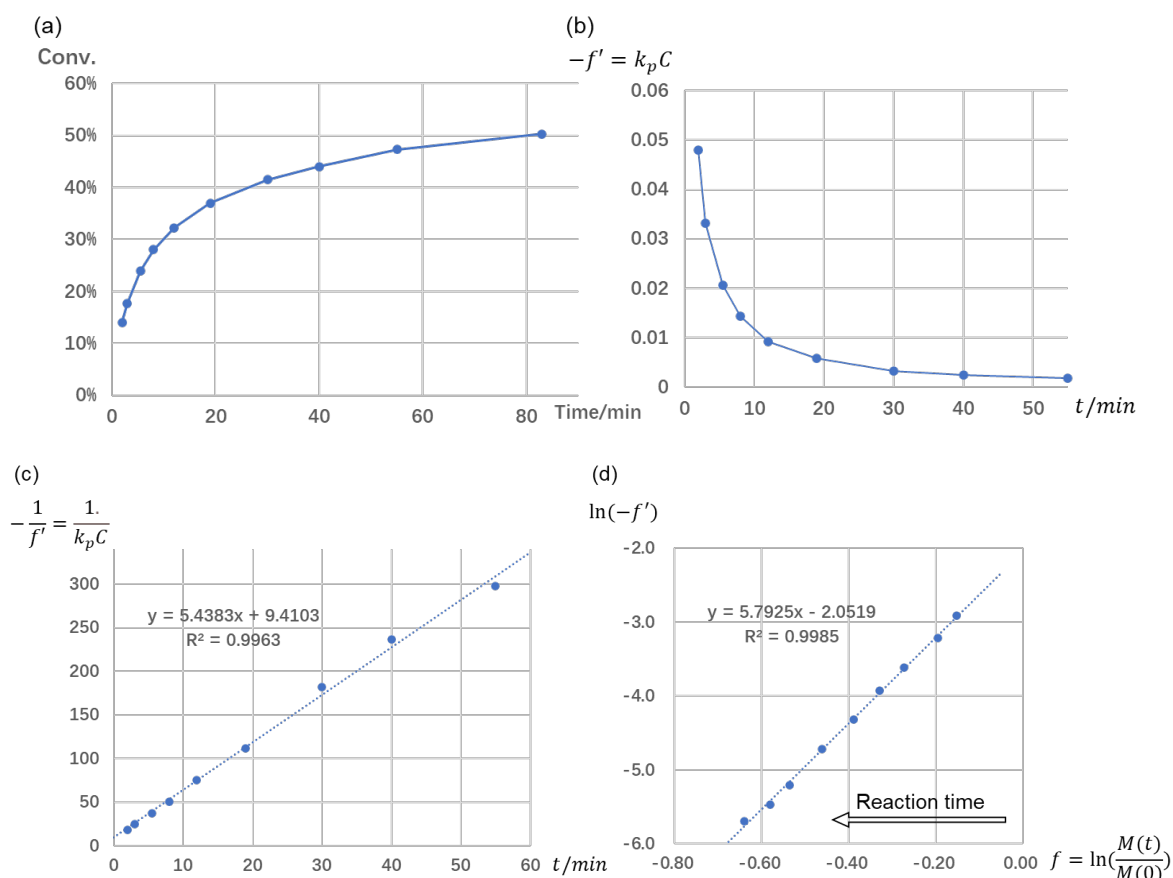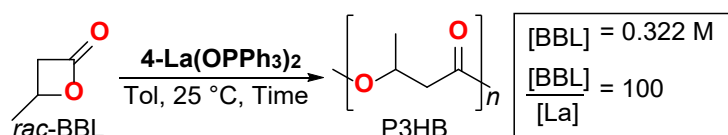
Figure 4.2. (a) Conversion of BBL (b) $k_p C$ and (c) $1/k_p C$ as functions of time. (d) Linear relationship of ln(-f') and f. Reaction was performed in toluene at ambient temperature with [BBL]/[**4-La(OPPh₃)₂**] = 100/1 and [BBL] = 0.322 M.

Dividing eq. (7) by eq. (6) can cancel the time differentials, which after separation of variables, leads to eq. (8):

$$\frac{dC}{C} = \frac{k_e}{k_p} \frac{dM}{M} \quad \Rightarrow d(\ln C) = \frac{k_e}{k_p} d(\ln M) \quad (8)$$

Let $C_0 = C(0)$ and $M_0 = M(0)$. At $t = 0$, $C = C_0$,* $M = M_0$, which gives:

$$\ln \frac{C}{C_0} = \frac{k_e}{k_p} \ln \frac{M}{M_0} \quad \Rightarrow C = C_0 \left(\frac{M}{M_0}\right)^{k_e/k_p} \quad (9)$$

*Note that we neglect the time needed for converting the pre-catalyst to the active catalyst. This works well for the current case according to Figure 4.2.b, but this may not hold under some other conditions.

Eq. (9) is an expression of C in terms of M. Using the expression of C in eq. (9) within eq. (6), we get an ordinary differential equation (ODE) of M.

$$\frac{dM}{dt} = -k_p C_0 M \left(\frac{M}{M_0}\right)^{k_e/k_p} \quad (10)$$

Solving eq. (10) with $M = M_0$ at $t = 0$ as the initial condition (see the procedures in 4.5.2):

$$\frac{M}{M_0} = (1 + k_e C_0 t)^{-k_p/k_e} \quad (11)$$

$$\text{i.e., } Conversion(t) = 1 - (1 + k_e C_0 t)^{-k_p/k_e} \quad (12)$$

In cases where the elimination rate is negligible ($k_e \sim 0$), the limit of eq. (12) is $Conversion = 1 - e^{-k_p C_0 t}$, which agrees with the kinetic of a 1st order reaction.

To determine the rate constants, eq. (10) can be divided by M and the natural logarithm can be taken for both sides to yield:

$$\ln(-f') = \frac{k_e}{k_p} f + \ln(k_p C_0) \quad (13)$$

$$\text{where } f(t) = \ln \frac{M(t)}{M_0}$$

The plot of $\ln(-f')$ vs f displays a linear relationship, where according to eq. (13), the slope and intercept are k_e/k_p and $\ln(k_p C_0)$, respectively (Figure 4.2.d). With a known C_0, we can readily extract k_p and k_e. Using $C_0 = 0.00322$ M in the case of Figure 4.2.d, we arrive at $k_p = 39.9$ (M·min)$^{-1}$ and $k_e = 231$ (M·min)$^{-1}$.

We then applied this method to various monomer concentrations while maintaining the same catalyst concentration to establish the monomer order for propagation and catalyst deactivation (Table 4.2 and 4.3). Linear regressions using eq. (13) display high coefficient of determinations (Figure 4.3.a). Furthermore, using the k_p and k_e extracted from these regressions and using eq. (12), reaction conversions can be simulated as functions of the reaction time. Under the conditions we have tested, all simulated conversion values display excellent agreement with the experimental results (Figure 4.3.b, Table 4.1, 4.2 and 4.3)
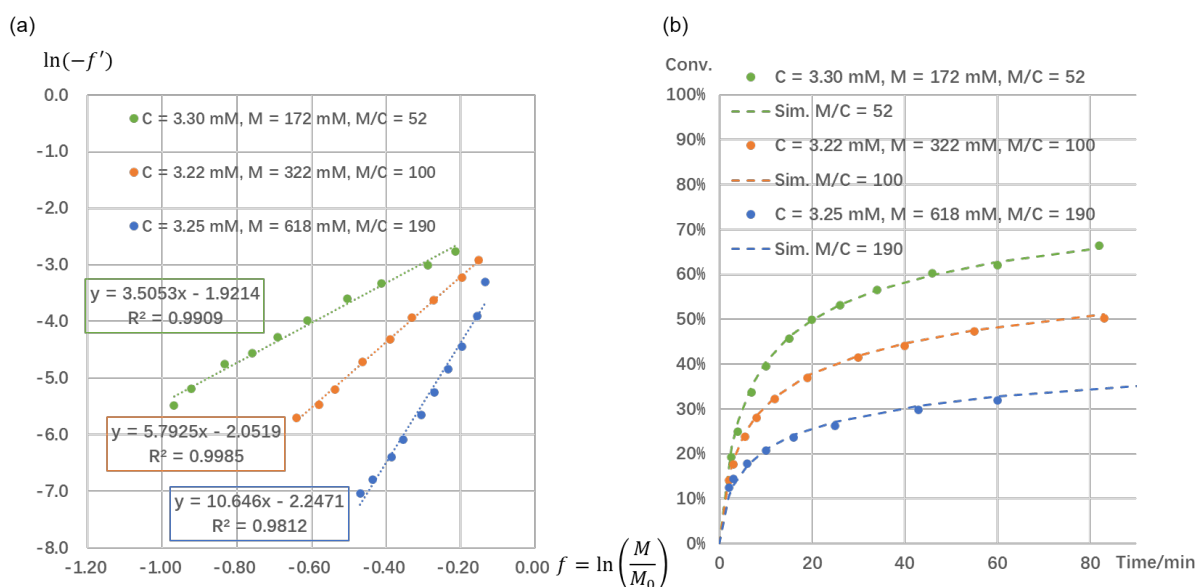
Figure 4.3. (a) Linear relationship of $\ln(-f')$ and f; (b) experimental (solid dots) and simulated (dash lines) conversions of BBL as functions of reaction time. Reactions were performed in toluene at ambient temperature with [BBL]/[**4-La(OPPh₃)₂**] = 52/1 and [BBL] = 0.330 M (green); 100/1 and [BBL] = 0.322 M (orange); 190/1 and [BBL] = 0.325 M (blue).

Table 4.2. ROP of *rac*-BBL (0.172 M) with **4-La(OPPh₃)₂** at different time points.
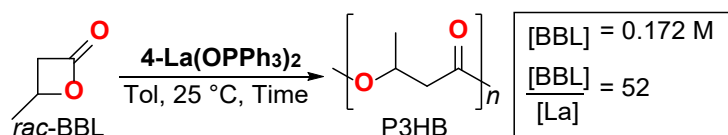
Entry	Time (min)	Conv. (%)[a]	$f = \ln(1\text{-Conv.})$	$-df/dt = k_pC$	$\ln(-df/dt)$	Sim. Conv. (%)[b]
0	0	0	0	-	-	0
1	2.6	19.2	-0.214	0.0633	-2.76	21.5
2	4	25.0	-0.288	0.0493	-3.01	27.3
3	7	33.7	-0.411	0.0360	-3.33	35.3
4	10	39.6	-0.504	0.0273	-3.60	40.4
5	15	45.7	-0.611	0.0186	-3.98	46.0
6	20	49.8	-0.690	0.0138	-4.28	49.9
7	26	53.2	-0.758	0.0105	-4.55	53.2
8	34	56.5	-0.833	0.00859	-4.76	56.5
9	46	60.3	-0.923	0.00556	-5.19	59.9
10	60	62.1	-0.969	0.00414	-5.49	62.7
11	82	66.4	-1.090	-	-	65.8

a – Determined by ¹H-NMR integration of BBL and PHB methine resonances in the crude reaction mixture.
b – Simulated conversions are calculated with eq. (12). k_p **= 44.4 (M·min)⁻¹** and k_e **= 156 (M·min)⁻¹**, determined by linear regression of eq. (13).

Table 4.3. ROP of *rac*-BBL (0.618 M) with **4-La(OPPh₃)₂** at different time points.
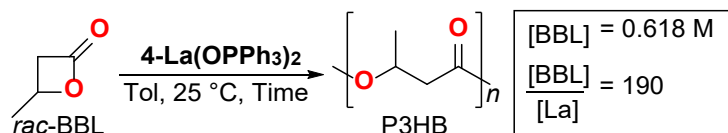
Entry	Time (min)	Conv. (%)[a]	$f = \ln(1\text{-Conv.})$	$-df/dt = k_pC$	$\ln(-df/dt)$	Sim. Conv. (%)[b]
0	0	0	0	-	-	0
1	2	12.4	-0.133	0.0371	-3.30	10.5
2	3	14.4	-0.155	0.0202	-3.90	12.9
3	6	17.8	-0.196	0.0117	-4.45	17.5
4	10	20.8	-0.233	0.00793	-4.84	21.0
5	16	23.6	-0.269	0.00522	-5.26	24.2
6	25	26.3	-0.305	0.00351	-5.65	27.1
7	43	29.8	-0.353	0.00227	-6.09	30.7
8	60	31.9	-0.385	0.00168	-6.39	32.8
9	100	35.3	-0.436	0.00112	-6.79	35.9
10	133	37.4	-0.469	0.00088	-7.04	37.6
11	180	39.5	-0.503	-	-	39.3

a – Determined by ¹H-NMR integration of BBL and PHB methine resonances in the crude reaction mixture.
b – Simulated conversions are calculated with eq. (12). k_p **= 32.5 (M·min)⁻¹** and k_e **= 346 (M·min)⁻¹**, determined by linear regression of eq. (13).

4.2.3. Effect of Equivalent of OPPh$_3$ and Induction Period

In Chapter 2, we qualitatively compared the ROP of BBL catalyzed by **1-La** in the presence of 0, 1, 2 and 3 equivalents of OPPh$_3$, where the equivalents of exogeneous donor led to remarkable changes in reaction rates and selectivity. With our method to evaluate the active catalyst concentration in hand, we set out to evaluate the impact of exogenous donor on the ROP of BBL catalyzed by **1-La**. To do this, we evaluated a series of reactions using $1 - 6$ equivalents of OPPh$_3$ with 3 mM **1-La** and 100 equivalents of BBL, by recording conversions at different times (Table 4.4 and Figure 4.4.a).

In all cases, increases in reaction conversion were insignificant after ~1 h reaction times compared to earlier time points. At this 1 h time point, increasing equivalents of OPPh$_3$ (1.0 to 6.0) led to large increases in the conversion of BBL (34% to 87%). Given that only modest increases in reaction conversion at 1 h were observed moving from $4 - 6$ equiv OPPh$_3$ (84 *vs* 87%), the upper limit of OPPh$_3$ equivalents we investigated was restricted to 6.

At the more dilute reaction conditions (0.3 *vs* 2.4 M BBL), there were significant differences in reaction conversion at 1 h for our optimal "standard" conditions (i.e., 2 equiv. OPPh$_3$; 48% conversion) and with large excesses of OPPh$_3$ (i.e., 6 equiv, 87% conversion). On the other hand, regardless of the higher final conversion, the reactions with large excesses of OPPh$_3$ led to much slower rates at early stages. The opposite effects of OPPh$_3$ equivalents in the early and late stages of the reaction suggested different kinetics associated with the evolution of the active catalyst.
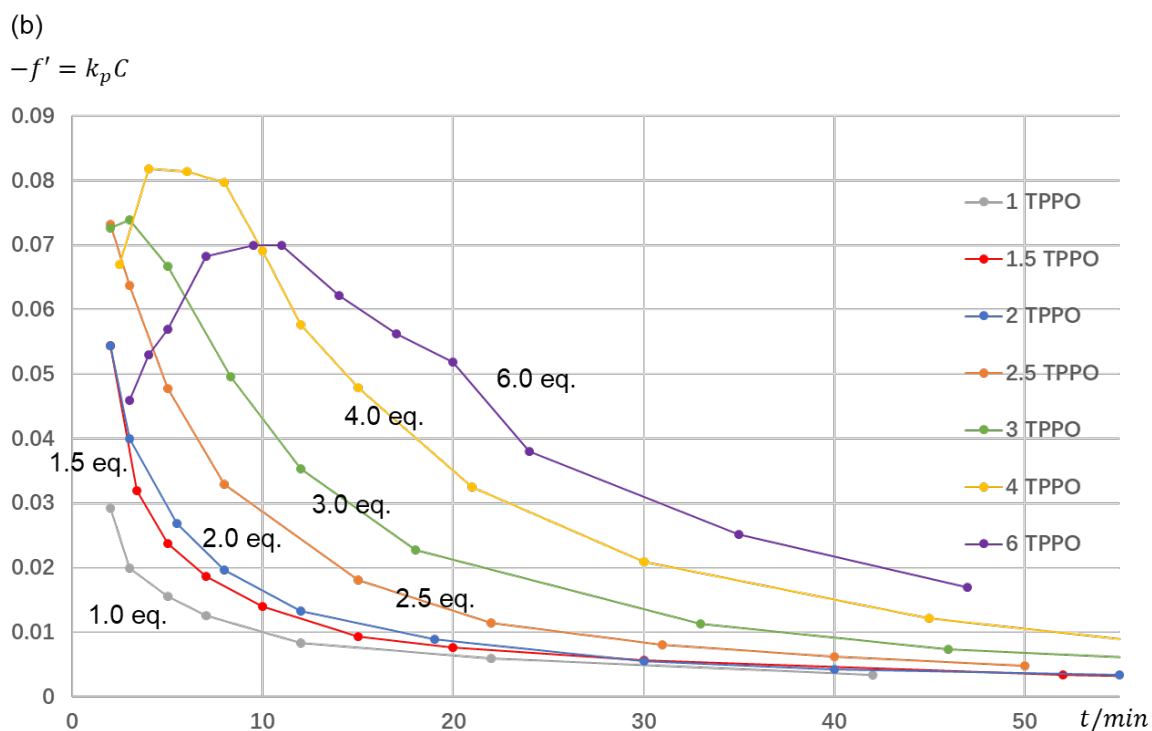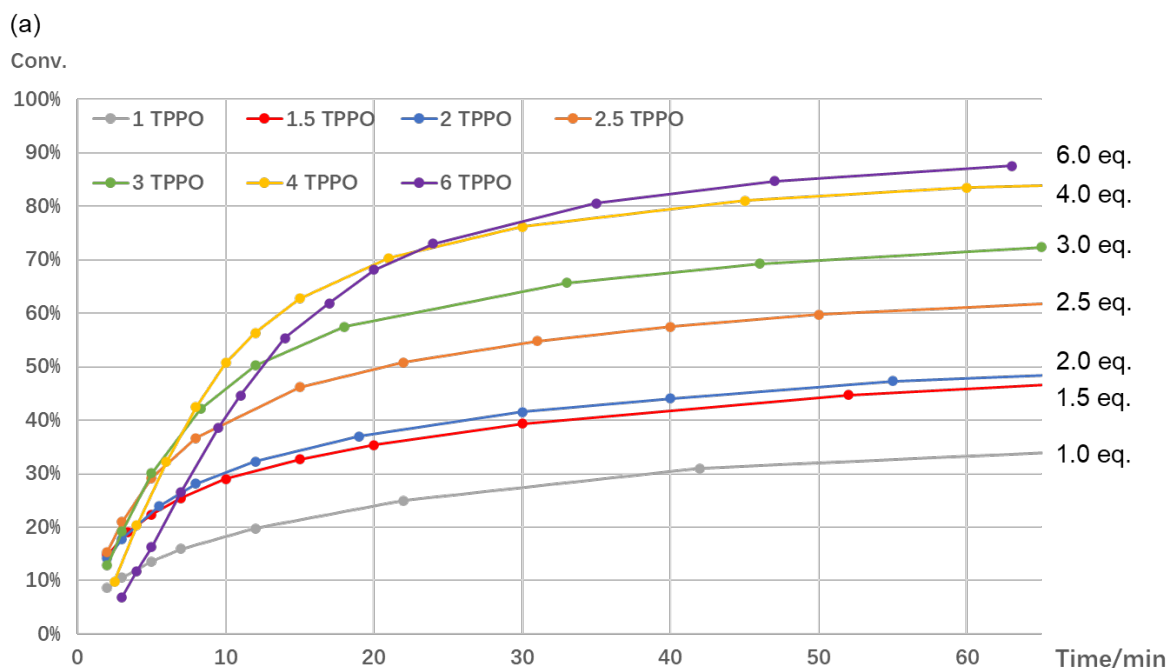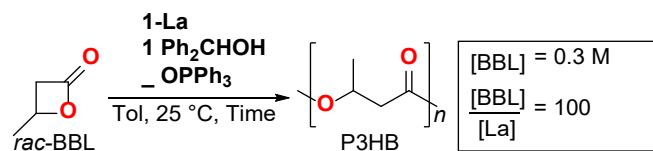
Figure 4.4. (a) Conversions of BBL and (b) relative catalyst concentration as functions of reaction time. Reactions were performed in toluene at ambient temperature with [BBL]/[**1-La**]/[Ph$_2$CHOH] = 100/1/1, [OPPh$_3$]/[**1-La**] = 1.0, 1.5, 2.0, 2.5, 3.0, 4.0 and 6.0, and [BBL] = 0.3 M.

Table 4.4. The ROP of *rac*-BBL (0.3 M) catalyzed by **1-La** with variable equiv. **OPPh₃**

1-La
1 Ph$_2$CHOH
_ OPPh$_3$
Tol, 25 °C, Time

rac-BBL → P3HB

[BBL] = 0.3 M
$\frac{[BBL]}{[La]}$ = 100

\multicolumn{4}{c}{1.0 equiv. OPPh₃}				\multicolumn{4}{c}{1.5 equiv. OPPh₃}			
Time (min)	Conv. (%)[a]	f[b]	$-df/dt = k_pC$	Time (min)	Conv. (%)[a]	f[b]	$-df/dt = k_pC$
2	8.6	-0.090	0.0292	2	14.7	-0.159	0.0545
3	10.5	-0.111	0.0200	3.4	19.0	-0.211	0.0320
5	13.6	-0.146	0.0156	5	22.4	-0.253	0.0237
7	15.9	-0.174	0.0126	7	25.4	-0.294	0.0187
12	19.7	-0.220	0.00840	10	29.0	-0.342	0.0141
22	24.9	-0.287	0.00587	15	32.6	-0.395	0.00937
42	30.9	-0.370	0.00339	20	35.3	-0.436	0.00761
81	35.9	-0.445	-	30	39.3	-0.500	0.00571
				52	44.7	-0.592	0.00343
				73	47.7	-0.649	0.00233
				110	50.9	-0.712	-

\multicolumn{4}{c}{2.0 equiv. OPPh₃}				\multicolumn{4}{c}{2.5 equiv. OPPh₃}			
Time (min)	Conv. (%)[a]	f[b]	$-df/dt = k_pC$	Time (min)	Conv. (%)[a]	f[b]	$-df/dt = k_pC$
2	14.1	-0.152	0.0544	2	15.3	-0.167	0.0732
3	17.7	-0.195	0.0400	3	20.9	-0.235	0.0638
5.5	23.9	-0.273	0.0268	5	29.2	-0.345	0.0478
8	28.1	-0.329	0.0197	8	36.6	-0.456	0.0330
12	32.2	-0.389	0.0133	15	46.1	-0.618	0.0181
19	37.0	-0.462	0.00897	22	50.8	-0.709	0.0114
30	41.5	-0.536	0.00551	31	54.8	-0.794	0.00807
40	44.0	-0.580	0.00423	40	57.4	-0.854	0.00618
55	47.3	-0.641	0.00336	50	59.8	-0.910	0.00486
83	50.3	-0.699	-	70	62.3	-0.977	-

\multicolumn{4}{c}{3.0 equiv. OPPh₃}			
Time (min)	Conv. (%)[a]	f[b]	$-df/dt = k_pC$
2	12.8	-0.137	0.0727
3	19.1	-0.212	0.0740
5	30.0	-0.357	0.0667
8.3	42.1	-0.546	0.0496
12	50.2	-0.698	0.0354
18	57.4	-0.854	0.0227
33	65.6	-1.07	0.0112
46	69.3	-1.18	0.00736
65	72.3	-1.28	0.00487
120	76.5	-1.45	-

a – Determined by ¹H-NMR integration of BBL and PHB methine resonances in the crude reaction mixture.
b – f = ln(1-Conv.).

Table 4.4. Continued

4.0 equiv. **OPPh$_3$**				6.0 equiv. **OPPh$_3$**			
Time (min)	Conv. (%)[a]	f [b]	$-df/dt = k_pC$	Time (min)	Conv. (%)[a]	f [b]	$-df/dt = k_pC$
2.5	9.8	-0.103	0.0671	3	6.9	-0.071	0.0459
4	20.3	-0.227	0.0819	4	11.7	-0.125	0.0530
6	32.2	-0.389	0.0814	5	16.3	-0.177	0.0570
8	42.4	-0.552	0.0797	7	26.5	-0.308	0.0682
10	50.7	-0.707	0.0691	9.5	38.6	-0.488	0.0699
12	56.3	-0.829	0.0576	11	44.6	-0.591	0.0699
15	62.8	-0.988	0.0480	14	55.4	-0.807	0.0621
21	70.3	-1.22	0.0325	17	61.9	-0.964	0.0562
30	76.2	-1.44	0.0210	20	68.1	-1.14	0.0519
45	81.0	-1.66	0.0122	24	73.0	-1.31	0.0380
60	83.5	-1.80	0.00741	35	80.5	-1.64	0.0252
84	85.2	-1.91	0.00396	47	84.7	-1.88	0.0170
120	86.8	-2.02	-	63	87.5	-2.08	-

a – Determined by ^{1}H-NMR integration of BBL and PHB methine resonances in the crude reaction mixture.
b – $f = \ln(1\text{-Conv.})$.

Relative catalyst concentrations during the reaction can be represented as $-f'$ according to eq. (3) (Table 4.4 and Figure 4.4.b). Note that among the curves of reactions with varied conditions, we cannot argue in which reaction the remained active catalyst is more than another at any given time, because it is k_pC rather than C we use as the vertical coordinate, where k_ps are undetermined and likely vary from one condition to another while they are considered as constants during each reaction. The interpretation of these curves is confined within each of themselves. Regardless of that, significant decreases of catalyst concentration were observed in all cases..

Plots of $-f'$ *vs* time reveal donor-dependent maxima, which reflect donor-dependent maxima in active-catalyst concentration. Notably, excess OPPh$_3$ (3.0, 4.0 and 6.0 equiv.) shifts the maxima of $-f'$ to later time, consistent with slower reaction rates at earlier timepoints. Such behavior is

consistent with increased delays in converting the pre-catalyst to authentically catalytic species, an induction period, where excess OPPh$_3$ appears to extend the induction period. Although we didn't observe a maxima in reactions with fewer than 2.5 equivalents of OPPh$_3$ were no more than 2.5, we attribute this to the actual maximum of catalyst concentration appearing much earlier than the first measurement we conducted (ca. 2 min).

Given these results, we hypothesize that activation of the pre-catalyst involves substitution of one of the two-bound OPPh$_3$ by the monomer, BBL. Before the addition of monomer, the pre-catalyst is in the state of a monomeric La alkoxide with two bound OPPh$_3$, e.g., **4-La**. We hypothesize that the precatalyst can be further converted to the relevant active catalyst for insertion and ring-opening through a ligand substitution reaction between free BBL and La-bound OPPh$_3$. The fraction of [La] species bound by BBL depends on the concentrations and binding strength of OPPh$_3$ and BBL, where higher binding strength and concentrations of OPPh$_3$ would lead to lower concentrations of active catalyst. This hypothesis is consistent with expectations based on the donor strength of OPPh$_3$[18] and BBL[19], as well as our experimental observations for (1) the positive correlation between OPPh$_3$ equivalent and length of induction period; (2) the presence of unbound OPPh$_3$ during reaction (see Chapter 2.).

Despite the lower catalyst concentration and slower reaction rates at earlier conversions, a slower composite reaction rate is beneficial to the final conversion. Because of the lower initial concentration of catalyst and the 2nd order dependence of catalyst degradation on its concentration, the irreversible consumption of catalyst is reduced at early stages of the reaction

with higher concentrations of OPPh$_3$. Therefore, reaction conversions are improved with higher concentrations of OPPh$_3$, due to an extended catalyst lifetime.

4.2.4. Effect of Electronic Property of Lutidine Oxide

In Chapter 3, we observed that the electron donating ability of groups located in the para-position of a family of lutidine oxides had a significant impact in the activity of ROP of BBL initiated by a La^{III} aminobisphenolate catalyst. Unlike increasing the equivalent of OPPh$_3$, which promotes the overall activity monotonically, the highest activity in our screen scale is supported by the lutidine oxide with OMe on para-position. More electron-rich (NMe$_2$) or electron-deficient (H) para-substituents than OMe lead to slower rates and lower conversions. In Chapter 3, we established that more electron-rich lutidine oxide bind more tightly to the La complex, while studies in Chapter 2 and the preceding section support that the substitution of the exogenous ligand is involved in catalyst activation and affects both the reaction rates and conversion. Herein, we continue to analyze the effects of donor electronic properties on the evolution of the active catalyst.

With the **1-La** as the precursor of catalyst of ROP of BBL, we chose ^{OMe}**LO**, ^{NMe2}**LO** and **LO** as the exogenous ligand with interest in this study. Monomer concentration and catalyst loading were set at 0.3 M and 1 mol% to maintain comparable conditions to our studies with OPPh$_3$. Conversions were measured by removal and quenching of aliquots at given time points, and this data was further converted to catalyst evolution according to eq. (3). The results of these experiments are shown in Table 4.5 and Figure 4.5.a.

The investigation of catalyst evolution shows that for the optimal lutidine oxide, ^{OMe}LO, the concentration of active catalytic species reaches a maximum at 1 min of the reaction (Figure 4.5.c.; 32% conversion). When a more electron-rich ligand is instead used, ^{NMe2}LO, the maxima is reached at longer time points (Figure 4.5.b.; 9 min, 17% conversion). The stronger donor suppresses the formation of active catalytic species, which leads to lower conversions and slower rates. In the reaction with a less electron-rich donor, ^{H}LO, the active species is found to decrease monotonically within the first measurement (Figure 4.5.d; 10 s, 5% conversion). This observation supports fast activation of the La benzhydrolate precursor with two LO coordinated.
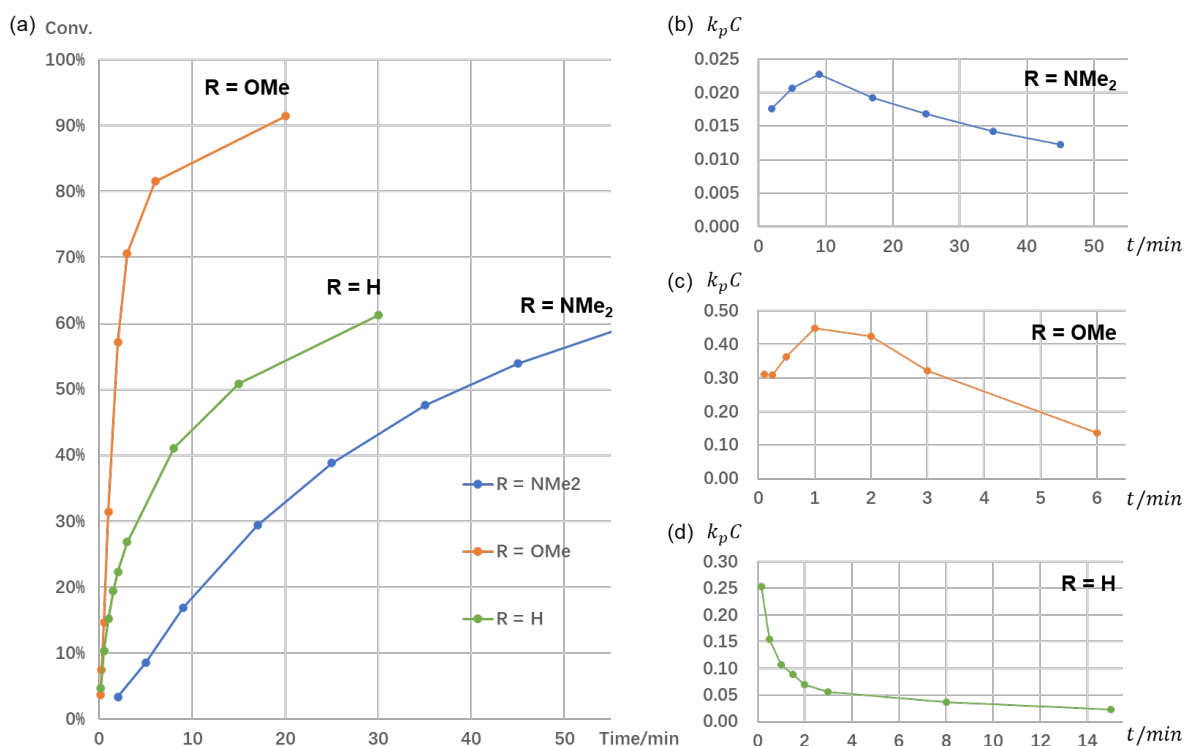
Figure 4.5. (a) Conversions of ROP of BBL with **1-La** and ^{R}**LO**, R = NMe$_2$ (blue), OMe (orange) and H (green), and relative catalyst concentration [(b) R = NMe$_2$ (blue), (c) R = OMe (orange) and (d) R =H (green)] as functions of reaction time. Reactions were performed in toluene at ambient temperature with [BBL]/[**1-La**]/[Ph$_2$CHOH]/[^{R}**LO**] = 100/1/1/2, and [BBL] = 0.3 M.

Table 4.5. ROP of *rac*-BBL (0.3 M) with **1-La** and $^\text{R}$**LO**.

Reaction scheme: *rac*-BBL → P3HB, conditions: **1-La**, 1 Ph$_2$CHOH, 2 $^\text{R}$LO, Tol, 25 °C, Time. [BBL] = 0.3 M, [BBL]/[La] = 100.

$^\text{NMe2}$LO			$^\text{OMe}$LO			LO		
Time (min)	Conv. (%) [a]	k_pC [b]	Time (min)	Conv. (%) [a]	k_pC [b]	Time (min)	Conv. (%) [a]	k_pC [b]
2	3.4	0.0176	0.12	3.7	0.311	0.17	4.7	0.254
5	8.5	0.0206	0.25	7.4	0.308	0.5	10.3	0.154
9	16.8	0.0227	0.5	14.7	0.363	1	15.2	0.106
17	29.4	0.0192	1	31.5	0.448	1.5	19.4	0.0886
25	38.8	0.0168	2	57.1	0.424	2	22.4	0.0698
35	47.6	0.0142	3	70.6	0.322	3	26.8	0.0564
45	53.9	0.0122	6	81.5	0.137	8	41.1	0.0362
60	61.1	-	20	91.5	-	15	50.9	0.0227
						30	61.3	-

a – Determined by ^{1}H-NMR integration of BBL and PHB methine resonances in the crude reaction mixture.
b – k_pC = df/dt, f = ln(1-Conv.).

Based on the strength of the exogenous ligand and the varying time of catalyst activation, the catalyst evolution is treated with two models. One is with a short induction period, in which the coordination of monomer is fast. In this scenario, activation of the pre-catalyst is effectively finished within the first seconds of the reaction, meaning that both the reaction time and conversion of BBL is negligible compared to the whole reaction time and final conversion. With this approximation, the reaction can be considered as one with a high initial concentration of catalytic species, where this amount equals that of the pre-catalyst used in the reaction. In this scenario, the reaction rate is predominantly affected by the rate of propagation *and* catalyst degradation (k_p and k_e). Catalysts using moderate donor-strength exogenous ligands (OPPh$_3$ and $^\text{H}$**LO**) are categorized in this type. In these cases, the catalytic species declines monotonically from the initial measurement, even at relatively low conversions. For these

systems, increasing the strength and concentration of the ligand enhances the reactivity by suppressing catalyst degradation (i.e., elimination, k_e).

The alternative model features an unignorable induction period, during which the amount of active species increases during times in which there is significant conversion of monomer. A significant portion of conversion takes place when active species reaches its maximum, so the catalyst evolution must still be evaluated as a competition between activation and degradation. In our studies, the reactions with highly electron-rich exogenous ligands (**^{NMe2}LO** and **^{OMe}LO**) showed this characteristic. We have found that donor strength not only impacts catalyst activation, but also attenuates the rate of propagation and catalyst degradation.

While further investigations are warranted, our initial experimental results suggest that catalyst activation can be rate-determining with stronger ligands, which can ultimately lead to lower reactivity. In the induction or activation dominated model, the activation rate can be qualitatively compared according to the time of the maximum of catalytic species. The more electron-rich the ligand is, the slower catalyst activation is (Figure 4.5.b and 4.5.c). This trend is consistent with our earlier hypothesis where the activation of catalyst involves substitution of one of the two coordinated ligands with BBL.

In summary, the electronic properties of the exogenous ligand can contribute oppositely in two different stages of the reaction. Increasing the electron-donating ability of the ligand decelerates monomer binding. This leads to an off-cycle intermediate (bis-donor coordinated

species), but also suppresses a key, irreversible catalyst degradation pathway (i.e., elimination). The underlying influence of these donors on enhancing the propagation rate still needs to be better understood, but it is clear that donors of intermediate strength, ^{OMe}LO, can balance these effects to reach unprecedented activity.

4.3. Conclusion

In this chapter, we proposed a method that can quantitatively evaluate the change in concentration of the catalytic species. This includes addressing a key catalyst deactivation process, elimination, which in previous chapters was found to considerably reduce the reaction rate. According to the relationship we have developed between the active species and reaction time, we have inferred that the elimination process is 2nd-order in catalyst and we have deduced rate constants for propagation and elimination in the ROP of BBL initiated by **4-La(OPPh$_3$)$_2$**. The kinetic model and derived rate constants are in excellent agreement with the experimental results. With this method, we evaluated key parameters surrounding exogeneous donor ligands in ROP of BBL initiated by **1-La** or its alkoxide derivative and assisted with such ligands, which included donor equivalents and donor electronic properties. These methods help categorize their effects and mechanistic roles in the ROP of BBL, and should enable the systematic design of future catalysts for ROP.

4.4. Experimental Section

4.4.1. General Methods

Instruments and measurements: Unless specified, all reactions were performed under inert conditions (N_2) using standard Schlenk techniques or in a MBraun drybox equipped with a standard catalyst purifier and solvent trap. Glassware was oven-dried for at least 2 h at 150 °C prior to use. Celite and 3 Å molecular sieves were heated under reduced pressure at 300 °C for at least 24 h and then cooled under vacuum prior to use. The following spectrometers were used for NMR characterization: Bruker Avance III HD Ascend (^{1}H: 600 MHz, ^{13}C: 151 MHz, ^{31}P: 243 MHz) and a Bruker DRX (^{1}H: 400 MHz, ^{13}C: 101 MHz, ^{31}P: 162 MHz). ^{1}H- and ^{13}C-NMR shifts are referenced relative to the solvent signal ($CDCl_3$: ^{1}H: 7.26 ppm, ^{13}C: 77.16 ppm; C_6D_6: ^{1}H: 7.16 ppm, ^{13}C: 128.06 ppm), while ^{31}P-NMR shifts are referenced relative to external solution standards (H_3PO_4, 0 ppm). Both instruments were equipped with Z-gradient BBFO probes.

Materials: Tetrahydrofuran, diethyl ether, toluene, hexanes, and pentane were purchased from Fisher Scientific. Solvents were sparged for 20 min with dry Ar and dried using a commercial two-column solvent purification system (LC Technologies). Solvents were further dried by storing them over 3 Å molecular sieves for at least 48 h prior to use. Ultrapure, deionized water (18.2 MΩ) was obtained from a Millipore Direct-Q 3 UV Water Purification System. Deuterated solvents were purchased from Cambridge Isotope Laboratories, Inc. C_6D_6 was degassed with 3 freeze-pump-thaw cycles and stored over 3 Å molecular sieves for at least 48 h prior to use. Qualitative assessment of moisture-content in these solvents was performed by

adding 1 drop of a concentrated solution of a sodium benzophenone radical anion (purple) to 10 mL of solvent where maintenance of a dark blue color for at least 5 minutes was sufficient for use.

2,6-ditertbutyl phenol (Oakwood Chemical; 99% purity), para-formaldehyde (Alfa Aesar; 97% purity), benzylamine (TCI; 99% purity), triphenylphosphine oxide (Acros; 99% purity), hexamethylphosphoramide (TCI; 98% purity), triphenylphosphate (Sigma-Aldrich; 99% purity), potassium hexamethyldisilazide (Sigma-Aldrich; 95% purity), 1,1,3,3-tetramethyldisilazane (TCI, 97% purity), $LaCl_3$ (Strem; RE = La; 99.9% purity), and acetyl chloride (Acros; 99% purity) were purchased and used as received. Racemic butyrolactone (Sigma-Aldrich; 98% purity) was freshly distilled from CaH_2 under nitrogen and degassed by freeze-pump-thaw cycles prior to use. $La[N(SiMe_3)_2]_3$,[20] $La[N(SiHMe_2)_2]_3(THF)_2$,[21] **BnL**, **1-La**, **1-La(OPPh₃)₂**,[22] were prepared according to reported procedures. **NMe2LO**, **OMeLO**, **LO** and **4-La(OPPh₃)₂** were prepared as described in Chapter 3.

4.4.2. Representative Example Measuring Conversion with a Pre-set Reaction Time

In a glovebox, a 4 mL scintillation vial was charged with **1-La** (10.0 mg, 0.0104 mmol, 1.0 equiv.; MW: 957.27 g•mol⁻¹), a toluene solution of $O(SiMe_3)_2$ (0.10% m/m, 3.20 mL, ρ = 0.867 g/mL; 2.77 g, 0.0171 mmol, 1.64 equiv.; MW: 162.38 g•mol⁻¹), and a magnetic stir bar. $O(SiMe_3)_2$ was used as an internal standard to accurately determine the amount and concentration of La complex and BBL.

Note: Despite the internal standard, the toluene solution of $O(SiMe_3)_2$ effectively acted as the solvent of the reaction and its amount regulated the reaction concentration. The amount of this solution was corrected according to the mass addition of the reaction vial before adding the stir bar. The ratio of **1-La** to $O(SiMe_3)_2$ was determined by ^{1}H-NMR of the mixed solution at this moment, which consumed 0.01 mL of the total volume (3.20 mL).

A toluene solution of $HOCHPh_2$ (2.0% m/m, 0.110 mL, ρ = 0.867 g/mL; 1.92 mg, 0.0104 mmol, 1.0 equiv.; MW: 184.24 g•mol^{-1}) and a toluene solution of ligand, e.g., ^{OMe}**LO** (5% m/m, 0.074 mL, ρ = 0.867 g/mL; 3.2 mg, 0.0209 mmol, 2.0 equiv.; MW: 153.18 g•mol^{-1}) were added to the clear, colorless solution. After approximately one minute, *rac*-BBL (0.085 mL, ρ = 1.06 g/mL, 90 mg, 1.04 mmol, 100 equiv.; MW: 86.09 g•mol^{-1}) was added to the stirring catalyst solution. After a pre-set reaction time, the conversion was checked by adding ca. 0.1 mL reaction solution to a 0.02 mL of a ca. 5 wt% toluene solution of benzoic acid (BzOH), followed by addition of 0.5 mL CDCl$_3$. The resulting solution was transferred to an NMR tube for ^{1}H-NMR analysis, yielding the conversion of BBL. The initial amount and concentration of BBL were corrected according to the ratio of the total area of methine peaks of BBL and P3HB to the signal of $O(SiMe_3)_2$.

4.5. Appended Math Procedures

4.5.1. 2nd Order Approximation of Derivatives of Discrete Functions with Different Step-Sizes (eq. 5)

In Section 4.2.2, we introduced $f(t)$ to represent the degree of the consumption of the substrate, that is the monomer in a polymerization, of which the derivative is proportional to the concentration of the catalytic species. If the independent variable of a function is given with equal interval, the derivative of the function at each point can be easily approximated with the function value at the point and those at its adjacent points. This is usually the case of an automated measurement. Limited by the nonautomated experimental method, the times when $f(t)$ is measured are set with unequal intervals, which are even deliberately assigned to increasing. This fact requires a more careful process to solve the derivative, as we expressed in eq. 5.

For value of function at the nth time point, eq. 4 gives 2nd order expansions from $f(t_n)$ to $f(t_{n\pm1})$:

$$f(t_{n+1}) - f(t_n) = f'(t_n)(t_{n+1} - t_n) + \frac{1}{2}f''(t_n)(t_{n+1} - t_n)^2 + O((t_{n+1} - t_n)^3) \quad (14)$$

$$f(t_{n-1}) - f(t_n) = f'(t_n)(t_{n-1} - t_n) + \frac{1}{2}f''(t_n)(t_{n-1} - t_n)^2 + O((t_{n-1} - t_n)^3) \quad (15)$$

$f(t_n)$, $f(t_{n-1})$ and $f(t_{n+1})$ are experimentally measured, $f'(t_n)$ and $f''(t_n)$ are unknown yet, and $f''(t_n)$ is what we interested in. Dividing eq. 14 by $(t_{n+1} - t_n)^2$ and neglecting 3rd order terms, we obtain

$$\frac{f(t_{n+1}) - f(t_n)}{(t_{n+1} - t_n)^2} = \frac{f'(t_n)}{t_{n+1} - t_n} + \frac{1}{2}f''(t_n) \quad (16)$$

Similarly, we reorganize eq. 15 as

$$\frac{f(t_{n-1}) - f(t_n)}{(t_{n-1} - t_n)^2} = \frac{f'(t_n)}{t_{n-1} - t_n} + \frac{1}{2}f''(t_n) \quad (17)$$

Subtracting eq. 17 from eq. 16, we cancel the unknown terms of second derivative.

$$\frac{f(t_{n+1}) - f(t_n)}{(t_{n+1} - t_n)^2} - \frac{f(t_{n-1}) - f(t_n)}{(t_{n-1} - t_n)^2} = \frac{t_{n-1} - t_{n+1}}{(t_{n+1} - t_n)(t_{n-1} - t_n)} f'(t_n) \quad (18)$$

Now, we can express $f'(t_n)$ as

$$f'(t_n) = \frac{1}{t_{n-1} - t_{n+1}} [(t_{n-1} - t_n) \frac{f(t_{n+1}) - f(t_n)}{t_{n+1} - t_n} - (t_{n+1} - t_n) \frac{f(t_{n-1}) - f(t_n)}{t_{n-1} - t_n}] \quad (19)$$

Rearranging eq. 19 to keep the convention that a subtraction involving two values of time is always the later minus the earlier, we obtain eq. 5.

$$f'(t_n) = \frac{1}{t_{n+1} - t_{n-1}} [(t_n - t_{n-1}) \frac{f(t_{n+1}) - f(t_n)}{t_{n+1} - t_n} + (t_{n+1} - t_n) \frac{f(t_n) - f(t_{n-1})}{t_n - t_{n-1}}] \quad (5)$$

This expression has a straightforward physical meaning: $f'(t_n)$ is approximated as the average of the slopes of its two adjacent intervals, weighted by how close an adjacent point is to the point of t_n.

4.5.2. Solution of Monomer Evolution with Time-dependent Catalytic Species (eq. 10)

In Section 4.2.2, the time derivative was obtained by combining the rate law of the evolution of monomer and catalytic species (eq. 10), where M and M_0 are the monomer concentration at any given time and the beginning of the reaction. The solution of this equation would express the monomer concentration as a function of time.

$$\frac{dM}{dt} = -k_p C_0 M \left(\frac{M}{M_0}\right)^{k_e/k_p} \quad (10)$$

Instead of M with a dimension of concentration, we herein are using $u = M/M_0$ as the variable, which is dimensionless and shows how complete the reaction has been.

Dividing eq. 10 by M_0 and substitute M/M_0 with u, we obtain

$$\frac{du}{dt} = -k_p C_0 u u^{k_e/k_p} = -k_p C_0 u^{k_e/k_p+1}$$

Separate terms of u and t:

$$k_p C_0 dt = -u^{-k_e/k_p-1} du$$

Integrate both side:

$$k_p C_0 t + Constant = -\frac{1}{-k_e/k_p} u^{-k_e/k_p}$$

Knowing $u = 1$ when $t = 0$, the constant is solved:

$$k_p C_0 t + \frac{k_p}{k_e} = \frac{k_p}{k_e} u^{-k_e/k_p}$$

Rearrange the equation to express u, namely M/M_0, we obtain the solution as eq. 11:

$$\frac{M}{M_0} = u = (1 + k_e C_0 t)^{-k_p/k_e} \qquad (11)$$

4.6. References

1. Kurcok, P.; Jedlinski, Z.; Kowalczuk, M., Reactions of β-lactones with potassium alkoxides and their complexes with 18-crown-6 in aprotic solvents. *J. Org. Chem.* **1993,** *58* (16), 4219-4220.

2. Kurcok, P.; Dubois, P.; Jèrôme, R., Polymerization of β-butyrolactone initiated with Al(OiPr)3. *Polym. Int.* **1996,** *41* (4), 479-485.

3. Shaik, M.; Peterson, J.; Du, G., Cyclic and Linear Polyhydroxylbutyrates from Ring-Opening Polymerization of β-Butyrolactone with Amido-Oxazolinate Zinc Catalysts. *Macromolecules* **2019,** *52* (1), 157-166.

4. Dominski, A.; Konieczny, T.; Zieba, M.; Klim, M.; Kurcok, P., Anionic Polymerization of beta-Butyrolactone Initiated with Sodium Phenoxides. The Effect of the Initiator Basicity/Nucleophilicity on the ROP Mechanism. *Polymers* **2019,** *11* (7).

5. Morikawa, H.; Marchessault, R. H., Pyrolysis of bacterial polyalkanoates. *Can. J. Chem.* **1981,** *59* (15), 2306-2313.

6. Ballistreri, A.; Garozzo, D.; Giuffrida, M.; Impallomeni, G.; Montaudo, G., Analytical degradation: An approach to the structural analysis of microbial polyesters by different methods. *J. Anal. Appl. Pyrolysis* **1989,** *16* (3), 239-253.

7. Kunioka, M.; Doi, Y., Thermal degradation of microbial copolyesters: poly(3-hydroxybutyrate-co-3-hydroxyvalerate) and poly(3-hydroxybutyrate-co-4-hydroxybutyrate). *Macromolecules* **1990,** *23* (7), 1933-1936.

8. Ariffin, H.; Nishida, H.; Shirai, Y.; Hassan, M. A., Determination of multiple thermal degradation mechanisms of poly(3-hydroxybutyrate). *Polym. Degrad. Stab.* **2008,** *93* (8),

1433-1439.

9.　Rieth, L. R.; Moore, D. R.; Lobkovsky, E. B.; Coates, G. W., Single-Site β-Diiminate Zinc Catalysts for the Ring-Opening Polymerization of β-Butyrolactone and β-Valerolactone to Poly(3-hydroxyalkanoates). *Journal of the American Chemical Society* **2002,** *124* (51), 15239-15248.

10.　Kricheldorf, H. R.; Scharnagl, N.; Jedlinski, Z., Polylactones 33. The role of deprotonation in the anionic polymerization of β-propiolactone. *Polymer* **1996,** *37* (8), 1405-1411.

11.　Kawalec, M.; Adamus, G.; Kurcok, P.; Kowalczuk, M.; Foltran, I.; Focarete, M. L.; Scandola, M., Carboxylate-Induced Degradation of Poly(3-hydroxybutyrate)s. *Biomacromolecules* **2007,** *8* (4), 1053-1058.

12.　Jaffredo, C. G.; Carpentier, J. F.; Guillaume, S. M., Controlled ROP of β-Butyrolactone Simply Mediated by Amidine, Guanidine, and Phosphazene Organocatalysts. *Macromolecular Rapid Communications* **2012,** *33* (22), 1938-1944.

13.　Altenbuchner, P. T.; Kronast, A.; Kissling, S.; Vagin, S. I.; Herdtweck, E.; Pöthig, A.; Deglmann, P.; Loos, R.; Rieger, B., Mechanistic Investigations of the Stereoselective Rare Earth Metal-Mediated Ring-Opening Polymerization of β-Butyrolactone. *Chemistry – A European Journal* **2015,** *21* (39), 13609-13617.

14.　Aluthge, D.; Ahn, J.; Mehrkhodavandi, P., Overcoming aggregation in indium salen catalysts for isoselective lactide polymerization. *Chemical science* **2015,** *6* (9), 5284-5292.

15.　Zhao, W.; Cui, D.; Liu, X.; Chen, X., Facile synthesis of hydroxyl-ended, highly stereoregular, star-shaped poly (lactide) from immortal ROP of rac-lactide and kinetics study. *Macromolecules* **2010,** *43* (16), 6678-6684.

16. Silvernail, C. M.; Yao, L. J.; Hill, L. M.; Hillmyer, M. A.; Tolman, W. B., Structural and mechanistic studies of bis (phenolato) amine zinc (II) catalysts for the polymerization of ε-caprolactone. *Inorganic chemistry* **2007,** *46* (16), 6565-6574.

17. Duda, A.; Penczek, S., Mechanisms of Aliphatic Polyester Formation. In *Biopolymers Online*, Wiley VCH: 2002; Vol. 3b, pp 371-429.

18. Laurence, C.; Gal, J.-F., Thermodynamic and Spectroscopic Scales of Hydrogen-Bond Basicity and Affinity. In *Lewis Basicity and Affinity Scales. Data and Measurement*, John Wiley & Sons: Chichester, U.K, 2010; p 159.

19. Laurence, C.; Gal, J.-F., Thermodynamic and Spectroscopic Scales of Hydrogen-Bond Basicity and Affinity. In *Lewis Basicity and Affinity Scales. Data and Measurement*, John Wiley & Sons: Chichester, U.K, 2010; p 151.

20. Bradley, D. C.; Ghotra, J. S.; Hart, F. A., Low co-ordination numbers in lanthanide and actinide compounds. Part I. The preparation and characterization of tris{bis(trimethylsilyl)-amido}lanthanides. *Journal of the Chemical Society, Dalton Transactions* **1973,** (10), 1021-1023.

21. Smith, A. R.; Livinghouse, T., Rapid and Efficient Procedure for the Synthesis of Group 3 Metal Tris[bis(dimethylsilyl)amide] THF Complexes. *Organometallics* **2013,** *32* (5), 1528-1530.

22. Dong, X.; Robinson, J. R., The role of neutral donor ligands in the isoselective ring-opening polymerization of rac-β-butyrolactone. *Chemical Science* **2020,** *11* (31), 8184-8195.